AD NUMBER

AD888652

NEW LIMITATION CHANGE

TO

Approved for public release, distribution unlimited

FROM

Distribution authorized to U.S. Gov't. agencies only; Test and Evaluation; SEP 1971. Other requests shall be referred to Air Force Materials Lab., Wright-Patterson AFB, OH 45433.

AUTHORITY

AFML ltr dtd 7 Dec 1972

AFML–TR–70–95
PART II

ABLATIVE MATERIALS FOR HIGH HEAT LOADS

PART II

HETEROCYCLIC RESINS, LAYERED COMPOSITES, ELASTOMERS,
AND FILAMENT WOUND COMPOSITES

P.W. Juneau, Jr.
J.W. Metzger
F.P. Curtis
R.M. Fenton

Document No. 71SD2066

General Electric Company

TECHNICAL REPORT AFML–TR–70–95, PART II

SEPTEMBER 1971

AIR FORCE MATERIALS LABORATORY
AIR FORCE SYSTEMS COMMAND
WRIGHT–PATTERSON AIR FORCE BASE, OHIO

NOTICE

When Government drawings, specifications, or other data are used for any purpose other than in connection with a definitely related Government procurement operation, the United States Government thereby incurs no responsibility nor any obligation whatsoever; and the fact that the government may have formulated, furnished, or in any way supplied the said drawings, specifications, or other data, is not to be regarded by implication or otherwise as in any manner licensing the holder or any other person or corporation, or conveying any rights or permission to manufacture, use, or sell any patented invention that may in any way be related thereto.

AFML-TR-70-95
PART II

ABLATIVE MATERIALS FOR HIGH HEAT LOADS

PART II

HETEROCYCLIC RESINS, LAYERED COMPOSITES, ELASTOMERS,
AND FILAMENT WOUND COMPOSITES

P.W. Juneau, Jr.
J.W. Metzger
F.P. Curtis
R.M. Fenton

Document No. 71SD2066

General Electric Company

TECHNICAL REPORT AFML-TR-70-95, PART II

SEPTEMBER 1971

AIR FORCE MATERIALS LABORATORY
AIR FORCE SYSTEMS COMMAND
WRIGHT-PATTERSON AIR FORCE BASE, OHIO

FOREWORD

This report was prepared by the Re-entry and Environmental Systems Division of the General Electric Company, Philadelphia, Pennsylvania, under AF Contract F33615-69-C-1503. This contract was initiated under Project 7340 "Nonmetallic and Composite Materials", Task No. 734001 "Thermally Protective Plastics and Composites". The work was administered under the direction of the Nonmetallic Materials Division, Air Force Materials Laboratory (AFML). The AFML project engineer was Mr. R. Farmer, AFML/LNC.

This report covers work performed between 30 March 1970 and 30 June 1971.

The manuscript of this report was released by the authors 22 July 1971.

This technical report has been reviewed and is approved.
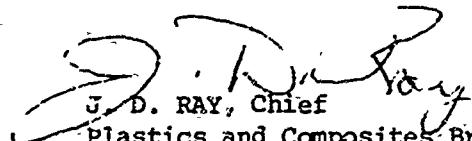
J. D. RAY, Chief
Plastics and Composites Branch
Nonmetallic Materials Division

ABSTRACT

Ablative plastic composite materials were investigated and developed for long time heating environments. The desirable materials performance goals were low surface ablation, insulative ability, and low weight without asymmetrical ablation, char instability, spallation or other thermomechanical effects.

The candidate materials consisted of (a) carbon, quartz, and silica cloth reinforced polyimide resin, (b) loom woven, low density quartz (LDQ) insulative layers using polyimide resin, (c) carbon-quartz bifilament tape reinforced phenolic resin, (d) filled ablative silicone elastomers, and (e) a multiple interlock, filament wound (MIFW) carbon filament reinforced phenolic resin cylinder.

Candidate materials and reference carbon and silica cloth reinforced phenolic resinous composites were evaluated. Polyimide resin composites were generally comparable to the reference materials. LDQ proved an effective light weight insulator when used between a heat shield and aluminum structure. Outstanding carbon-quartz bifilament tape performance was obtained, but the results could not be adequately reproduced. There were no attractive performance features for the two remaining concepts.

The test environment was generated by a 5 megawatt air arc heater, which was operated stepwise over 300 seconds to give a 36,550 Btu/ft^2 heat load. Other nominal conditions over the 230- and 70-second heating intervals were 5000 and 5000 Btu/lb enthalpy; 25 and 440 Btu/ft^2-sec heat flux; 0.4 and 2.5 lb/ft^2 shear stress.

A high heat flux, dual channel characterization procedure was developed to investigate the ablative performance of materials under conditions more representative of advanced missile entry missions. Preliminary characterizations were conducted for selected reference and candidate composites.

An analytical study was made of materials response and to confirm experimental results. Good agreement was generally found between analytical and experimental results for carbon cloth reinforced phenolic resin and other composites.

FORMAT TRANSMITTAL LETTER

SUBJECT: AFML-TR-70-95, Part II, AF Contract No. F33615-69-C-1503

TO: Recipient

1. Furnished herewith for your review, information, and permanent retention is Part II of Technical Report AFML-TR-70-95 for the subject contract. This Interim Summary Technical Report is entitled "Ablative Materials for High Heat Loads, Part II", and was prepared by the Re-Entry and Environmental Systems Division, General Electric Company.

2. This document is subject to special export controls and each transmittal to foreign governments or foreign nationals may be made only with prior approval of the Plastics and Composites Branch, Nonmetallic Materials Division, Air Force Materials Laboratory (MANC), Wright-Patterson Air Force Base, Ohio 45433.

3. Technical comments will be appreciated. They should be forwarded to AFML (MANC), Wright-Patterson AFB, Ohio 45433.

1 Attch
AFML-TR-70-95, Part II

LIST OF SYMBOLS

A	–	Collision Frequency
C_p	–	Specific Heat
e	–	Base, natural logarithm
E	–	Activation Energy
F	–	Coefficient
h	–	Enthalpy
H	–	Latent Heat
k	–	Thermal Conductivity
$M, \overline{M}$	–	Molecular weights
m	–	Summation Integer
$\dot{m}$	–	Mass flow
n	–	Exponent
P_r	–	Prandtl Number
$\dot{q}$	–	Heat Transfer Rate
R	–	Gas Constant
$\dot{s}$	–	Recession Rate
T	–	Temperature
t	–	Time
x	–	Depth dimension
X'	–	Specified Depth
Z	–	Reaction Rate Coefficient

β	–	Constant
Δ	–	Difference
∇	–	Del, vector operator
∂	–	Partial differential
ρ	–	Density
σ	–	Boltzmann Constant
Σ	–	Summation
Φ_0	–	Variable coefficient, defined in text

Subscripts

GF	–	gas–fluid
K	–	cracking/recombination
g	–	gas
c	–	char (except us/$\dot{q}$)
v	–	virgin
i	–	counter (of n components)
cv	–	convective
RR	–	reradiative
f	–	film (= $\dot{q}/\Delta h$)
e	–	emissivity
a	–	geometric viewfactor
r	–	recovery (stagnation)
w	–	wall
BL	–	Boundary Layer
vap	–	Vapor

TABLE OF CONTENTS

LIST OF ILLUSTRATIONS

LIST OF ILLUSTRATIONS (Continued)

LIST OF ILLUSTRATIONS (Continued)

LIST OF TABLES

I. INTRODUCTION

Ablative heat shield materials are usually exposed to peak high heat flux and peak high shear force environments for relatively brief periods of time. A low rate of surface recession is thus a prime performance requirement. There are advanced missile entry systems, however, that will require efficient insulative ability in addition to low recession for lengthy, high heat load missions.

The selection of ablative materials for high heat loads can be made only if the total environment effects are clearly understood and practical performance criteria are applied to the problem. The long period of heating first imposes a requirement for a high degree of insulative ability in addition to the usual ablative resistance. Secondly, it must be recognized that early decomposition and loss of resin may result in thermomechanical phenomena such as asymmetrical erosion, char instability, spallation, and surface roughness. The effects are of particular importance during the increasing heat flux and shear stress period at the lower entry altitudes.

This program was initiated to examine materials response under the advanced environmental requirement of high heat loads and to conduct exploratory development to provide new and improved materials for maximum efficiency. The desirab'e performance goals were high ablative resistance against thermochemical surface removal, insulative ability for structural thermal protection, and low total weight per unit area, without thermomechanically induced deleterious phenomena.

In the first years' work, an investigation was made of the adequacy, limitations and materials problems associated with the use of state-of-the-art tape wrapped carbon cloth and silica cloth reinforced phenolic resin composites. The erosive resistance, insulative ability, and structural integrity of ablative materials was evaluated using a high heat load characterization environment. The effects of composition and construction were investigated for a series of three reference and four candidate composites. The variables included cloth type, fiber orientation within the cloth, fiber size, resin type, and weave pattern. The ablative responses were highly dependent upon composition and construction. Asymmetrical erosion, excessive erosion, or high internal temperatures was found for several composites.

Certain carbon cloth and silica cloth reinforced phenolic resin composites gave acceptable ablative surface patterns, mass loss rates, and internal temperatures. These materials were relatively heavy. Consequently, multilayer lighter weight concepts were examined. A low density quartz (LDQ) construction was shown to be an effective and light weight insulator when bonded between the heat shield and aluminum structure. The LDQ consisted of phenolic impregnated quartz strands, which alternated at right angles to yield a square wall, non-laced patterned construction.

A considerable effort was devoted to the development of an appropriate environmental simulation capability. The unique facility features a five minute run in two steps for a large specimen. An exposure of 230 seconds at a low heat flux is followed by a step-change to a high heat flux period of 70 seconds. The nominal heat flux, enthalpy and shear stress environmental conditions are further summarized by Figure 1. Specimen dimensions were 5 inches length by a 1.75 inch width by a variable thickness. There was a bonded aluminum structure, five thermocouples, and a 20 degree fiber angle for the simulated tape wrapped specimen.

The exploratory development program was continued a second year to develop improved concepts as described by this report. The emphasis was on heterocyclic resins, abla-tive-insulative layer composites, low density elastomers, and a filament wound cylinder. The candidate concepts included: carbon, quartz and silica cloth reinforced polyimide resin (which is more thermally stable than phenolic resin); LDQ using polyimide resin; carbon-quartz bifilament tape reinforced phenolic resin composites; filled ablative silicone elastomers; and a simulated multiple interlock, filament wound (MIFW) carbon filament reinforced phenolic resin cylinder with promising ease of manufacture.

In addition to materials exploratory development, improvements were made in the design and operation of the air arc heater for high heat load characterization. Additional improvements were made in calibration procedure and the reporting of experimental data.

A dual channel characterization was developed to examine ablative performance under conditions more representative of advanced missile entry missions with a higher heat flux pulse and shorter period of heating. The nominal environmental conductions con-sisted of a calorimetric heat flux of 1200 Btu/ft^2-sec, enthalpy of 7000 Btu/lb, and run time of 15 seconds for a heat load of 22,500 Btu/ft^2. Specimens dimensions were 5 inches/length by a 1.75 inch width by a variable thickness. There were four thermo-couples and a 20 degree fiber angle for the two matching simulated tape wrapped speci-mens. Preliminary characterizations were conducted for reference carbon cloth and silica cloth reinforced phenolic resin composites, candidate carbon cloth and silica cloth reinforced polyimide resin composites and a graphite.

An existing computer code was modified to permit the analytical study of materials response and to confirm experimental results. Good agreement was generally found between analytical and experimental results for the reference carbon cloth reinforced phenolic resin composite and LDQ composites for the two types of ablative charac-terizations.

II. TECHNICAL APPROACH

FABRICATION

Fabrication of new concepts and specialized test specimens continued. There were some process failures and not all specimens were successfully completed. For simulated tape wrapped specimens, the fabrication process outlined in the interim annual report was used.

P13N (B-138) AND REFRASIL C-100-48

Five small scale process studies were made to determine a final process for the production of 20° oriented-bias tape flat panels utilizing P13N/Refrasil and autoclave equipment.

The studies included "B" stage times and coating applications (Resin pick-up). "B" stage temperatures were constant as well as laminating pressures. The gel time of the resin was 65 seconds at 190°C. Resin solids was 40 percent.

The initial three attempts resulted in a porous laminate having little structural integrity after post cure through 600°F. Little flow was noted and the cured laminate could be delaminated, ply by ply with little pressure exerted.

The fourth attempt included a consolidation step under vacuum bag pressure (14 psi) at 300°F for 15 minutes—followed by 150 psi (press) and 300°F for one hour. Resin flow was evident at 300°F - 150 psi and the laminate appeared structurally stable on cool-down. Several small voids were noted.

The fifth study included an additional time cycle in the consolidation step. This time was increased to minimize volatile entrapment.

Three oriented layups were made, and processed in the autoclave. All three were lost when the post cure oven temperature control failed and they were exposed to 1200°F. They all showed evidence of delamination prior to post-cure.

3

The fifth study included an additional time cure in the consolidation step from 15 to 30 minutes followed by 150 psi pressure at 300°F for one hour. The resulting laminate showed evidence of flow, structural integrity, but still evidence of small voids.

The sixth study included a consolidation step at a lower temperature (200°F) for a longer period of time (one hour) in an attempt to minimize volatile entrapment. Subsequent processing at 150 psi pressure and 300°F produced an acceptable, structurally stable flat panel.

The above process was scaled-up to the standard model configuration—20° oriented—45° bias tape model and processed by autoclave techniques at 150 psi and 350°F temperature. The resulting panel appeared structurally stable. Resin content at this point – 36%. On post cure through 300°F the oven control and override mechanisms failed, the oven temperature reaching a minimum of 900°F. Resin burn out and delamination was evident.

The process was repeated, the cured laminate post cured through 600°F. Samples were machined to model test size. These machined pieces showed some porosity, and low density areas. Further work with the P13N material was abandoned due to processing difficulties.

Gemon L - Quartz Sample Processing

    Reinforcement   581/9073 Quartz Fabric

    Resin Content   36 to 39%

    Solvent Content   9.4% average

The material as received was cut into 2 in.-wide tapes at 45° orientation and further sectioned into 12 in. lengths. These were then stacked into a 12 x 8 in. mold at 20° angle.

The panel was consolidated under vacuum bag pressure (14 psi) for 1 hour at 200°F.

This panel was further processed at 150 psi autoclave pressure and 350°F for six hours.

Post cure included 12 hours at 400°F plus 8 hours at 500°F.

Samples were machined to test model configuration—t.0 x 1.75 x 0.5 in. Density was –1.71 g/cc.

A previous panel processed in the identical manner, post cured in a run-away oven—estimated temperature 900 °F—survived sufficiently to be machined into test panels.

Resin content after (900 °E) post-cure - 36 percent.

Specific gravity - 1.70 g/cc

One specimen of each post cure condition was submitted for test. The fact that the composite was able to survive a very high temperature exposure for a substantial period of time made it of increased interest in this program.

Silicone Elastomer: Two specimens based on TBS 542 silicone rubber were prepared. They were identified as GEM 1 and 2.

GE TBS 542 Experimental Silicone (Modified with Sic)

Sample Preparation

Formulation	grams	%
TBS 542	200	84.1
RTV 9811 Catalyst	16	6.7
Silicon carbide 600 mesh	22	9.3
Total	238	100.0

Process

The TBS 542 was thoroughly blended by mechanical stirring with the RTV 9811 paste catalyst until a uniform green color was observed (5 minutes). Silicon carbide powder was added slowly until a uniformly dispersed (10 minutes). The mix was then dearated under 14 - 15 psi vacuum pressure. The mix although somewhat thixotropic was capable of being transferred into a 6 in. x 3 in. x .5 in. cavity by utilizing a vibrating table.

Cure

Initial Cure	16 hours at 75 °F
Post Cure	8 hours at 200 °F
	16 hours at 250 °F
	8 hours at 300 °F

5

Test Sample

The cured TBS 542 sample was bonded under moderate pressures to a 0.0625 in.-thick 6 x 2 in. aluminum plate (2024 T3) using RTV 560 0.5% T-12 catalyst.

Post cure of the bonded sample	8 hrs @ 160°F 8 hrs @ 200°F 8 hrs @ 300°F

On completion of the cure the sample was sectioned and surface ground to the test configuration 5.0 x 1.75 x 0.5 in. The density was 1.5g/cc.

In addition to the modified material, an unmodified specimen was prepared for comparison purposes. Both materials were used to complete the evaluation of the DCM-1 specimen.

Table I outlines the properties of the unmodified resin casting.

Multiple Interlocked Filament Wound (MILFW) Cylinder

The objective of this effort was to filament wind a MILFW cylinder composed of two (1/4 in.-wide) PX505/2510 helical bands interlocked into five (1/16 in-wide) PX505/2510 circumferential bands. The phenolic resin used was DP 2510.

Previous investigations have indicated that the quality of a filament wound structure is highly dependent upon the tension applied to the circumferentials. In this instance, it was not possible to apply tension to the circumferential band because of the separation of the two PX505 yarns which made up the 1/16 in.-wide band. One yarn would carry all the tension applied to the spool while the other yarn would not be under any tension.

Rather than return the PX505/2510 band to the material processor, attempts were made to utilize the material by applying supplemental individual tension to each yarn. This was done by constructing individual spring actuated tension arms which would apply tension to each yarn while still utilizing the basic spool tension brake.

Extensive trials revealed that the tension arms would not provide adequate circumferential winding tension on a consistent basis for the time span necessary to construct a MILFW cylinder. The process has been abandoned as being impractical with current materials.

6

As a substitute for the multiple interlocked filament wound specimen, a helically rewound PX510/DP2510 specimen was prepared and cured. Upon sectioning it was noted that this first winding contained a circumferential crack about midway through the piece. A second winding was prepared and cured, and showed no evidence of cracking when sectioned. This second specimen has been reimpregnated with additional phenolic resin, and prepared for test.

Figure 4 shows the cast, impregnated specimen, and Figure 5 shows the machined cylinder.

Combination Tape - Quartz/Carbon

The combination tape as supplied by the vendor consists of a three-inch wide, unimpregnated carbon, quartz cloth having a ratio of 2-1 carbon to quartz. It is interwoven with strands of organic yarn. The combination tape is shown in Figure 6.

Ablation samples were prepared by the following process:

1. Sixteen, 60-inch lengths of tape were cut and dried in an air circulating oven at 275°F for two hours.

2. On removal they were immediately impregnated with a 40 percent solution of DP-2510, phenolic resin, in Ethanol.

3. The tape was then "B" Staged 1 hour at 180°F.

4. A second coat of DP-2510 was applied.

5. The tape was "B" Staged 2 hours at 180°F.

6. The impregnated tape was then cut into 5-inch lengths.

7. These 5-inch segments were trimmed leaving a carbon layer of 1-inch and a quartz layer of 0.5-inch. This was done to facilitate molding.

8. The 5-inch segments were laid up at 20° wp in an eight inch mold.

9. The lay-up was consolidated at 180°F (vacuum bag pressure approx. 14 psi) for one hour.

10. Rebagged and cured in an autoclave at 150 psi under the following scheduled:

350°F	2 hours
375°F	2 hours
400°F	4 hours

11. Specimens were machined to 5-inches x 1.75-inches x *0.375-inch.

*Total material thickness after cure - 0.395-inch.

7

The resin content of the impregnated tape was 50 percent.

The density of the cured part was -1.34 g/cc.

The ratio of carbon to quartz in the cured part was six to one.

The line of demarkation between quartz and carbon was excellent.

No other properties were measured since the thickness of the quartz layer was less than desired. A 10X view is shown in Figure 7. A second set of ablation samples were prepared using the techniques outlined. Two exceptions were made:

1. The tape was molded as a 3-inch width without trimming.

2. Quartz scrim cloth (J. P. Stevens) was inserted between each layer of combination tape to achieve a more uniform quartz thickness.

Arc Modifications

As a result of previous tests, minor water leakage around ar. O-ring seal in the second plenum was observed. The problem was attributed to apparent progressive shrinkage of the copper liner of the plenum. Although the leakage was not serious, remedial action was taken; despite the repair and improvement in water flow, the plenum developed a leak during the subsequent run.

Because there has been increasing difficulty with the secondary plenum hardware, a new plenum design was prepared. The modified set-up is shown in Figures 2 and 3.

Construction of the dual channel components and specimens for the high heat transfer tests was completed. The test specimens will consist of 20° tape wrapped carbon phenolic and ATJ graphite. The dual channel test exhibited the following basic operating characteristics:

Heat Transfer 1500 BTU/sec-ft^2 (Extreme - 5.3%, -9.3%)

Enthalpy 6740 BTU/lb (Max. variation: -8.0%)

Delivered Power 2220 KW (Max. variation: -2.6%)

Specimen Pressure 54 psia (Variation -3.0%)

The configuration of the dual channel equipment is shown in Figure 8.

8

MATERIALS AND CONCEPT SELECTION

A number of new concepts were prepared during the second half of this study program, including some tape wrapped specimens utilizing a low density insulator, and some cast elastomeric materials and a filament wound specimen.

Table II outlines the specimen materials and gives details of construction. With the exception of A4-2B, all shield materials were of high density and uniformly good quality. A4-2B was a specimen prepared from CCA1-1641 Carbon fabric and Skybond 700, a material that characteristically produces composites with a high void content (Reference 1). A newly developed polyimide resin that cures by an addition polymerization process was selected to overcome the difficulties experienced with Skybond 700 (a condensation polymer), and specimens A4-3, 4, and 5; and A3-4 were prepared. The resin is code named H7B1000B. * The carbon composites exhibited a density of 1.42 g/cc, and the silica composites had a density of 1.88 g/cc. Neither showed any evidence of voids upon microscopic examinations. For comparison, specimen A2-2, a standard silica phenolic, was tested during this period. The C-4 specimens were based on a combination tape composed of VYB yarn and quartz yarn. The tape and fabricated specimens were described in the fabrication section.

Specimen C1-5 was a 0.2 inch thick carbon heat shield over a low density quartz phenolic insulator with a radiation barrier.

It should be noted that specimen C1-6 contained only 5 thermocouples, two in the shield material, one at the shield/insulator interface, one at the cold side of the radiation barrier, and one at the aluminum bond line. The sketch below gives details of construction.
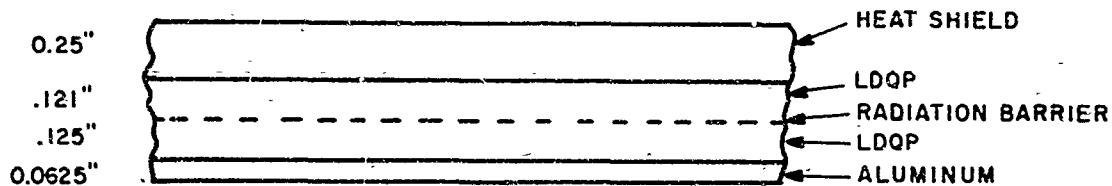
The heat shield thickness was selected based on the results obtained on C1-5 during a previous run.

The Quartz/Gemon (polyimide) composites, A7-1 and A7-3, were not as uniform in appearance as the silica/Gemon, A3-4 and A3-8, material, but showed high density properties in spite of the presence of some small cracks. DCM-1 (DC93-104) was supplied in cured form, and tested as supplied.

---

*GemonL

9

ABLATION TESTING

TWO PHASE HEATING

The data acquired during this program are given in Table III. A review of data acquired during the last group of ablation tests shows that significant improvement has been achieved in controlling input energy to the arc. Correspondingly, plenum pressure and secondary plenum pressure values are also relatively uniform. This can be readily seen by comparing plots in Figures 9 through 28. While this indicates an improved operational procedure, subsequent testing may provide even better repeatability. The general behavior of the channel wall pressures is attributed to the variation in performance of the nozzle as a result of specimen ablation. Although there is no immediately evident correlation between the types of materials and the gross channel pressure curve characteristics, it is difficult to identify any other mechanism which has the potential for producing the changes observed. Ineffective sealing of the specimen to the channel may be basically ruled out because the various tests nearly all exhibit sustained pressures below atmospheric. In some cases values of the order of 2/3 atmosphere were recorded. Note that no pressure responses are recorded for dual channel tests.

With reference of the heat balance, the results were more uniform than in the early series. Naturally, in part, this was due to more uniform application of the available electrical energy, but more improvement may be obtained when the recommended thermocouple array is installed in the water circulatory system.

The next set of figures show the surface temperature responses of the tested composites. Figure 29 shows the high heat flux environment portion of the C1-5 test; the low heat flux environment indicated a steady reading. Note the jagged shape of the first part of the curve, which then smooths out and has two peaks at about 4000 °R and 4400 °R. This composite consisted of a standard CP heat shield 0.2 inches thick over an insulating structure. Figures 30 and 31 show the surface temperatures attained by the specimen during the high heat flux portion of the test on A4-3 and A4-4. These were CCA-1 polyimide composites. Note the large differences in surface temperature, possibly caused by the change in total enthalpy in the two tests. It is of interest to note that radiation changes were observed after the arc was shut down. Figure 32 shows the total run response of Specimen A4-4.

Figure 33 shows the surface temperature of Specimen C4-1, which was a composite prepared from a bicomponent tape, with the carbon portion at the surface. One peak after power shutoff can be seen. The low heat flux environment showed a stable surface temperature, while the high heat flux portion showed a wide temperature variation.

10

Figure 34 shows the high heat flux portion of the surface temperature of A4-2B, a low density CCA1 polyimide composite. This specimen ablated through to the aluminum backing plate. Figure 35 shows the total run temperature, showing variation during the low heat flux portion of the run.

Figures 36 and 37 show the surface temperature response of specimen A3-4, a silica polyimide (GE) composite. Variable temperatures at the surface during the high heat flux environment are apparent, with one flash occurring after shutdown.

Figures 38 and 39 show the surface temperature response of specimen A2-2, a silica phenolic having the same approximate density as A3-4. Note the extreme differences in response between the two.

Figures 40 and 41 show the surface temperature response of C4-2, a bicomponent tape composite similar to specimen C4-1. Surface temperature variability is again apparent. The rest of the figures also show variability. It is necessary to point out that full length temperature response curves were not drawn for all specimens in which the low heat flux portion was uniform, since the major area of interest and most of the variations, took place during the high heat flux portion of the run.

The specimens based on GE polyimide (A4-3, A4-4 and A4-5) emitted energy after the arc was shut down. One other specimen, also a polyimide based composite (A4-2B), did not display this property, but showed a rapid decay in surface temperature. C4-1, a phenolic resin based material, also showed one flash of energy after arc shutdown. All the specimens showed considerable surface temperature variability during the high heat flux portion of the run. A comparison of Figures 45 and 53 is interesting, since it shows the surface temperatures of two different silicone resin formulations. Figure 55 will be supplied.

Figures 56 through 70 show the internal temperature response modes of the tested specimens.

Figures 77 through 96 show the recession profiles of the tested specimens.

Figures 97 and 98 show the ablated C1-5 specimen, both full view and in cross section. Note the melting of the quartz insulator layer, shown by the disassembled specimen in Figure 99.

Figure 100 shows a specimen typical of both A4-3 and A4-4 before test. Figures 101 and 102 show A4-3 and A4-4 after test. No cracks are apparent in either piece.

Figure 103 shows C4-1 prior to test. Figure 104 shows the full face post test appearance, and Figure 105 is a three quarter view. Since this was an unusual orientation of fiber in which the yarns are not biased, the relatively good performance of this specimen is of interest.

11

Figure 106 shows the appearance of A4-2B, a carbon polyimide (Skybond 700) composite after test. This was a low density composite, and it performed poorly.

Figure 107 shows A3-4, a silica polyimide (addition type) prior to test. Figures 108 and 109 show the ablated specimen.

Figures 110 and 111 show specimen A2-2, silica phenolic, after ablation. Contrasted with A3-4, the appearance of the two materials is similar. Figure 112 shows the ablated surface of specimen C4-2, displaying erosion to the quartz portion of the bicomponent tape.

Figures 113, 114 and 115 show the ablated surface of specimen C1-6. This concept utilizes a radiation barrier in the low density component.

Concept C1-8 is shown in Figures 116, 117, 118 and 119. DCM-1 (a silicone elastomer) is shown in Figure 120, unablated. The cross section (Figure 121) shows the clear demarcation between virgin material and char.

Figures 122 through 126 show specimens C5-1 and C5-2, utilizing low density insulative components. Specimen R2-9 is shown in Figures 127 and 128; this was a retest of a standard material. Figures 129 and 130 show specimen C1-7. Two quartz/Gemon composites are shown in Figures 131 through 136. In spite of the presence of small cracks, the materials performed as well as silica phenolic.

A modified silicone is shown in Figures 137 through 142. The full length run on GEM-1 showed that this elastomer performed poorly when compared to DCM-1.

C4-1A is shown in Figures 143 and 144. A filament wound concept is shown in Figures 145 and 146.

Dual Channel Test

The dual channel test which examine the relative performance of ATJ graphite and tape wrapped carbon phenolic, was conducted in a structure fabricated from ATJ graphite. (Fig. 8) Fitted to the standard arc hardware, the graphite structure consists of three components. The first is a graphite transition nozzle. The flow directed through the nozzle enters a circular section and exits through a rectangular section measuring 1.0" x 0.5". The channel proper, formed between the remaining two graphite plates accepts the flow at this point and is tapered to an exit measuring 1.0" x 0.35". The later dimensions constitute the throat at which the flow attains mach one. Evaluated at the measured enthalpy and the pressure within the channel, calculations place the flow velocity at several thousand feet per second. The present test was unique, in that both faces of the channel incorporated instrumented specimens. For this reason evaluation of heat transfer and channel pressure were based upon current, voltage and plenum pressure records compared with accumulated data obtained during previous channel flow tests. The enthalpy was obtained directly from the heat balance data acquired during the test. The results are summarized in Table III.

12

The data generated by the thermocouple instrumentation is shown in Figures 147, 148, and 149. The latter figure gives indication of the cooling profile of the carbon phenolic in which three thermocouples survived. All thermocouples failed on the ATJ graphite. Even without quantitative evaluation, it is readily evident that thermal conductivity in the carbon phenolic is much less than in the ATJ graphite.

Following test, both specimens were sectioned longitudinally and measured. Although the ablated face of the ATJ graphite appears relatively uniform to visual inspection, the profile plotted to an expanded scale (Figure 150) exhibits more irregularity.

The section of the carbon phenolic exhibits fissures as did the ATJ. However, these appear to extend only to the depths to which degradation has progressed. It is quite evident, as has been described previously[2] ("Ablation Test of a Modified Four Harness Interlock Fabric in the Hyperthermal Arc", J. Metzger, TDM 8151-020, 11/21/69), that removal or softening of the resin results in a relaxation of the fibers compressed during fabrication. When raised to their relaxed position, the resin depleted fibers effectively obscure the true recession. A heat of ablation model based on specimen recession can report highly optimistic values. The basic profile of the specimen is recorded in Figure 151.

Figure 152 is a photograph showing the ATJ and carbon phenolic specimens prior to test. Figures 153 and 154 show the two specimens in the mounts, after test. Figures 155 and 156 are sectional views of the ablated specimens. The presence of cracks in both specimens after test should be noted.

Since it was obvious that the fiber structure had expanded, the problem existed of estimating the true recession which had been realized. To make such an estimate, the positions of the thermocouple holes were measured, based on the photographed scale. These were compared to the thermocouple depths originally measured when the specimen was instrumented. It was found that the disparity in measurements increased as the holes approached the ablated surface (Figure 157). The values were referenced to the original hole measurements and the growth factor, extrapolated to 0.452 (the original surface) suggested net expansion of 38 mils above the original surface In actuality, the ablated surface above the uppermost thermocouple was profiled at 0.458", or six mils more than the original face, from which actual recession is deduced to be 33 mils. A measurement of the distance from the thermocouple hole to the ablated face on the photograph yields 0.14/2.08 - 0.067". Since the original depth was 0.100", this also indicates a recession of 33 mils. The recession values tabulated and plotted were obtained by difference from the unablated edges of the specimen after test. Since these were restrained, their tendency to grow was less than the unrestrained center region. Nevertheless a maximum net growth of 28 mils was recorded.

Two additional dual channel tests were conducted. In this configuration, a pair of specimens was exposed simultaneously in the same test configuration. The configuration, a channel, was prepared to accept a test specimen in the two opposite walls.

13

Tests were at a heat transfer rate of approximately 1200 BTU/sec-ft^2 and an enthalpy estimated at 7000 BTU/lb and lasted fifteen seconds each.

One channel was fitted with two carbon/polyimide specimens of slightly different manufacture (A4-5 and A4-7). Performances were not dramatically different, although the specimen of more recent manufacture (A4-7) appeared to show a greater tendency to increase dimensionally. The tendency to increase dimensionally has been noted on tape wrapped carbon phenolic materials numerous times. At present it is not known what factors contribute to the growth patterns. The second dual channel tends to further accentuate the phenomenon and arouses speculation on possible factors exerting influence up on it.

The second dual channel had installed in it a silica phenolic (A3-8) opposite a carbon polyimide (A4-6). In the course of the test, the silica phenolic was deeply (and uniformly) eroded. Even lateral undercutting of the specimen was noted. The carbon composite was unique. It gave evidence of tremendous dimensional increase. Following test, even with ablative erosion, the centerline region was elevated about 1/8" above its original location. The growth observed was the largest noted to date. Since rapid ablation of the silica polyimide created an abnormally large flow cross section, speculation centers on the possibility that local changes in test conditions might have contributed to the dimensional increase. The basic test data reveal that the gross environmental conditions (mass flow, power, pressure) were quite comparable on each of the two tests. Since a similar specimen was exposed in the other channel test and showed a lesser material expansion, it appears most probable that locally variable conditions led to the observed differences in performance.

The silica polyimide suffered ablative recession of about 200 mils. Since the test was 15 seconds in duration, about 13 mils per second were removed, except at the aft end. At the aft end ablation completely penetrated the specimen. This is the result of the development of a forward facing step at the specimen-holder interface. A vortex or similar disturbance at this region results in enhanced heat transfer rates and correspondingly increased erosion. The effect is more pronounced when the step is large.

The dual channel specimens offered several unusual results. In run 22-71, specimens A4-5 and A4-7 were exposed. Subsurface temperature responses (Figures 158 and 159) and the ablation profiles of both specimens are presented (Figures 160 and 161).

The ablation performance of A4-7 is of interest. Although the recession was measured to be irregular, when taken over the measured ablated surface, a mean recession of

14

approximately 90 mils was observed. Examination of the depth of the thermocouple holes in this model, leads to the conclusion that the specimen suffered a dimensional expansion which tends to hide the actual recession value. The post test locations of the thermocouple holes are shown on the profile (Figure 161). An appreciable change in location is evident. The numerical values of dimensional changes were plotted against the original thermocouple depth and a nearly linear trend in the changes of the various holes can be observed (Figure 162). Projected to a zero depth, the curve suggests that the position of the original surface would have shifted higher by 100 mils, had there been no ablation.

Since a mean value of 90 mils of recession was noted, it can be estimated that net true ablation was 190 mils, which is quite high. Expansion of the fiber matrix was quite extensive. However, the behavior is consistent with materials property measurements. Under controlled heat loading tests, samples of carbon phenolic have exhibited a hysteresis-like phenomenon with respect to thermal expansion (Figure 163).

The second dual channel test incorporated specimens A3-8 and A4-6. Their subsurface responses are given in Figures 164 and 165. The silica phenolic specimen (A3-8) ablation profile is depicted in Figure 166. Note that the one thermocouple hole which remained indicated a very slight tendency of the material to retain an expanded dimension. The ablation was severe, having removed nearly three-quarters of the specimen thickness. The ablation resistant graphite downstream of the specimen was more ablation resistant and created a rear-facing step. Locally enhanced heat transfer resulted in increased ablation in the specimen and penetration at the aft end as shown by the profile.

The carbon polyimide specimen ablation profile is shown in Figure 167. Note the apparent increase in thickness, due to ply distortion. Photographs of the ablated specimens are shown in the next six figures. Figure 168 shows a top view of specimens A4-5 and A4-7 after test. Cross sections are shown in Figures 169 and 170. A4-6 and A3-8 are shown in Figures 171, 172, and 173.

15

MISCELLANEOUS TESTS

ELEMENTAL ANALYSES

Elemental analyses were performed on four samples for percent carbon, hydrogen, and nitrogen. The samples were designated R1-4, R2-4, R3-6 and A3-4, consisting of: Silica/Phenolic C-100-48/USP95 FM5020; Carbon/Phenolic CCA1-1641/USP95 FM5055A; Carbon/Phenolic Pluton B1/DP 251J MXC-31HP and Silica/Polyimide C100-48/GE Polyimide respectively. The structural layer consisted of 2024-T3 Aluminum.

The analyses were all performed on the Perkin Elmer model 240 Elemental Analyzer. Because of the high carbon content of the samples, the analyses were rather erratic until the allowed combustion time was increased from 2.25 to 5.25 minutes. At the lower combustion time the samples were not receiving enough of an oxygen supply for complete oxidation. The finalized results are presented in Table IV and are within an accuracy of $\pm$ 0.3 percent absolute.

FLEXURAL STRENGTH TESTS

Flexural strength determinations were made on standard materials, and on a carbon/polyimide composite. The data are presented in Table V. The polyimide specimen is in the same strength range as the phenolic specimen, in spite of its slightly lower density.

SURFACE TEMPERATURE ANOMALIES

A review of a number of test runs has emphasized an interesting characteristic of the high heat rate surface temperature response of the carbon phenolic specimens. In many of the profiles, the surface temperature data generated at the high heat transfer rate is characterized by a smooth rate of rise, initially nearly vertically but rapidly inclining toward a constant level. After a few seconds (approximately 10) there is generally an abrupt decline in the temperature. The data may indicate a fall of several hundred degrees within one or two seconds. This is followed by another rise in temperature similar to the first but extending over a longer interval. The pattern may or may not be repeated at various intervals thereafter, but the initial characteristic has been reproduced on a number of test runs. The surface temperature response is real and appears primarily as a response of carbon phenolic specimens. Therefore, it is appropriate to consider an interpretation of the cause. The extremely rapid imposition of the higher heat transfer closely approximates a step function. The sudden presence of the greater thermal flux will drive the immediate surface toward an equilibrium temperature which is higher. The driving rate can

be postulated to force the surface temperature much faster than heat may be conducted internally. However, conduction does persist and a portion of the resin content of the material is volatilized. The generated gases vent, resulting in a rapid cooling momentarily. The surface temperature tends to recover as resin seeking the surface must percolate from progressively greater subsurface depths. It is possible to attribute subsequent abrupt changes in surface temperature to the emission of volatiles from resin occlusions (perhaps locally) at various depths, which can increase the mass addition momentarily. The discussion is speculative, but the acquired evidence indicates that the response characteristic that it attempts to explain is real and reasonably reproducible.

ANALYTICAL MODELING

Analytical modeling of the various ablation processes (charring, subliming, melting, etc.) are all adapted to machine computation through the introduction of various simplifications. While the adaptations make the actual process more amenable to machine computational techniques, they none-the-less provide results which are reasonable representations of the actual physical responses of an ablator. Consider a charring ablator. It may be depicted as shown in Figure 174. The location of the initial face of the ablator is shown. At time zero, it is in equilibrium with the ambient environment. Convective and radiative heat transfer impose time dependent thermal flux upon the ablator surface. It will be assumed that the impressed environment is sufficient to result in ablation. The applied thermal flux elevates the temperature of the surface layer rapidly and conduction within the ablator results in a temperature rise profile which advances through the material as a function of time. When the temperature at a depth is sufficient, degradation of the plastic material will initiate. The complex organic molecules begin to decompose progressively, producing gaseous hydrocarbons and other vapors and leaving a porous char residue. In many charring ablators, the char is comprised of carbon. Other principal constituents usually present (H_2, O_2, N_2), enter the gaseous products. As gaseous products of degradation evolve, they produce increases in internal pressure, which is relieved as the full, more porous char is developed. The graduation of char density and decline of internal pressure approaching the ablating surface tend to direct the evolved gases to issue from the surface. If inert, these gases will help block incoming heat and help suppress transfer of heat toward the interior. If combustible, the evolved gases may actually contribute additional heat to the surface when combining with oxygen diffusing through the boundary layer. It is significant to note that some porous structures in an ablator may sustain pressures locally which are in the tens of atmospheres (Reference 3). Consequently, blowing of the generated gases into the boundary layer may be at appreciable velocities in some cases. With continued application of the source of heating, the plastic at the surface will be completely degraded. No additional gas will be generated in this region through the degradation process. The region involving such chemical changes will advance further within the material. If the external environment is sufficiently severe, the surface will be removed by structural failure, oxidation or even sublimation. Thus the surface recedes, following the totally charred region and the region of chemical reaction.

17

The process described and the analogues for other ablative processes have been described mathematically and modified for automated computation. The computational system developed is the REaction Kinetics Ablation Program (REKAP). In the case of a charring ablator, the REKAP considers the thermal balance of an infinitesimal element of the dynamic system, incorporating

1. Net heat conducted into the element

2. Heat stored in the solid

3. Heat absorbed in the chemical reaction

4. Heat stored in gas generated

5. Heat absorbed in cracking or recombination

6. Heat generated due to friction

In considering the contributions of the various factors involved in the ablation of a charring ablator, it was found that some factors contributed negligibly to the thermal balance. Consequently, these were eliminated, reducing the complexity of the defining equation. The defining equation, upon simplification, is given as

$$\nabla \cdot k \nabla T = \rho C_p \frac{\partial T}{\partial t} + H_{GF} \left[\rho - \rho_c \right] Ze^{-E/RT} - \left(C_p + \frac{\partial H_k}{\partial T} \right) \dot{m}_g \cdot \nabla T$$

Described in one-dimensional form, the expression has been generalized to accommodate greater latitude in variation of the char density.

$$\frac{\partial}{\partial x} \left[k \frac{\partial T}{\partial x} \right] = \rho C_p \frac{\partial T}{\partial t} + H_{GF} \dot{m}_g - \left(C_g + \frac{\partial H_k}{\partial T} \right) \frac{\partial T}{\partial x} \int_{x = X'}^{x = \text{backface}} \dot{m}_g \, dx$$

$$\dot{m}_g = \rho_v \left[\frac{\rho - \rho_c}{\rho_v} \right]^n \sum_{i=1}^{m} A_i e^{-\Delta E_i/RT}$$

Subject to the boundary conditions imposed, the equation describes events modeled to occur within the reaction zone, which, by definition, lies between the original surface and the backface. The boundary conditions relate the exchange of heat across the front surface to the internally distributed heat as described above and to the mass transfer due to issuance of evolved gases and the recession of the specimen surface. The machine computation considers mathematically the thermal equilibrium between the two active regions: the reaction zone and the surface.

18

As a boundary condition, the surface of the specimen is the source of the primary thermal energies. The thermal balance at the surface is represented by

$$\dot{q}_{net} = \dot{q}_c - \dot{q}_{RR} - \dot{q}_{Block} - \dot{q}_{vaporization}$$

where

$$\dot{q}_c = \text{hot wall convective heat flux} = H(h_r - h_w)$$

$$\dot{q}_{RR} = \text{re-radiated heat flux} = \sigma F_e F_a T_w^4$$

$$\dot{q}_{block} = \text{transpiration cooling due to injected gases}$$

For laminar flow

$$\dot{q}_{block} = \dot{q}_c \left[\left(\frac{\overline{M}_{BL}}{M_{gas}} \right)^{1/3} (0.69) \frac{\Phi_o}{Pr^{1/3}} \right]$$

For turbulent flow

$$\dot{q}_{block} = \dot{q}_c \left[1 - e^{-0.38 \left(\frac{C_{p_{gas}}}{C_{p_{BL}}} \right) \Phi_o} \right]$$

$$\Phi_o = \int_{frontface}^{Backface} \dot{m}_g \, dx \left[\frac{h_r - h_w}{\dot{q}_c} \right]$$

$$\dot{q}_{vap} = \text{phase change energy associated with surface}$$

Surface recession rate is assumed to be a reaction rate controlled process that can be best described by an expression of the form suggested by Munson and Spindler, (Ref. 2)

$$\dot{S} = \beta_1 T_w^{\beta_2} e^{-\beta_3 / T_w}$$

At the backface of the virgin plastic or supporting substructure, the second boundary condition on the equation is

$$k \left(\frac{\partial T}{\partial x} \right)_{BF} = 0$$

19

Mechanical computation solves the foregoing equations simultaneous and continuously through the heating period. Input environmental parameters are distributed in accord with the mathematics among effects which include thermal conduction, heat storage, material degradation, gas formation and emission, and surface recession. The functional REKAP incorporates a group of mathematical tolerance standards with which the computations are constantly compared in order that the continual summation process has a realizable terminal result.

The model described was that employed to model a material of specific characteristics. However, as presently written, the REKAP has been programmed in a generalized form. There exist at least six options which can be applied to the generalized program in order to accommodate different material characteristics. These include the charring ablators, the sublimers, materials which develop a liquid layer as well as several specific special cases.

The REKAP uses the basic measured properties of a material. These normally include experimental recession performance, thermal conductivity, emissivity and perhaps others. It has been found that the complex organic materials employed in ablative materials undergo complicated, difficult-to-measure thermochemical processes such as chemical cracking. These processes may be either endothermic or exothermic and will modify the controlling parameters. Lacking appropriate experimental data, the analytical model is adjusted to provide a properly calibrated response accounting for these processes. The model is modified to respond in a manner consistent with experimental behavior which is measured, using relevant parameters to coordinate the results. The calibrated model can then be employed to determine material performance during re-entry along a specific trajectory.

In developing an adequate model for the composite consisting of carbon phenolic overlaid on a highly insulative substructure of open weave quartz yarns, very satisfactory progress has been made. The development was an extension of the model of carbon phenolic previously described. The system required a two layer model. Therefore, in addition to the thermal properties of the carbon phenolic, suitable values for the appropriate properties of low density quartz were required. An appropriate system for estimating the specific heat of the material assumed the sum of the products of specific heat and density of the principal constituents divided by the sum of the densities will yield a weighted mean value of the specific heat. Since the ρ_{c_p} product for air is relatively small, the weighted value for the LDQ is

similar to that of the silica fibers in the structure. Fortunately the values of the principal components are not greatly disparate. In the case of the thermal conductivity, values approaching those of air were employed. Although the fibers are more conductive they occupy a very small portion of the low density quartz volume, and only about one third can be considered as conductive paths which will admit heat to the rear of a specimen.

The results obtained with the model indicate that little further profitable revision may be made to improve the model evolved on the basis of tests in the channel. For the computations utilizing the properties, a model was assumed which incorporated a 3/8" thick heat shield atop a 1/4 in. layer of LDQ. The results are given in the accompanying series of graphs generated from the computed results. Char developed to a depth of more than three tenths of an inch (Figure 175). The model indicates that about half of the char developed during the low thermal flux application and half during the high. It is of incidental importance to note that previous tests of heat shield materials of less than three tenths of an inch in thickness actually were charred completely through.

Ablative recession (Figure 176) was predicted to be a little over 125 mils. The value is very similar to that predicted for the carbon phenolic alone. The result suggests that the insulative layer does little to modify the response of the heat shield exposed on the environment. Also submitted are surface temperature profiles (Figure 177) and subsurface response curves (Figures 178 and 179) both as a function of time and of depth. The latter plot indicates the markedly different rate of conduction in the insulative layer.

One possible region in which the insulative layer may be further refined is relative to its thermal conductivity. It may be recognized that as temperatures at the interface between the shield and the LDQ exceed 500 to 600°F, the resins which are subject to degradation may begin to generate some gases or vapors of high molecular weight. These gases can find their way into the interstices in the LDQ. As a result, the thermal conductivity of the insulator as a whole may be subject to transient variations. Higher temperatures may further modify this property by cracking or further degradation of the gas or vapors of high molecular weight. Presently, it appears that such transient changes do little to affect the net conductive response of the material, but their possible effects are recognized. Figures 180 and 181 show the thermal histories used in the analyses. These are computer inputs.

The initial problem to be resolved in applying the REKAP computer program to the High Integrated Heat Load investigation was that of providing a data input compatible with the limitations of the basic computer program. The REKAP is comprised of various equations designed to describe mathematically the interrelations among physical phenomena which contribute to the thermochemical removal of material from an ablator. For a material exposed to a severe thermal environment, it attempts to establish a balance among the energy exchanged at the surface, the mass

21

removed from the surface and the thermal energy conducted internally from the surface. The numerical solution of the equations is a process which operates consecutively and repetitively on discrete numerical elements. The accuracy with which various numerical operations are performed constitutes an inherent part of the program and represents a source of operational problems; the inability to compute a solution within the specified accuracy limits will result in cessation of the computational sequence. Effecting the necessary calculations within the accuracy limits programmed is achieved by selection of suitable magnitudes in both the time and the dimensional computation intervals. The heat transfer applied in the Integrated Heating program is characterized by an abrupt twenty-fold increase. In order for the computer to handle the abrupt change in heating without failure, the computational time intervals were greatly decreased in the temporal vicinity of the change.

In preparing the inputs, the nominal conditions specified for the ablation test program were entered. The program was applied to twenty degree tape wrapped carbon phenolic, using the existing model of this material as it has been calibrated for flight applications. Since calibration of the 20° TWCP for flight includes response to conditions in excess of those achievable in the test facility and provides compensation for the more significant shear and pressures encountered in flight, it was anticipated that the ablation obtained by using this model would exceed that experienced in the test facility. Indeed, since the model for flight has been thoroughly proven, the relative difference in the performance of test specimens compared to the computer predictions constitute a method of extrapolating for flight prediction any new material modeled on the basis of the facility tests.

A successful computer run was obtained. The program provides a continuous account of the accuracy of the results obtained by piece-wise summation, and the data indicated that the thermal input model provided a good approximation of the continuous equation. As might be expected the largest local excursion of the accuracy figures was at the change in heat transfer. Nevertheless the net heat balance was quite good. The surface temperature profile, the recession behavior and the subsurface thermal responses at various depths are depicted in Figures 182, 183, and 184 respectively.

In general, the predicted results are consistent with expectations. The magnitude of surface temperature at the low rate of heat transfer is in good agreement with those obtained experimentally. While somewhat higher than surface temperatures reported for the experiments, the computer prediction for the high rate of heat transfer is consistent with these data.

Since the cold wall heat transfer rates obtained in the experiments have been generally below the anticipated nominal values, the observed difference in surface temperature is plausible. Ablation was predicted to be larger than has been attained in the facility test, as had been expected. However, the problem is not solely due to the calibration of the model for flight; evidence has accumulated that under some heat load conditions the fabric in the 20° TWCP tends to expand and take a permanent set, which tends to render the net recession as unduly small. The net dimensional change on both Run 51-70 and Run 62-70 was apparently affected by such growth.

It is interesting to examine some specimen surface temperature data superimposed on the computer prediction. The selection of runs was arbitrary. Reference specimen R2-4 was selected as representative of data acquired early in the program. It consisted of the basic carbon (CCA1-1641) and phenolic (USP95) systems constructed directly adjacent to the aluminum backing plate in a manner analogous to tape wrapped carbon phenolic. In contrast, specimen C1-8 was among those recently tested. Although the shield portion was fabricated from the same materials as the reference specimen and in the same manner, it was separate from the aluminum backing plate by an insulative layer. Both specimens produced nearly identical response curves. The data tend to reconfirm the generally good reproducibility obtainable in the test facility. Reviewing the facility data it may be observed that the energies delivered to the arc heater during these runs differed by less than 4-1/2% of their nominal value. The relative change in magnitude of current and voltage between the two runs and the corresponding pressure differences result in different enthalpies. It is inferred that the decline in experimental surface temperature is a consequence of the erosion of the specimen ablative erosion produces an increase in flow area and an attendent increase in the expansion of the flow gas.

Comparisons of actual and predicted values of surface temperature are shown in Figures 182; other computed results are shown in Figures 183, and 184.

After having developed the basic computer model designed to accept the abrupt rise in thermal input, the program was applied in two consecutive steps. The first generated predictions for conditions representing idealizations of the actual test environment and the second examined predictions for a closer approximation of typical test environments. The input models are shown in Figure 185. Note that the second model considers variable pressure and the correspondingly modified heat transfer. A notable difference in the net recession was achieved (Figures 186 and 187). Although the effect of the changes introduced into the second model are negligible at low heat input, a significant decrease in the net recession is produced. The predicted recession appears to agree favorably with results obtained experimentally. Specimen R2-9, for example, experienced an average recession of 135 mils, which exceeds the value predicted by the more accurate model by only 6%.

If one considers the char layer predicted, both models predict thicknesses in excess of three hundred mils (Figures 188 and 189). Again, considering the results obtained on R2-9, it was reported that the char had penetrated the entire thickness of the shield. Since the original thickness was 420 mils, ablation, on the average has reduced the thickness to 285 mils. This is significantly less than the predicted chars. Hence the experiments are consistent with the predictions. Until actual composite predictions are generated, it will be difficult to assess the net effects produced on the thermal balance of the shield material.

23

Surface temperatures were little affected by the differences in the two models (Figures 190 and 191). Low heat transfer inputs resulted in a maximum surface temperature of 2200°R while peak heating during the application of high heat transfer rates was approximately 4600°R. It is of interest to note (Figure 192) that the change in pressure with attendant heat transfer rate changes produces a "saddle" in the high temperature plateau.

It is of interest to compare the conventional analytic ablation model with that developed in evaluating data in this program. For this purpose, a high integrated heating trajectory was employed, with a heat transfer profile representative of a region on the frustum. (Figure 193). The most unusual result deriving from the comparison of the two is the difference in recession behavior. The difference is shown in Figure 194. When the incident heat transfer is very low, the two models show no difference. However, when the heat transfer rate is increased, after about 70 seconds into re-entry, the standard model first trails the one developed in this program, then accelerates until it yields a net recession two mils in excess of it. The difference amounts to less than 1% of the total recession predicted. Also, there are but slight differences in the chars predicted. Both the recession profiles and the char densities are presented for both models in Figures 195, 196, 197 and 198 respectively.

REFERENCES

1. Juneau, P.W. (Jr.), Carbon and Silica Fiber Reinforced Polyimide Resin Composites. Proceedings: 22nd Annual Technical Conference, Society of Plastics Engineers, March 7-11, 1966, Montreal, Canada.

2. Munson, T., and Spindler, R., "Transient Thermal Behavior of Decomposing Materials, Part I; General Theory and Application to Convective Heating," paper presented at IAS 30th Annual Meeting, N.Y., N.Y., January 1962.

3. "The Ablative Degradation Chemistry of A Low Density Elastomeric Silicone Formulation", T.F. McKeon, Jr., General Electric TIS-67SD274, August 15, 1967.

III. SUMMARY AND CONCLUSIONS

The principal objective of the program was to seek new material concepts capable of sustaining a high integrated heat load. The developmental materials were designed to provide lighter weight and more efficient thermal protection than conventional tape wrapped constructions. The program initially examined the thermal response of three reference materials and six developmental materials. Twenty-six additional concepts have been tested. Most of the test specimens were exposed to a long time two step heat flux environment in the five megawatt air arc heater. Six were exposed to a dual channel test. Despite some rather wide variations in the response of the materials, it was possible to make comparative evaluations of the groups of specimens. The following summary outline highlights the details of program.

a. It was the objective of the program to evaluate the ablation performance and insulative properties of a group of composite candidate materials subjected to a high integrated heat load. To this end, performance goals consisted of high resistance to thermomechanical surface erosion, good insulative characteristics for structural thermal protection and low total weight per unit area. Detailed study was planned for asymmetrical ablation char instability, and dimensional changes resulting from pyrolysis, in-depth heating, lack of physical integrity, spallation or other thermomechanically induced deleterious phenomena.

b. An investigation was made of the adequacy, limitations, and materials problems associated with the use of conventional tape wrapped carbon and silica reinforced phenolic resin materials. Consideration was given the specific components, fiber sizes, weave patterns and resin systems as well as the geometrical orientation of the cloth fibers in the conventional materials. Three were selected as reference materials. These were a silica cloth/phenolic resin (C-100-48/USP95, Code R1) and two different carbon cloth/phenolic resin systems: 1) CCA1-1641/USP95, Code R2 and, 2) Pluton B1/DP-2510, Code R3.

c. To compare with these reference heatshield materials, four developmental heatshield combinations were considered. Different carbon cloths and silica cloth were combined with phenolic resins and polyimide resin. The combinations consisted of VCX/DP2510 (Code A1), C-100-48/DP-2510 (Code A2), C-100-48/Skybond 700 (Code A3) and CCA1-1641/Skybond 700 (Code A4).

d. In order to effect a structure of lower weight per unit area, the heatshield materials were incorporated into two layer composites. The subsurface layer was designed to be highly insulative and of a low density. It consisted

25

of a loom woven low density quartz (LDQ), which was bonded to each of the shield materials. The LDQ was made with silica phenolic strands alternating at right angles to give a square wall pattern simulating a filament wound structure. The composites were described as R2/LDQ (Code C1). R3/LDQ (Code C2) and R1/LDQ (Code C3).

e. Additional development specimens were fabricated and tested in the second half of the program, and are reported herein. They included: polyimide resin reinforced with carbon cloth (composite Code A4), quartz cloth (Code A7), and silica cloth (Code A3); two composites using LDQ-polyimide resin insulative layers, R2/LDQ-polyimide (Code C1) and A3/LDQ-polyimide (Code C5); carbon-quartz bifilament tape reinforced phenolic resin (Code C4); filled silicone elastomers (Codes DCM and GEM); simulated multiple, interlock, filament wound carbon filament reinforced phenolic resin (Code FW).

f. Specimens for ablation test were obtained from larger fabricated plates of the various materials. The finished specimens measured 5.0 x 1.75 inches. Thicknesses were appropriate to the materials and material combinations. All specimens were processed to simulate a tape wrapped heatshield element. An aluminum plate was bonded to the shield or the LDQ insulative layer. Each specimen was equipped with five thermocouples. They were installed in isothermal planes at progressively increasing depths. For dual channel testing, an aluminum backup plate was not used.

g. The specimens were tested in a facility powered by a five megawatt arc. The equipment was arranged to provide an integrated heat transfer of $36,550$ BTU/ft^2 in two discrete heating pulses during a 300 second interval. The nominal conditions achieved during the 230 and 70 second heating intervals were 5,000 and 5,000 BTU/lb enthalpy; 25 and 440 BTU/sec-ft^2, heat transfer and 0.4 and 2.5 lb/ft^2 shear stress. The stepwise change in heat transfer was obtained by redirection of portions of a constant net mass flow of air. Dual channel testing was done in a modified holder in the arc.

h. The test facility equipment was constructed around a rectangular two dimensional flow nozzle. The nozzle was designed to provide an expansion ratio of four from a plenum pressure of 60 psia at an enthalpy of 5,000 BTU/lb. The corresponding Mach Number was approximately 1.5. Calculations were based on an assumed frozen flow. The specimens were mounted to form one wall of the rectangular nozzle during test.

i. After test, recession profiles and char depths were determined from the longitudinally sectioned specimen. The material performance was determined as a function of distance along each specimen. The most representative, average values were those obtained near the middle of the specimen. In each case, a time resolved history of surface temperature, subsurface temperatures and local pressures was also obtained.

26

j. The specimens tested in the arc channel configuration using a two stage heating set-up can be separated by reinforcement and resin type into carbon, silica, quartz, and silicone composites. Of the carbon composites, the CCA-1 based material (R2-9) exhibited the lowest recession rate and the most stable char layer. The insulative composites (C1-5, C1-6, C1-7, C1-8, C5-1, C5-2) showed the improved back face response due to a low density insulation layer.

k. The silica and quartz Materials (A2-2, A7-1, A7-3) were fairly close in response to the arc environment, but the polyimide quartz specimens (A7-1, A7-3) were hampered by the presence of cracks.

l. The combination tape specimens (C4-1, C4-2, C4-1A) behaved very erratically. Two of the three specimens were consistent in response, and demonstrated the effects of a non-biased fiber orientation. The fibers were oriented normal to the heated air, and the composite was therefore more conductive than a bias tape specimen.

m. The silicone elastomer specimens ablated rapidly. Of the three specimens tested, only DCM-1 survived the full test environment--the GEM materials ablated through before completion of the high heat portion of the run.

n. Of the dual channel experiments the carbon composites survived very well, displaying some cracks after test. Comparing the phenolic and polyimide resin materials, the two appear to be equal in ablation properties.

o. The filament wound material ablated rapidly and showed an extremely uneven char layer.

p. Irregular erosion was found at the specimen-nozzle edge. This was possibly due to a combination of irregular flow and thermochemical erosion. It may be noted that the disturbed region is less pronounced in the more ablation resistant materials.

q. A second disturbed region frequently occurs at the nozzle exit. This region is dependent on the pressure gradient within the nozzle. If the pressure within the nozzle departs greatly from one atmosphere, a shock will be created at the exit. Enhanced local heat transfer will result. The ability of the system to maintain approximately one atmosphere is strongly influenced by the amount of specimen erosion which occurs. Obviously the ablation changes the area of the nozzle exit, the effective area ratio, and the characteristics of local conditions furnished by the heated gas.

r. The design of the two-step heating nozzle has been improved. An optimization of the design has been achieved by incorporating elements tending to reduce the surface area through which heat is transferred to the cooling water. This lowered the requirements of arc heat operation and provided longer operating life for the arc heater components.

27

s. An improved high heat flux facility has been developed in the dual channel test set-up.

t. The analytical study demonstrated the development of a computer code that was able to predict actual test performances in a consistent and accurate manner.

28

IV. RECOMMENDATIONS

Based on the results obtained thus far in the program, the following recommendations are made:

a. Develop higher temperature insulative components based on carbon microspheres, reflective radiation barriers, and ceramized plastics. Based on the information obtained in LDQ, these material approaches seem promising.

b. Utilize newly developed open-weave, low thermal conductivity carbon fibers as both ablative and insulative components.

c. Continue to investigate new, high char yield heterocyclic resins.

d. Further refine the performance of the arc facility in both the arc tunnel and dual channel modes.

e. Several tests have demonstrated dramatically the thermally induced enlargement of carbon fiber composites. It is recommended that, in the interest of more precise design, an investigation be made of the enlargement phenomenon, as related to incident heat flux and duration of application. In developing optimized shield design, it is believed that the detailed behavior of carbon phenolic must be understood.

TABLE I. TBS-542 EXPERIMENTAL PRODUCT DATA

Material: TBS-542

Curing Agents: Dibutyl tin dilaurate (0.1 to 0.5 wt. %)
RTV-9708 (0.75 to 1.5 wt. %)
060-127-823 (0.1 to 0.5 wt. %)

I. Physical Properties (Typical)

A. Uncured Compound

- Appearance: white paste, non-Newtonian flow characteristics
- Viscosity: Brookfield RVF cps 80,000 No. 6 spindle at 10 rpm

B. Catalyzed Compound – compound catalyzed with 0.5 wt. % dibutyl tin dilaurate $77 \pm 2°F/50\%$ R.H.

Application Rate, gm/min at 1 hour: 20
Tack Free Time: 4 hrs.
Hardness, Shore A:
  24 hours: 45
  72 hours: 65

C. Cured Compound – Compound cured 24 hours in 5 x 6 x 0.080 in. ASTM mold followed by 144 hours/ $77 \pm 2°F/50\%$ R.H. Compound catalyzed with 0.25 wt. % dibutyl tin dilaurate.

Specific Gravity: 1.34
Hardness, Shore A: 60 to 70
Tensile, Strength, psi: 300 to 450
Elongation, %: 20 to 50

II. Thermal Properties

A. General

- Thermal Coefficient of Expansion: (in./in./°F) 26×10^{-5} Range: (100 to 450°F)
- Thermal Conductivity: (Btu/ft/hr/ft^2/°F): 0.163 at 108°F
  0.14 at 478°F
- Specific Heat: (Cal/gm/°C)

Temperature°C	Value

● Specific Heat: (Cal/gm/°C)

Temperature°C	Value
60	0.318
100	0.329
125	0.342
150	0.348
175	0.353
210	0.360
240	0.372

B. Ablative Properties

Test Conditions:

Type: Oxy-kerosene Torch
Torch: Linde FSJ-3 Blowpipe
Sample Size: Cylinder, 0.50" dia., flatface
Sample to Flame Tip Distance (Initial): 1.5 inches
Flame Temperature: 3700°F
Gas Velocity: Mach 2
O_2 Flow Rate: 1.25 lb/min
Kerosene Flow Rate: 0.513 lb/min
Mass Flow: 0.0294 lb/sec
Stagnation Pressure: 50 psia
Gas Enthalpy: 180 Btu/lb
Cold Wall Heating Rate: 800 Btu/ft^2 sec

Test Data

Sample	Exposure (sec) Time	Mass (gm/sec)	Loss Rate (lb/ft^2/sec)
1	4	0.147	0.23
2	6	0.134	0.22
3	8	0.129	0.21
4	10	0.133	0.21

*The properties shown in this table have been determined from laboratory tests and are typical of the product. However, a reasonable degree of variation will occur in commercially produced material. The typical values shown here should not be used as a basis for specifications.

TABLE II. CONCEPTS FOR TEST

Specimen	Run	Heat Shield	Insulator	Structure
C1-5	15	CCA1-Carbon Phenolic	LDQP	Aluminum
A4-3	16	CCA1-Carbon-Polyimide (Addition Type)	None	Aluminum
A4-4	17	CCA1-Carbon-Polyimide (Addition Type)	None	Aluminum
C4-1	19	Combination Tape	Carbon-Quartz Phenolic	Aluminum
A4-2B	20	CCA1-Carbon Polyimide (Low density)	None	Aluminum
A3-4	22	Silica Polyimide (Addition Type)	None	Aluminum
A2-2	23	Silica Phenolic	None	Aluminum
C4-2	25	Combination Tape	Carbon-Quartz Phenolic	Aluminum
C1-6	49	CCA1-Carbon Phenolic	Gemon/Quartz Low Density Layer	Aluminum
ATJ/CP	51	DUAL CHANNEL TEST		
C1-8	60	CCA1-Carbon Phenolic	Gemon/Quartz Low Density Layer	Aluminum
DCM1	61	DC 93-104 Silicone Elastomer	None	None
C5-1	62	Gemon/CCA1 Heat Shield	Gemon/Quartz Low Density Layer	Aluminum
C5-2	63			
R2-9	64	CCA1-Carbon Phenolic	------------	Aluminum
C1-7	65	Similar to C1-8		
A7-1	4(71)	Quartz/Gemon PI	------------	Aluminum
A7-3	6(71)	Quartz/Gemon (900°F Post Cure)	------------	Aluminum
GEM-2	7(71)	TBS 452 (unmodified)	------------	Aluminum
GEM-1	8(71)	TBS 452 (modified)	------------	Aluminum
C4-1A	9(71)	Combination Tape Composite	------------	Aluminum
A4-7	22	CCA1/Gemon Polyimide Dual Channel Run	------------	Aluminum
A4-5	22			
A4-6	23	CCA1/Gemon Polyimide	------------	Aluminum
A3-8	23	Silica/Gemon Polyimide	------------	Aluminum
FW-1		Filament Wound PX505/510 Phenolic	ESM	Aluminum

33

TABLE III. ABLATION TEST RESULTS

MATERIAL

SAMPLE NO.	C1-5	A4-3	A4-4	C4-1	A4-2B	A3-4	A2-2	C4-2
RUN NO.	15	16	17	19	20	22	23	25
RUN TIME (Low $\dot{q}$/High $\dot{q}$), sec.	238/51	238/50	238/51	238/50	239/51	239/50	238/50	231/52
CURRENT, Amp	1900	1840	1780	1980	1980	2020	1920	1820
VOLTAGE, volt	933	939	981	900	900	870	906	963
POWER, kw	1735	1735	1754	1781	1782	1757	1740	1753
AIR FLOW - in, lb/sec	0.0650	0.0650	0.0650	0.0650	0.0650	0.0650	0.0650	0.0650
AIR FLOW - exh, lb/sec	0.0139	0.0126	0.0128	0.0135	0.0136	0.0144	0.0138	0.0139
AIR FLOW - nozz., lb/sec	0.0511	0.0524	0.0522	0.0515	0.0514	0.0506	0.0512	0.0511
COOLING WATER, gal/min FLOW, lb/sec	447 / 62.0	444 / 61.6	445 / 61.8	444 / 61.6	442 / 61.4	445 / 61.8	443 / 61.5	445 / 61.8
COOLING WATER ΔT, °F	22.75	22.33	23.2	23.08	23.8	22.95	21.9	21.55
ARC POWER, BTU/sec	1663	1645	1665	1687	1688	1663	1650	1663
ENERGY LOSS, BTU/sec	1410	1376	1434	1421	1460	1419	1330	1353
ENERGY TO AIR, BTU/sec	253	269	231	246	228	244	320	310
AIR ENTHALPY, BTU/lb	4950	5130	4430	4770	4450	4820	6250	6070
PLENUM PRESSURE, psia	93.0	95.8	97.5	94.7	95.0	91.8	94.7	102.0
PLENUM (2) PRESSURE, psia	61.4	61.5	65.3	60.8	60.4	65.8	62.6	63.1
WALL PRESSURE, St.1, psia	14.7/14.5	15.0/16.6	14.7/15.8	14.8/15.1	14.8/15.8	14.7/16.1	14.7/15.3	14.0/17.4
WALL PRESSURE, Sp.3, psia	14.7/10.5	15.0/13.8	14.7/12.2	14.7/12.0	14.8/12.8	14.5/14.5	14.5/13.5	14.7/13.7
WALL PRESSURE, Sp.4, psia	14.7/9.7	14.7/10.4	14.8/13.5	14.8/12.5	15.2/13.5	14.8/13.1	14.7/13.8	14.7/16.3
HEAT FLUX (calc'd), BTU/ft² sec	23.8/332	24.7/321	21.3/288	23.0/30.2	21.4/302	23.1/323	29.9/402	29.2/395
INTEGRATED HEAT TRFR (BTU/ft²) LOW HEAT INPUT	5660	5880	5070	5470	5120	5520	7110	6750
HIGH HEAT INPUT	16920	16050	14690	15100	15400	16140	20130	20530
TOTAL HEAT INPUT	22580	21930	19760	20570	20520	21660	27240	27280

34

TABLE III. ABLATION TEST RESULTS (Cont.)

MATERIAL	C1-6	ATJ/20 TWCP	Silicone Elastomer					
SAMPLE NO.	C1-6	-	C1-8	DCM-1	C5-1	C5-2	R2-9	C1-7
RUN NO.	49	51	60	61	62	63	64	65
RUN TIME (low $\dot{q}$/High $\dot{q}$), sec.	236/67	15.6	236/69	234/69	144	236/67	234/68	234/67
CURRENT, amp	1840	1860	1920	1826	1920	1720	1727	1880
VOLTAGE, volt	981	1033	939	960	954	909	1002	954
POWER, kw	1805	2064	1808	1753	1832	1717	1730	1792
AIR FLOW-in, lb/sec.	0.0700	0.1200	0.0700	0.0700	0.0700	0.0700	0.0700	0.0700
AIR FLOW-exh, lb/sec.	0.0144	0.0187	0.0154	0.0154	0.0150	0.0150	0.0155	0.0131
AIR FLOW-nozz., lb/sec.	0.0556	0.1013	0.0546	0.0546	0.0550	0.0550	0.0545	0.0569
COOLING WATER, gal/min. FLOW, lb/sec.	447	426	447	446	446	446	444	445
	62.0	59.1	62.0	61.9	61.9	61.9	61.7	61.8
COOLING WATER ΔT, °F	23.00	21.76	22.82	22.93	23.20	20.78	22.28	22.90
ARC POWER, BTU/sec	1711	1952	1714	1662	1737	1626	1640	1699
ENERGY LOSS, BTU/sec	1425	1284	1412	1419	1437	1296	1385	1415
ENERGY TO AIR, BTU/sec	286	669	302	243	300	330	255	284
AIR ENTHALPY, BTU/lb	4740	6604	5520	4450	5450	5995	4940	5000
PLENUM PRESSURE, psia	101.95	72.5	102.5	105.0	98.5	103.2	102.3	105.0
PLEN'M (2) PRESSURE, psia	15.4/64.4	---	15.0/64.7	15.1/61.8	14.3	14.7/63.2	14.8/64.1	15.0/64.2
WALL PRESSURE, St.1, psia	14.3/18.6	56.0	14.6/17.5	15.0/16.2	14.9	14.6/13.0	14.7/15.2	14.8/15.2
WALL PRESSURE, St. 3, psia	14.7/10.8	56.0	14.9/10.8	14.9/13.0	14.3	14.5/7.4	15.7/10.3	14.9/8.8
WALL PRESSURE, St. 4, psia	14.5/10.0	56.0	15.2/10.3	15.2/13.6	14.6	14.7/9.9	14.8/13.9	14.8/9.7
HEAT FLUX BTU/sec-ft² (calc'd)	22.3/548	1200	27.0/535	21.9/292	25.9	28.7/318	23.8/331	23.9/294
INTEGRATED HEAT TRANSFER $\int \dot{q}_{low}$	5263	---	6372	5125	3730	6745	5509	5593
$\int \dot{q}_{hi}$	23316	---	23115	20148	---	21306	22508	19698
$\int \dot{q}_{tot}$	28579	18720	29487	25273	3730	28051	28077	25291

TABLE III. ABLATION TEST RESULTS (Cont.)

MATERIAL

	AT-1	AT-3	GEM 2	GEM 1	C4-1A	A4-7	A4-5	A4-6	A3-8
SAMPLE NO.	71-4	71-6	71-7	71-8	71-9	71-22	71-22	71-23	71-23
RUN NO.	231/67	232/76	203	232/47	234/63	15.5	15.5	15.3	15.3
RUN TIME (Low q/High q), sec.									
CURRENT, amp	1980	2020	2040	1940	1880	2080	2080	2080	2080
VOLTAGE, volt	927	909	909	921	945	1026	1026	1026	1026
POWER, kw	1835	1836	1854	1757	1777	2134	2134	2134	2134
AIR FLOW - in, lb/sec	0.0700	0.0700	0.0700	0.0700	0.0700	0.1100	0.1100	0.1100	0.1100
AIR FLOW - exh, lb/sec	0.0184	0.0188	0.0195	0.0134	0.0145	0.0232	0.0232	0.0463	0.0263
AIR FLOW - nozz., lb/sec	0.0516	0.0512	0.0505	0.0566	0.0565	0.0868	0.0868	0.0887	0.0637
COOLING WATER, gal/min.	447	447	447	447	451	419	419	420	420
FLOW, lb/sec	62.2	62.1	62.1	62.1	62.6	58.2	58.2	58.3	58.3
COOLING WATER ΔT, °F	23.75	23.9	24.40	22.5	22.65	23.55	23.55	24.0	24.0
ARC POWER, BTU/sec	1740	1741	1758	1666	1685	2023	2023	2023	2023
ENERGY LOSS, BTU/sec	1473	1484	1513	1397	1417	1371	1371	1399	1399
ENERGY TO AIR, BTU/sec	267	257	248	269	268	652	652	624	624
AIR ENTHALPY, BTU/lb	5180	5020	4850	4750	4840	7510	7510	7455	7455
PLENUM PRESSURE, psia	93.0	93.0	90.5	93.5	100.0	69.6	69.6	75.8	75.51
PLENUM (2) PRESSURE, psia	14.7/60.2	14.7/59.6	15.2	14.7/61.3	14.7/66.0	---	---	---	---
WALL PRESSURE, St.1, psia	14.3/6.0	15.7/26.0	15.0	14.3/25.7	14.7/27.2	58.5	58.5	59.2	59.2
WALL PRESSURE, St.3, psia	14.6/5.8	14.7/13.2	14.7	14.1/22.0	14.1/22.5	58.5	58.5	59.2	59.2
WALL PRESSURE, ST.4, psia	14.5/4.8	14.2/19.5	14.7	14.7/20.4	14.2/20.7	58.5	58.5	59.2	59.2
HEAT FLUX (calc'd), BTU/ft²-sec	24.9/260	24.2/252	23.8	22.8/515	23.9/538	1355	1355	1210	1340
INTEGRATED HEAT FLUX									
Low q Portion	5752	5614	4831	5290	5593	---	---	---	---
High q Portion	17420	19152	---	21205	33894	---	---	---	---
TOTAL HEAT, BTU/ft²	23172	24766	4831	29495	39487	21003	21003	20502	20502

TABLE IV. ELEMENTAL ANALYSES

Sample	% N	% C	% H
R1-4 No. 1	0.09	22.31	0.01
No. 2	0.13	20.23	0.18
No. 3	0.06	20.67	0.78
No. 4	0.08	23.12	1.40
R2-4 No. 1	0.13	98.49	0.22
No. 2	0.53	96.99	0.42
No. 3	0.52	93.50	1.44
No. 4	1.25	88.75	2.08
R3-6 No. 1	0.99	87.37	0.10
No. 2	1.37	86.93	0.67
No. 3	1.27	85.50	1.82
No. 4	1.81	78.14	2.84
A3-4 No. 1	0.60	13.93	0.11
	0.80	14.19	0.08
No. 2	0.56	15.14	0.05
	0.85	15.00	0.05
No. 3	2.72	18.32	1.23
	2.80	19.35	1.36
No. 4	3.00	22.69	1.61
	2.81	23.52	1.69

The designation of No. 1 through No. 4 indicate the area of the specimen
from which the sample was obtained: No. 1 is the charred surface;
No. 2 midway through the char layer; No. 3 is from the transition zone;
No. 4 is virgin material.

TABLE V. FLEXURAL STRENGTH OF COMPOSITES

Material	Sample Number	Flexural Modulus 10^6 psi	Ultimate Flexural Strength (psi)	S.G.
Refrasil Phenolic 20° Comp (R-1)	-1	1.45	13,748	1.68
	-2	1.44	13,863	
Carbon Phenolic 20° Comp (R-2)	-1	2.31	23,325	1.50
	-2	2.17	24,912	
Carbon Phenolic 20° Comp (Low Density—Comparison only)	-1	1.72	16,638	1.35
	-2	1.54	16,247	
Carbon Phenolic 20° Comp (R-2)	-1	1.89	22,631	1.48
	-2	2.20	23,490	
GE Polyimide 20° Comp A4-3	-1		18,926	1.43
	-2	1.68	27,417	
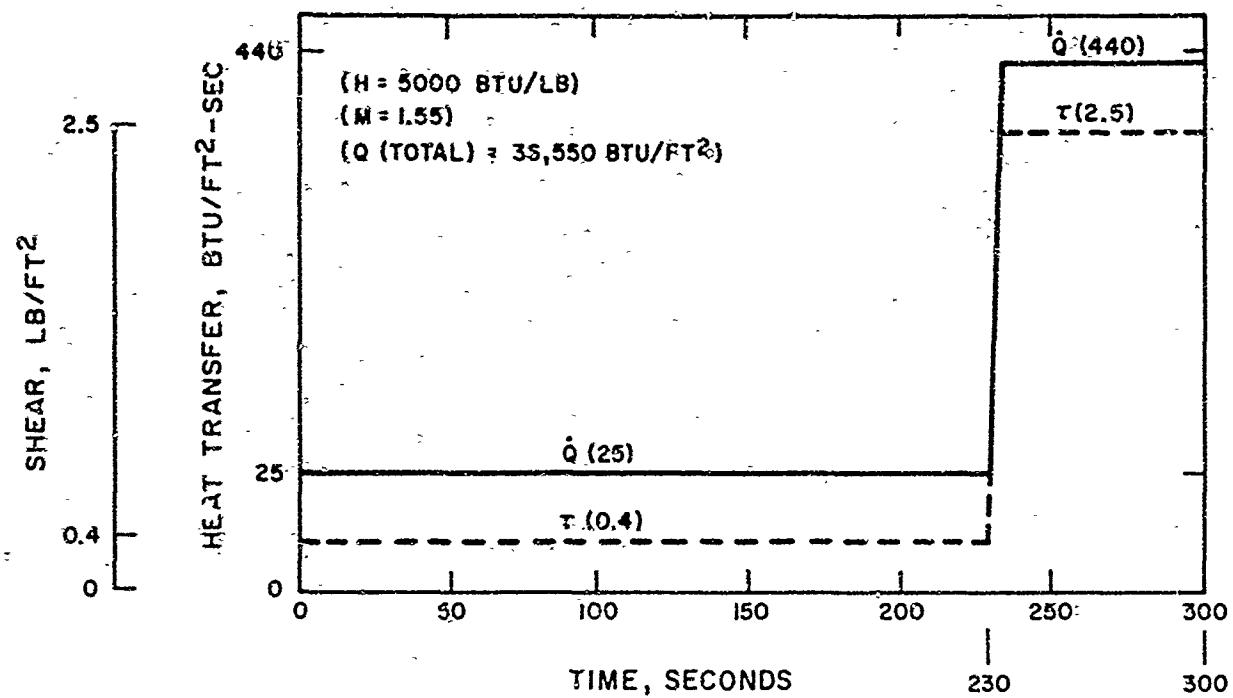
Figure 1. Nominal Shear and Heat Transfer Ablation Test Program
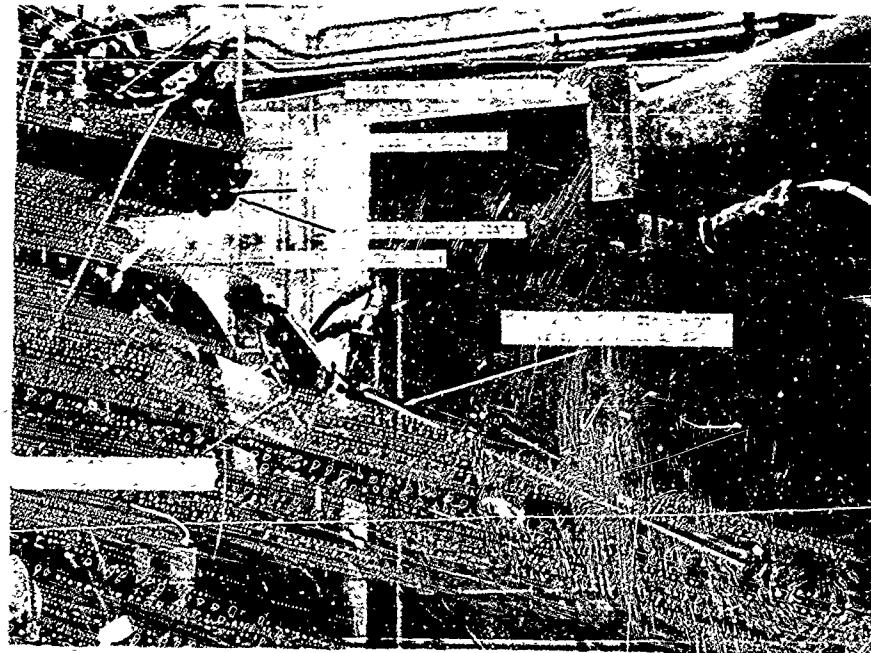
Figure 2. Close-up View of Water Cooled Nozzle Assembly
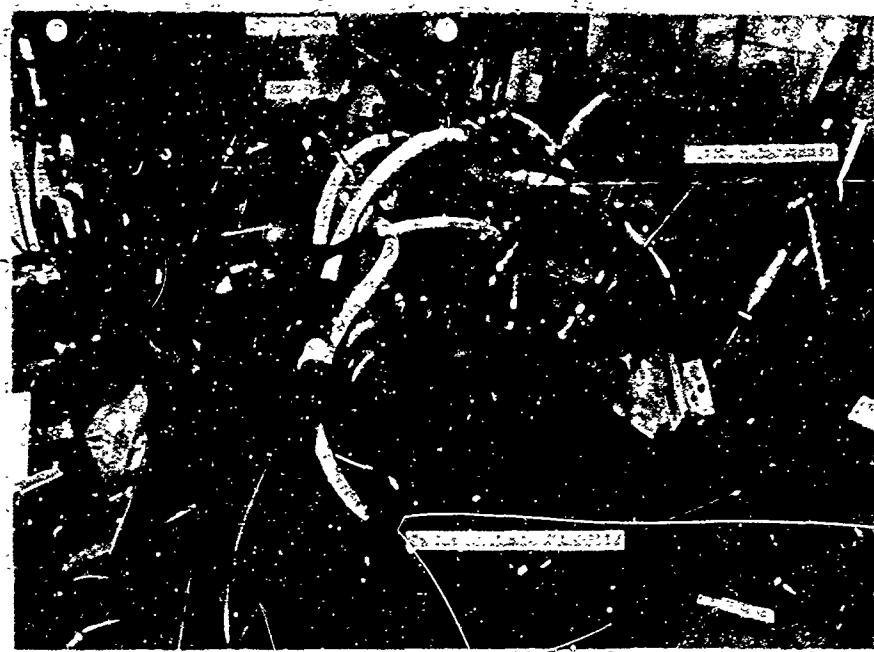
Figure 3. Over View of Wedge Plenum Gerdien Arc with Water Cooled Copper Nozzle Assembly Attached

Figure 4. Cast, Impregnated Cylinder

40

Figure 5. Machined Cylinder
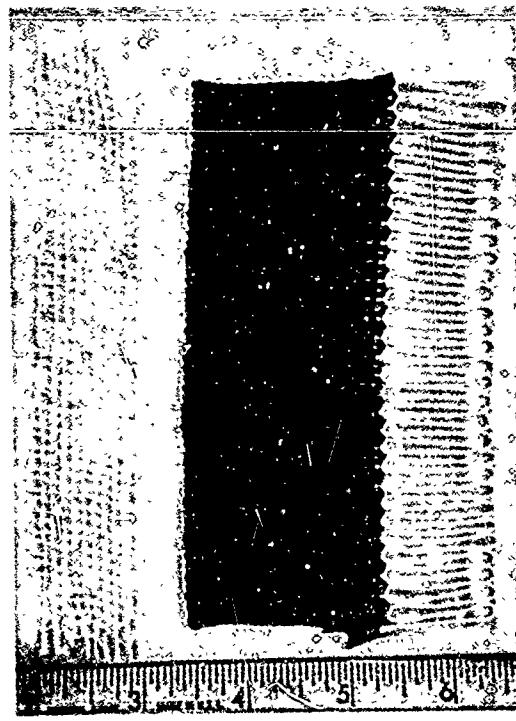
Figure 6. Combination Tape
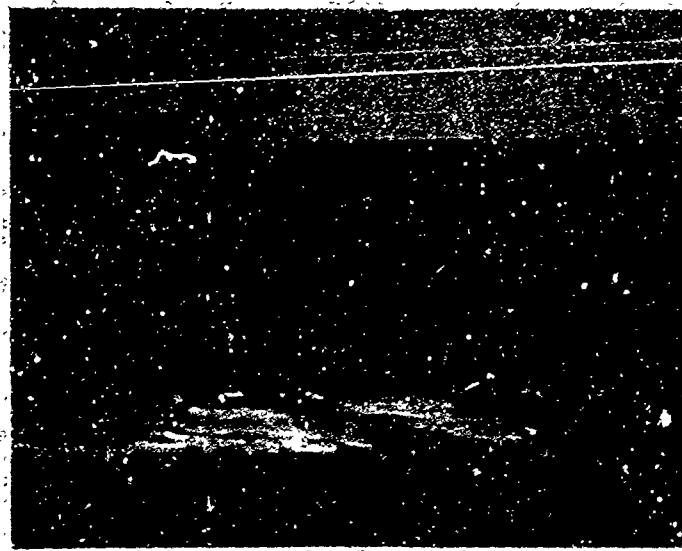
Figure 7.   Combination Composite, 10X
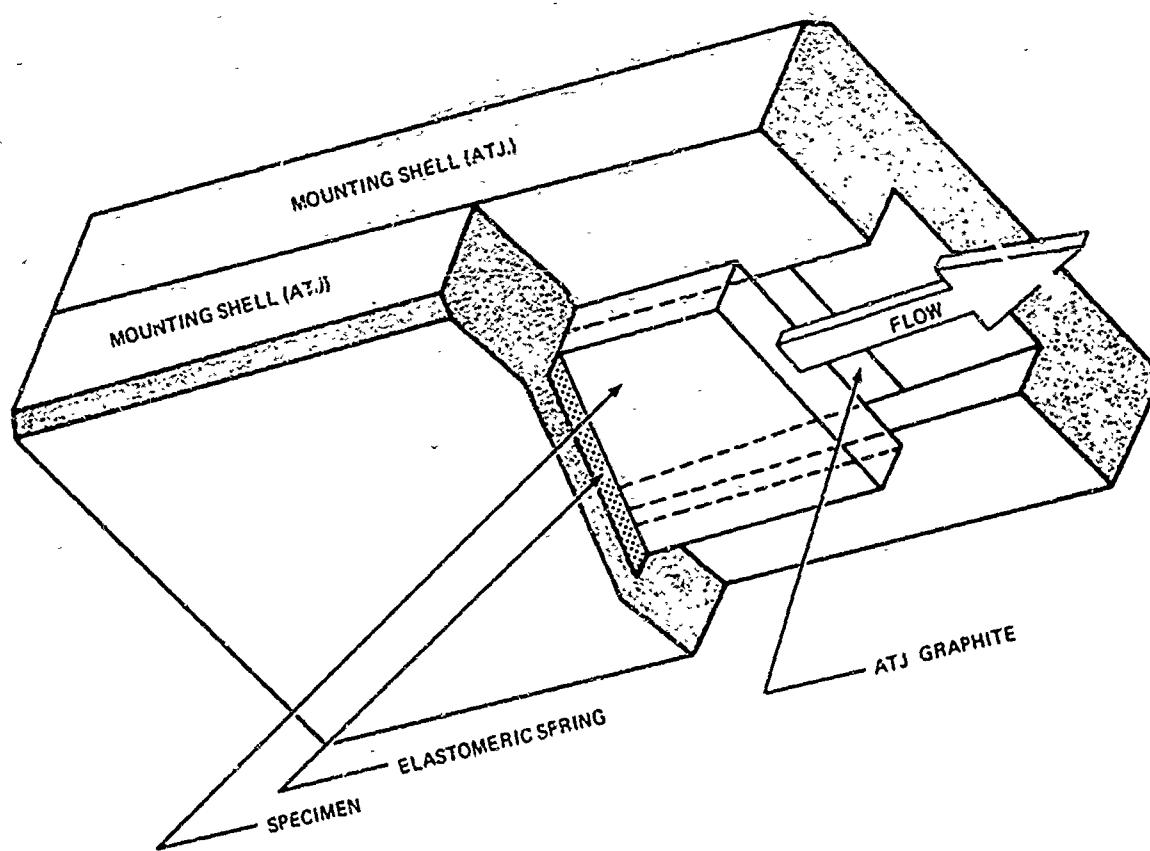
Figure 8.   Dual Channel Set-Up

42
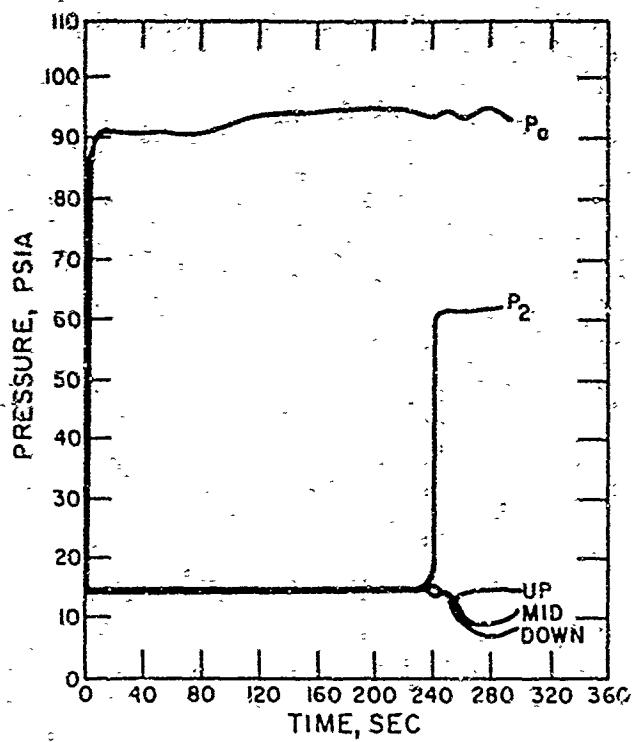
Figure 9. Plenum Pressures Specimen C1-5 Run 15-70
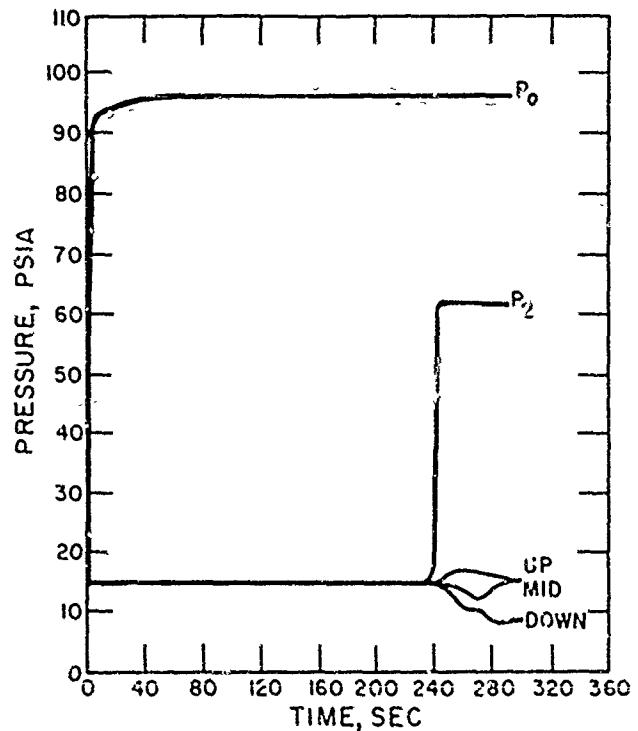
Figure 10. Plenum Pressures Specimen A4-3 Run 16-70

43
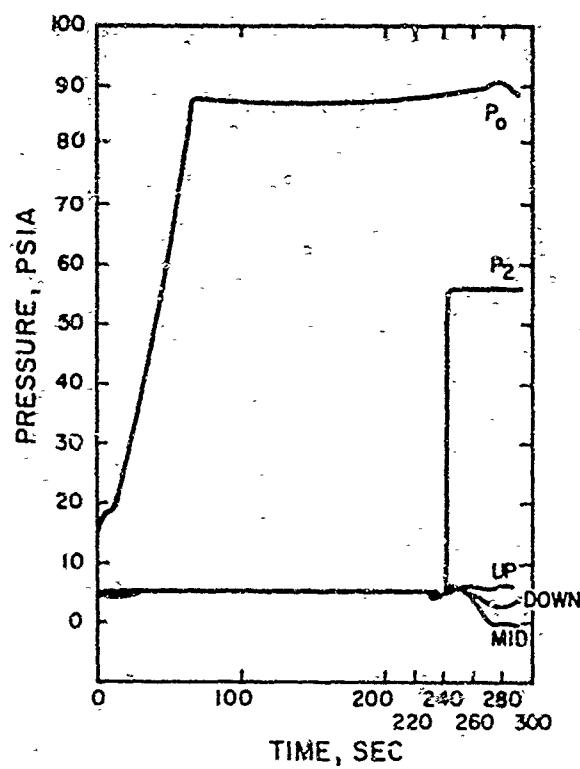
Figure 11.   Plenum Pressures Specimen A4-4 Run 17-70
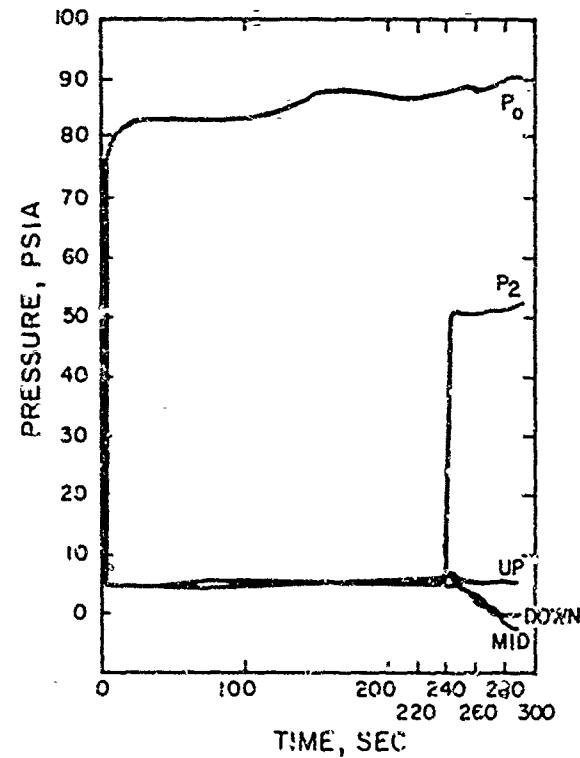
Figure 12.   Plenum Pressures Specimen C4-1 Run 19-70
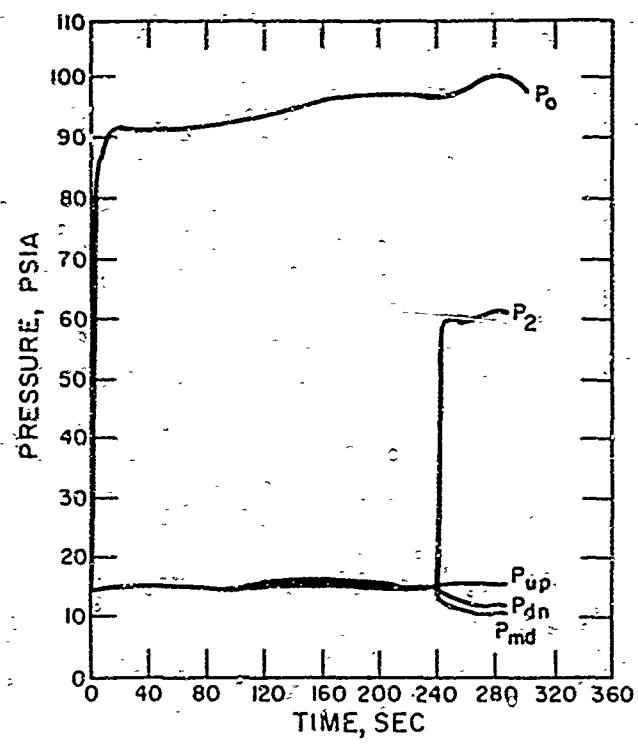
Figure 13. Plenum Pressures Specimen A4-2B Run 20-70
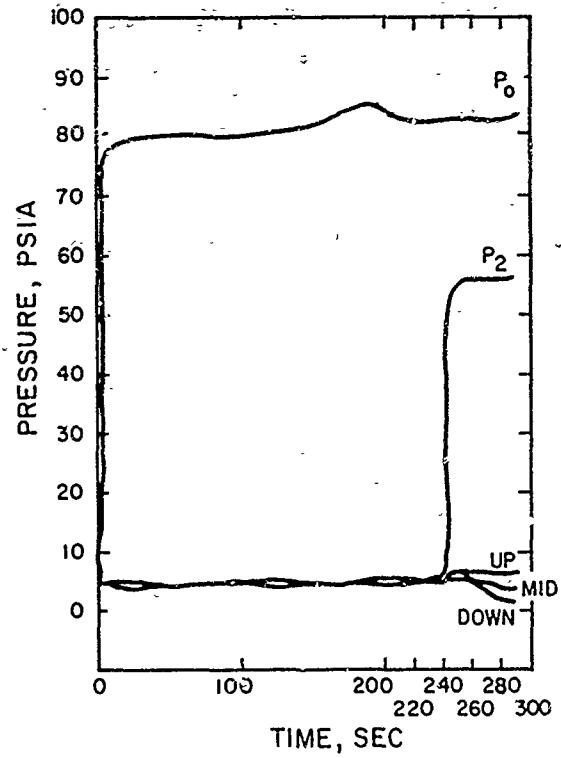
Figure 14. Plenum Pressures Specimen A3-4 Run 22-70

45
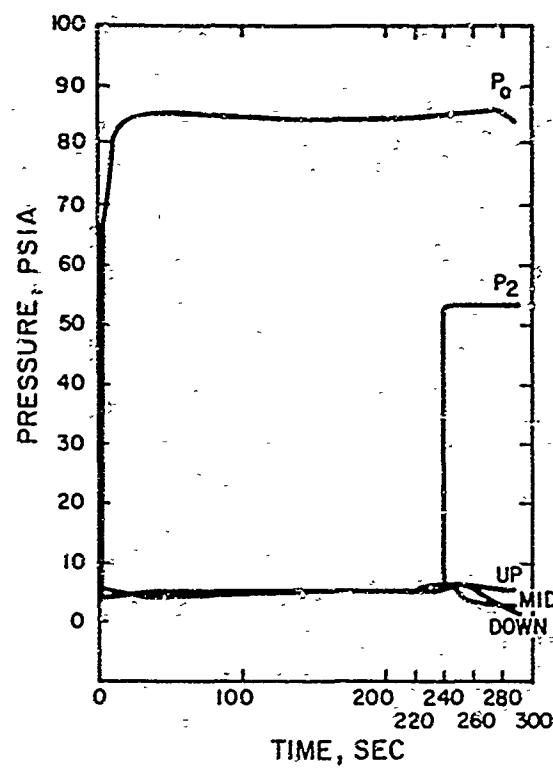
Figure 15. Plenum Pressures Specimen A2-2 Run 23-70
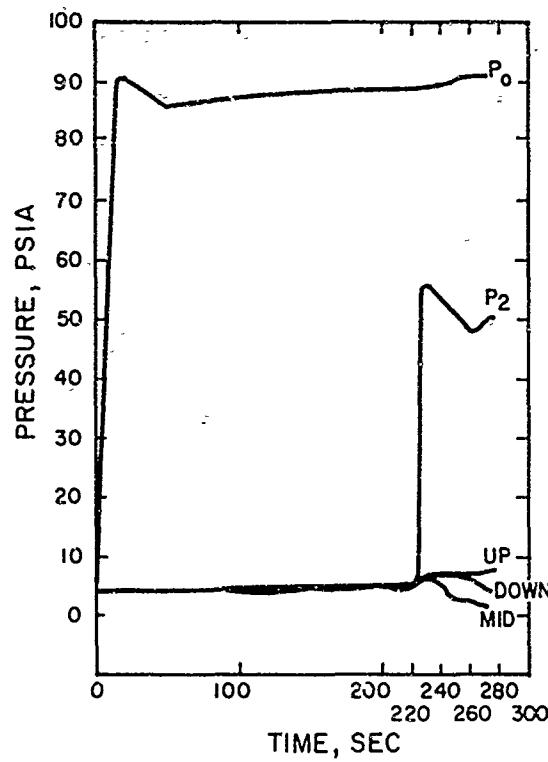
Figure 16. Plenum Pressures Specimen C4-2 Run 25-70

46
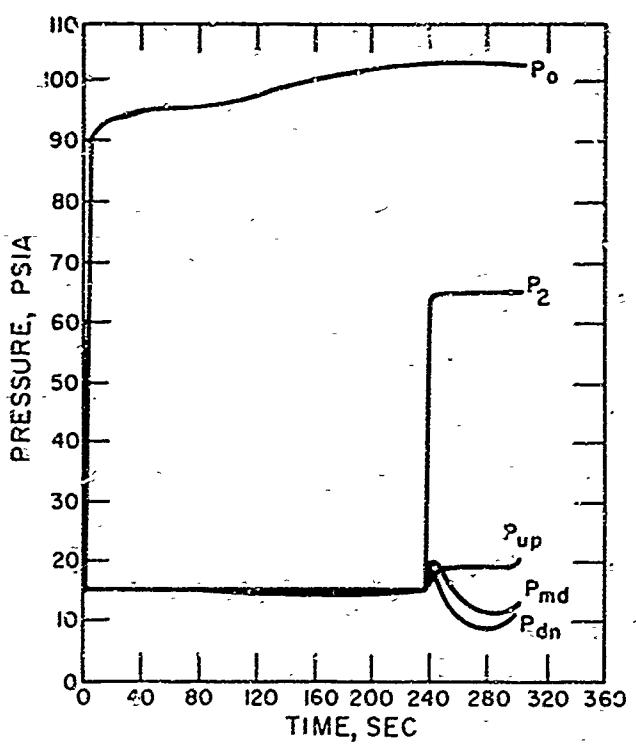
Figure 17. Plenum Pressure, Specimen C1-6, Run 49-70
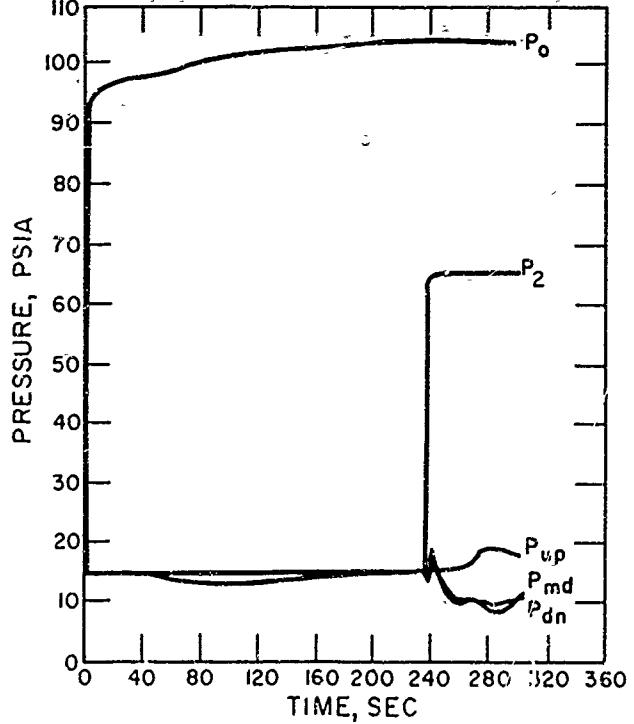
Figure 18. Plenum Pressure, Specimen C1-8, Run 60-70

47
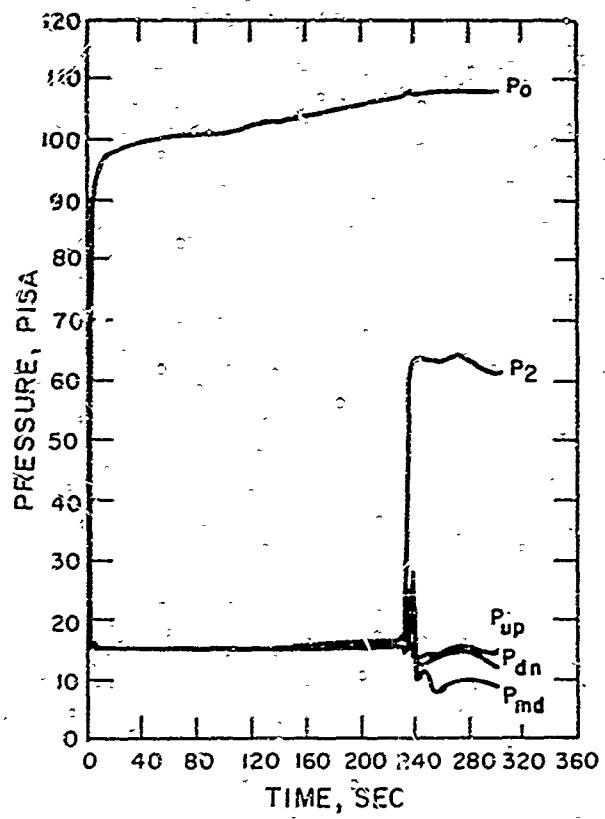
Figure 19. Plenum Pressure Specimen DCM-1 Run 61-70
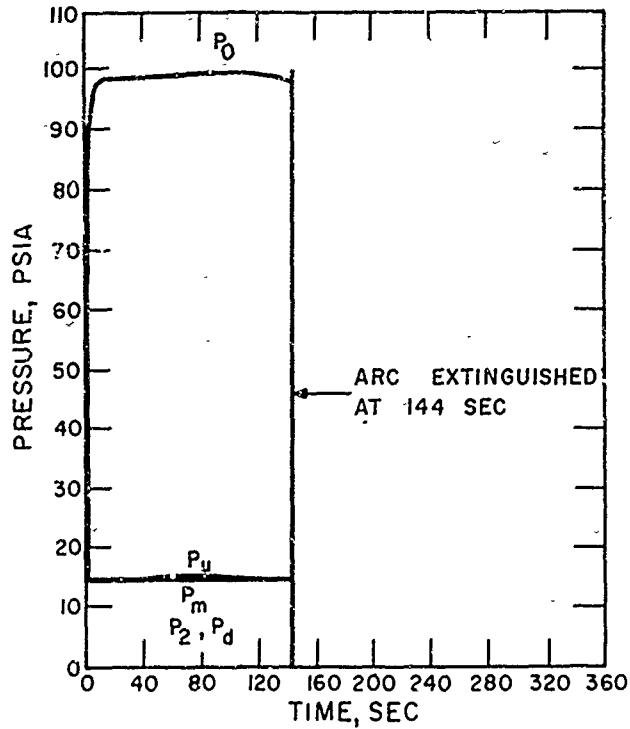
Figure 20. Plenum Pressure, Specimen C5-1, Run 62-70
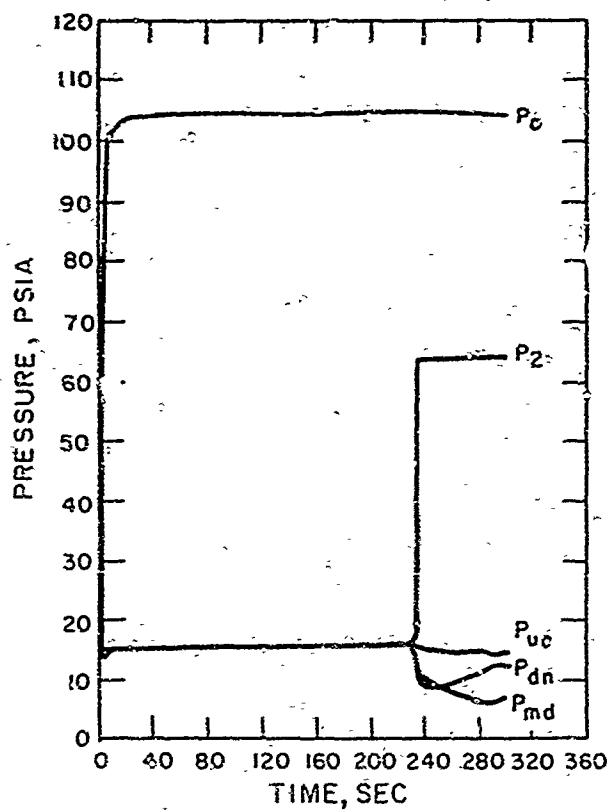
Figure 21. Plenum Pressure Specimen C5-2 Run 63-70
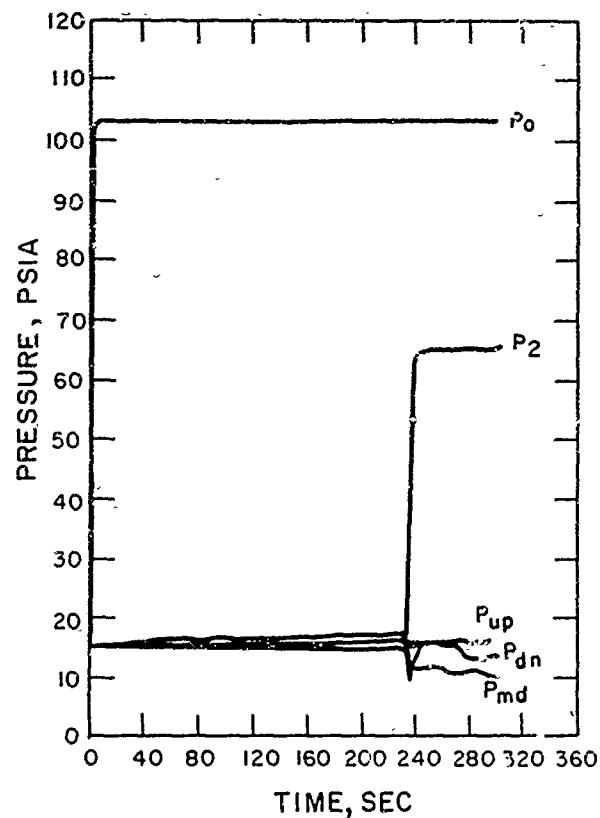
Figure 22. Plenum Pressure Specimen R2-9 Run 64-70
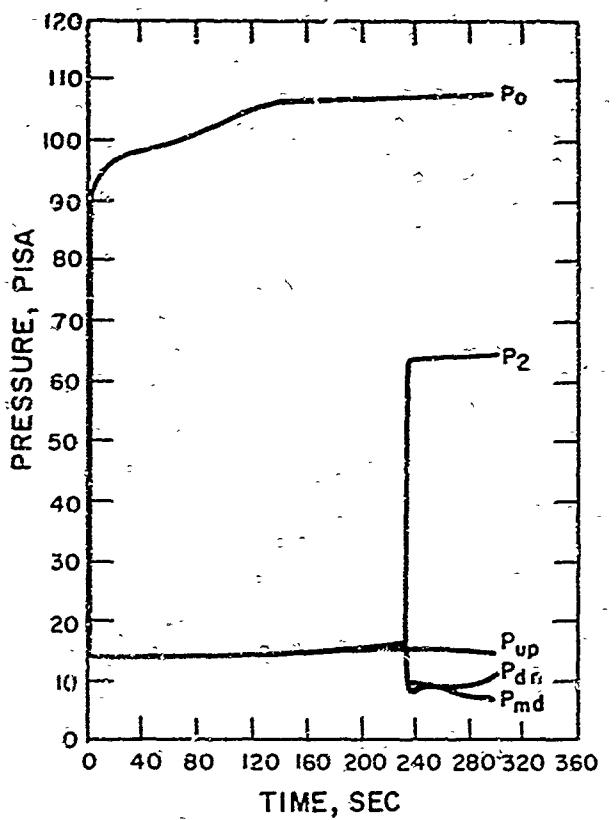
Figure 23. Plenum Pressure Specimen C1-7 Run No. 65-70
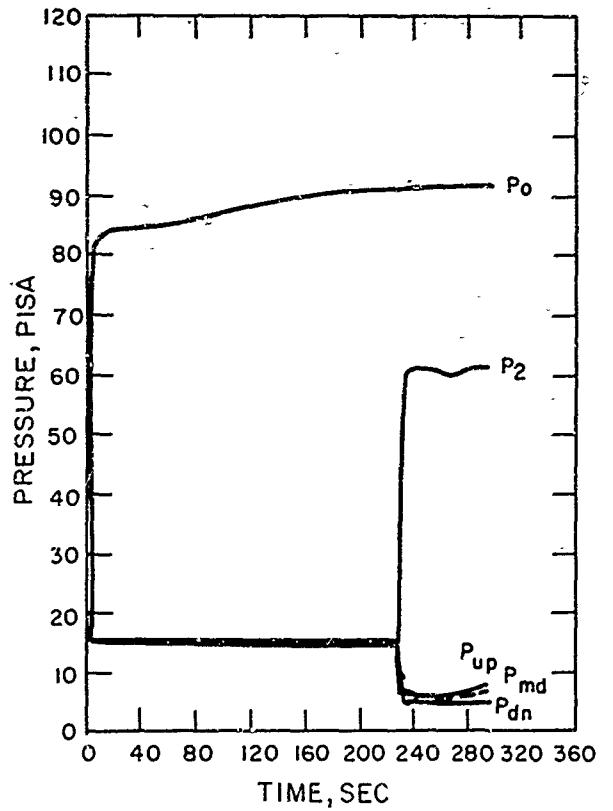
Figure 24. Plenum Pressure Run 4-71 Specimen A7-1
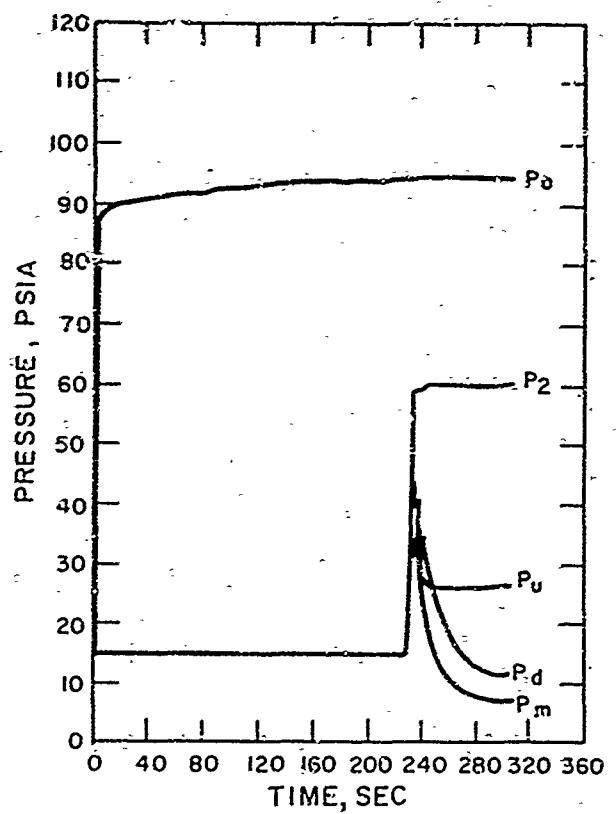
Figure 25. Plenum Pressure Specimen A7-3 Run No. 6-71
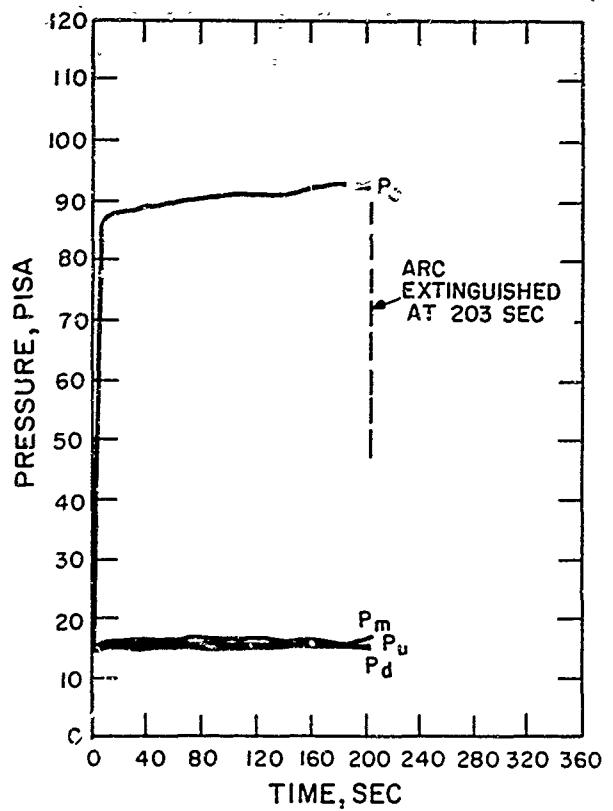
Figure 26. Plenum Pressure Specimen Gem 2 Run 7-71

51
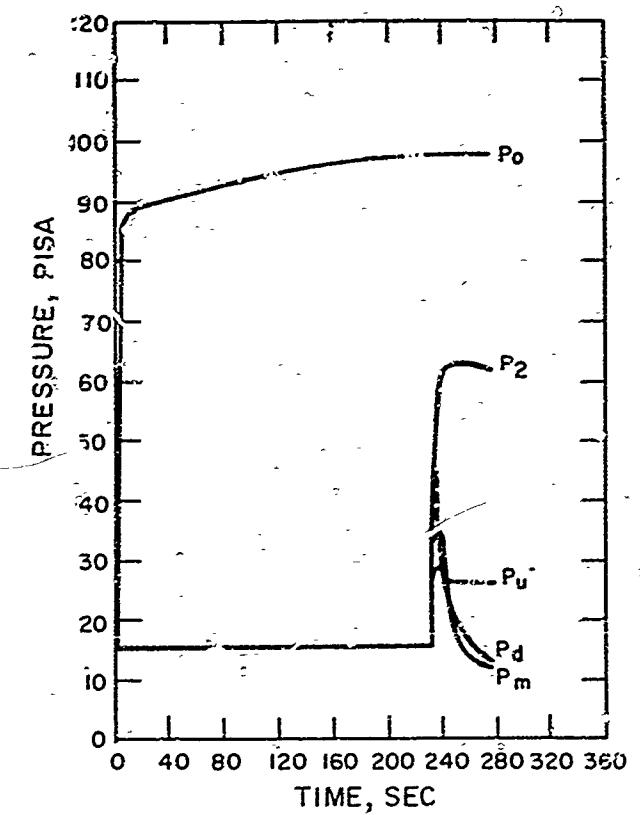
Figure 27. Plenum Pressure Specimen Gem-1 Run No. 8-71
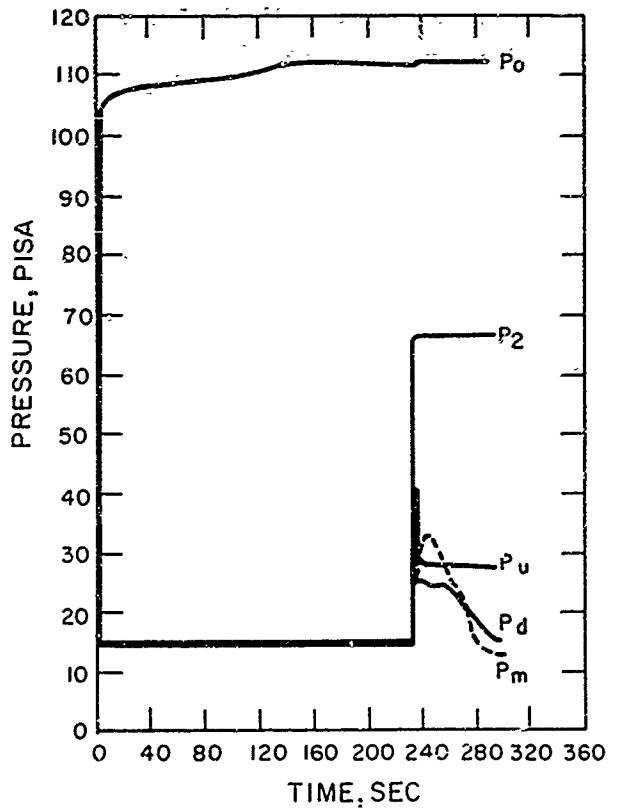
Figure 28. Plenum Pressure Specimen C4-1A Run No. 9-71

52
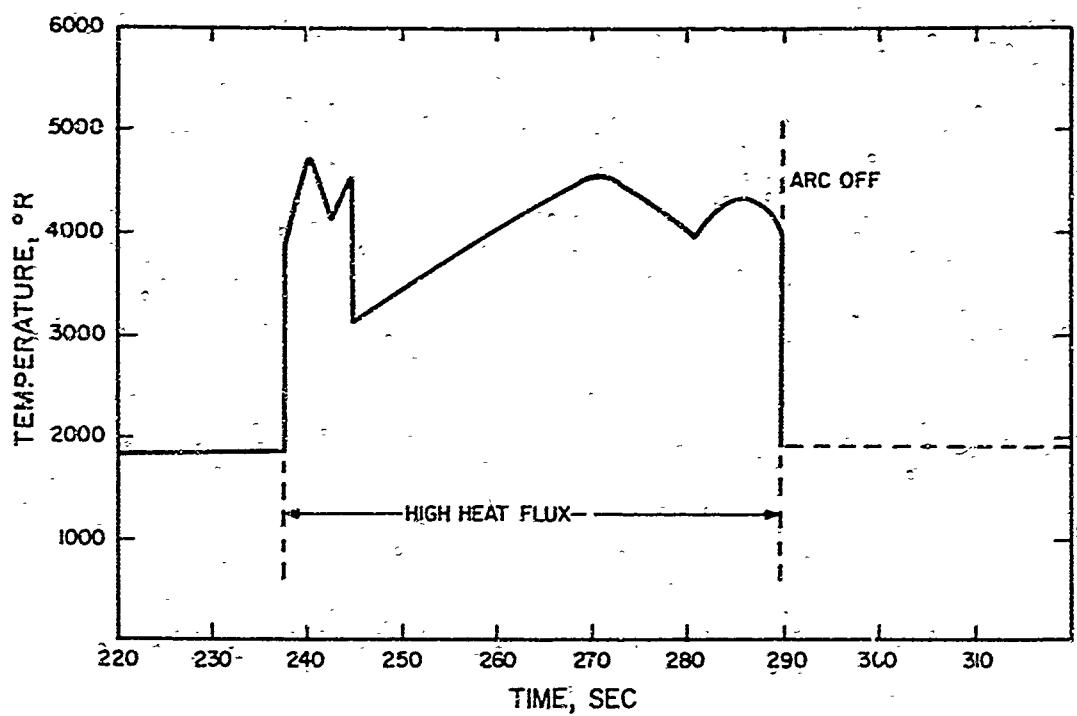
Figure 29. Surface Temperature Expanded Scale Specimen C1-5 Run 15-70
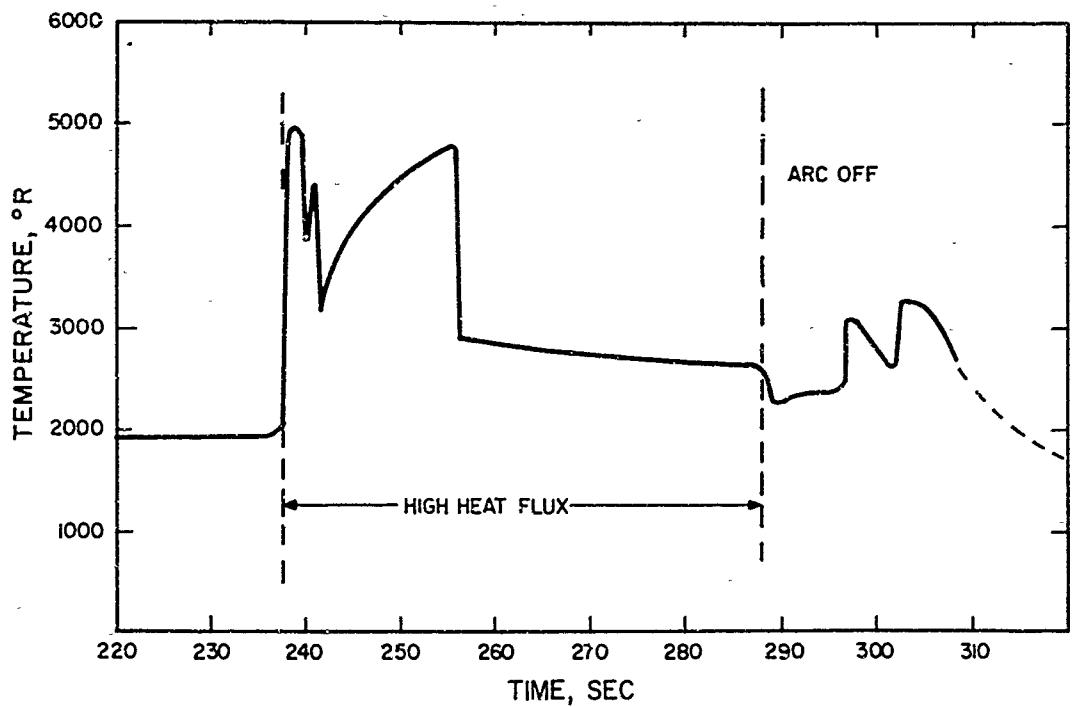
Figure 30. Surface Temperature Expanded Scale Specimen A4-3 Run 16-70

53
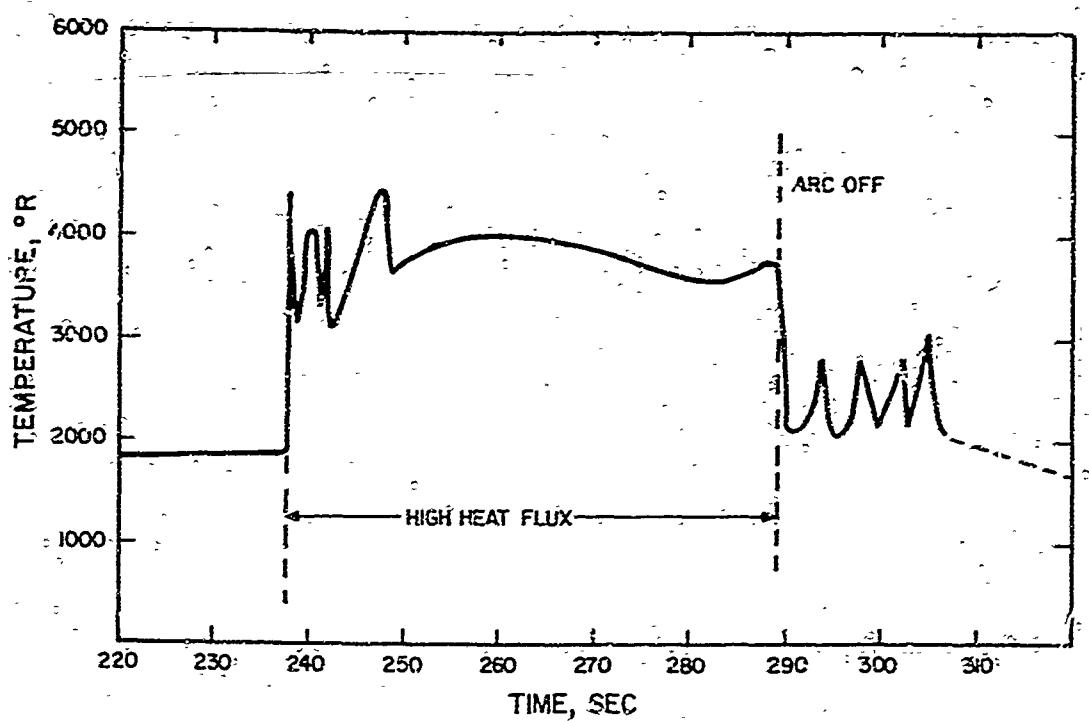
Figure 31. Surface Temperature Expanded Scale Specimen A4-4 Run 17-70
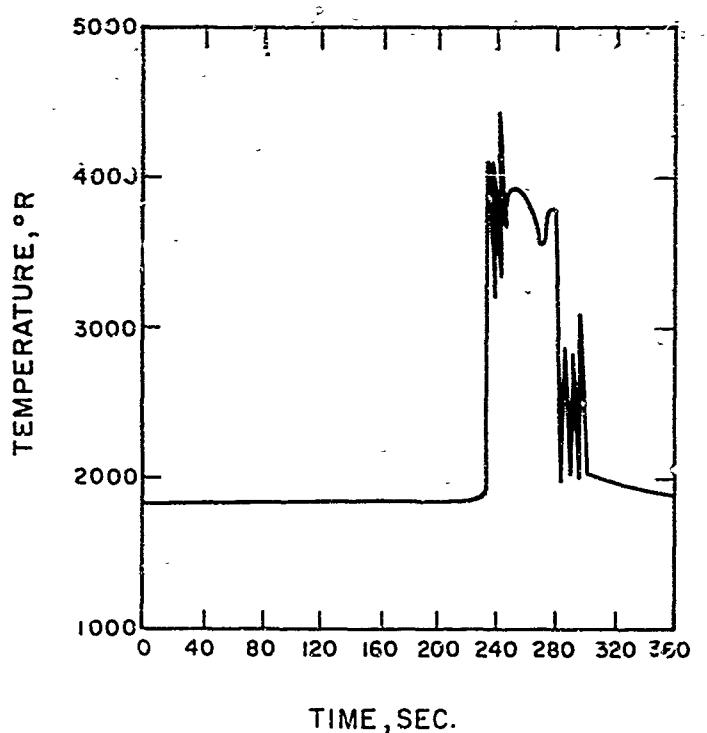
Figure 32. Surface Temperature Full Scale Specimen A4-4 Run 17-70

54
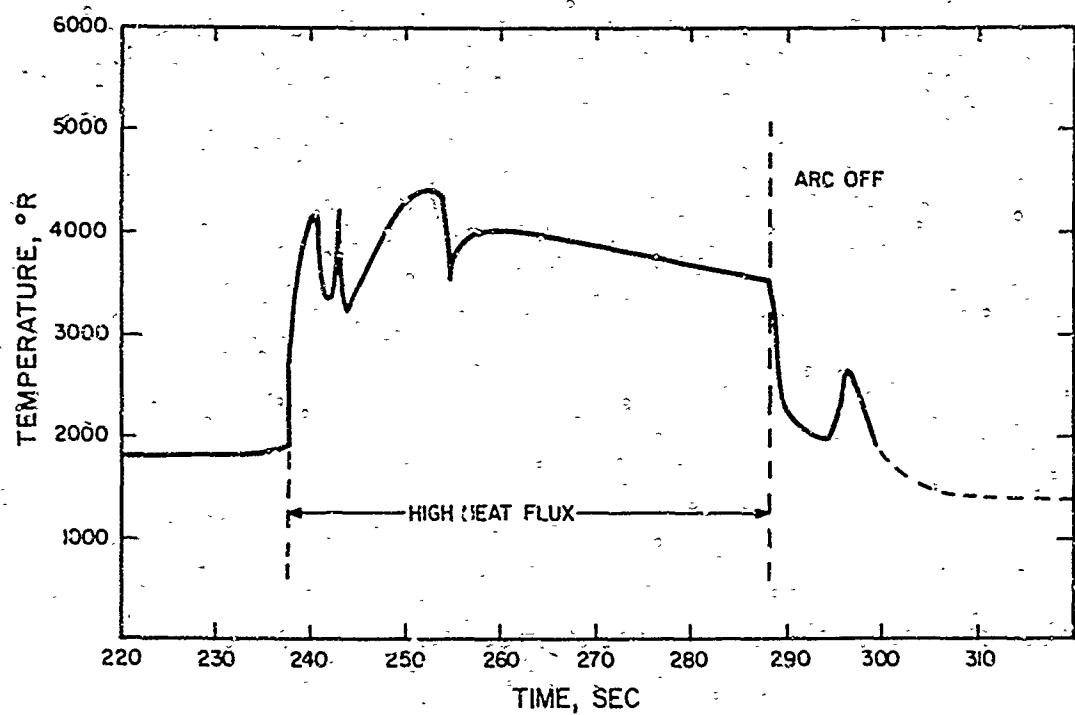
Figure 33. Surface Temperature Expanded Scale Specimen C4-1 Run 19-70
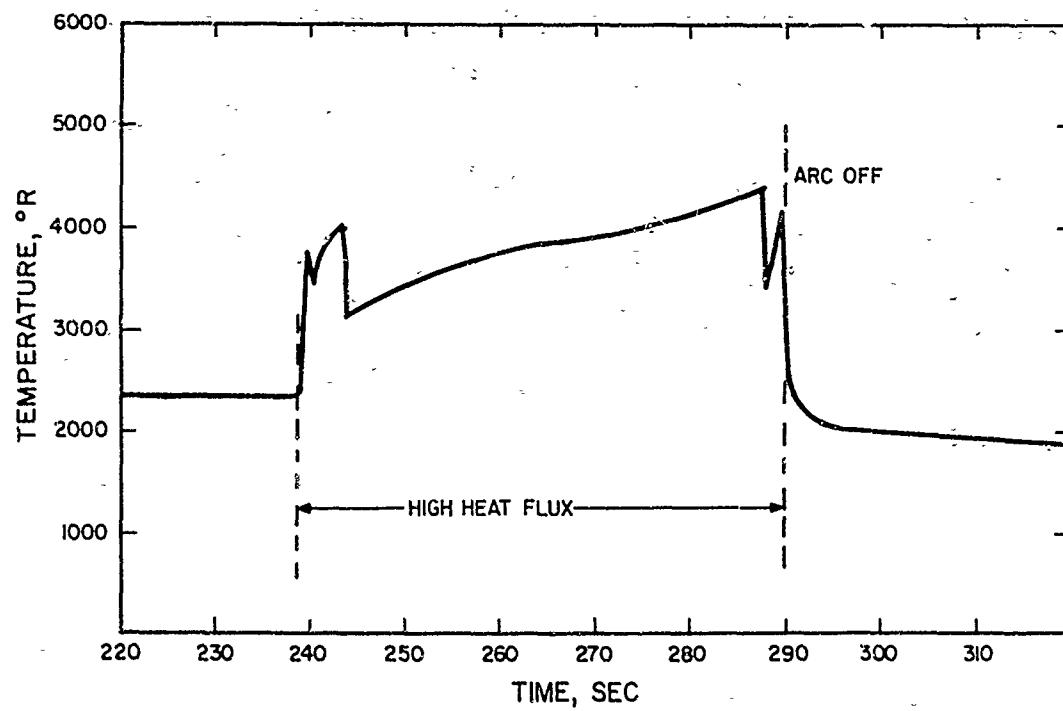
Figure 34. Surface Temperature Expanded Scale Specimen A4-2B Run 20-70
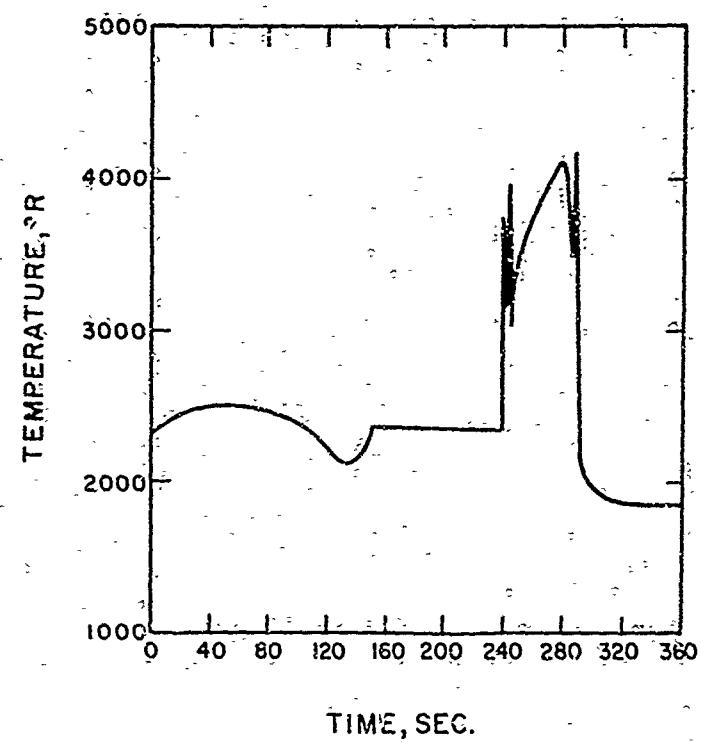
Figure 35. Surface Temperature Full Scale Specimen A4-2B Run 20-70
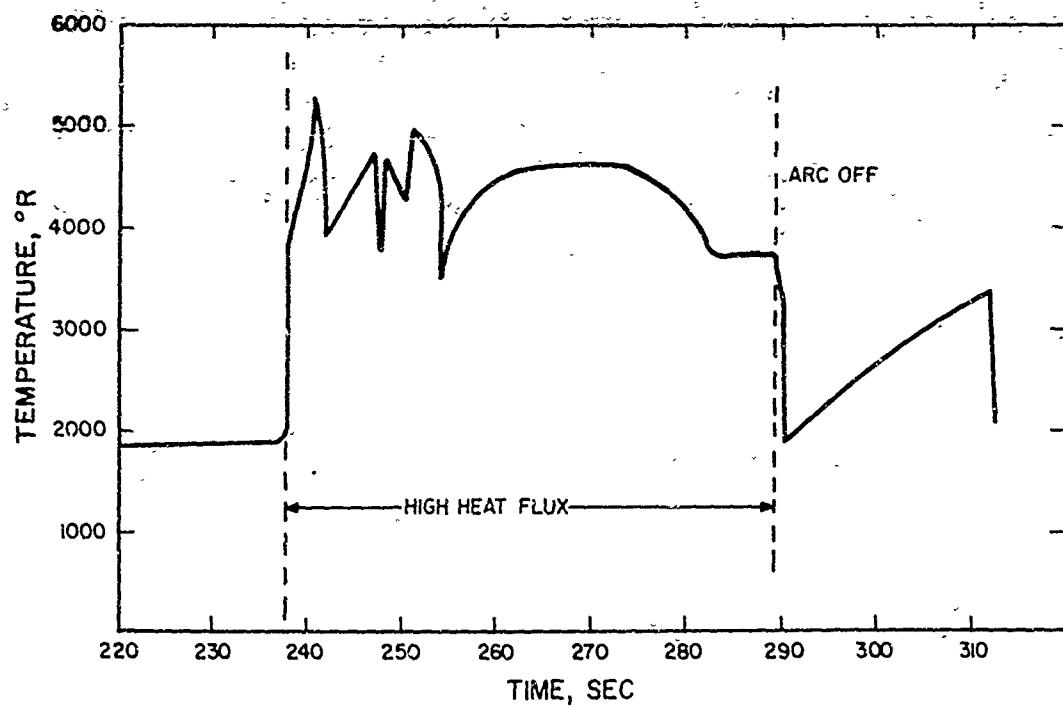
Figure 36. Surface Temperature Expanded Scale Specimen A3-4 Run 22-70
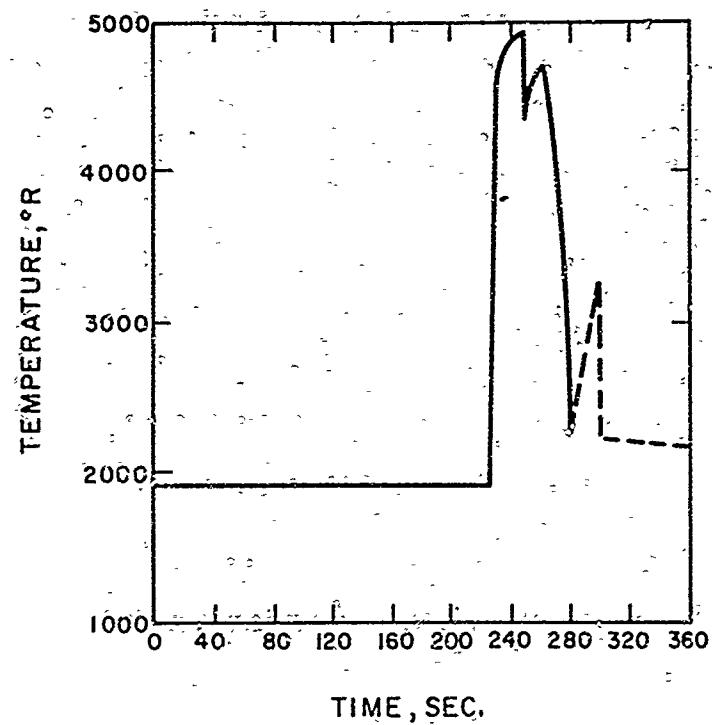
Figure 37. Surface Temperature Full Scale Specimen A3-4 Run 22-70
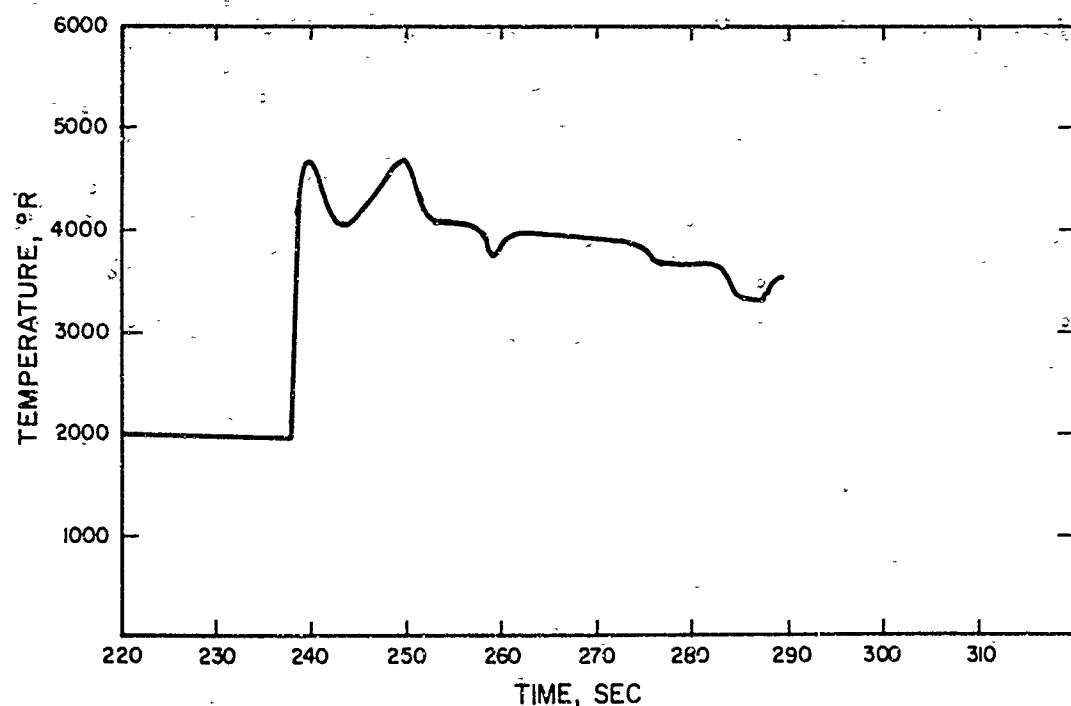
Figure 38. Surface Temperature Expanded Scale Specimen A2-2 Run 23-70

57
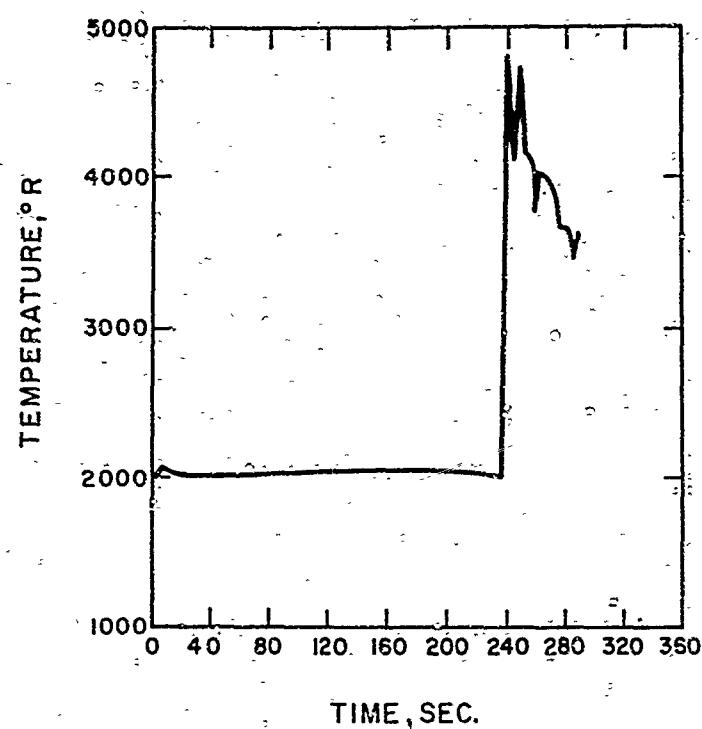
Figure 39. Surface Temperature Full Scale Specimen A2-2 Run 23-70
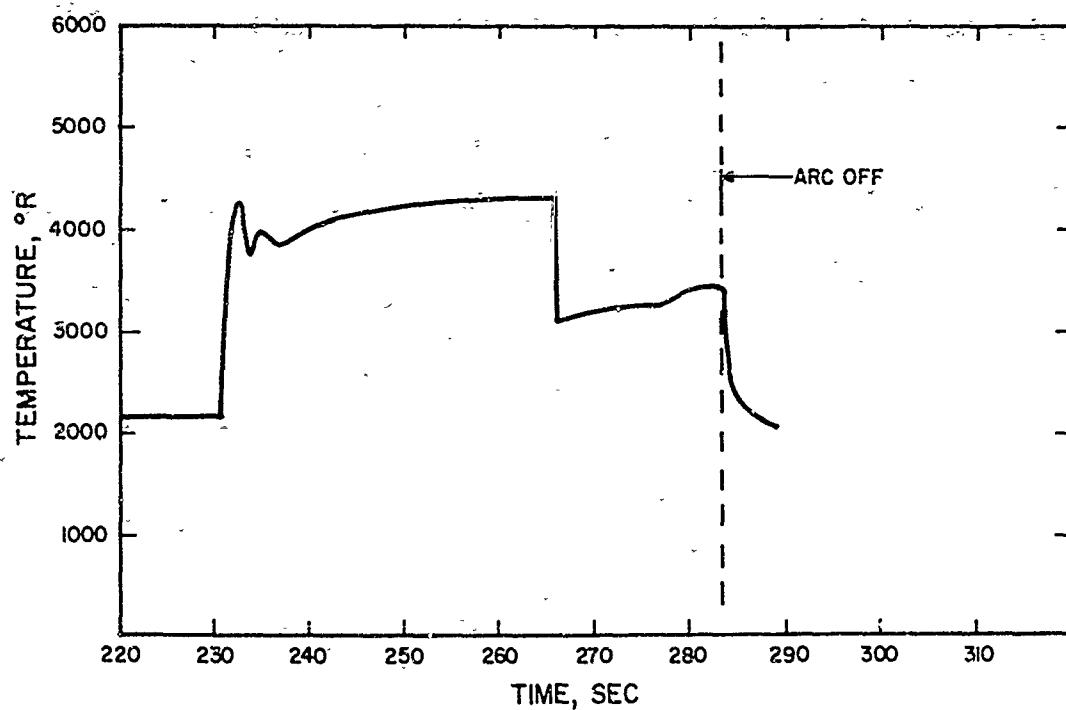
Figure 40. Surface Temperature Expanded Scale Specimen C4-2 Run 25-70

58
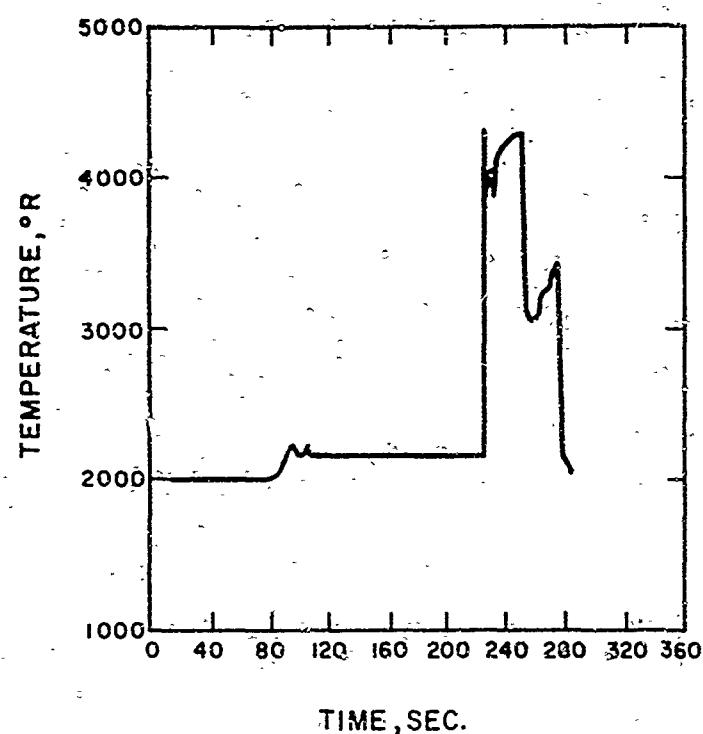
Figure 41. Surface Temperature Full Scale Specimen C4-2 Run 25-70
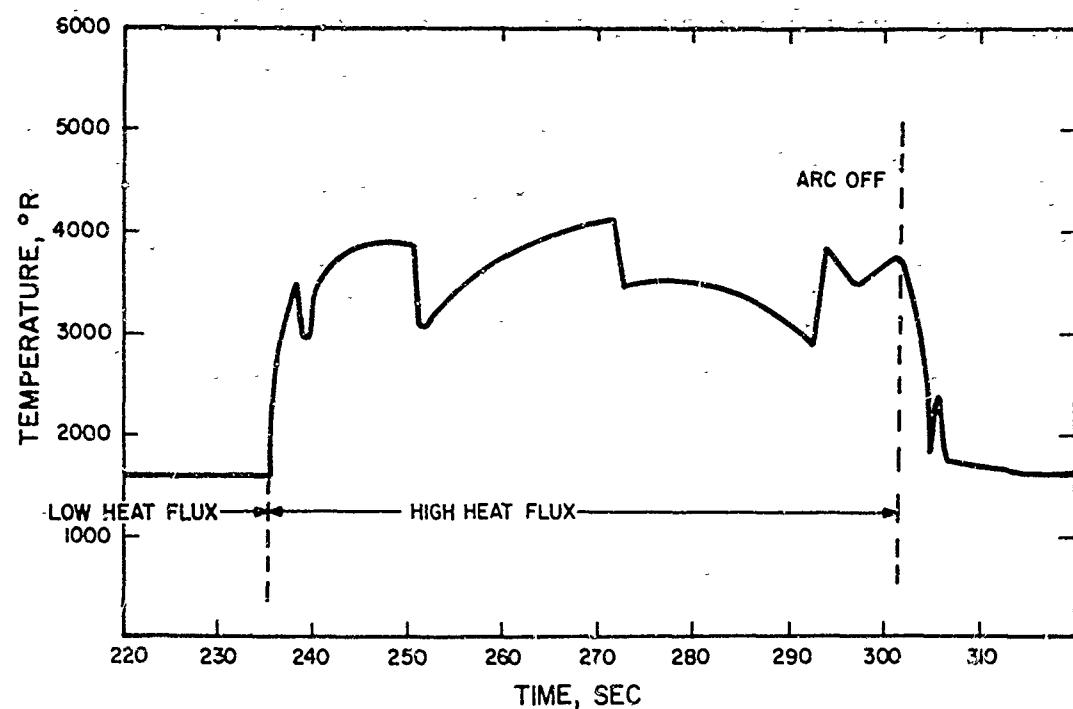
Figure 42. Surface Temperature, Expanded Scale - Specimen C1-6 Run 49-7

59
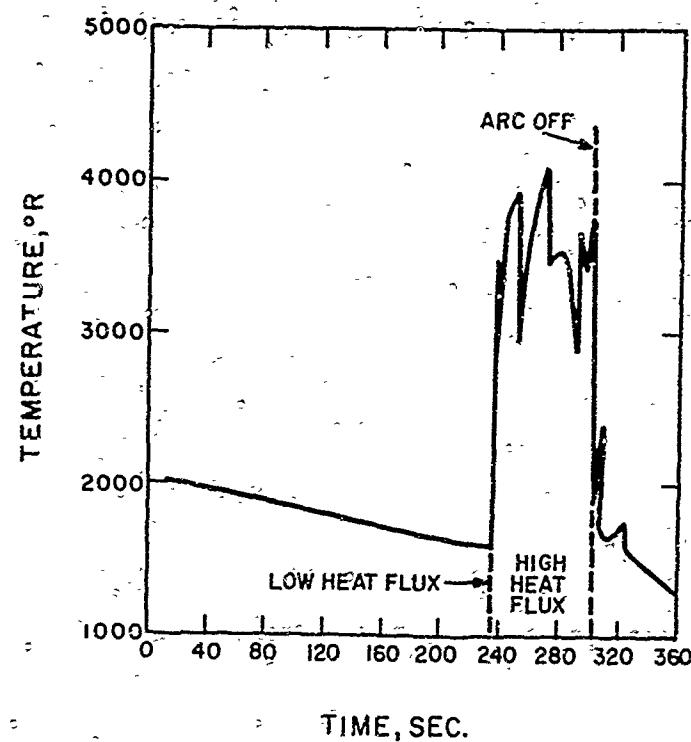
Figure 43. Surface Temperature, Full Scale, Specimen C1-6, Run 49-70
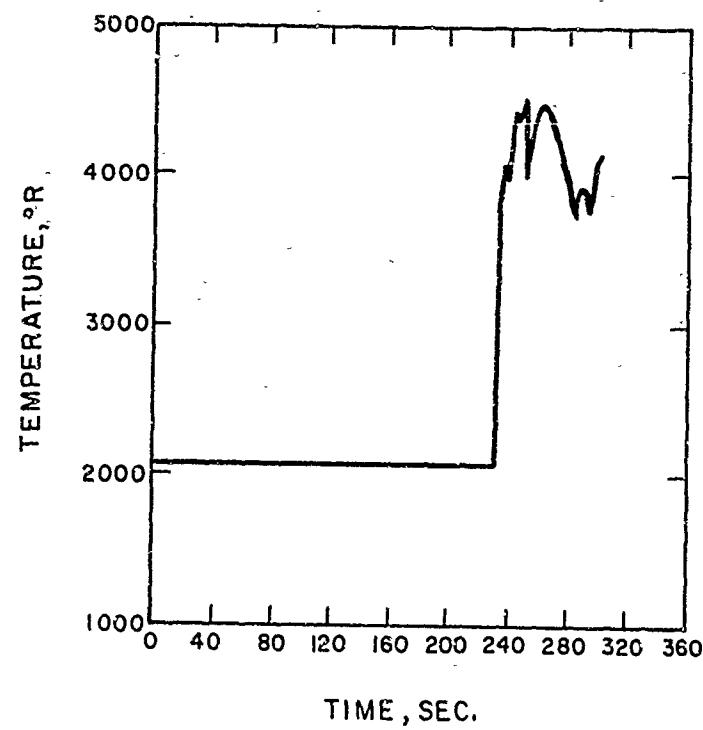
Figure 44. Surface Temperature, Specimen C1-8, Run 60-70
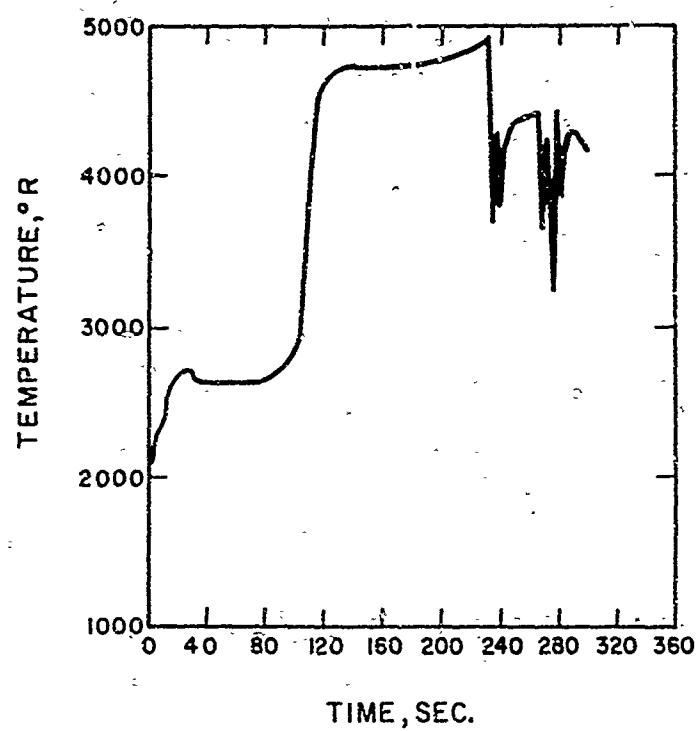
Figure 45. Surface Temperature, Specimen DCM-1, Run 61-70
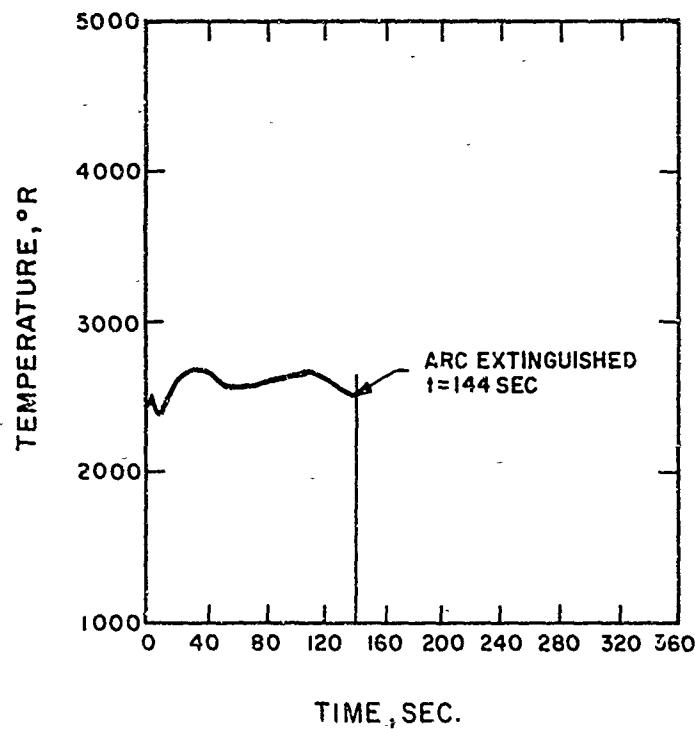
Figure 46. Surface Temperature, Specimen C5-1, Run 62-70
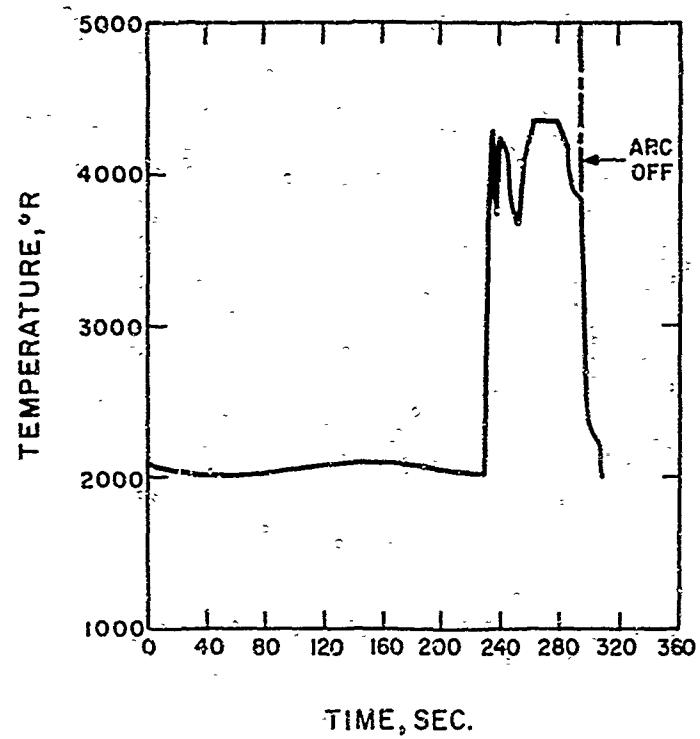
Figure 47. Surface Temperature, Specimen C5-2, Run 63-70
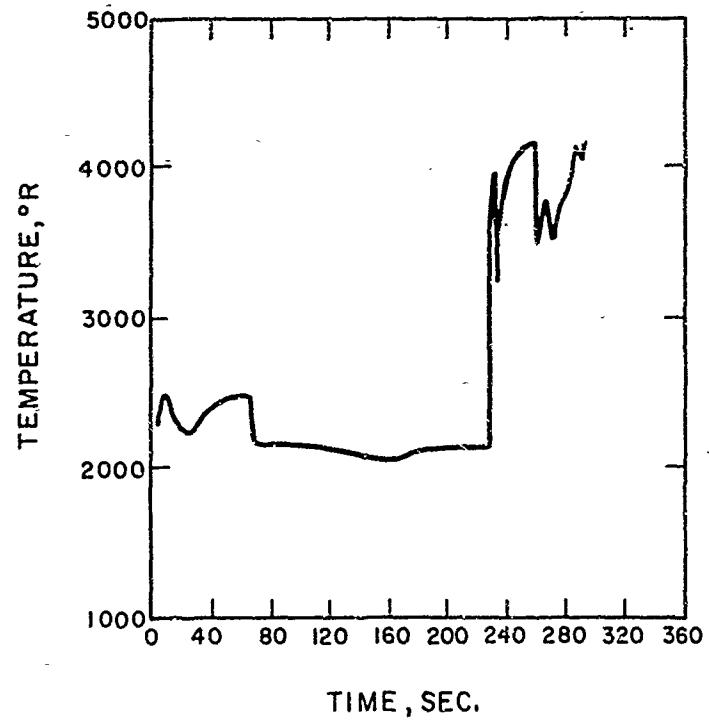
Figure 48. Surface Temperature, Specimen R2-9, Run 64-70

62
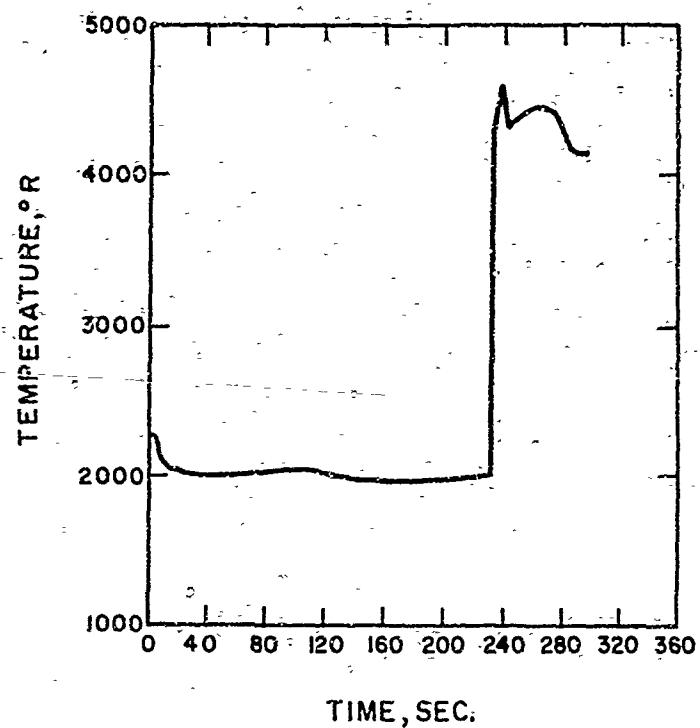
Figure 49. Surface Temperature, Specimen C1-7, Run 65-70
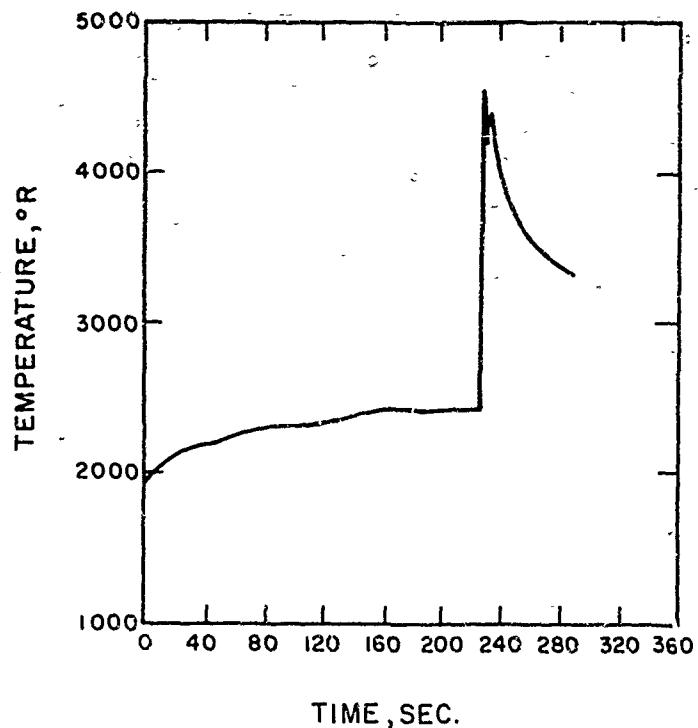
Figure 50. Surface Temperature, Specimen A7-1, Run 4-71

63
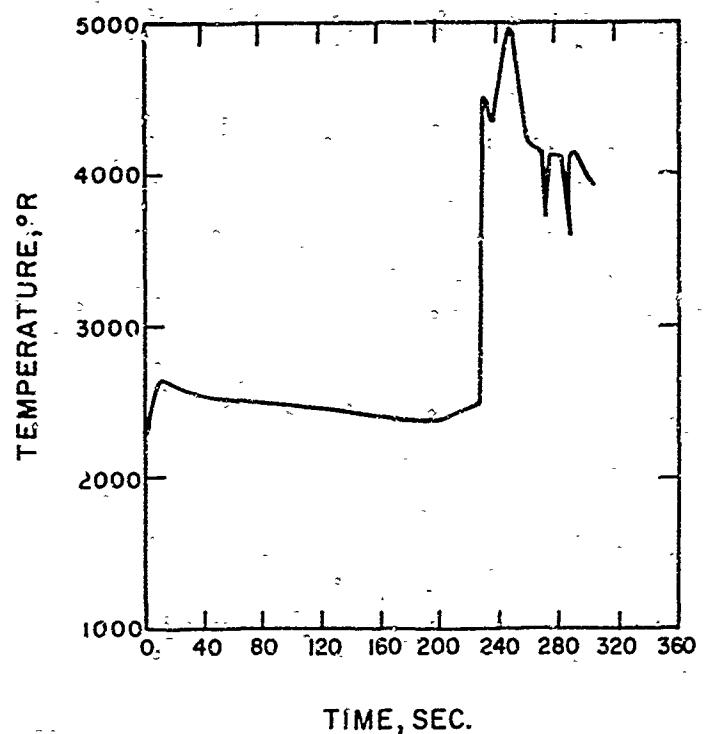
Figure 51. Surface Temperature, Specimen A7-3, Run 6-71
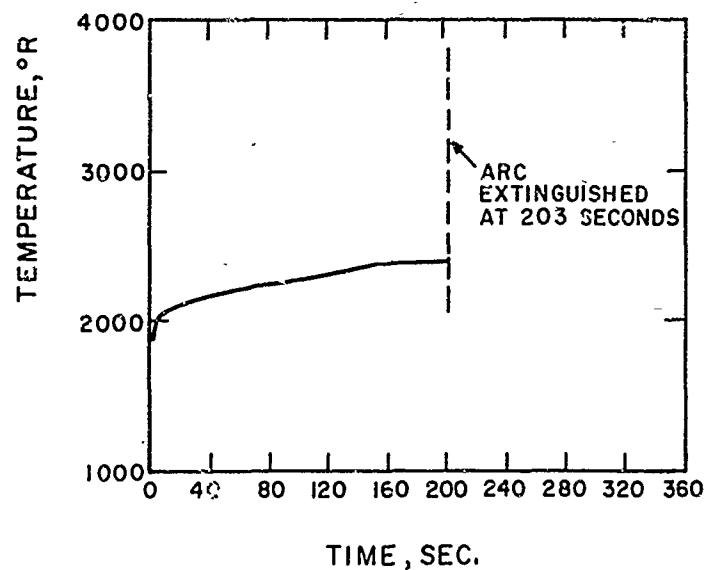
Figure 52. Surface Temperature, Specimen GEM2, Run 7-71

64
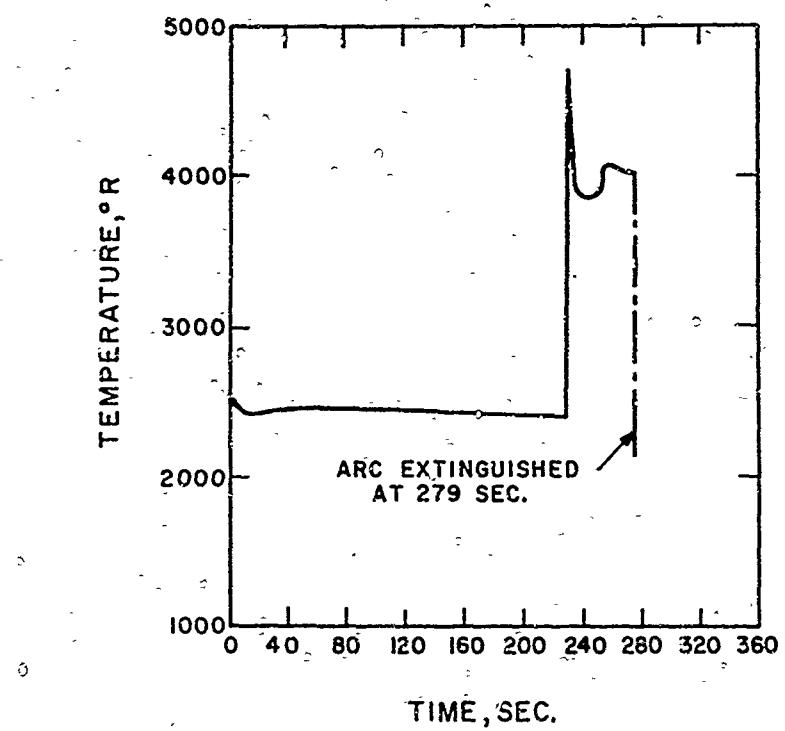
Figure 53. Surface Temperature, Specimen GEM1, Run 8-71
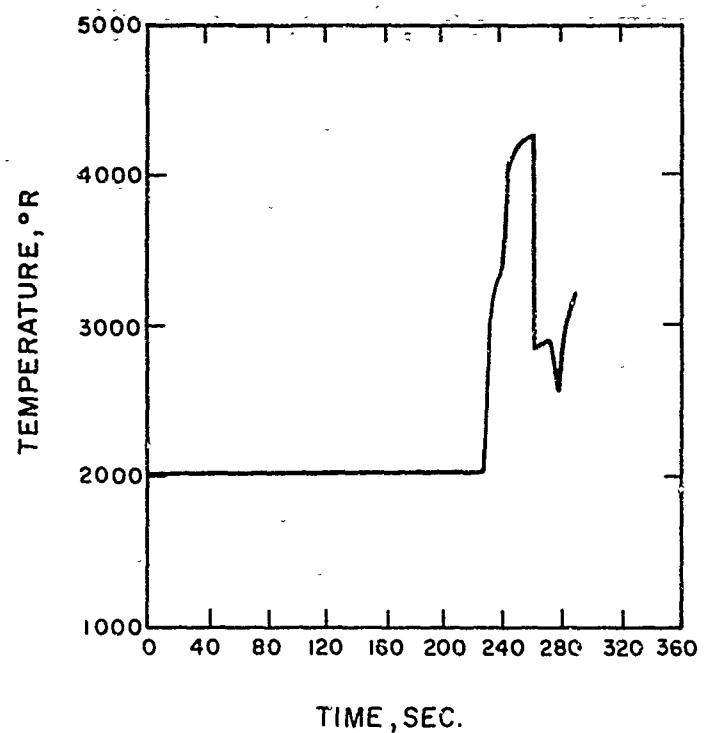
Figure 54. Surface Temperature, Specimen C4-1A, Run 9-71

65
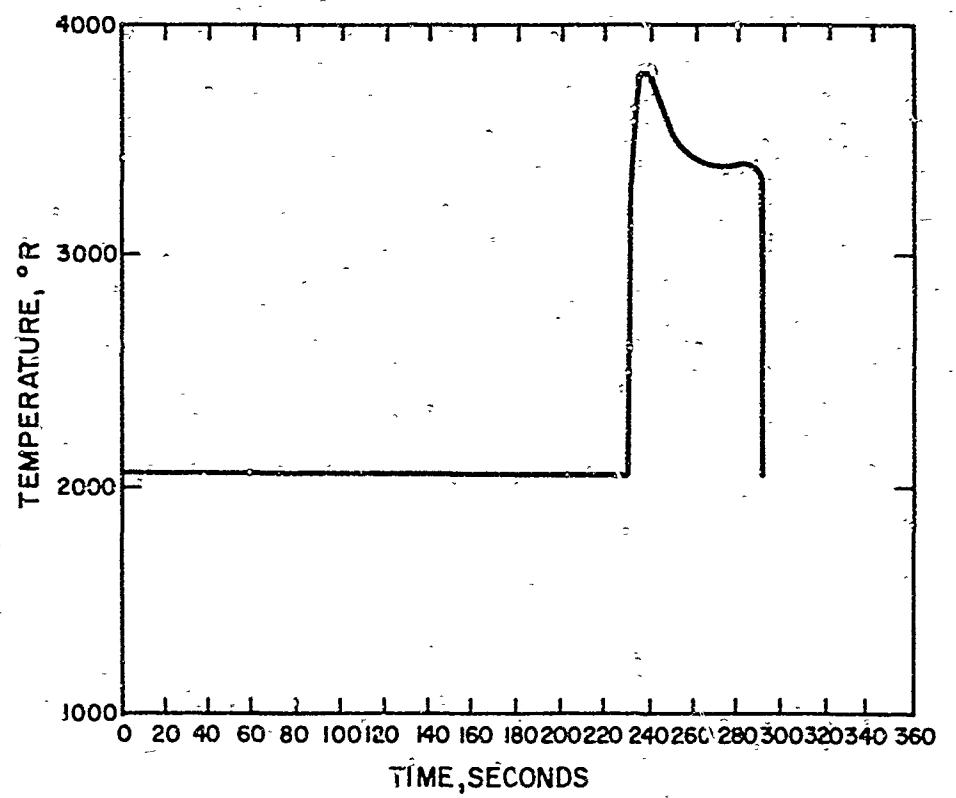
Figure 55. Surface Temperature Full Scale Specimen FW-1 Run 42-71
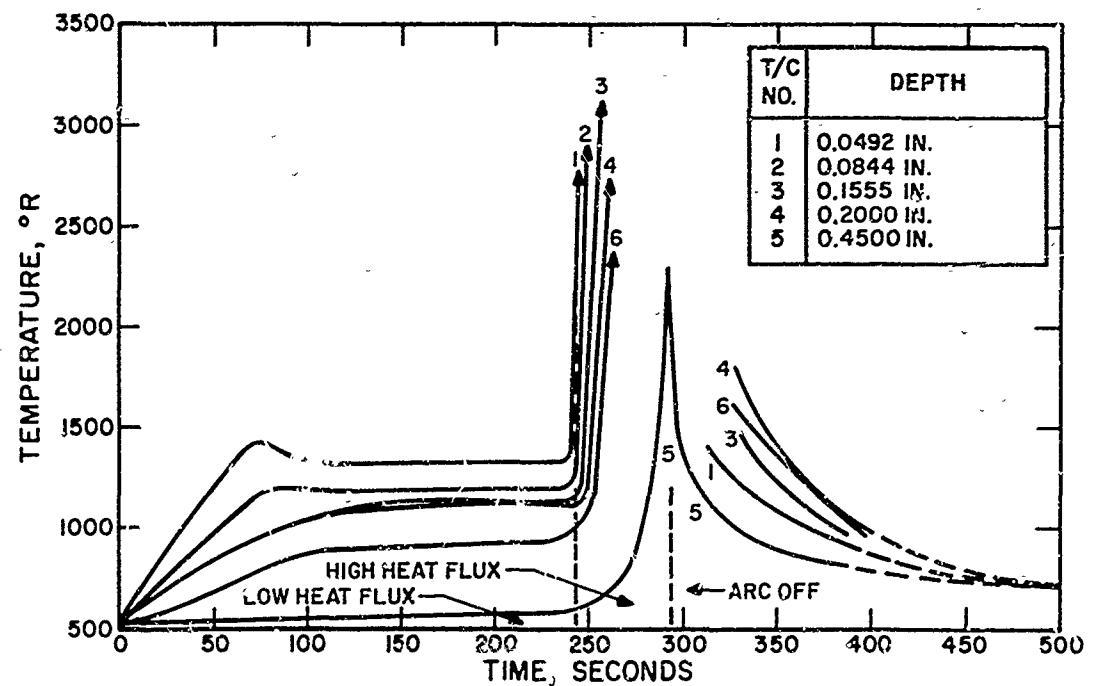
Figure 56. Thermocouple Response Specimen C1-5 Run 15-70

66
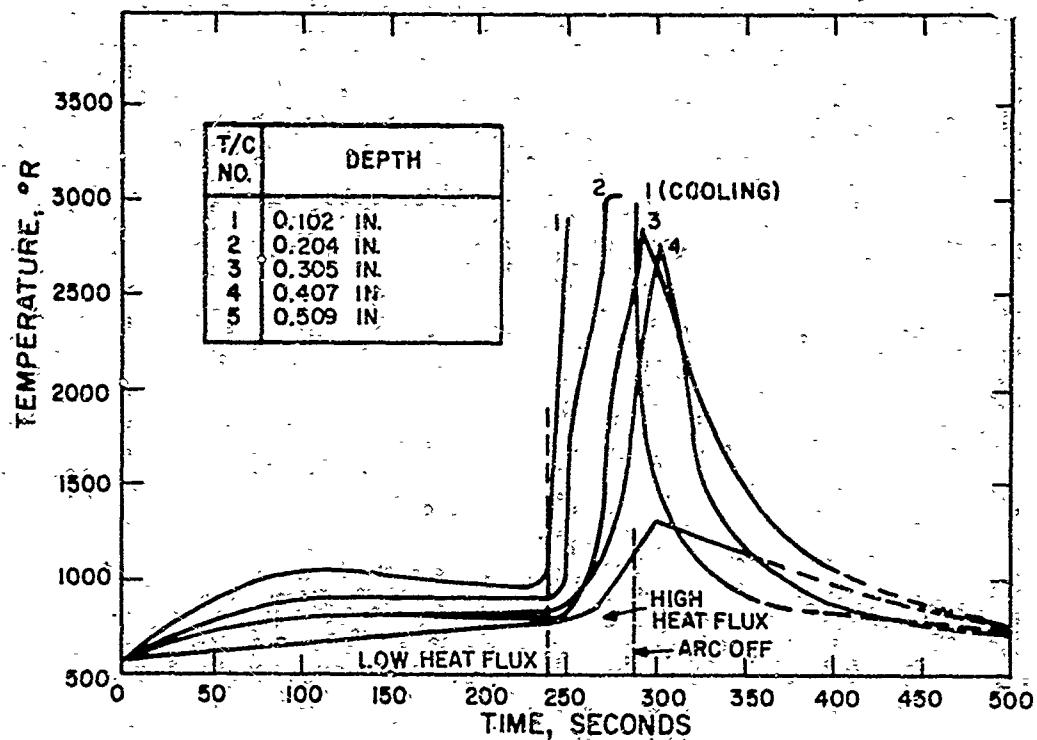
Figure 57. Thermocouple Response Specimen A4-3 Run 16-70
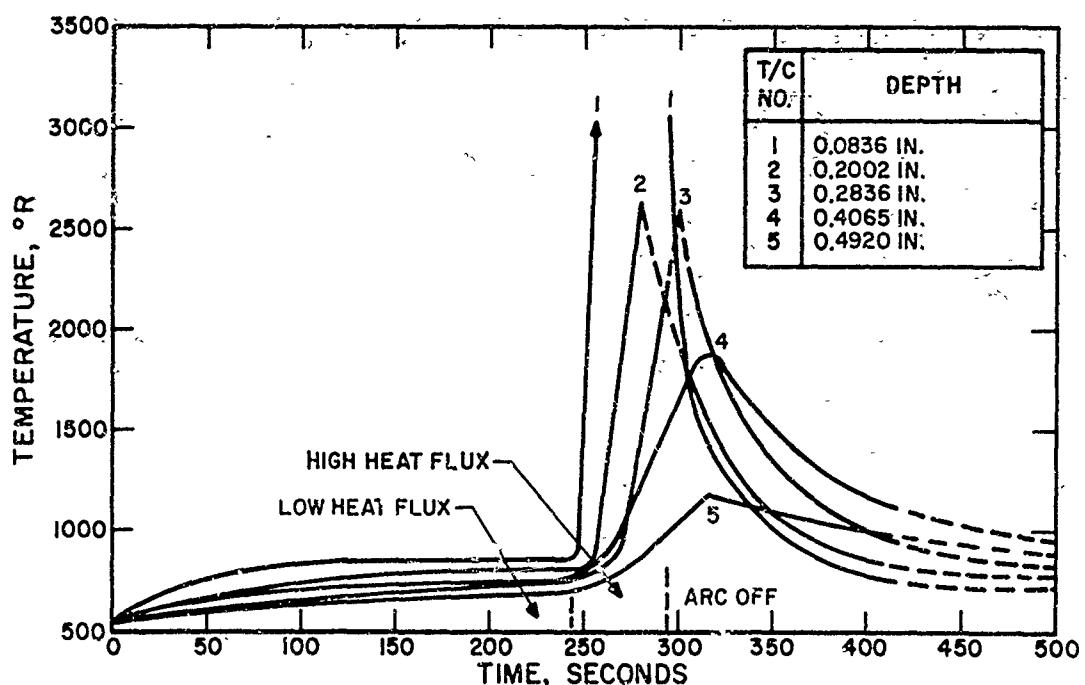
Figure 58. Thermocouple Response Specimen A4-4 Run 17-70

67
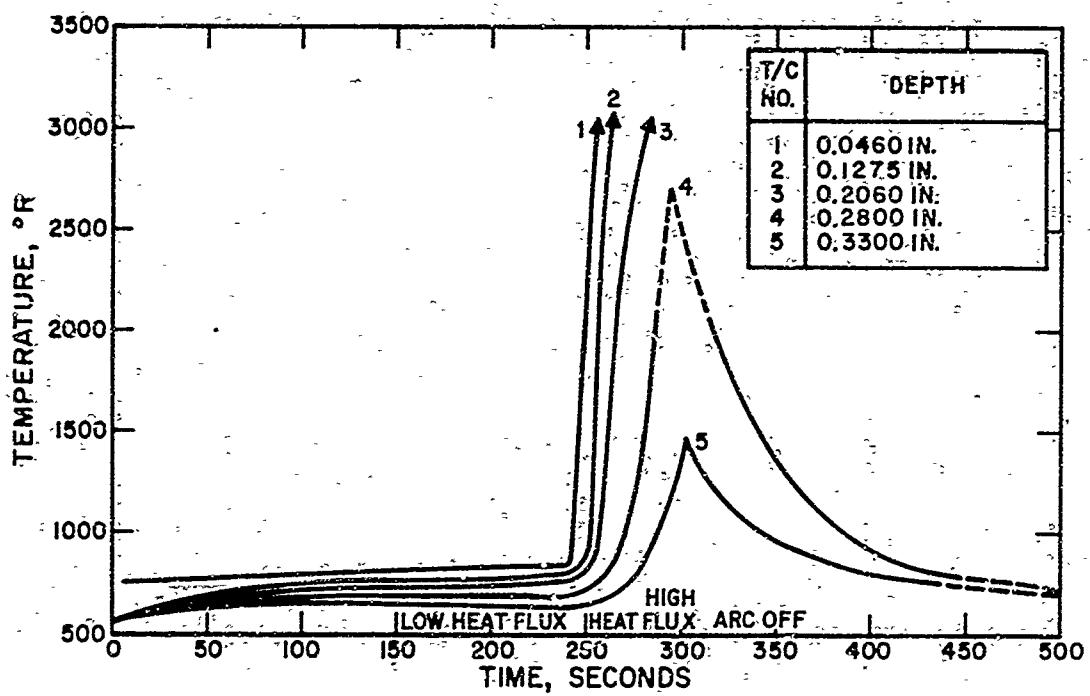
Figure 59. Thermocouple Response Specimen C4-1 Run 19-70
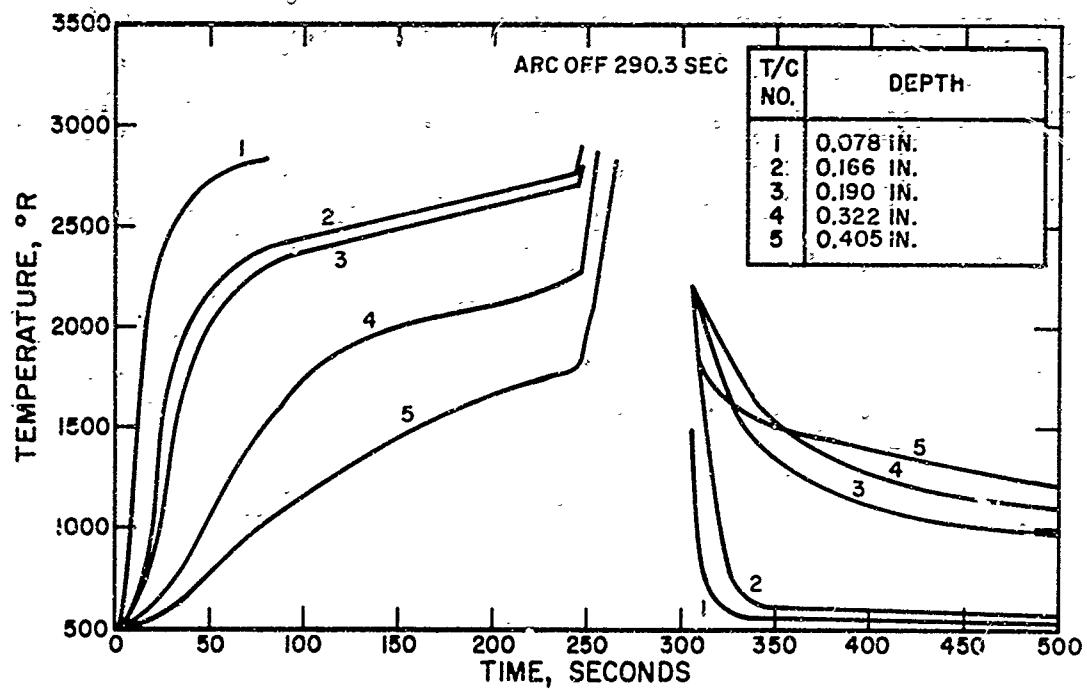
Figure 60. Thermocouple Response Specimen A4-2B Run 20-70

68
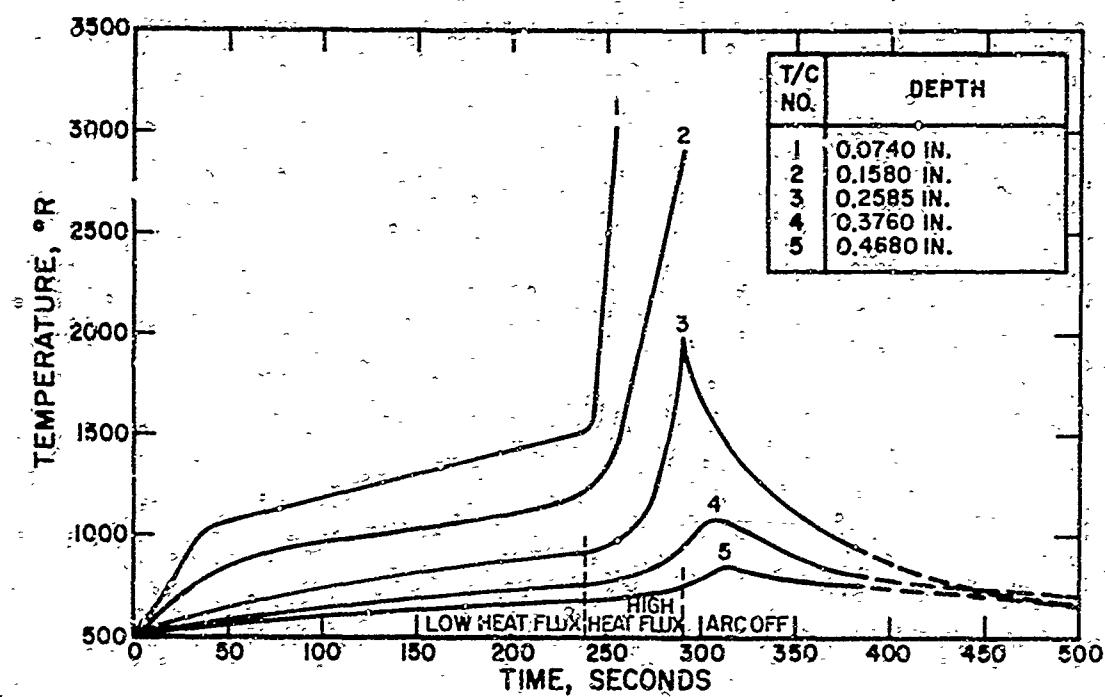
Figure 61. Thermocouple Response Specimen A3-4 Run 22-70
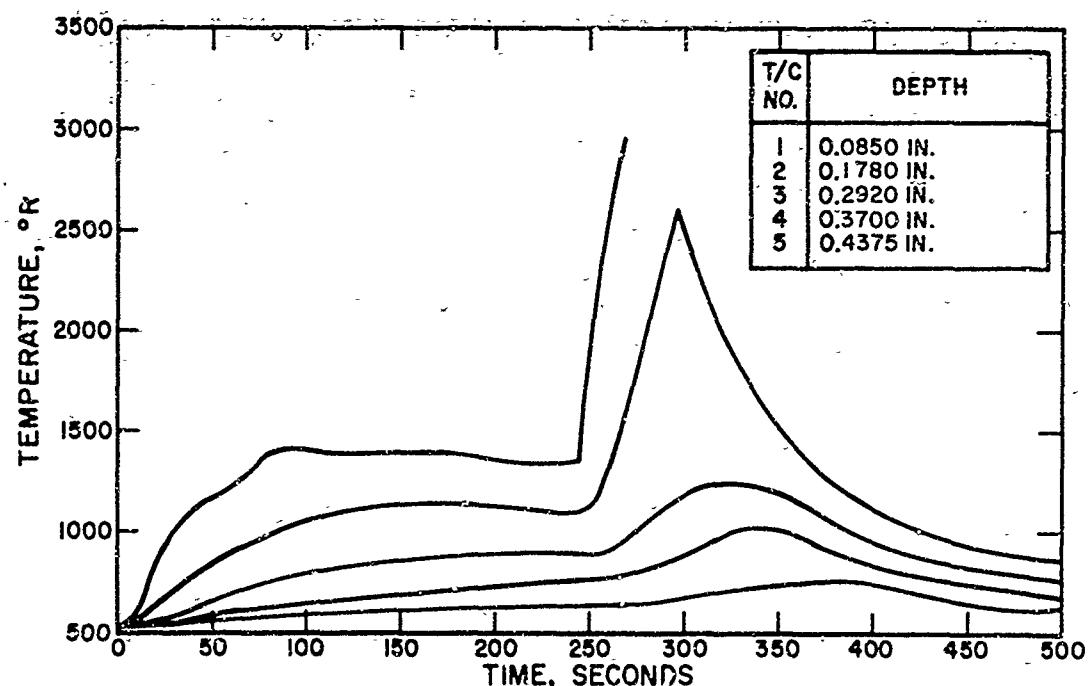
Figure 62. Thermocouple Response Specimen A2-2 Run 23-70

69
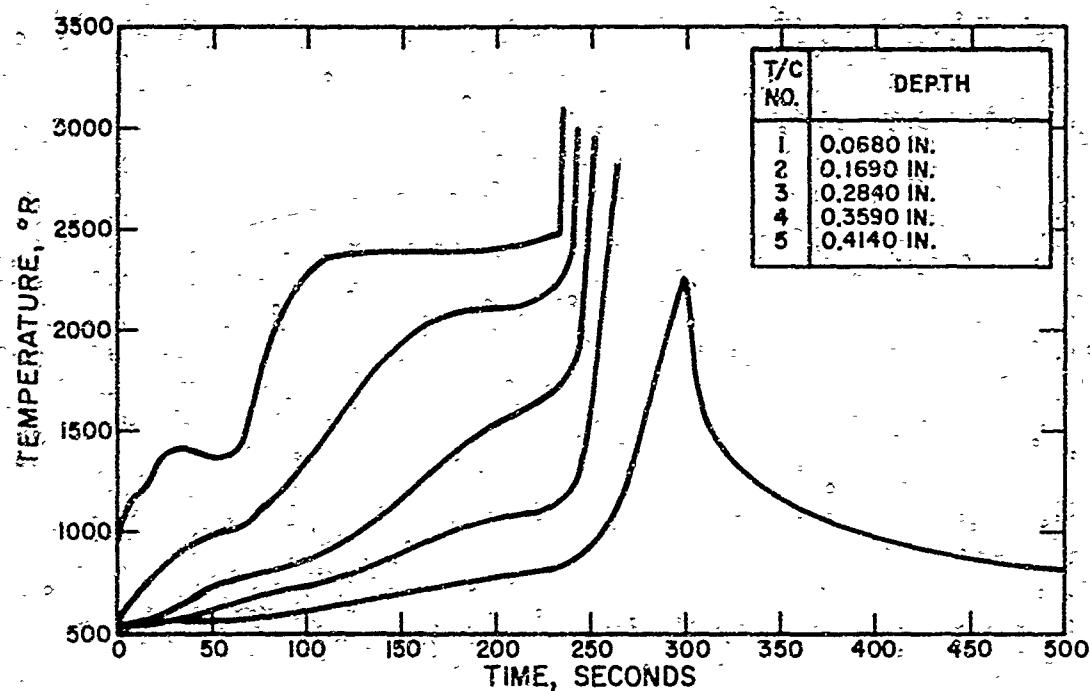
Figure 63.   Thermocouple Response Specimen C4-2 Run 25-70
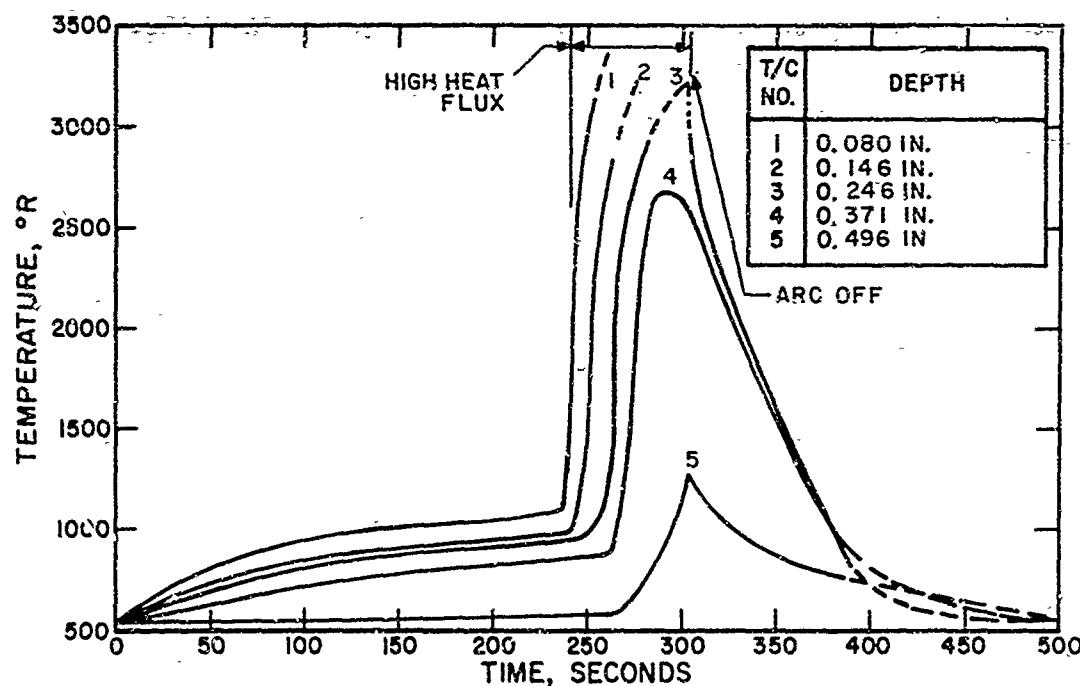
Figure 64.   Thermocouple Response Specimen C1-6 Run 49-70

70
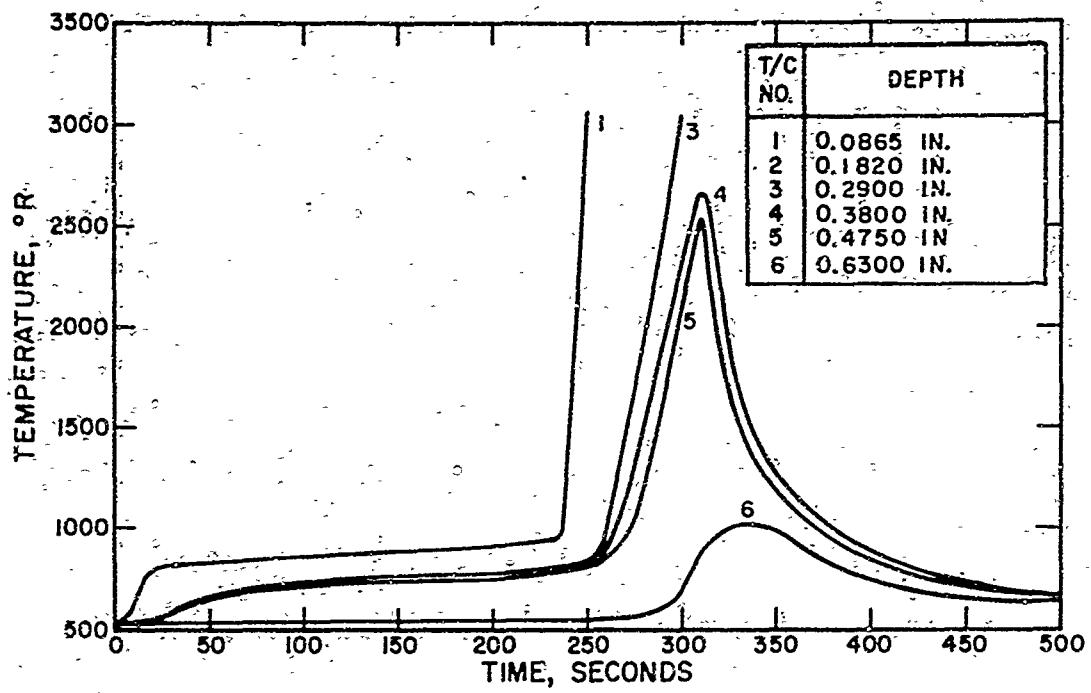
Figure 65. Thermocouple Response Specimen C1-8 Run 60-70
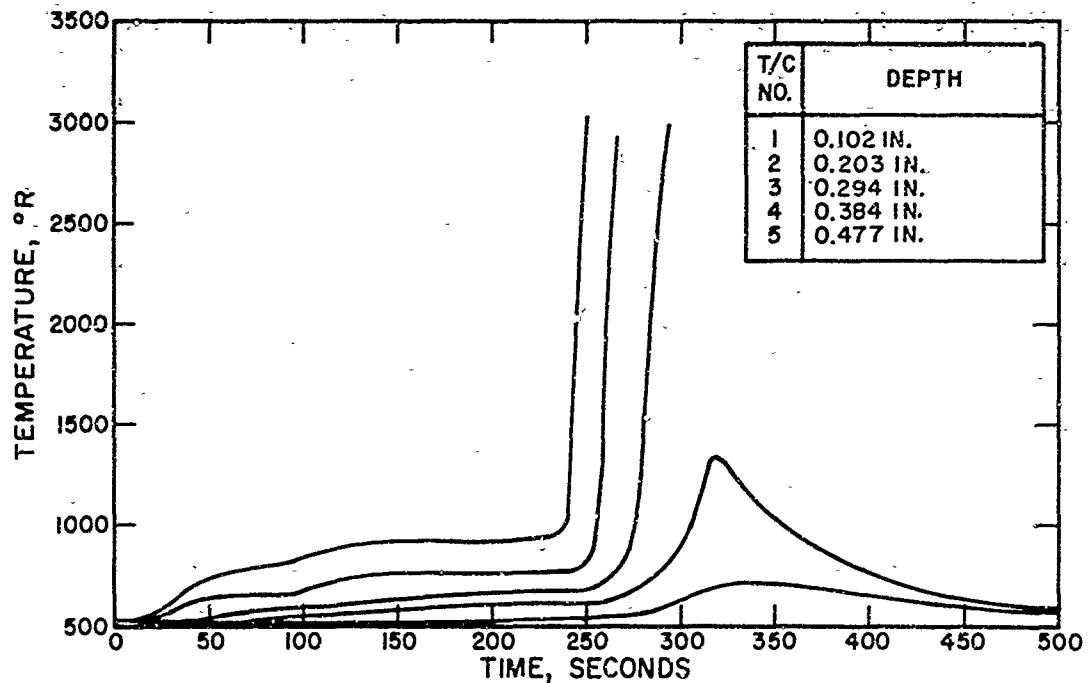
Figure 66. Thermocouple Response Specimen DCM-1 Run 61-70

71
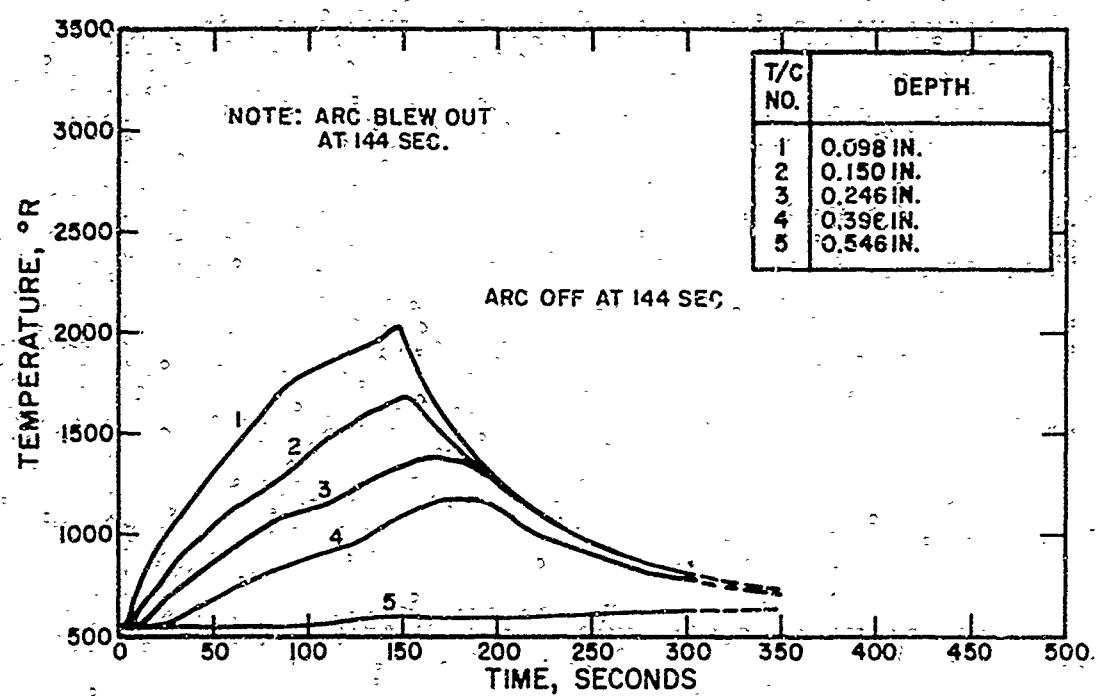
Figure 67. Thermocouple Response Specimen C5-1 Run 62-70
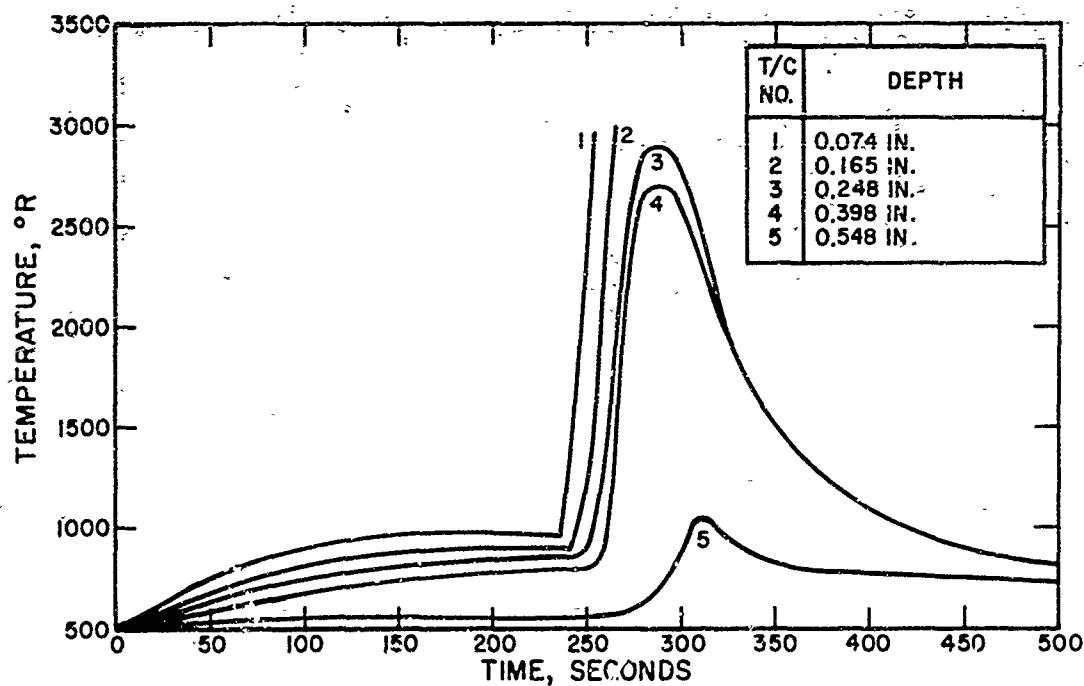
Figure 68. Thermocouple Response Specimen C5-2 Run 63-70

72
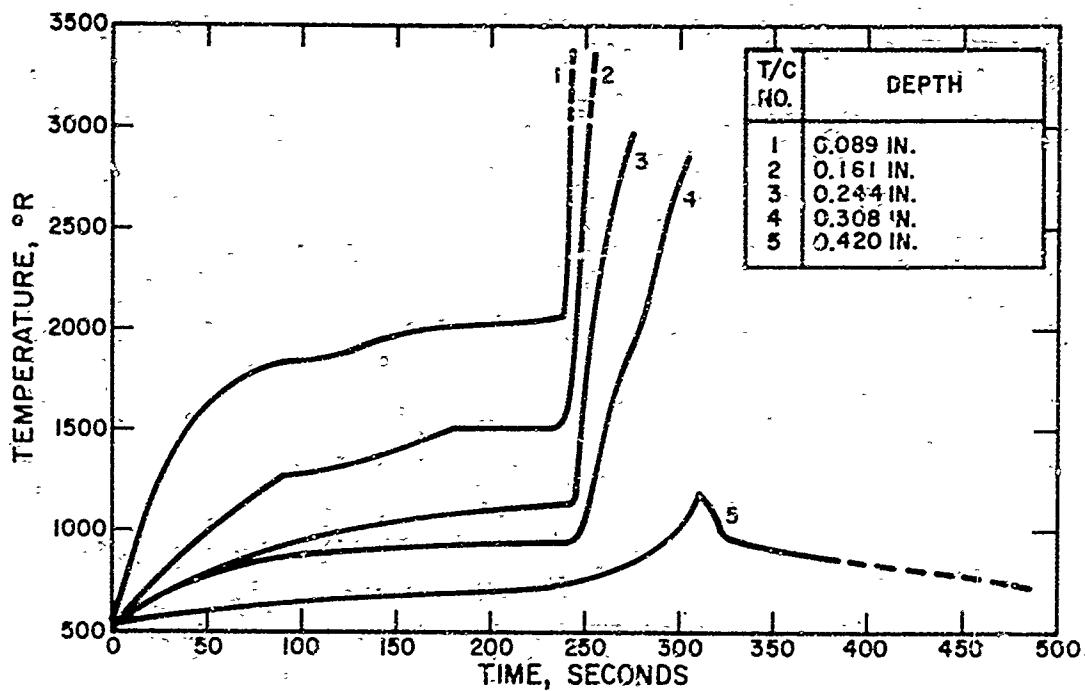
Figure 69. Thermocouple Response Specimen R2-9 Run 64-70

T/C NO.	DEPTH
1	0.089 IN.
2	0.161 IN.
3	0.244 IN.
4	0.308 IN.
5	0.420 IN.
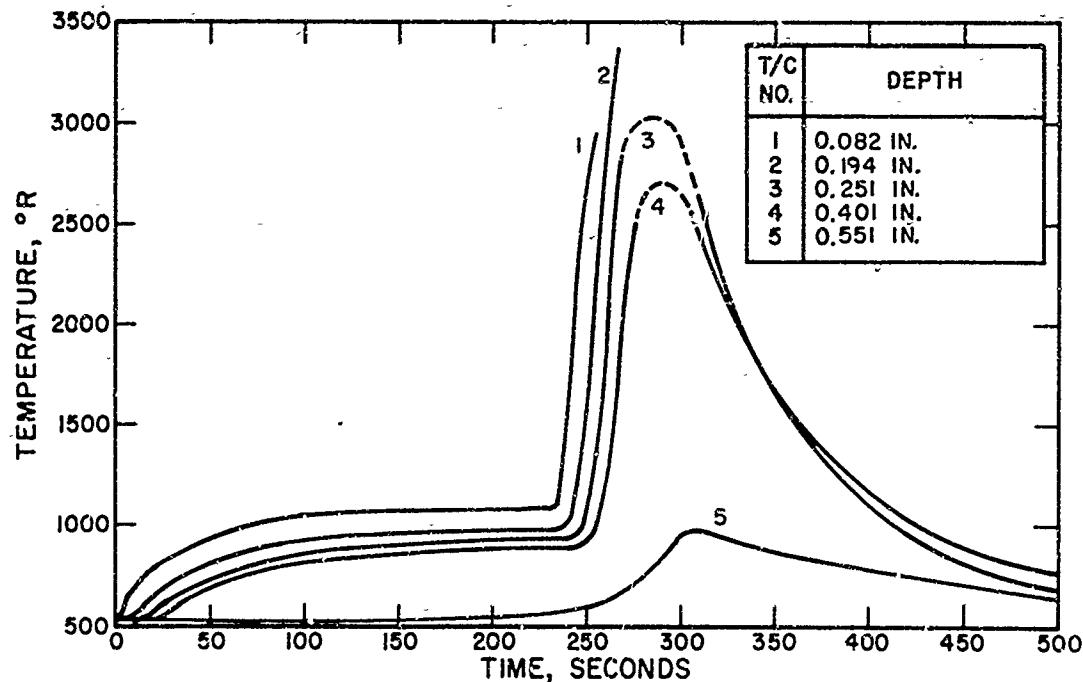
Figure 70. Thermocouple Response Specimen C1-7 Run 65-70

T/C NO.	DEPTH
1	0.082 IN.
2	0.194 IN.
3	0.251 IN.
4	0.401 IN.
5	0.551 IN.
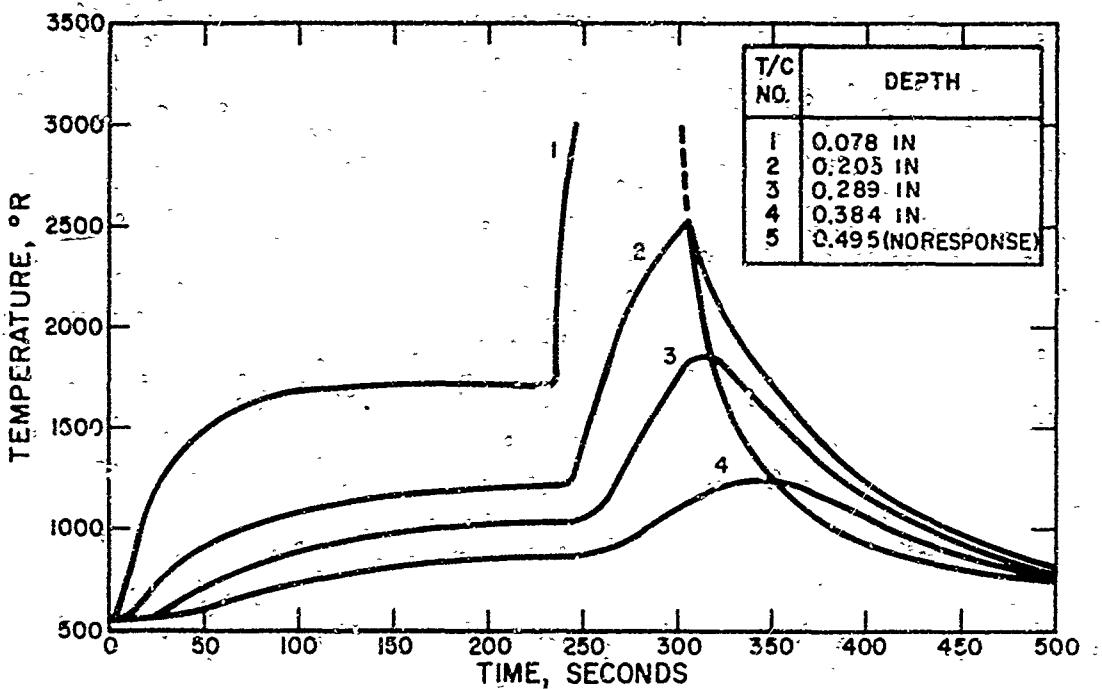
Figure 71. Thermocouple Response – Specimen A7-1 (Run 4-71)
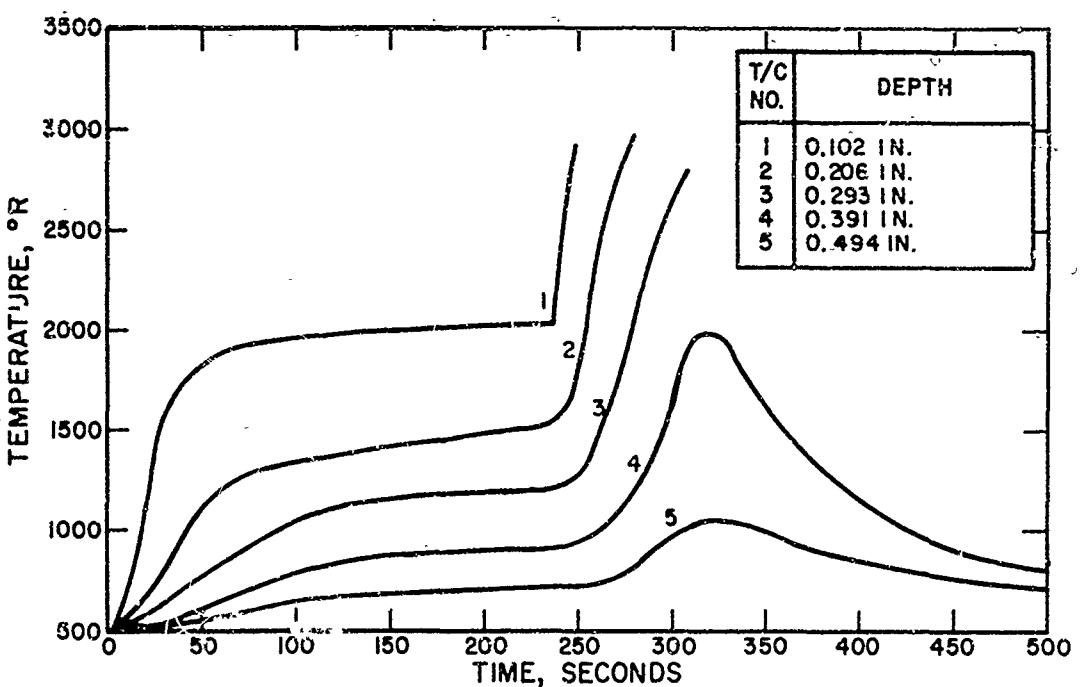
Figure 72. Thermocouple Response – Specimen A7-3 (Run 6-71)

74
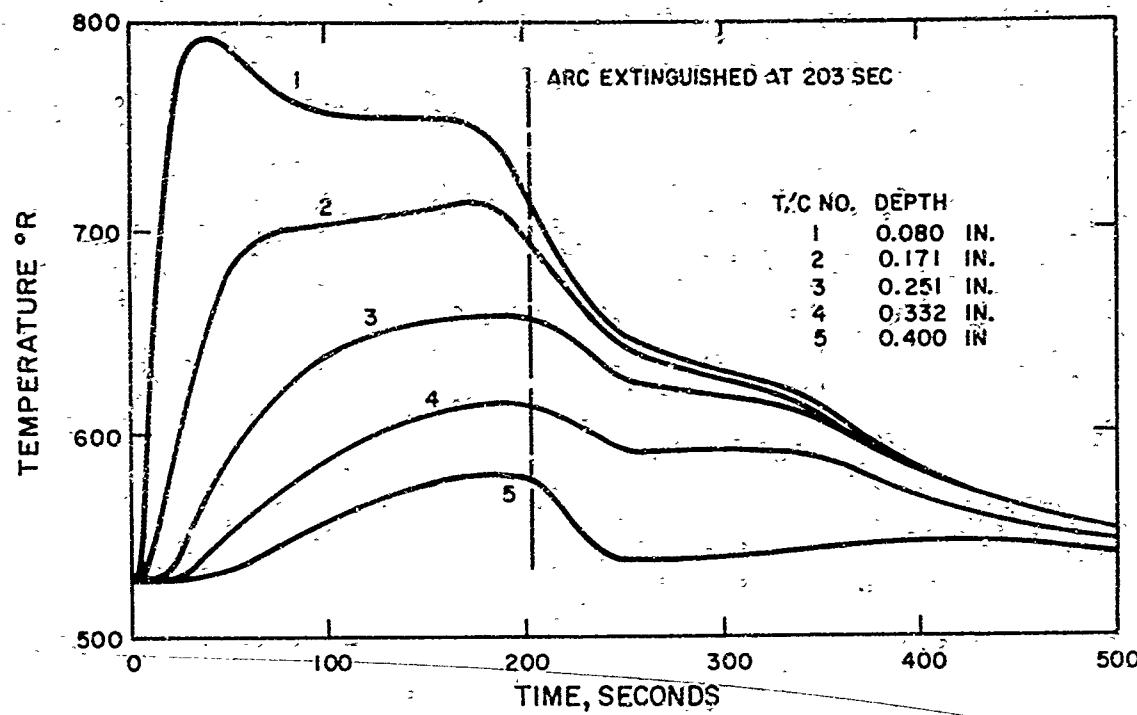
Figure 73.   Thermocouple Response Specimen GEM-2 Run No. 7-71
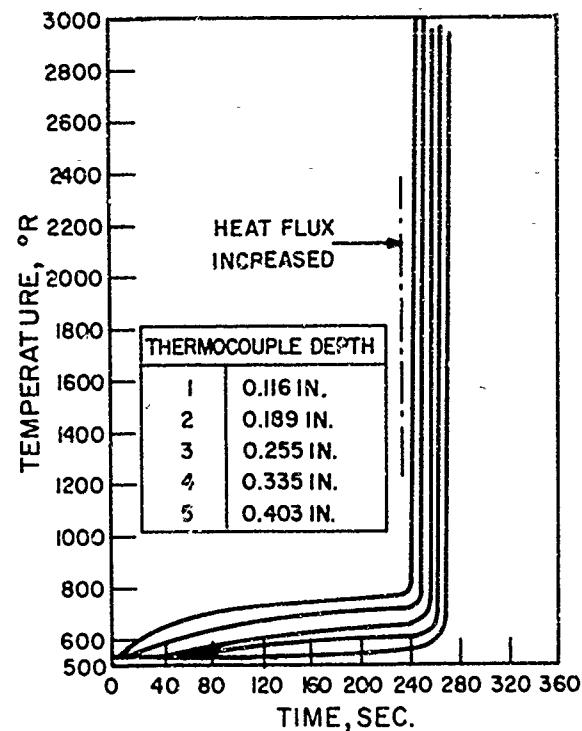
Figure 74.   Thermocouple Response Specimen GEM-1 Run No. 8-71

75
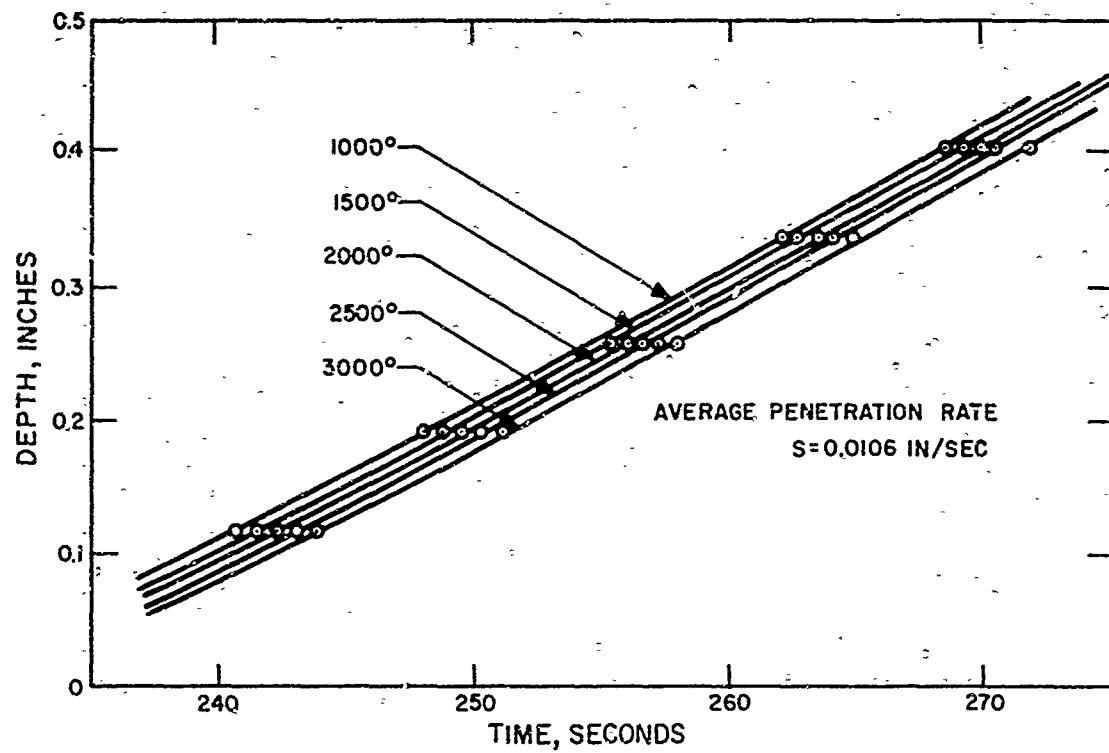
Figure 75. Thermocouple Isotherms Specimen GEM-1 Run No. 8-71
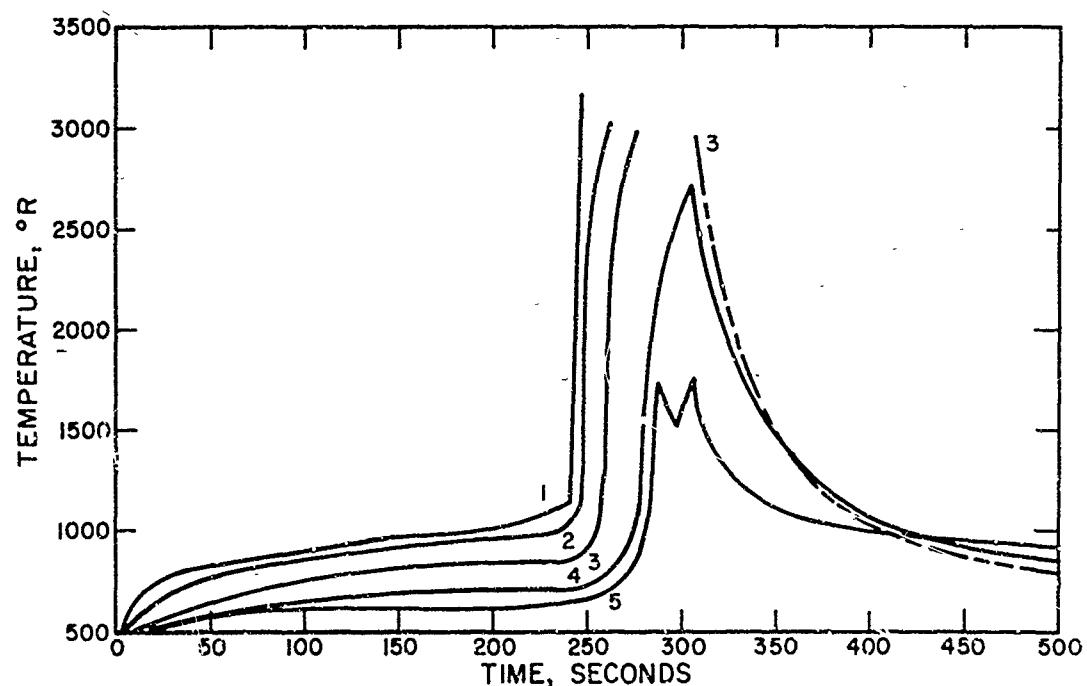
Figure 76. Thermocouple Response Specimen C4-1A Run No. 9-71

76
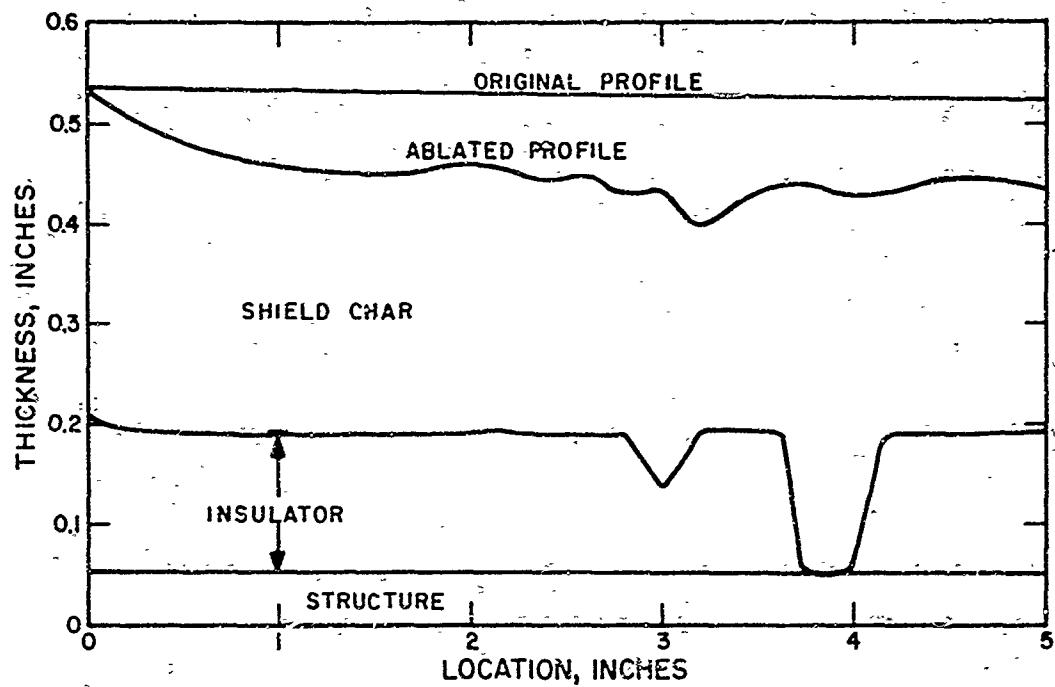
Figure 77. Recession Profile Specimen C1-5 Run 15-70
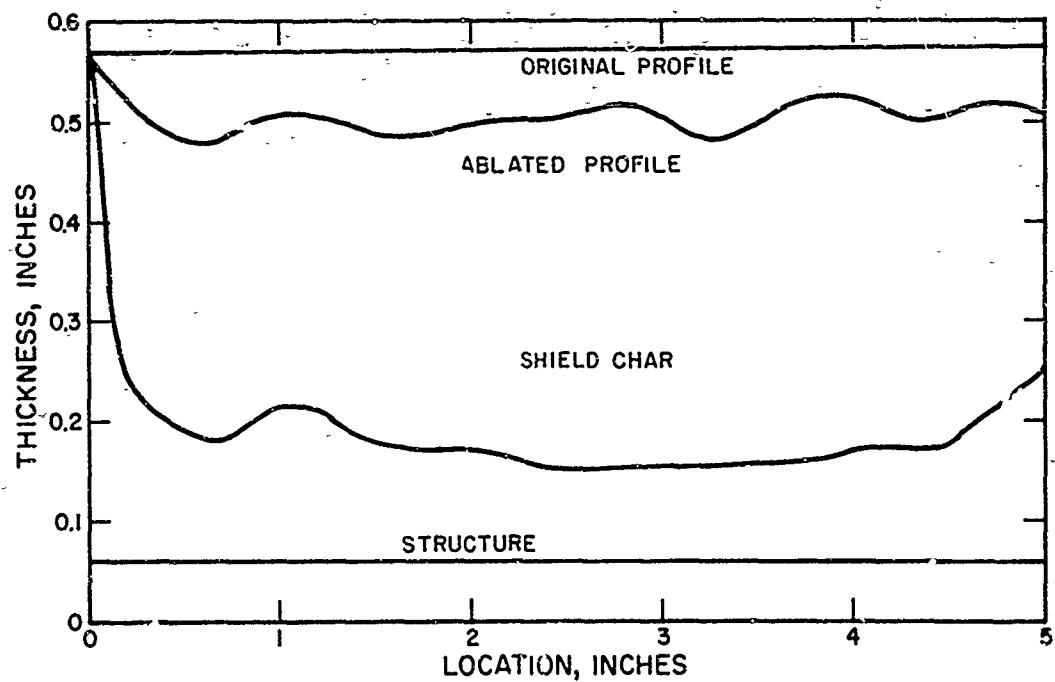
Figure 78. Recession Profile Specimen A4-3 Run 16-70

77
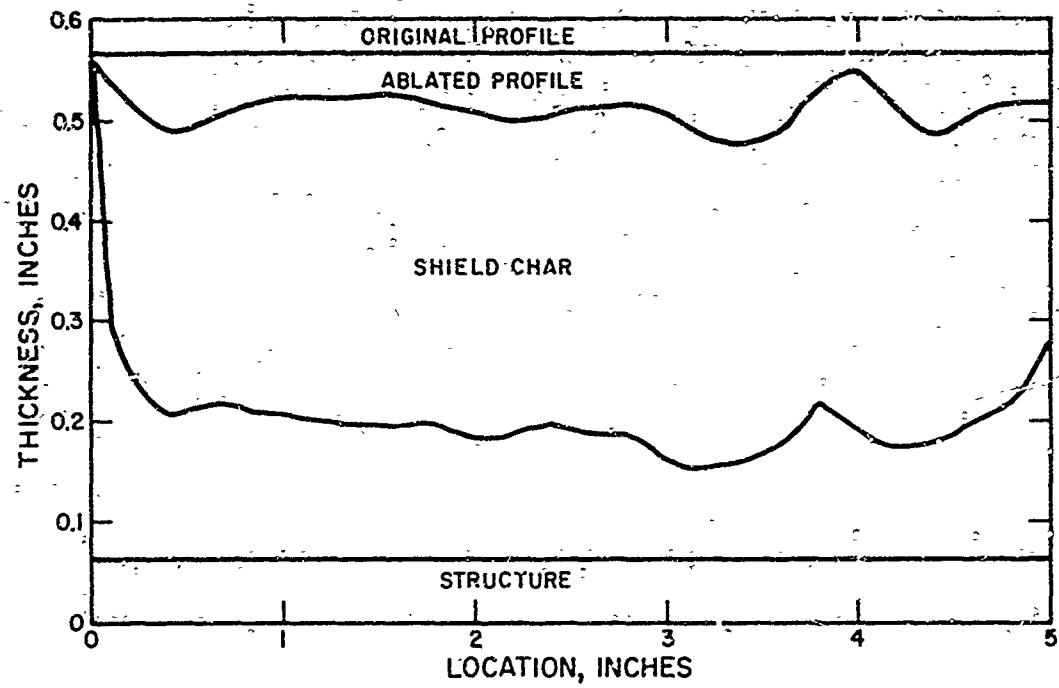
Figure 79. Recession Profile Specimen A4-4 Run 17-70
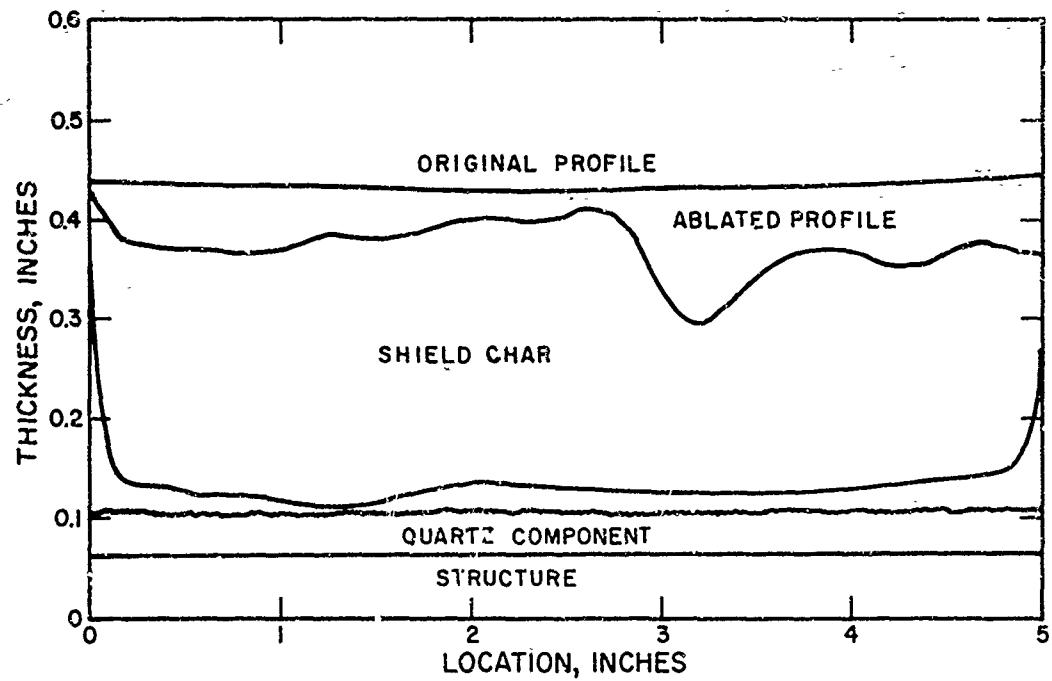
Figure 80. Recession Profile Specimen C4-1 Run 19-70
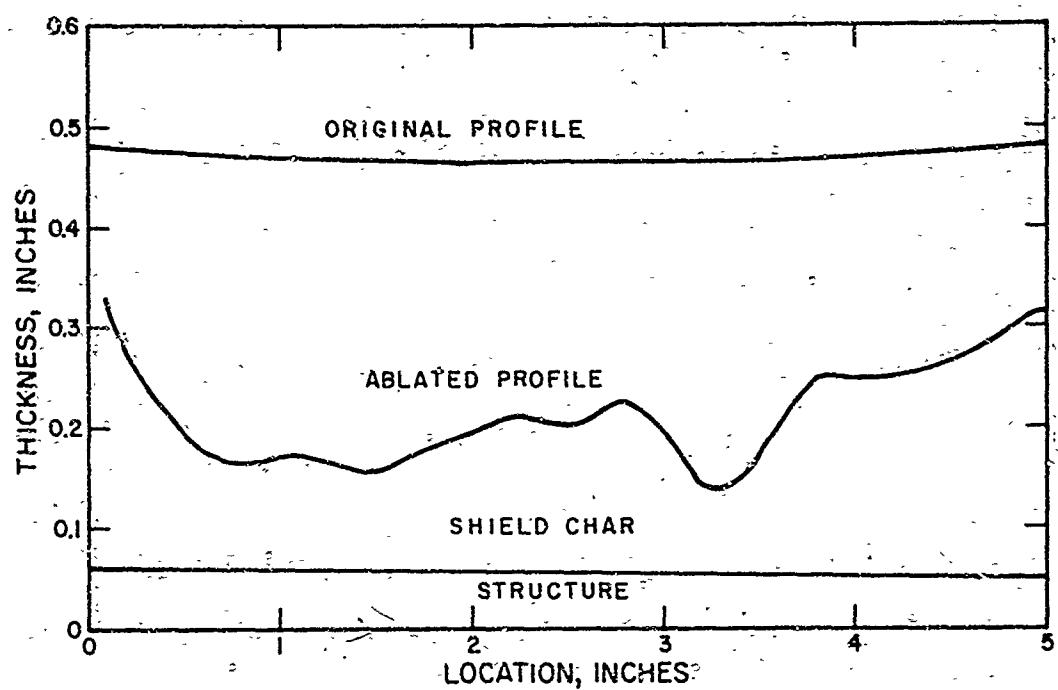
Figure 81. Recession Profile Specimen A4-2B Run 20-70
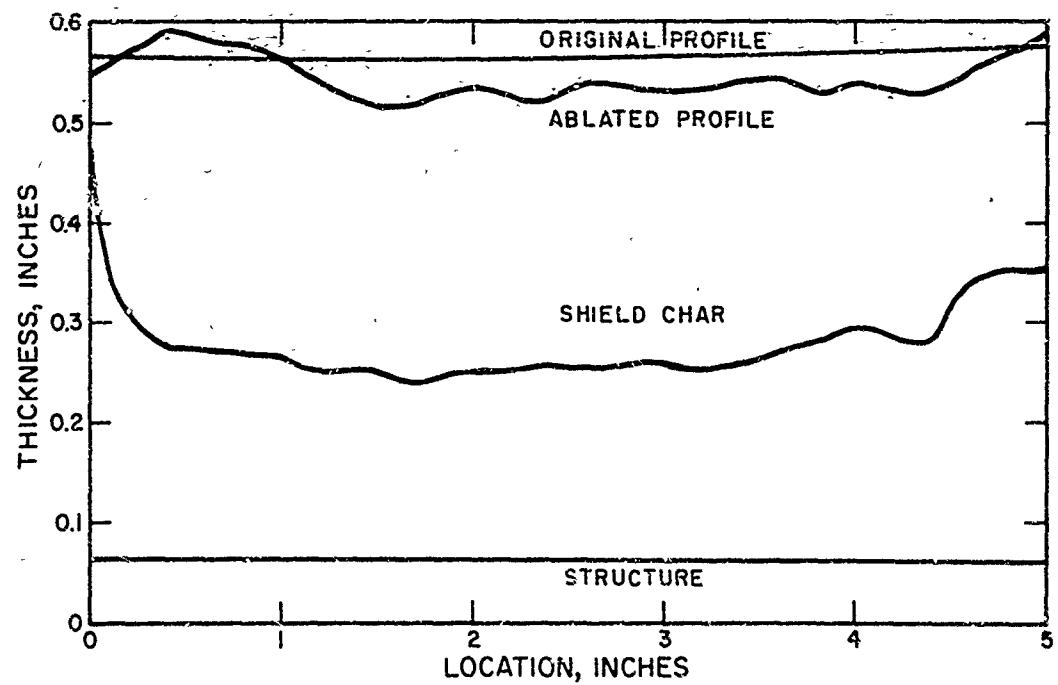
Figure 82. Recession Profile Specimen A3-4 Run 22-70

79
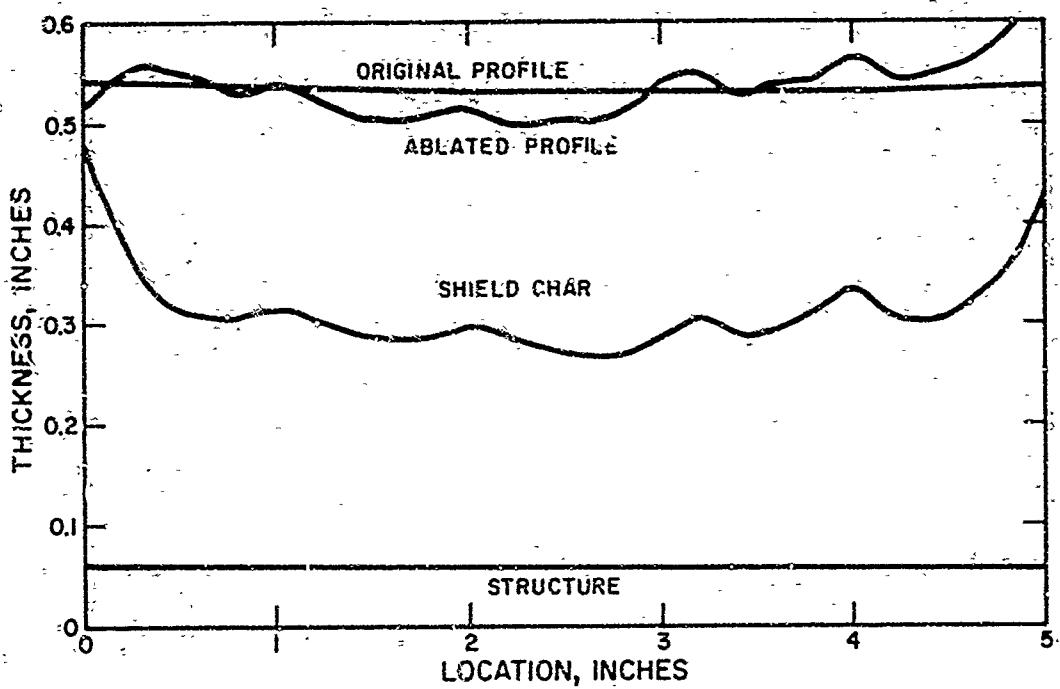
Figure 83. Recession Profile Specimen A2-2 Run 23-70
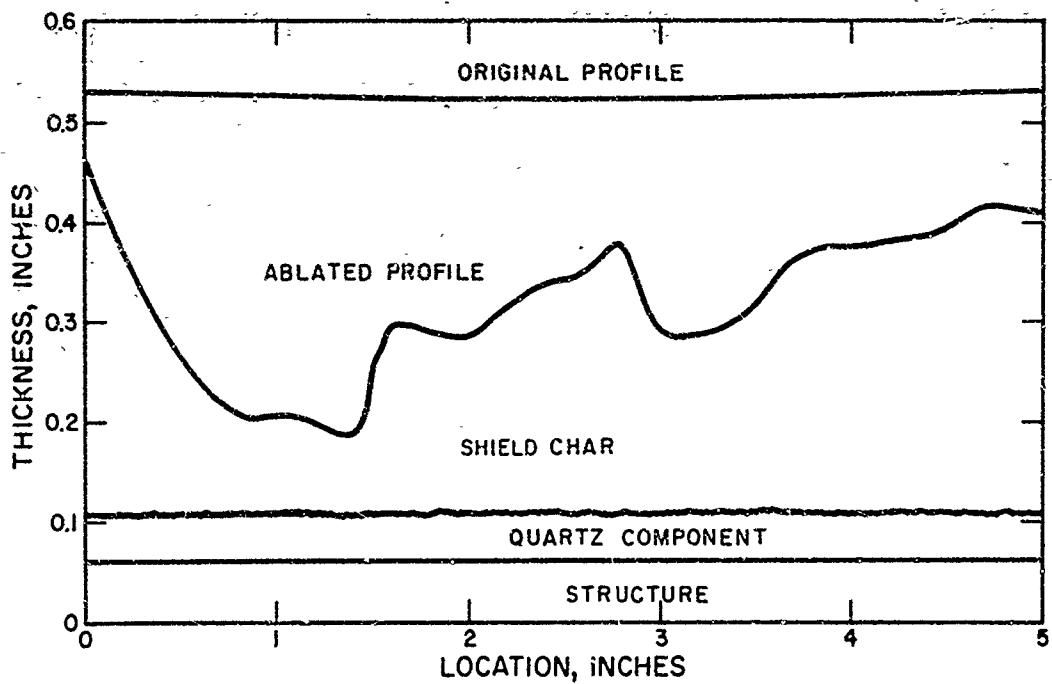
Figure 84. Recession Profile Specimen C4-2 Run 25-70

80

ORIGINAL SURFACE PROFILE

ABLATED PROFILE

THICKNESS, INCHES

SHIELD MAT'L

NOTE: CHAR HAD
PENETRATED
SHIELD COMPLETELY

INSULATOR

(BARRIER)

INSULATOR

+NORMAL T/C DEPTHS

STRUCTURE - 0.062 IN. (AL)

LOCATION, INCHES
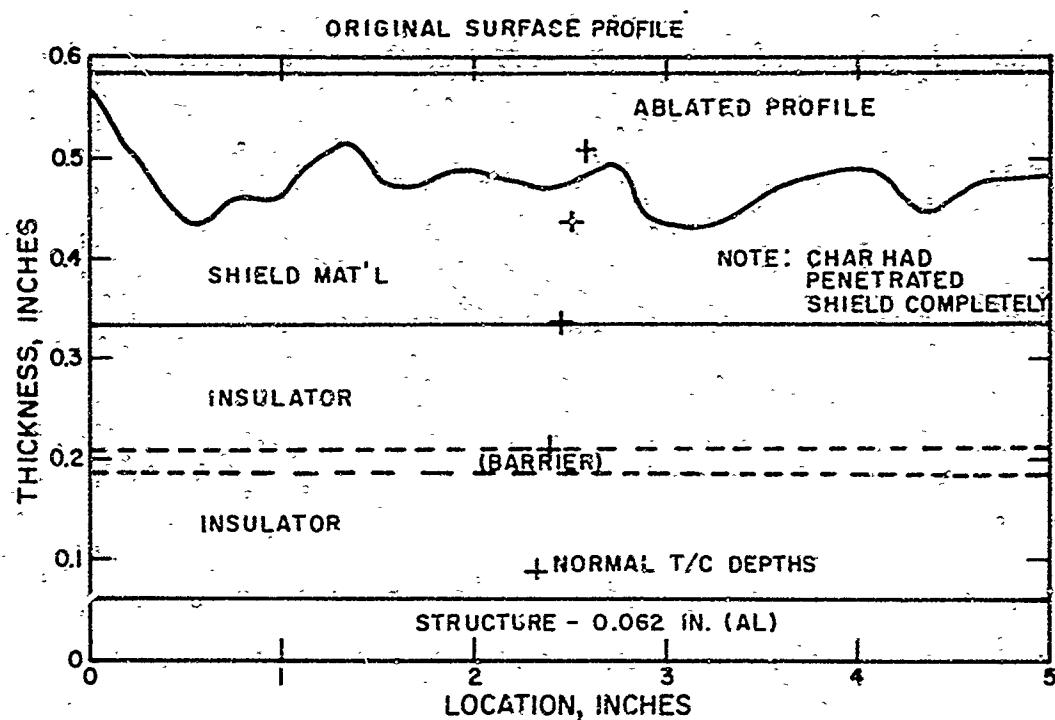
Figure 85. Recession Profile Specimen C1-6 Run 49-70

ORIGINAL SURFACE PROFILE

ABLATED SHIELD

THICKNESS, INCHES

SHIELD MAT'L

+ NOMINAL T/C DEPTHS

INSULATOR - INCLUDING BARRIER LAYER

STRUCTURE 0.062 IN (AL)

LOCATION, INCHES
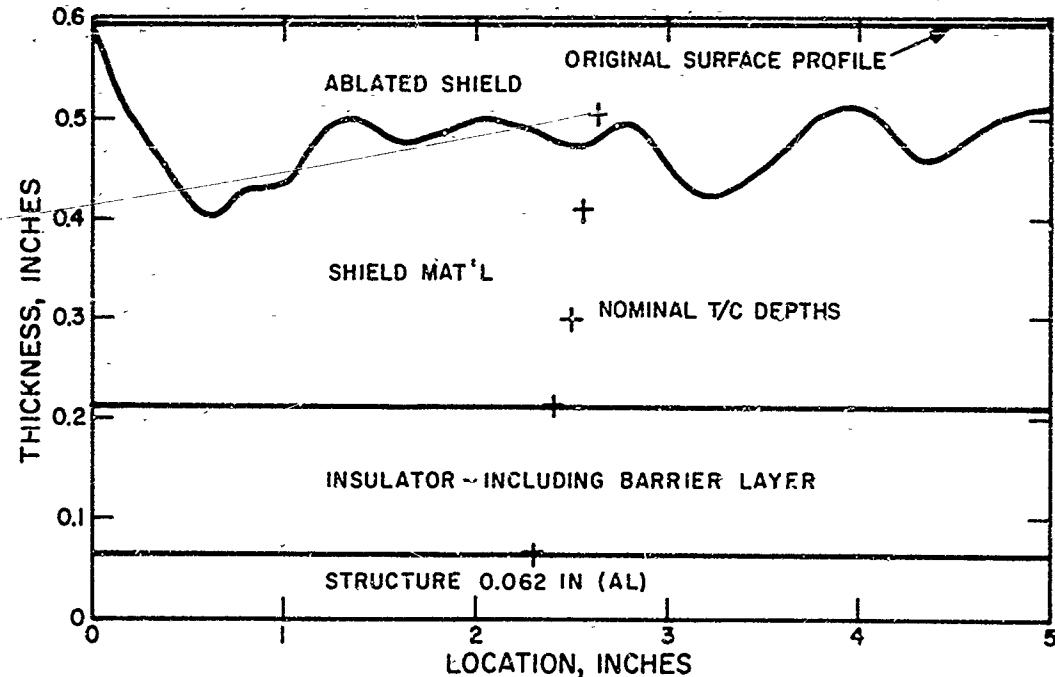
Figure 86. Recession Profile Specimen C1-8 Run 60-70

81
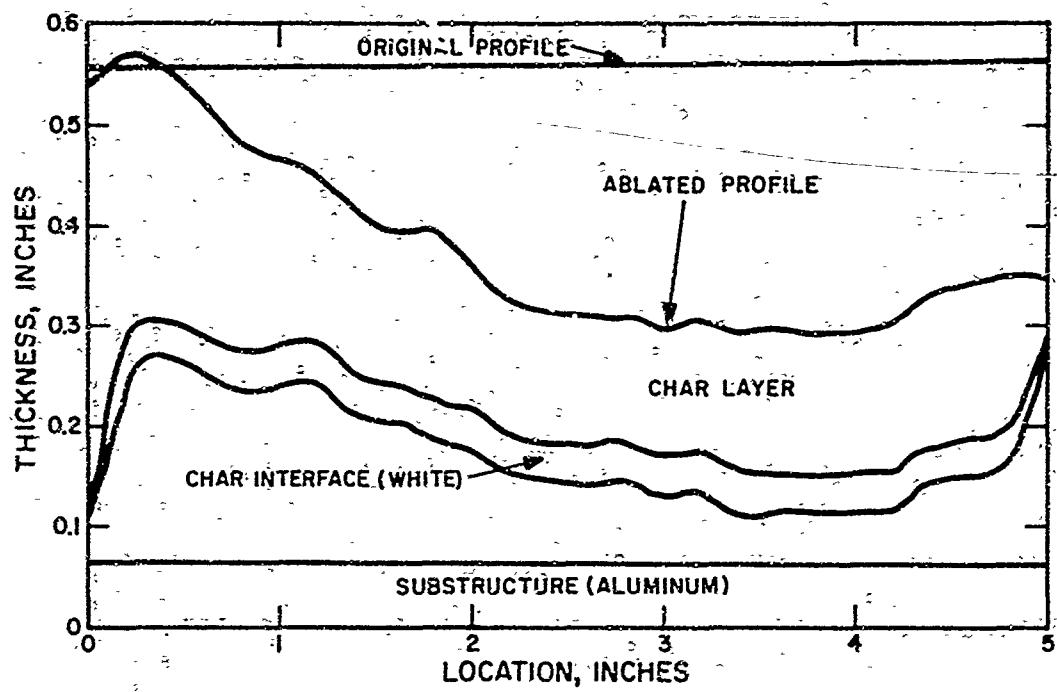
Figure 87. Recession Profile Specimen DCM-1 Run 61
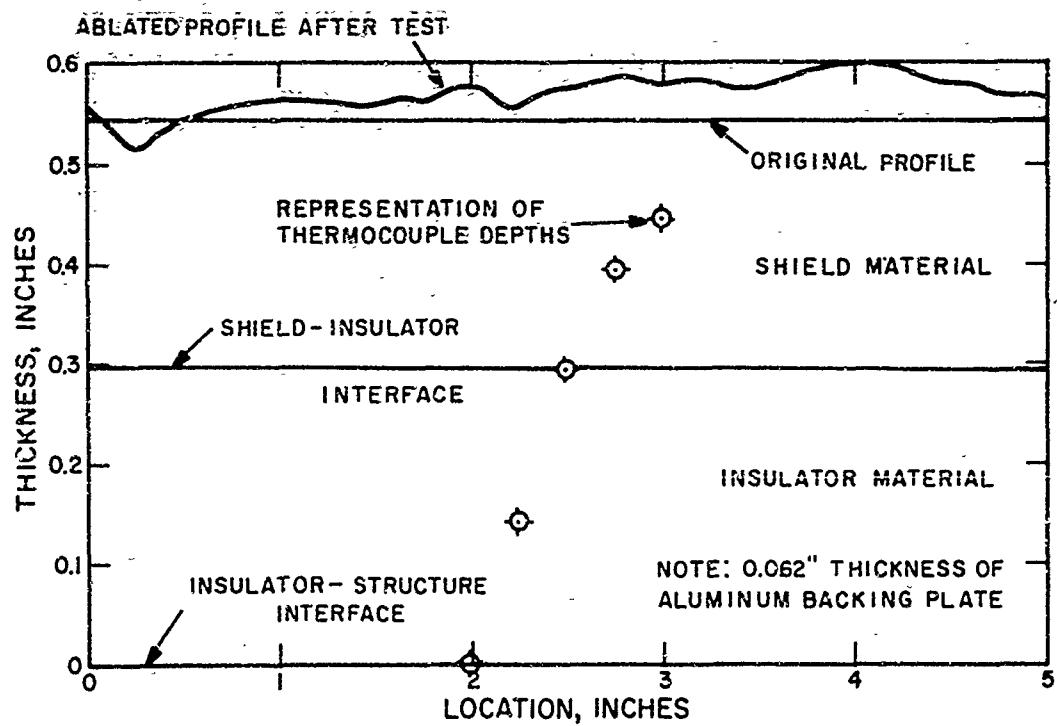
Figure 88. Recession Profile Specimen C5-1 Run 62-70

82
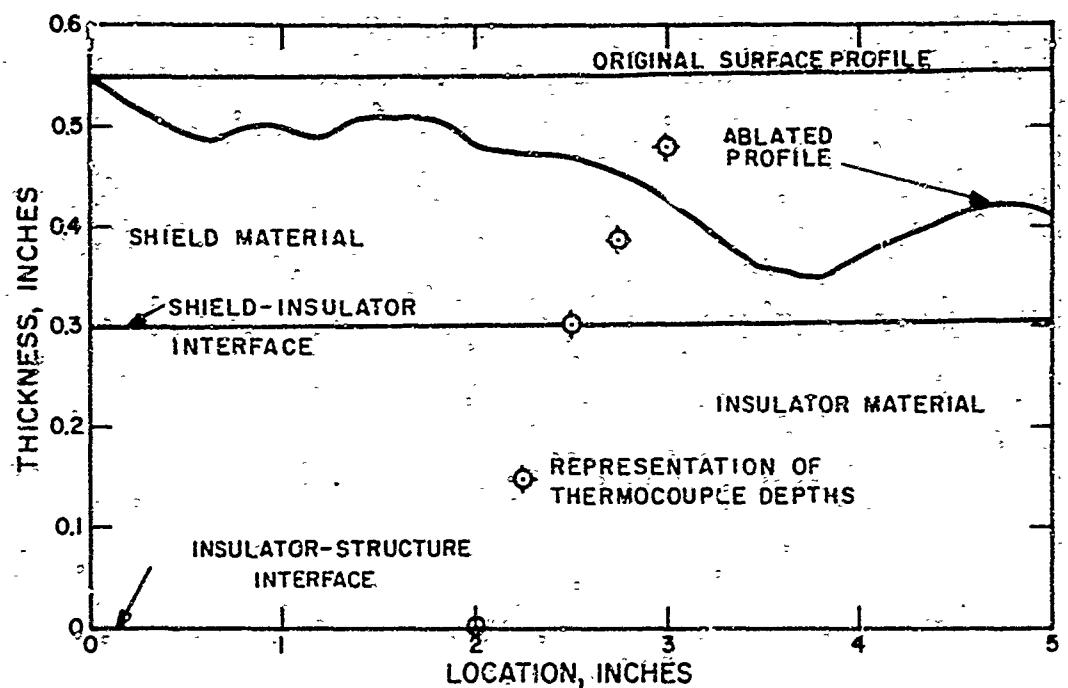
Figure 89. Recession Profile Specimen C5-2 Run 63-60
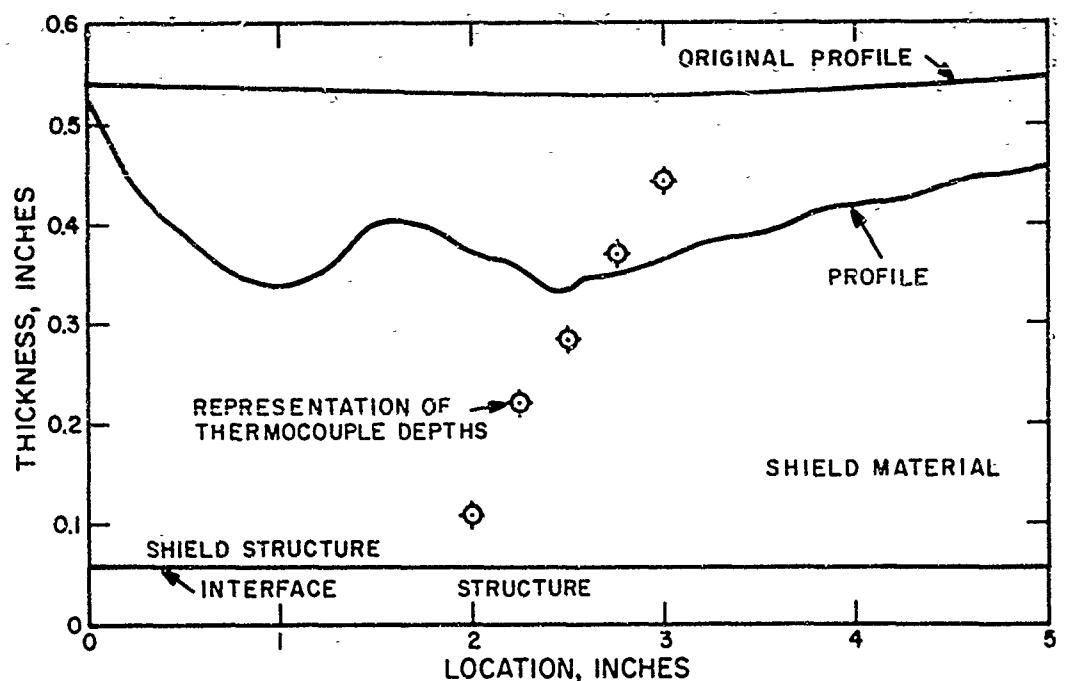
Figure 90. Recession Profile Specimen R2-9 Run 64-70

83
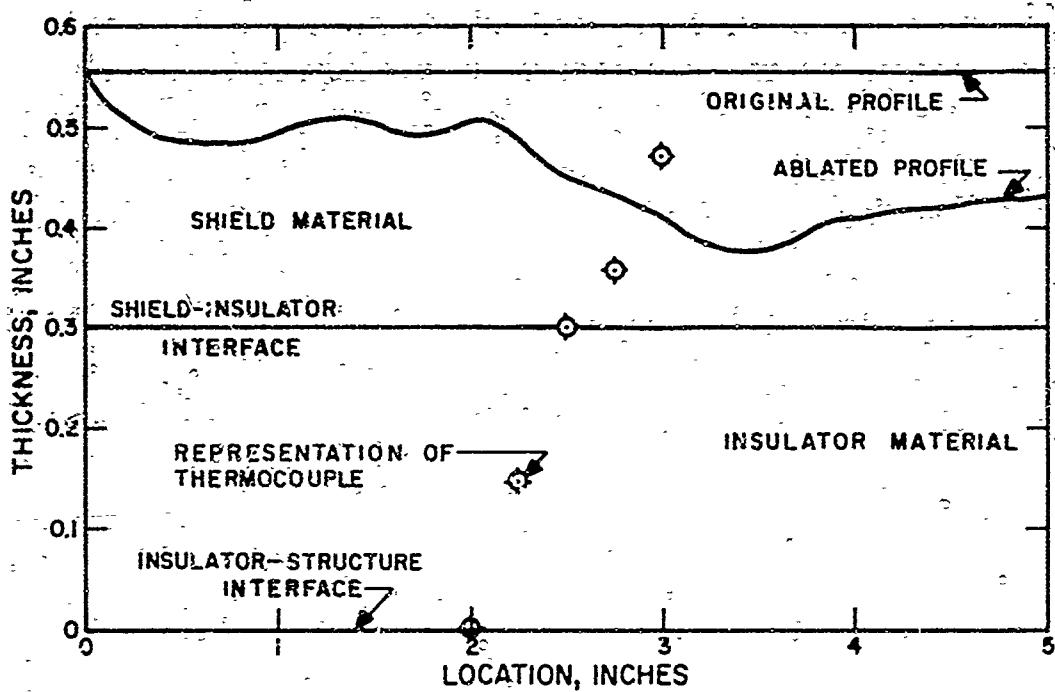
Figure 91. Recession Profile - Specimen C1-7 Run 65-70
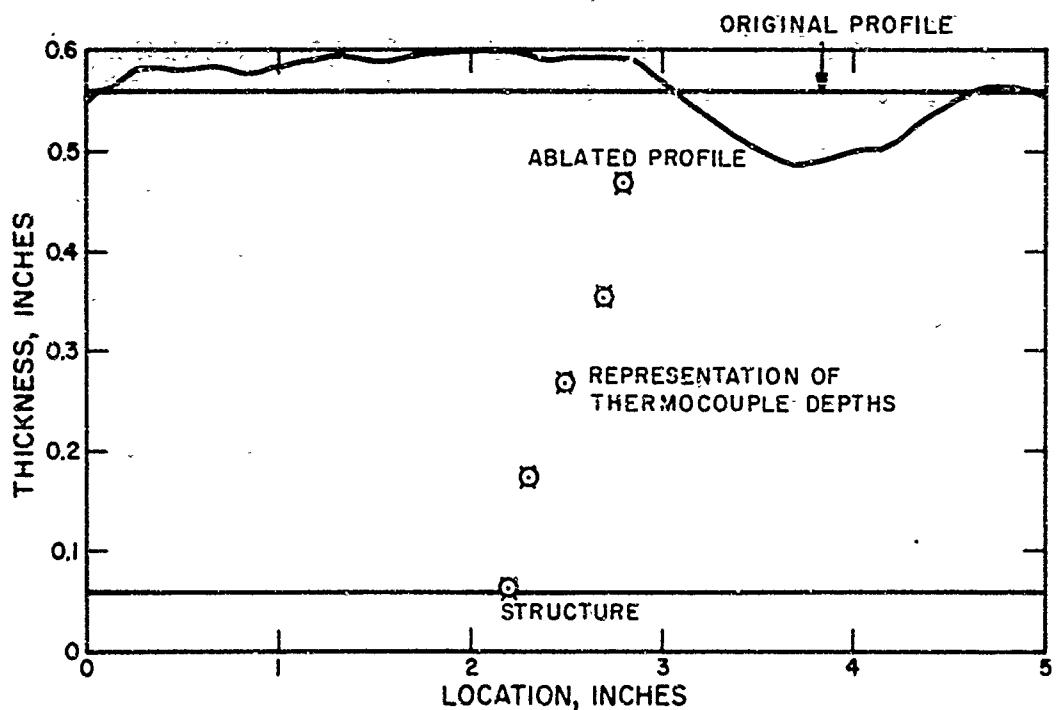
Figure 92. Recession Profile - Specimen A7-1 Run 4-71

84
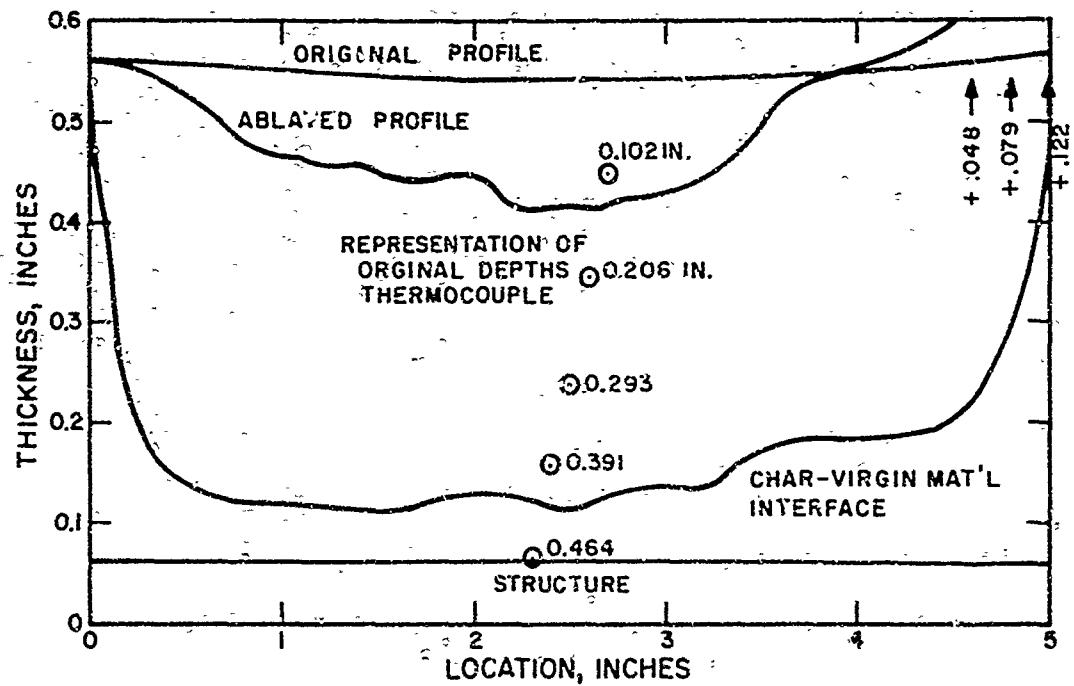
Figure 93. Recession Profile - Specimen A7-3 Run 6-71
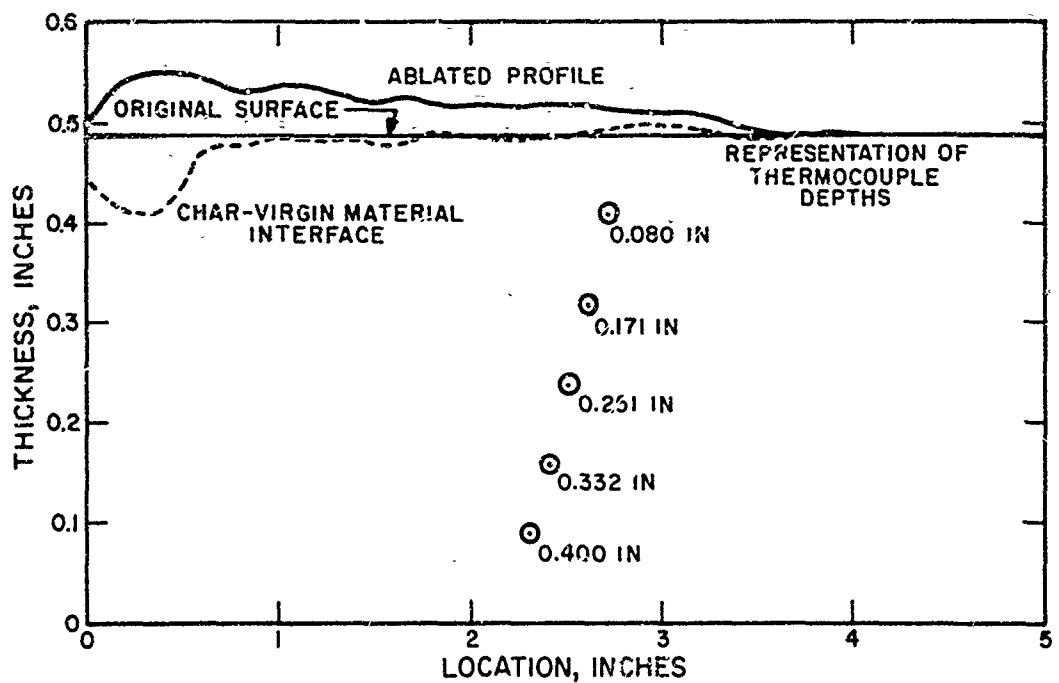
Figure 94. Recession Profile - Specimen GE-M2 Run 7-71

85
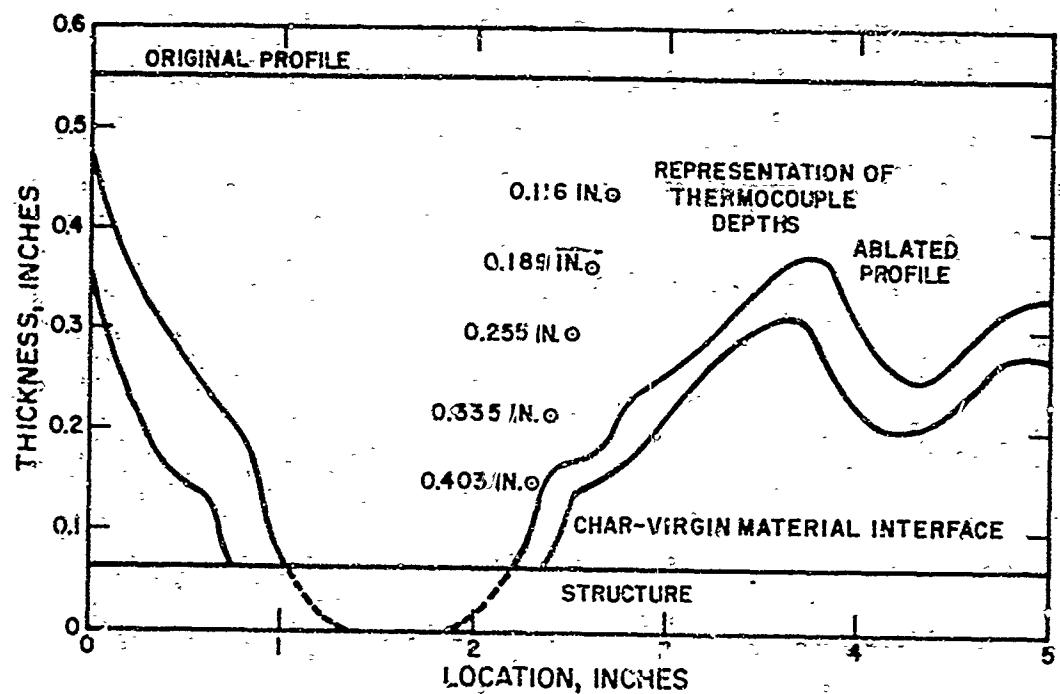
Figure 95. Recession Profile – Specimen GE-M1 Run 8-71
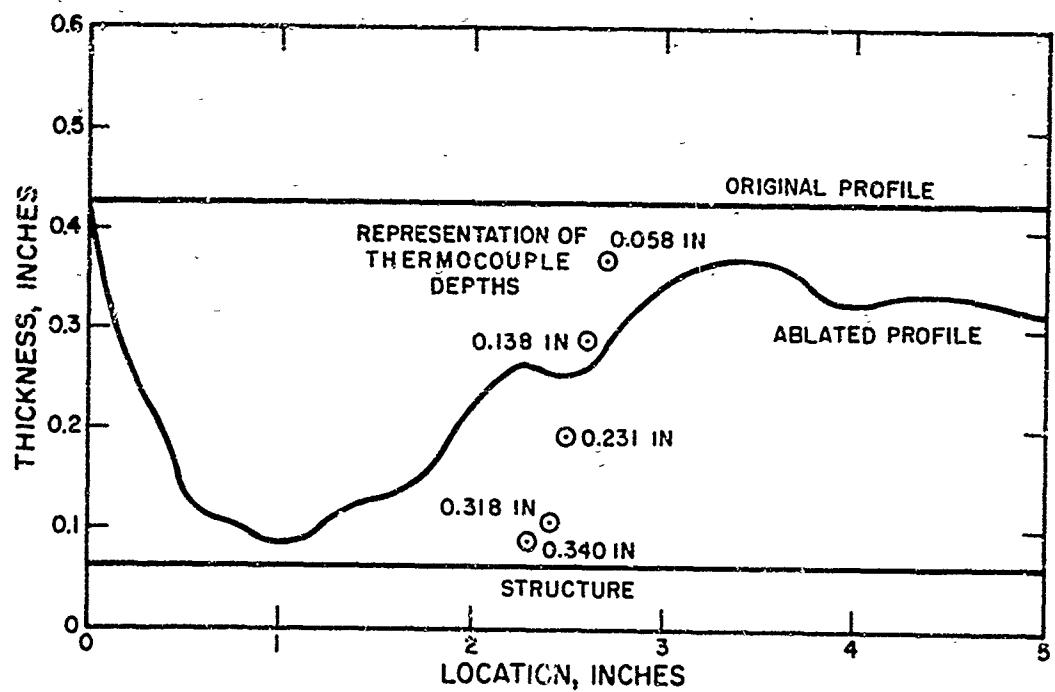
Figure 96. Recession Profile – Specimen C4-1A Run 9-71

86
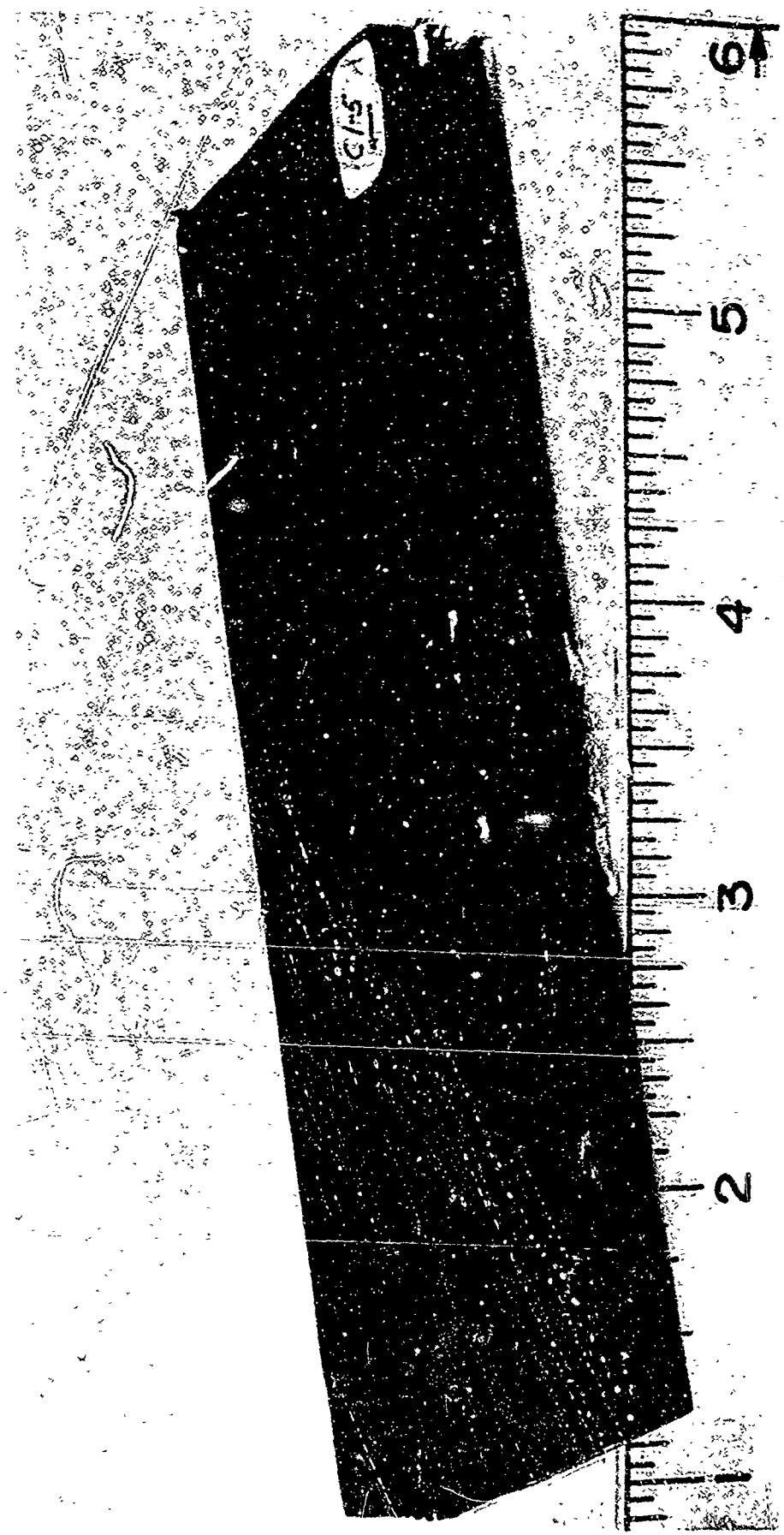
Figure 97. Ablated Specimen – Three Quarter View C1-5

87
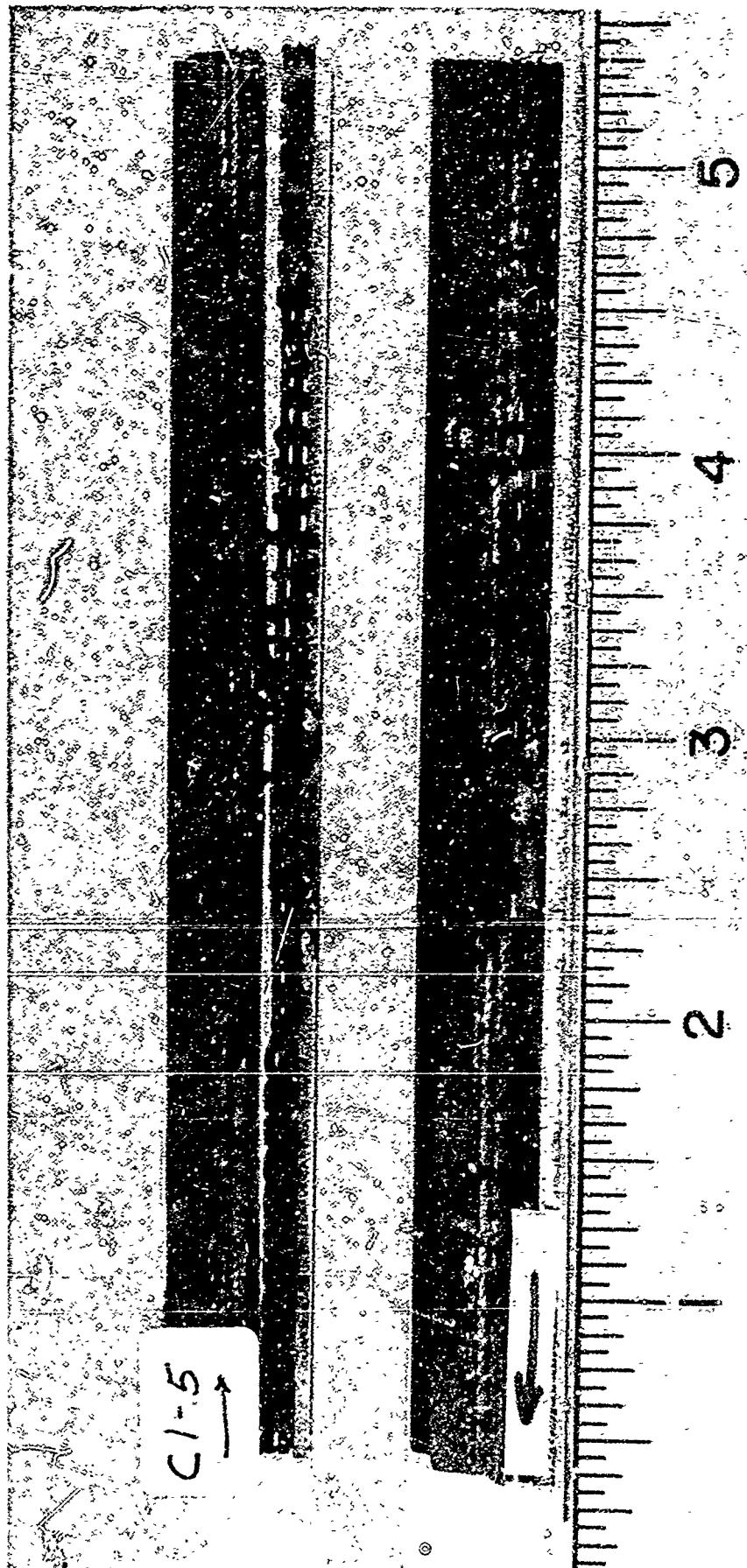
Figure 98. Ablated Specimen – Cross Section C1-5

88
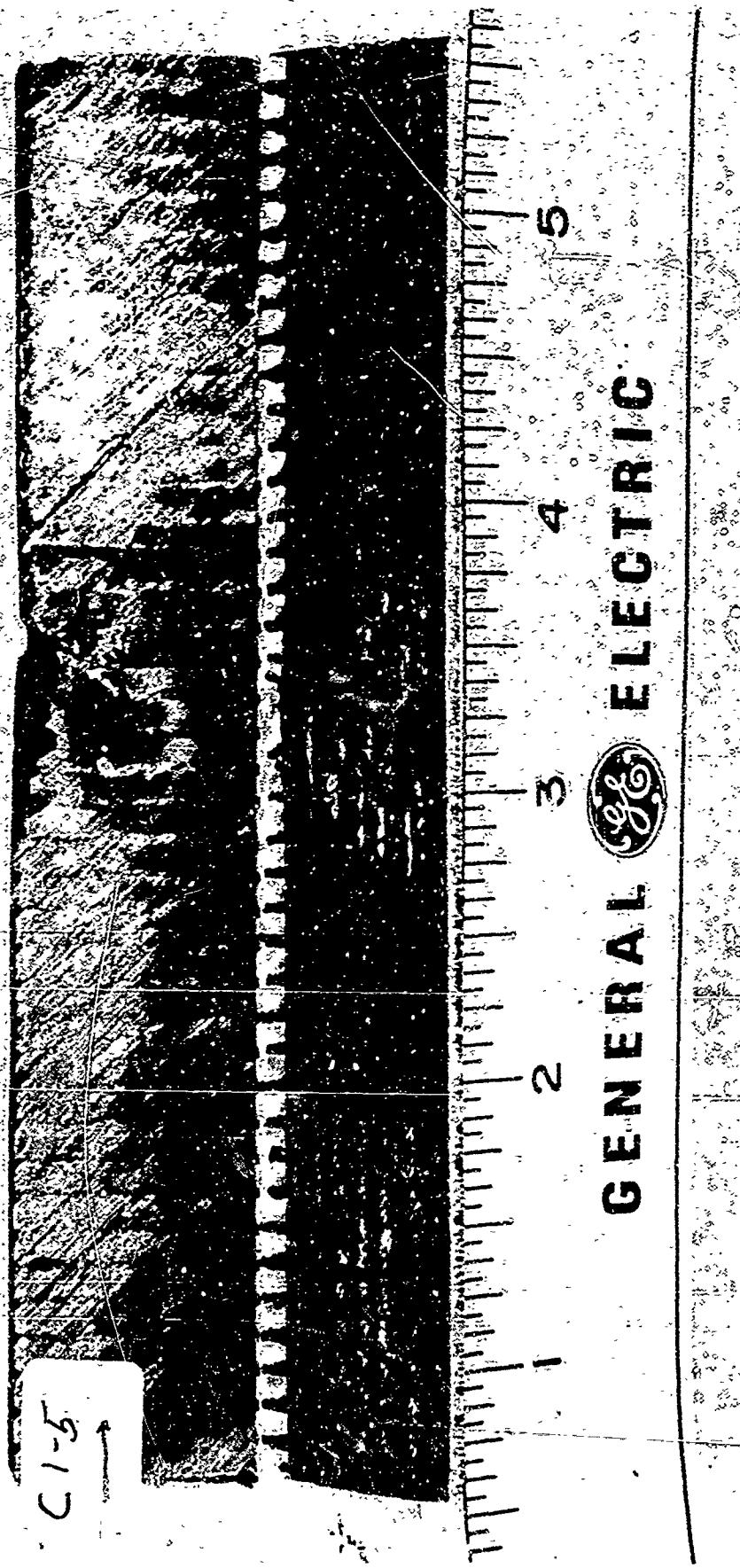
Figure 99. Ablated Specimen – Disassembled C1-5
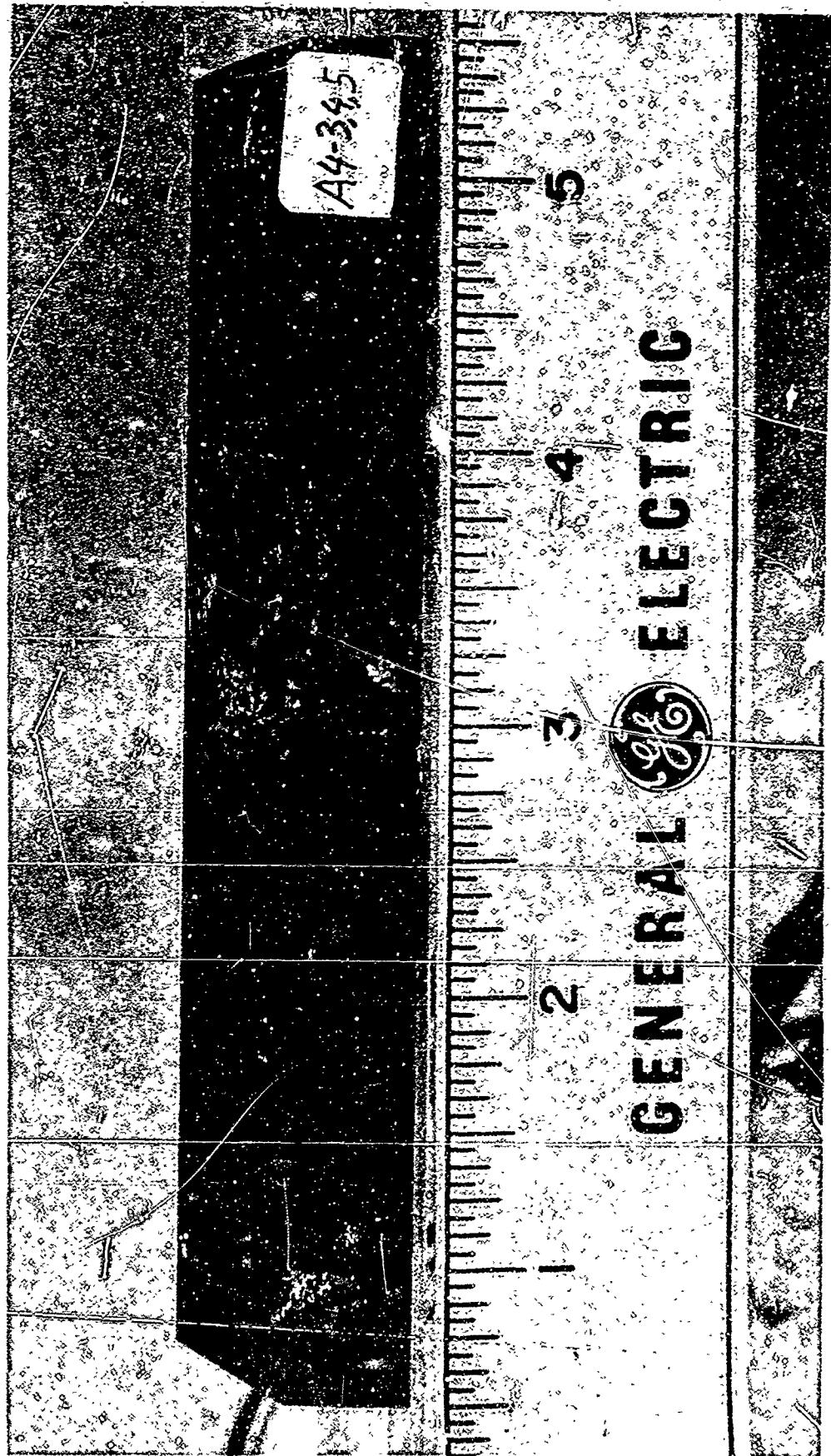
Figure 100. Untested Specimen – Three Quarter View A4–3, 4, 5

A4-3 →
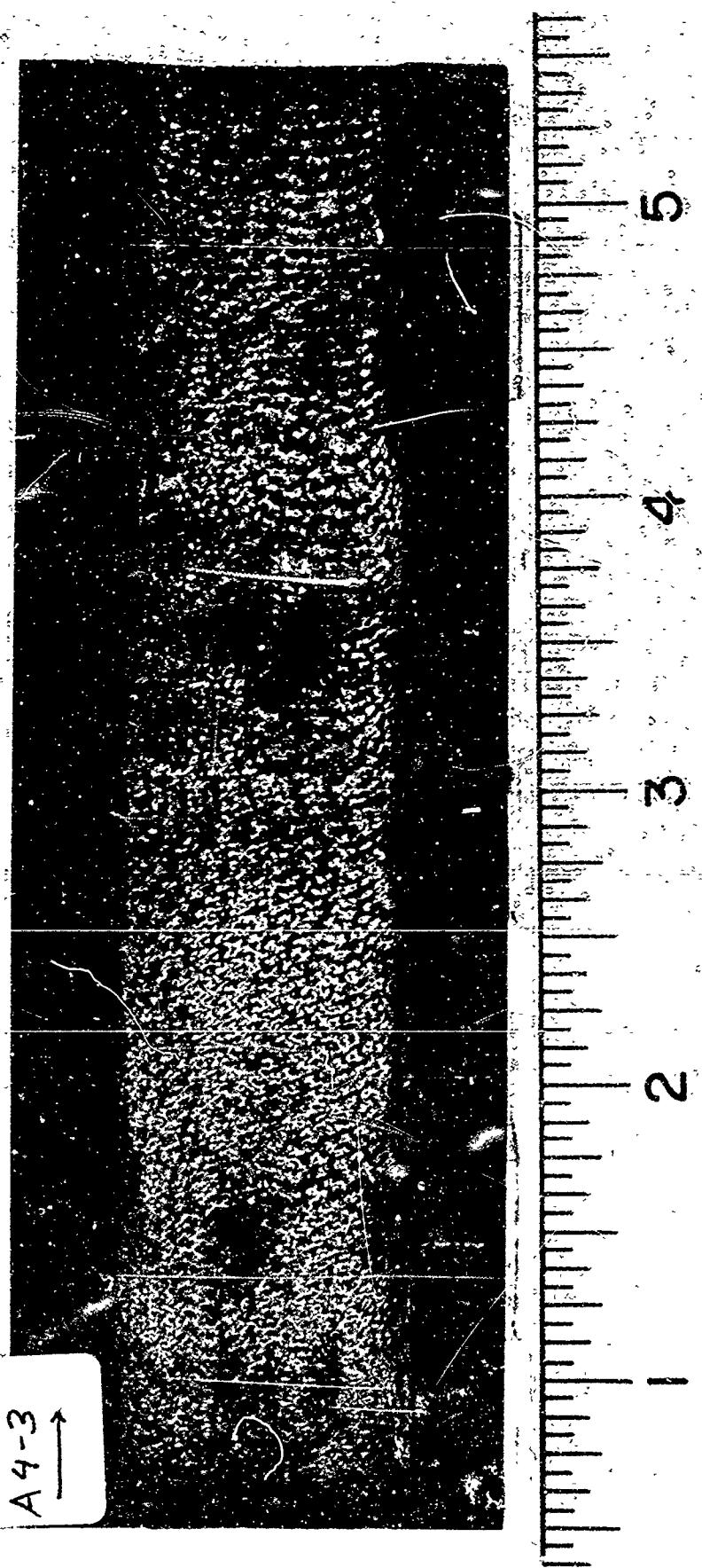
Figure 101. Ablated Specimen – Top View A4-3

91

Figure 102. Ablated Specimen – Top View A4-4
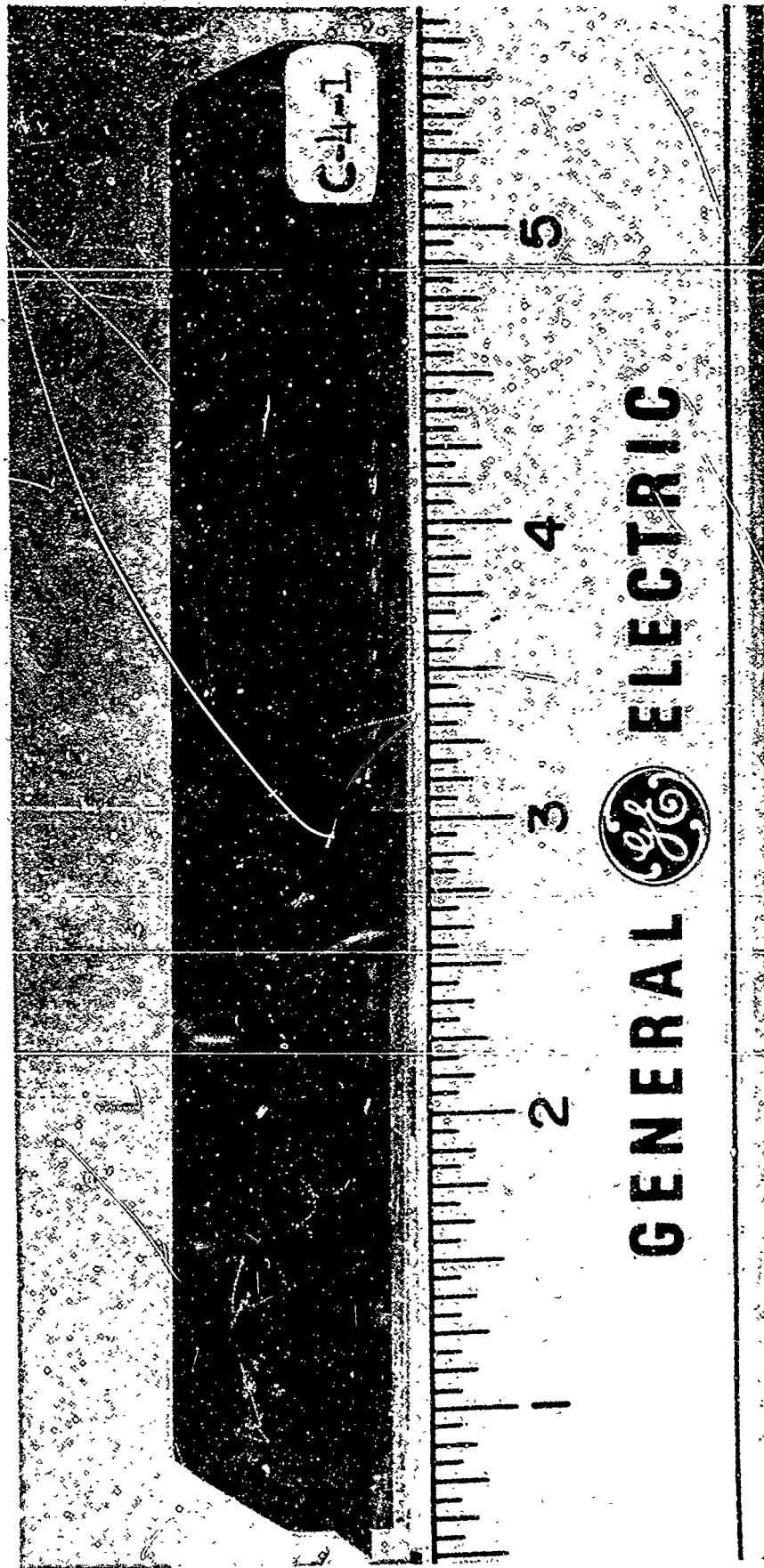
Figure 103. Untested Specimen – Three Quarter View C4-1

Figure 104. Ablated Specimen – Three Quarter View C4-1

94
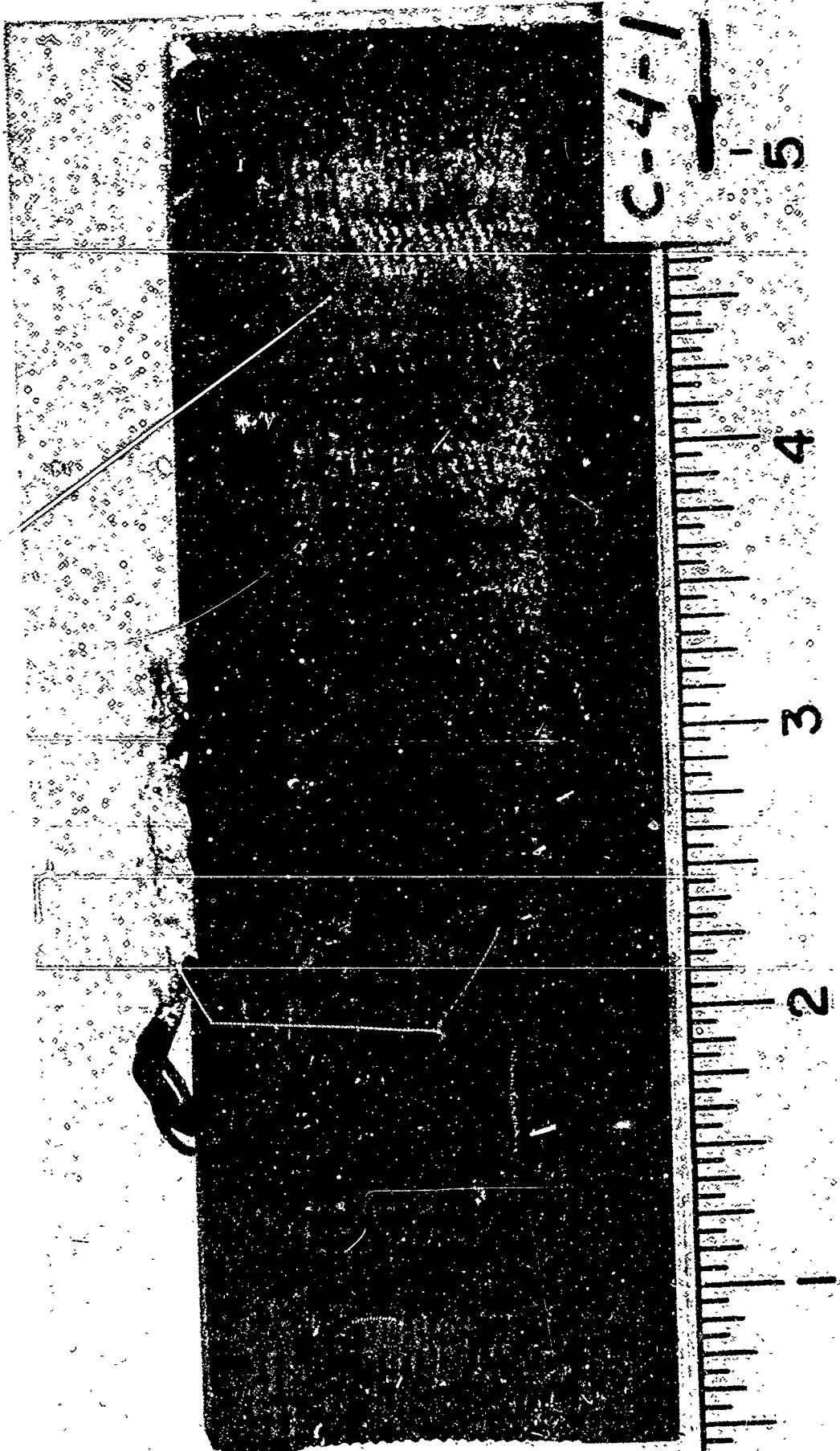
Figure 105. Ablated Specimen – Top View C4-1

95
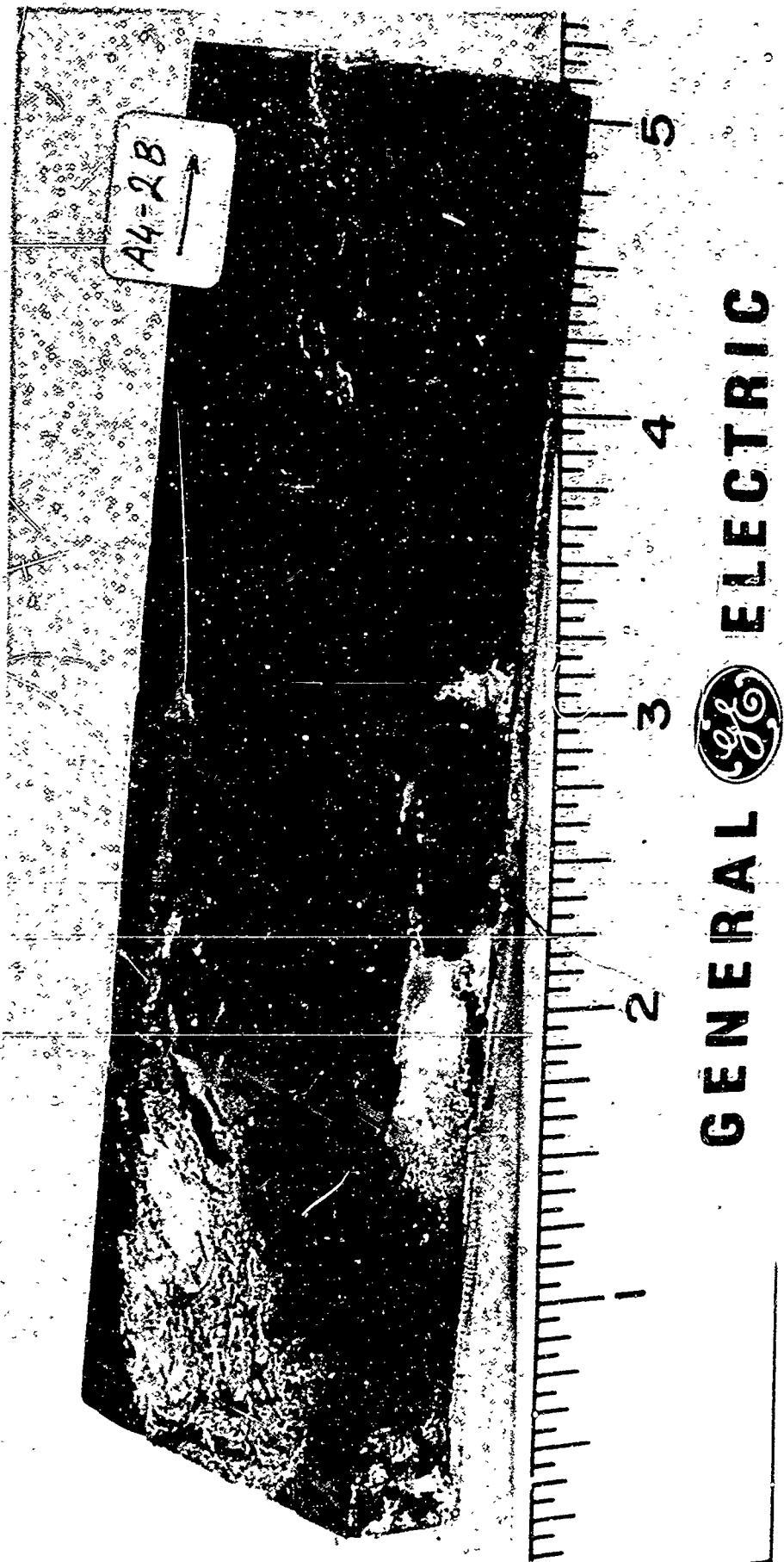
Figure 106. Ablated Specimen – Three Quarter View A4-2B
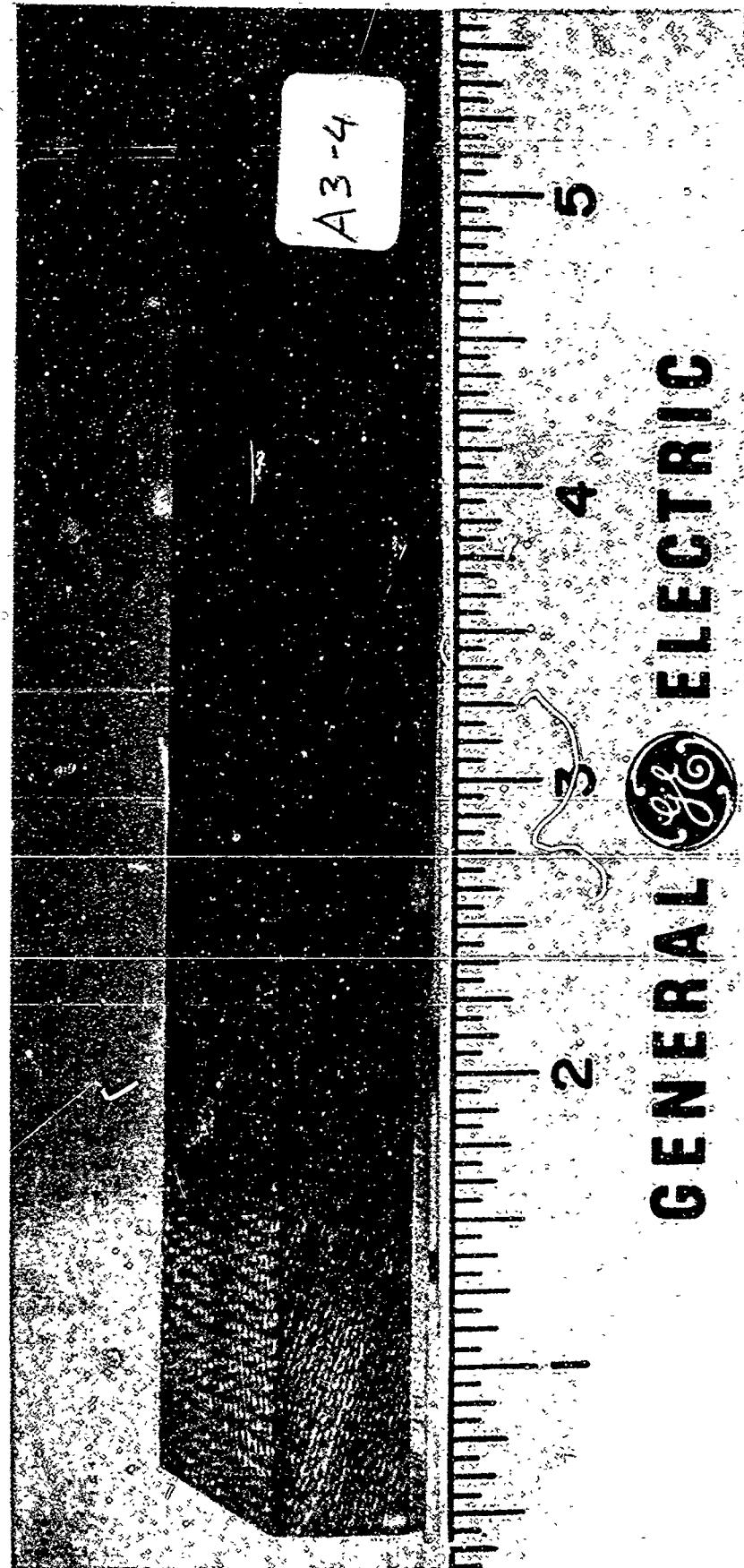
Figure 107. Untested Specimen – Three Quarter View A3-4
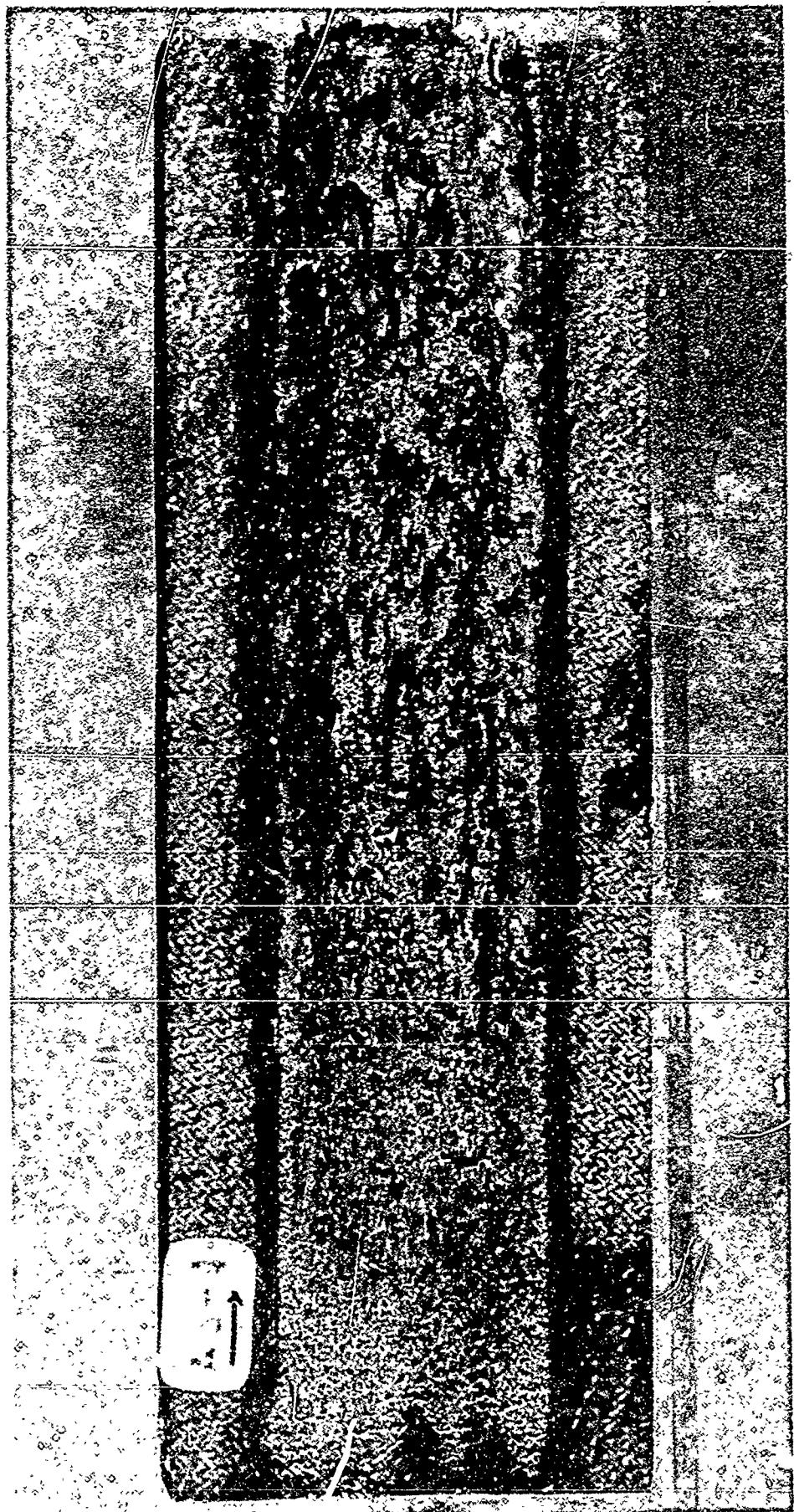
Figure 108. Ablated Specimen – Top View A3–4
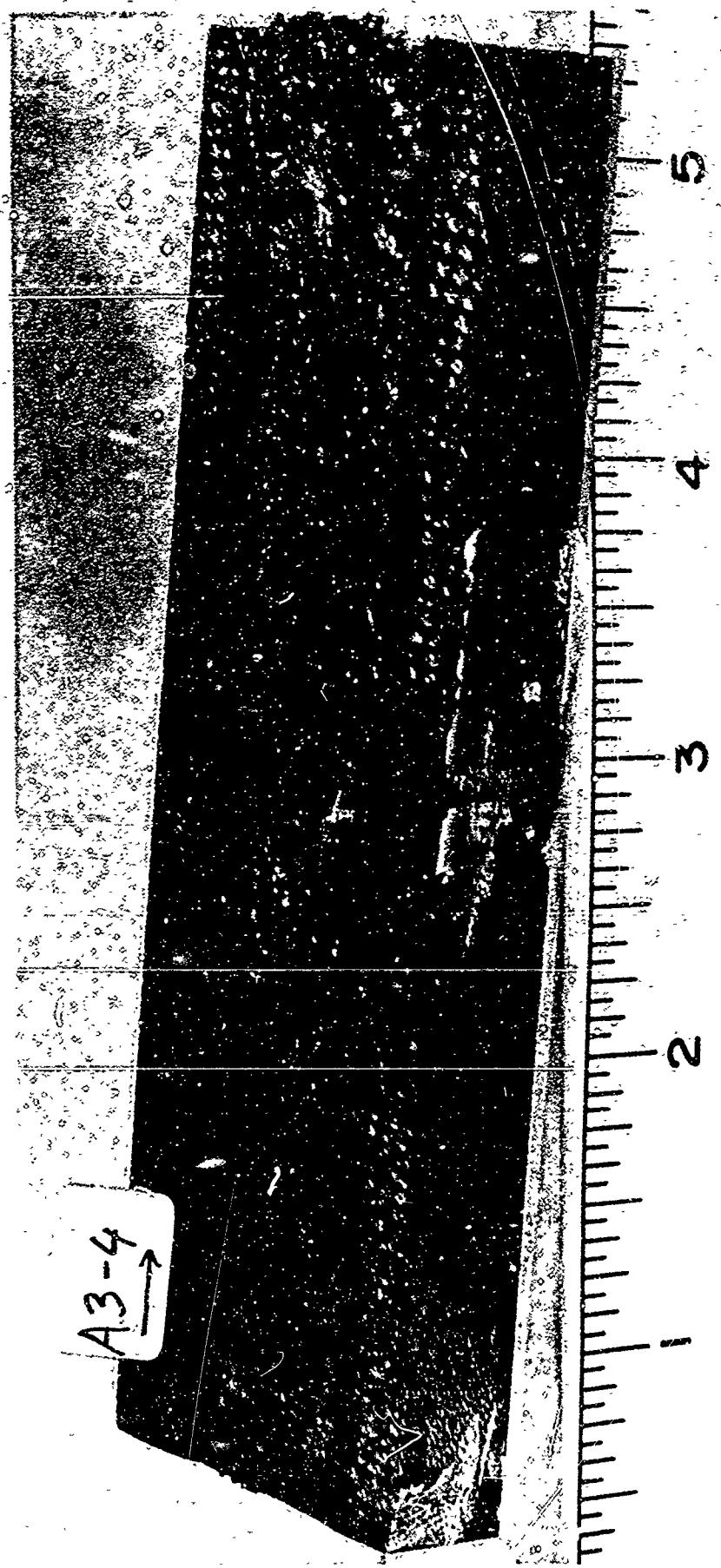
Figure 109. Ablated Specimen – Three Quarter View A3-4

99
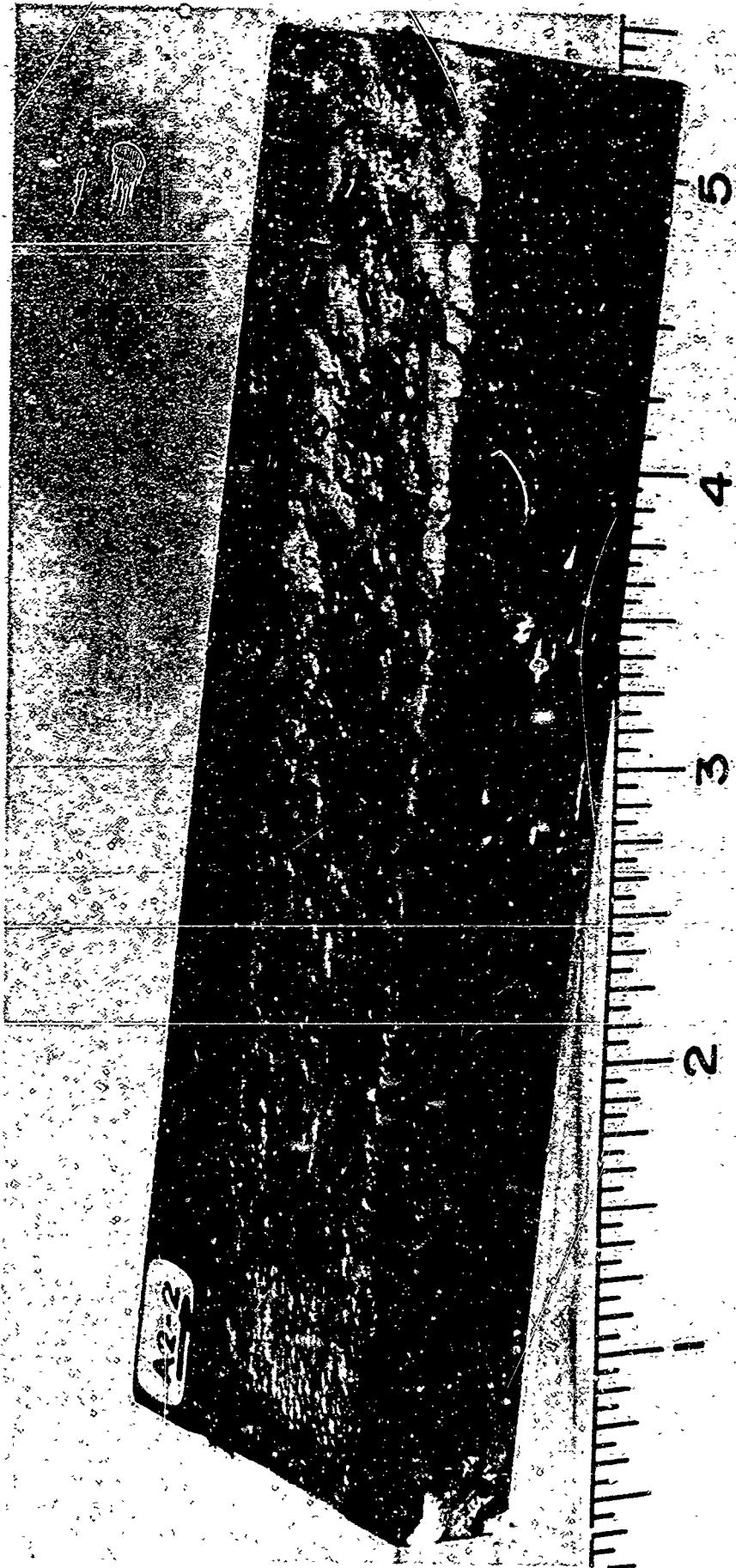
Figure 110. Ablated Specimen – Three Quarter view A2-2

100
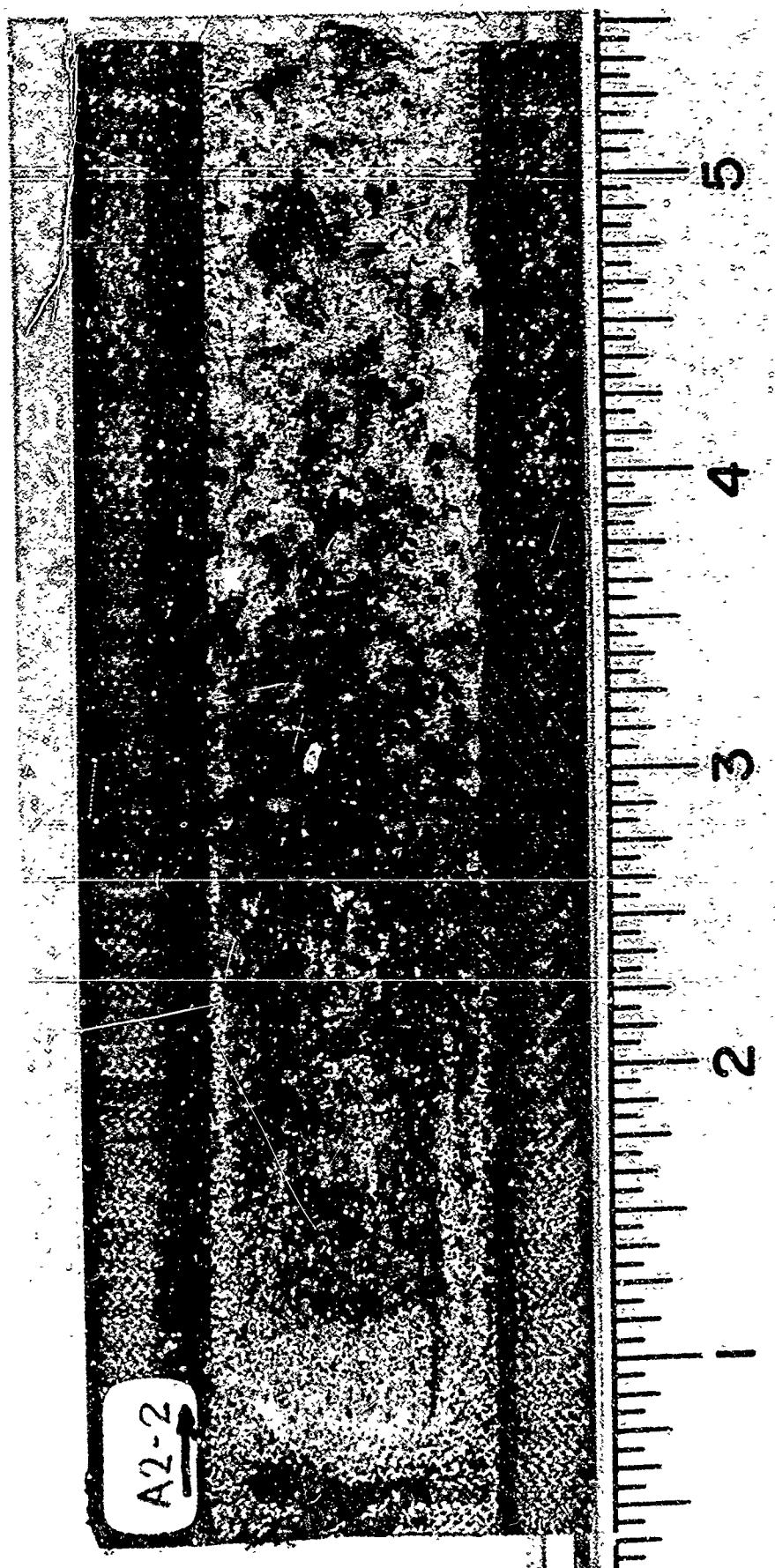
Figure 111. Ablated Specimen – Top View A2-2
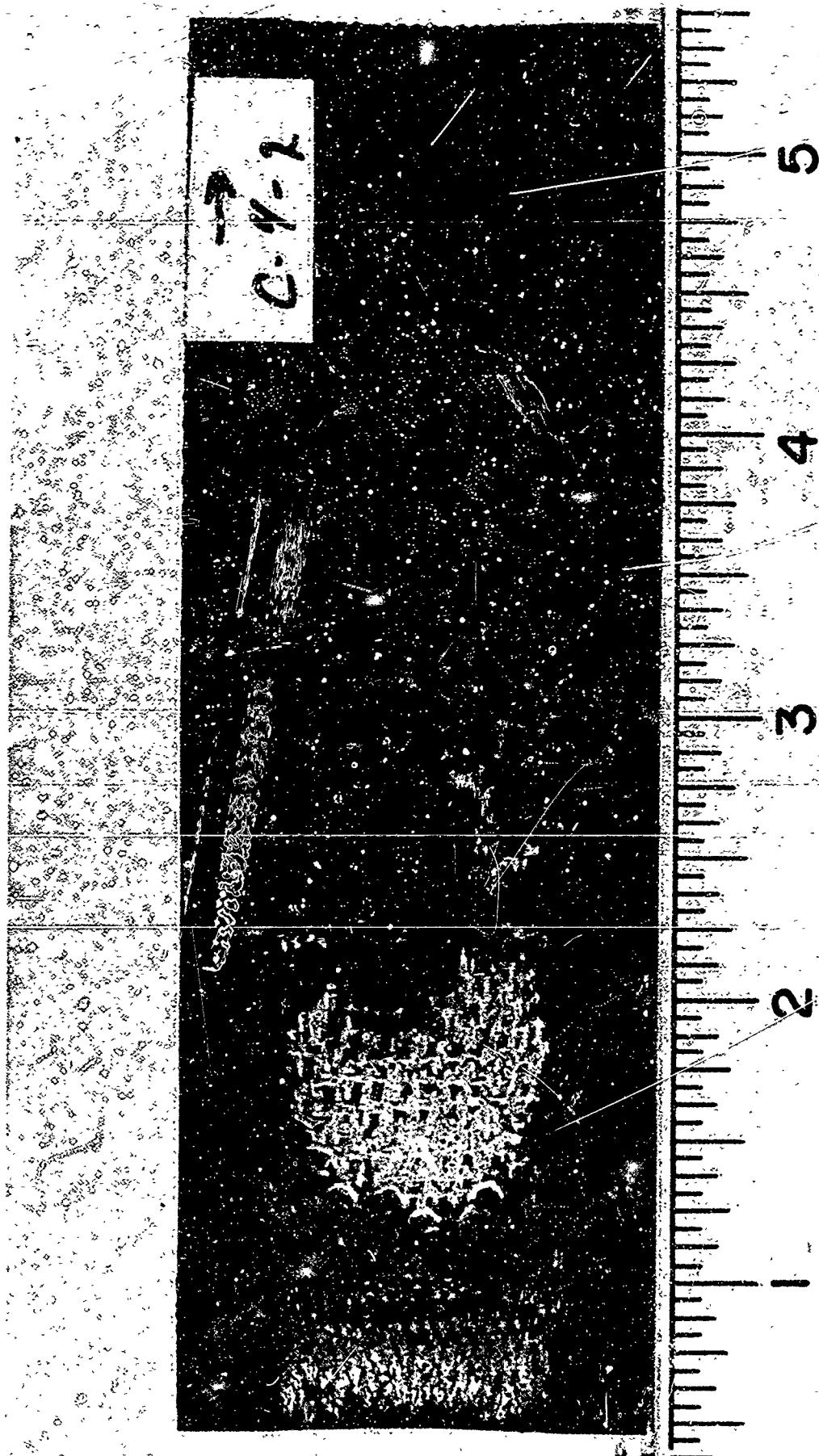
Figure 112. Ablated Specimen – Top View C4-2

C-1-6   flow ⟶
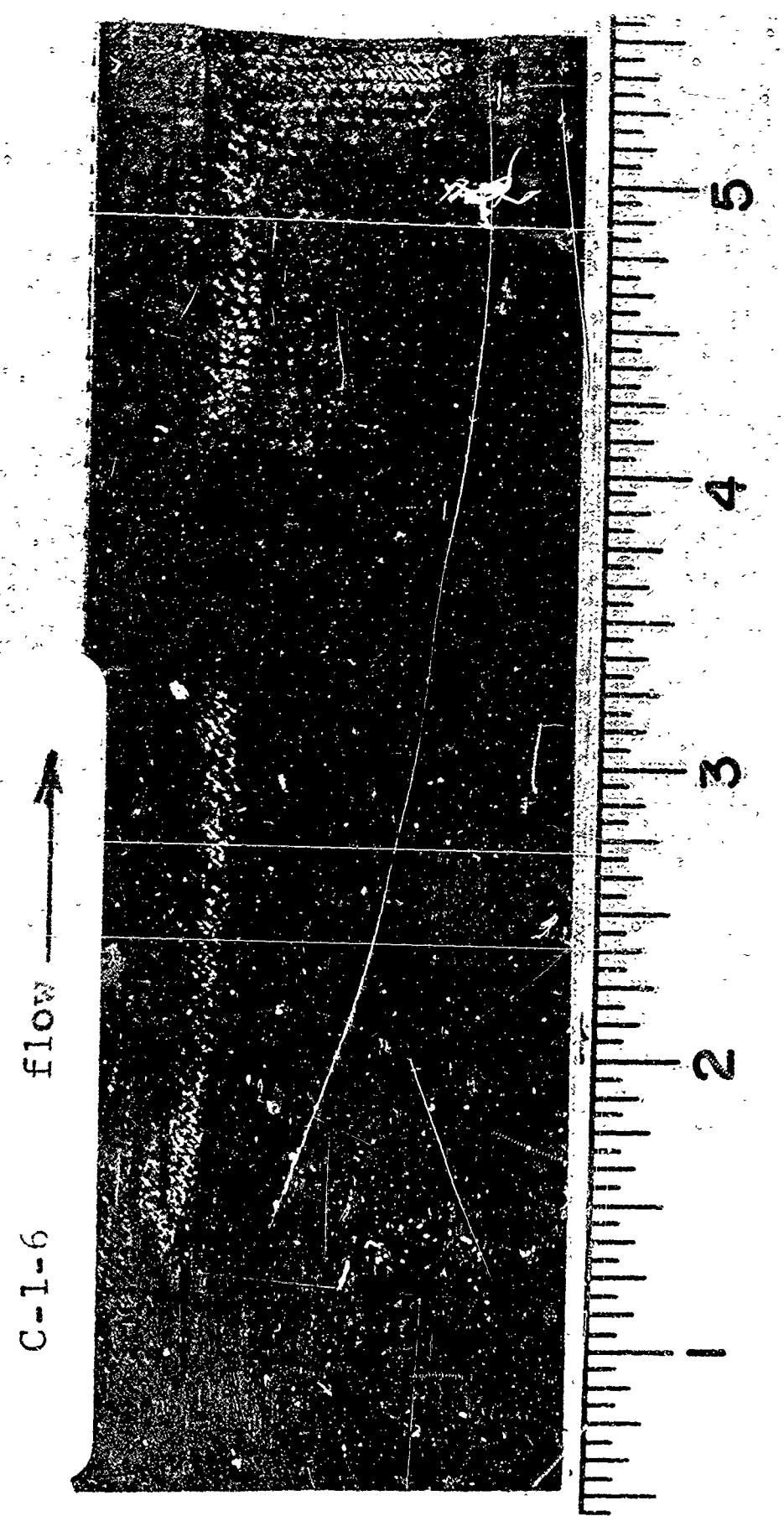
Figure 113. Ablated Specimen, Top View Specimen C1-6

103
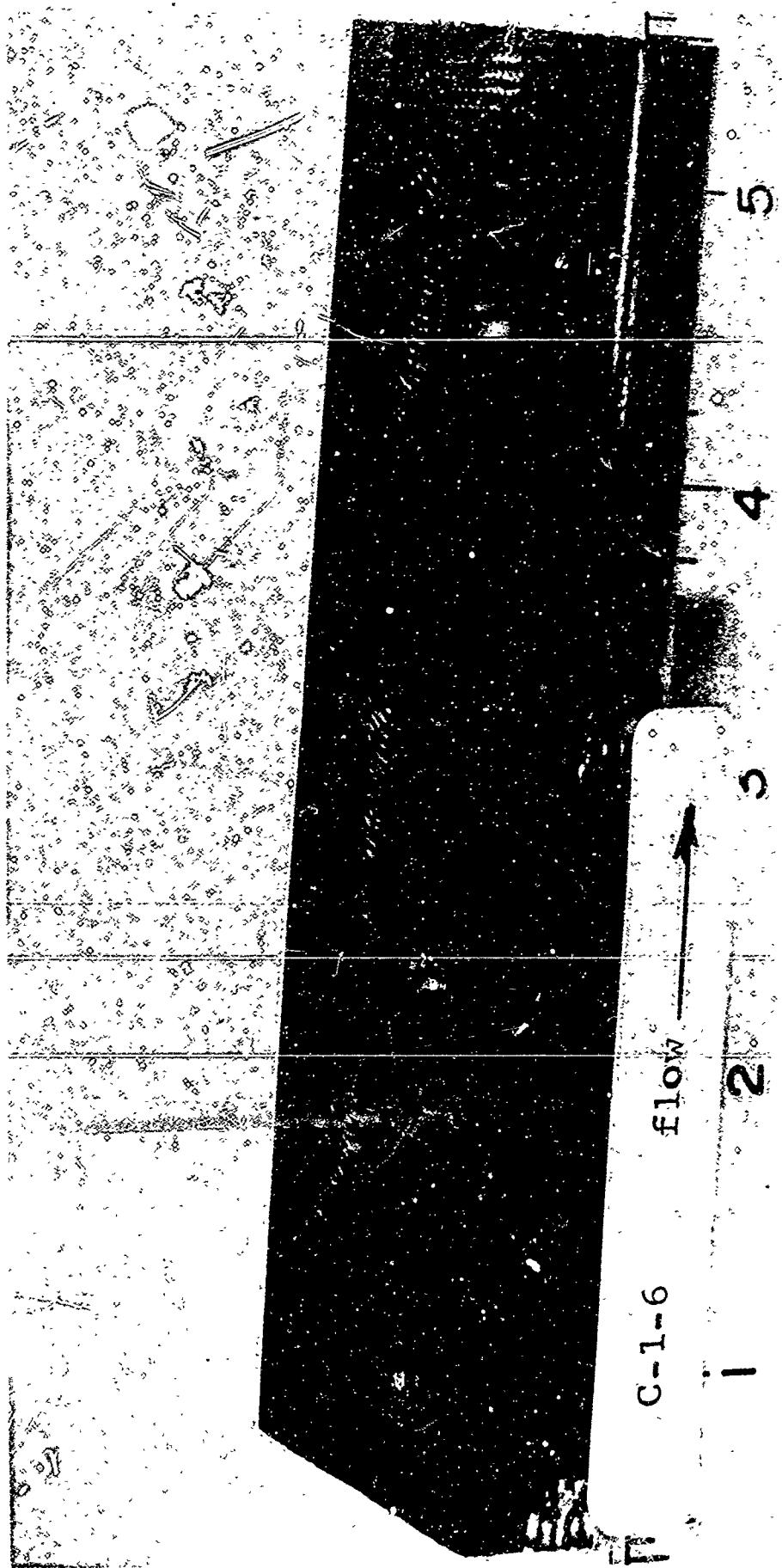
Figure 114. Ablated Specimen, Three-Quarter View, Specimen C1-6

104

C-1-6

flow

flow
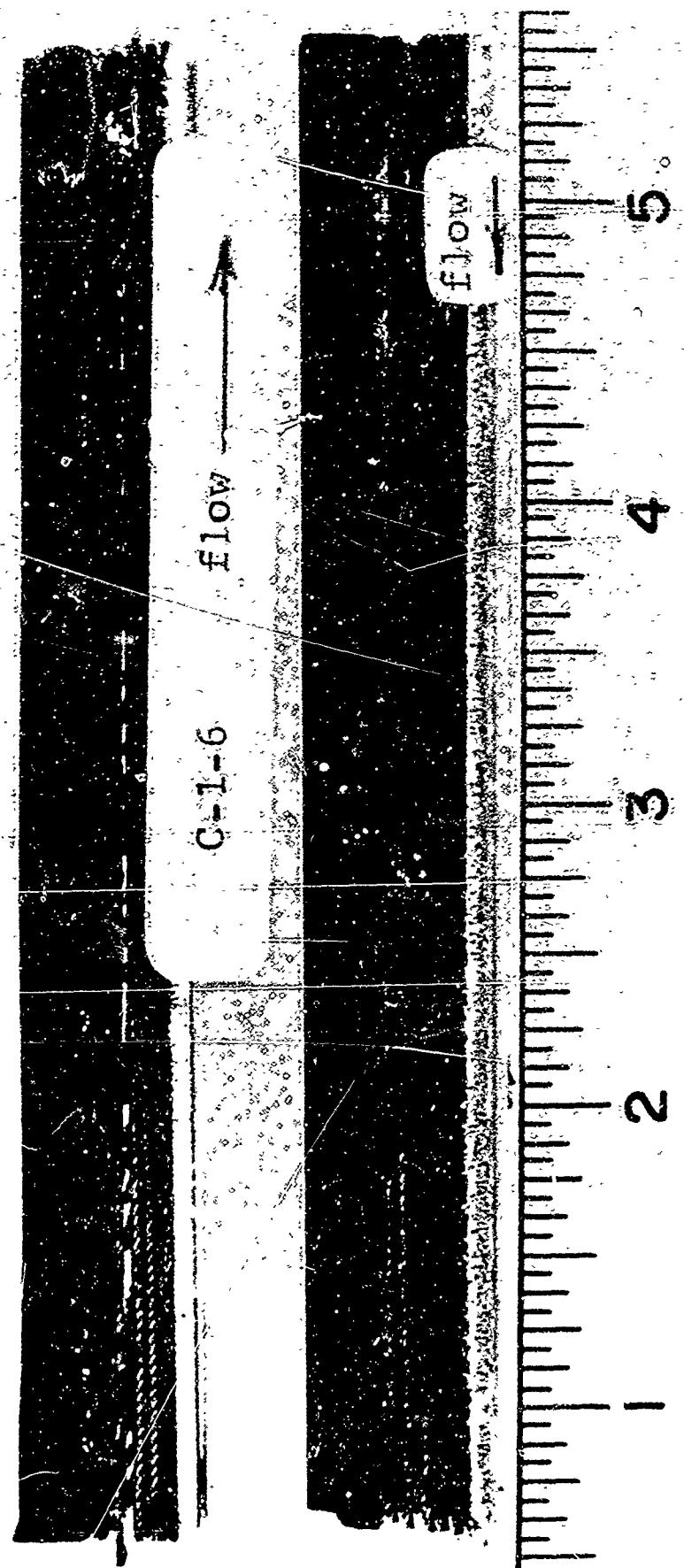
Figure 115. Ablated Specimen Cross Section, C1-6
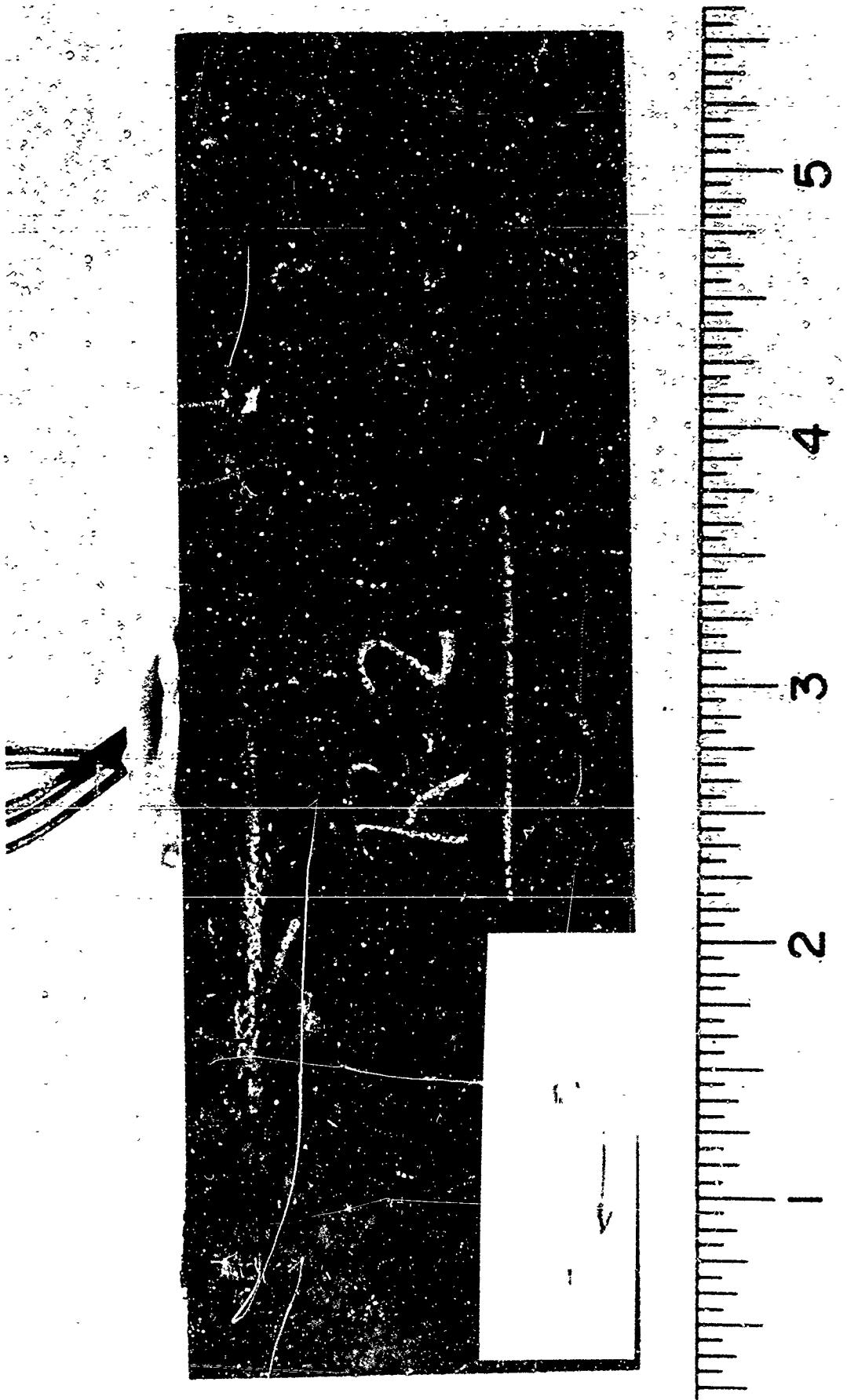
Figure 116. Untested Specimen C1-8
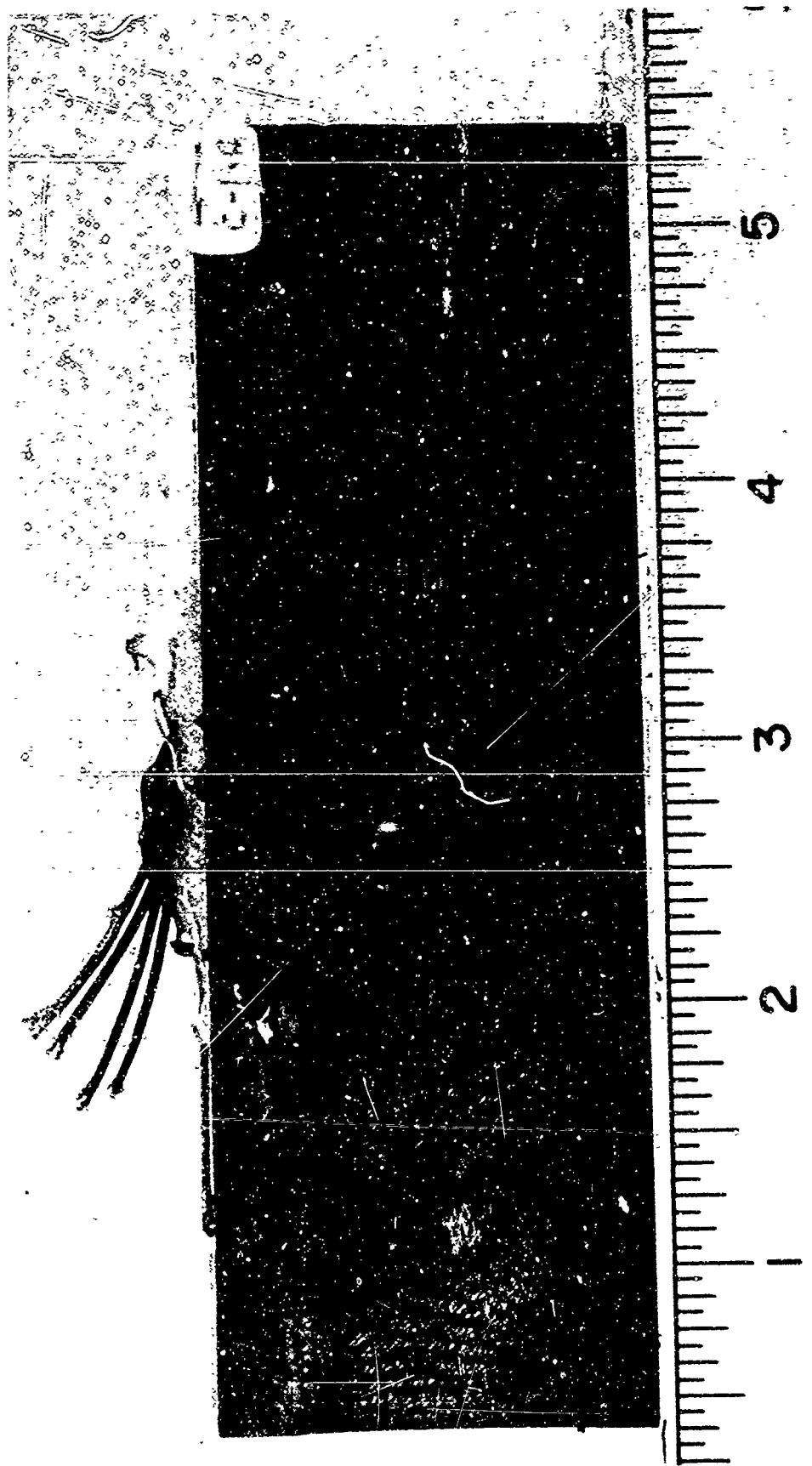
Figure 117. Ablated Specimen Top View C1-8

107
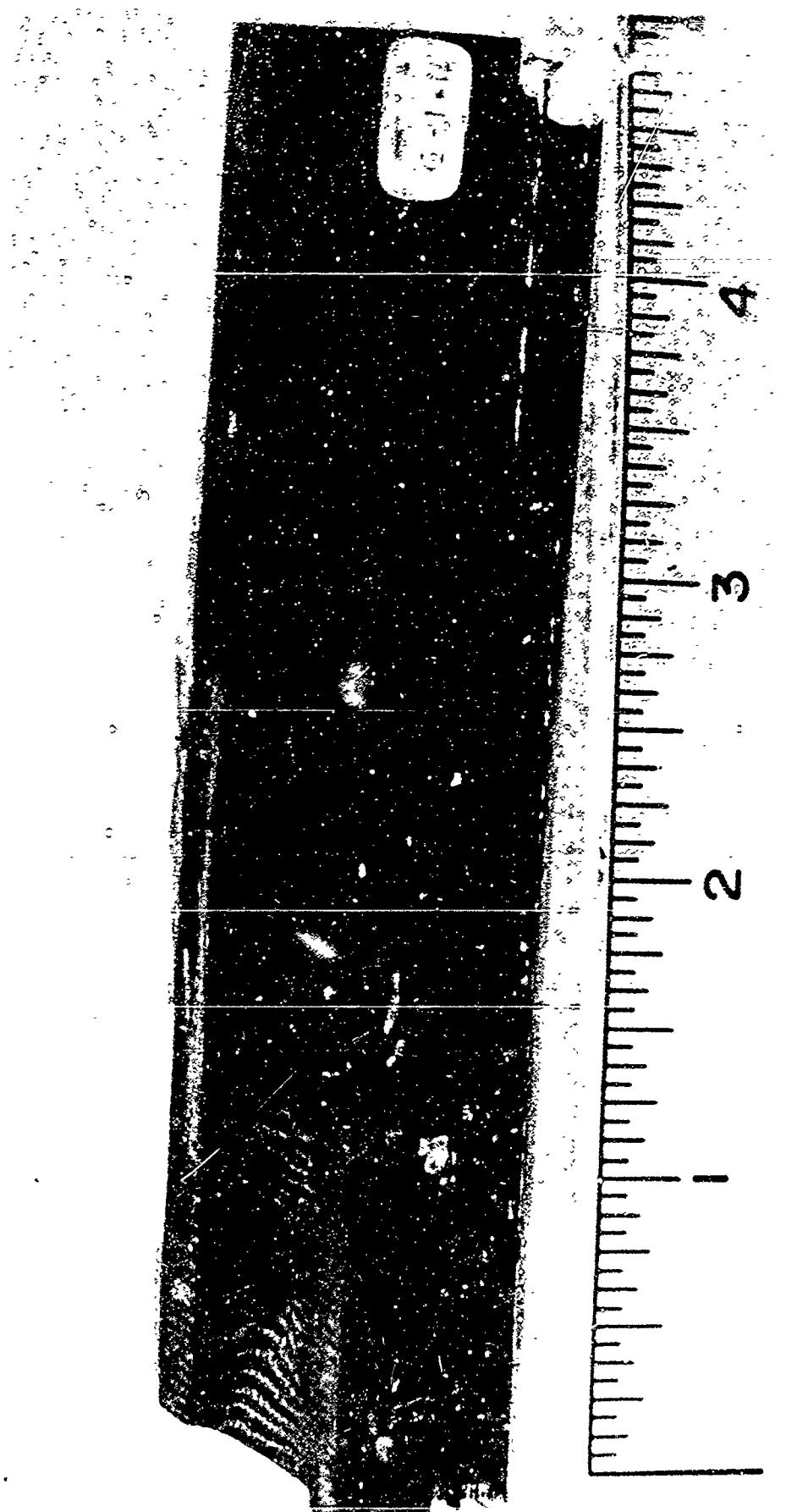
Figure 118. Ablated Specimen Three-Quarter View C1-8
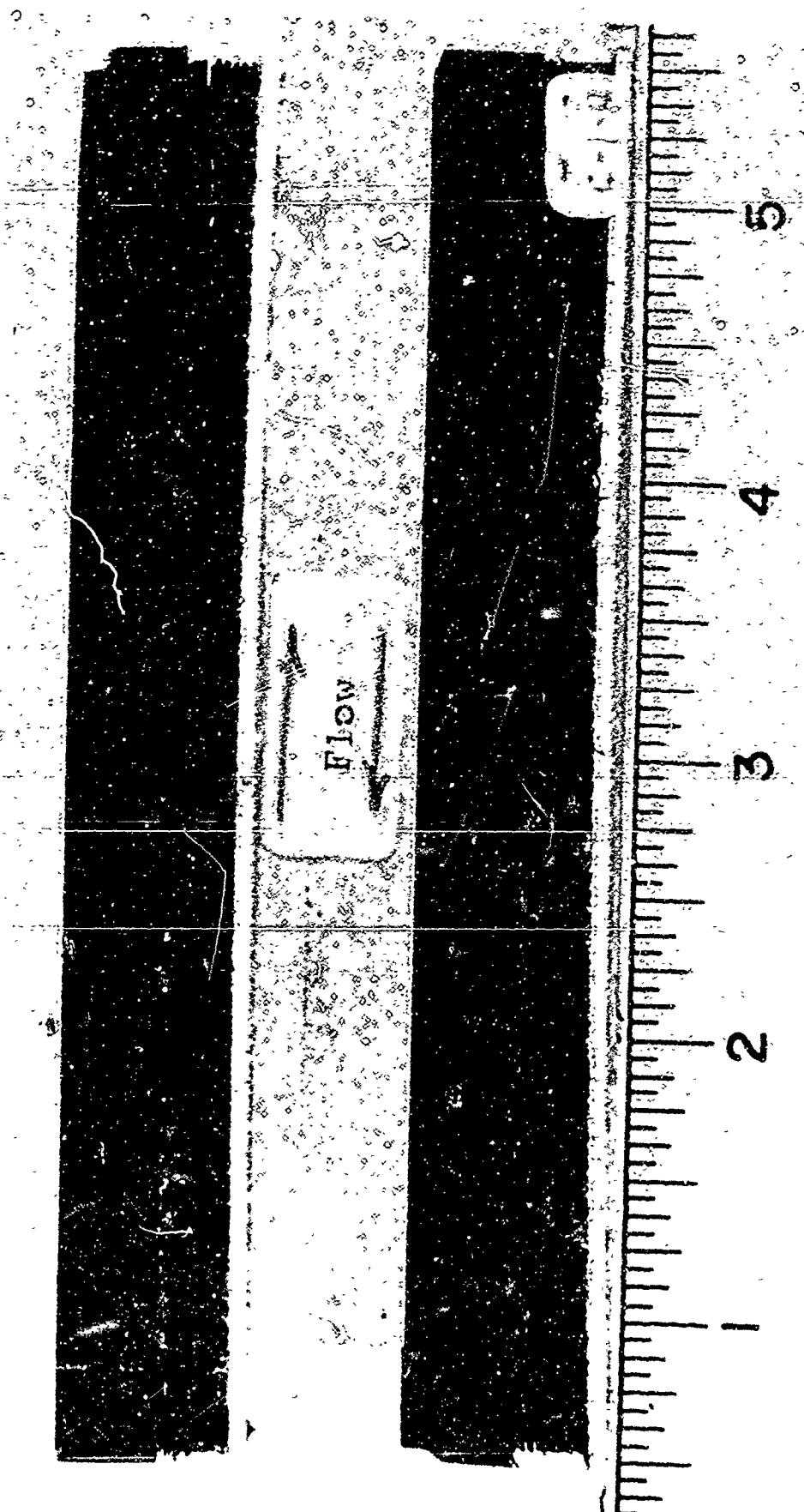
Figure 119. Ablated Specimen Cross Section C1-8

Flow

109
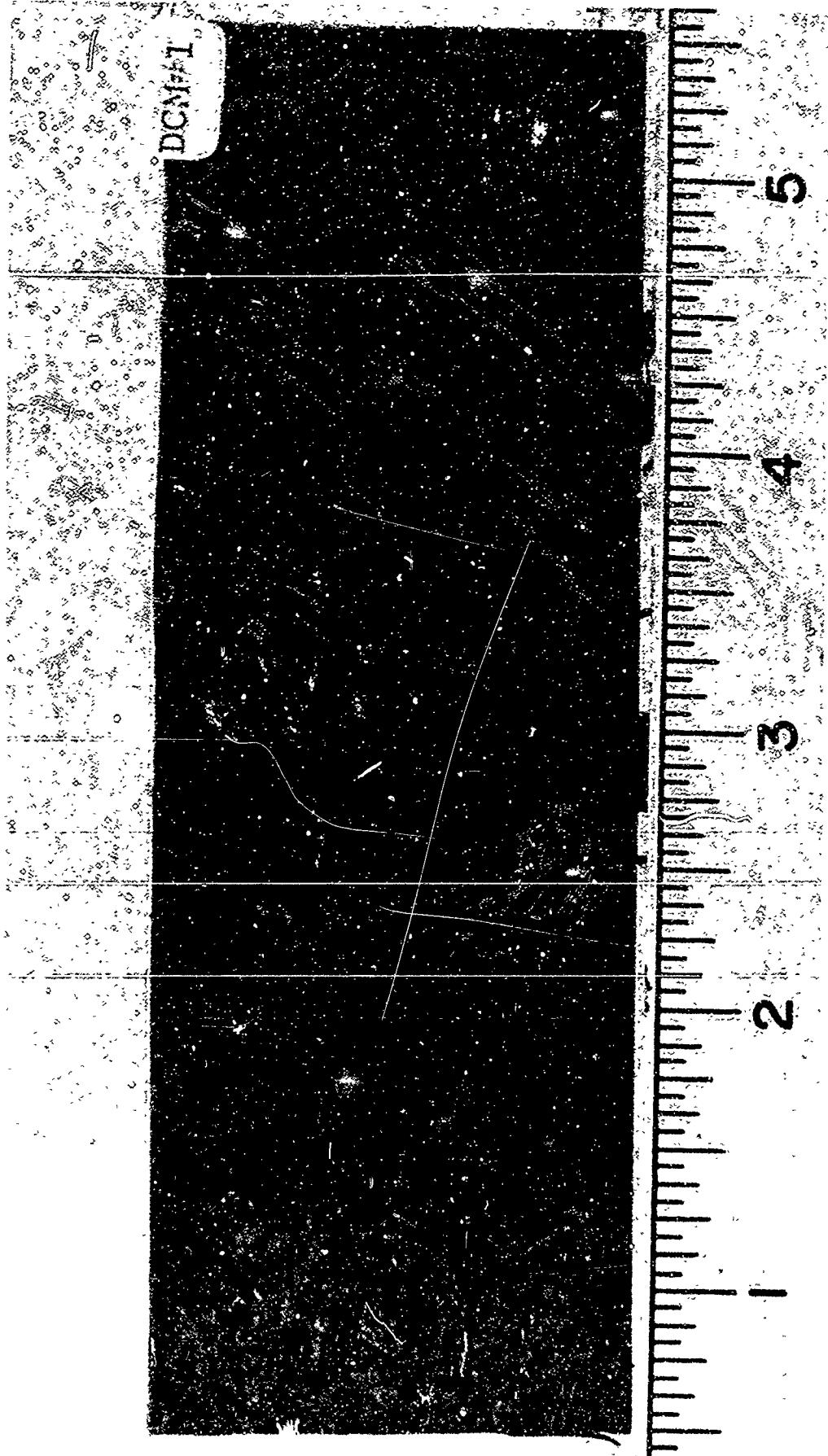
Figure 120.   Untested Specimen DCM-1

110
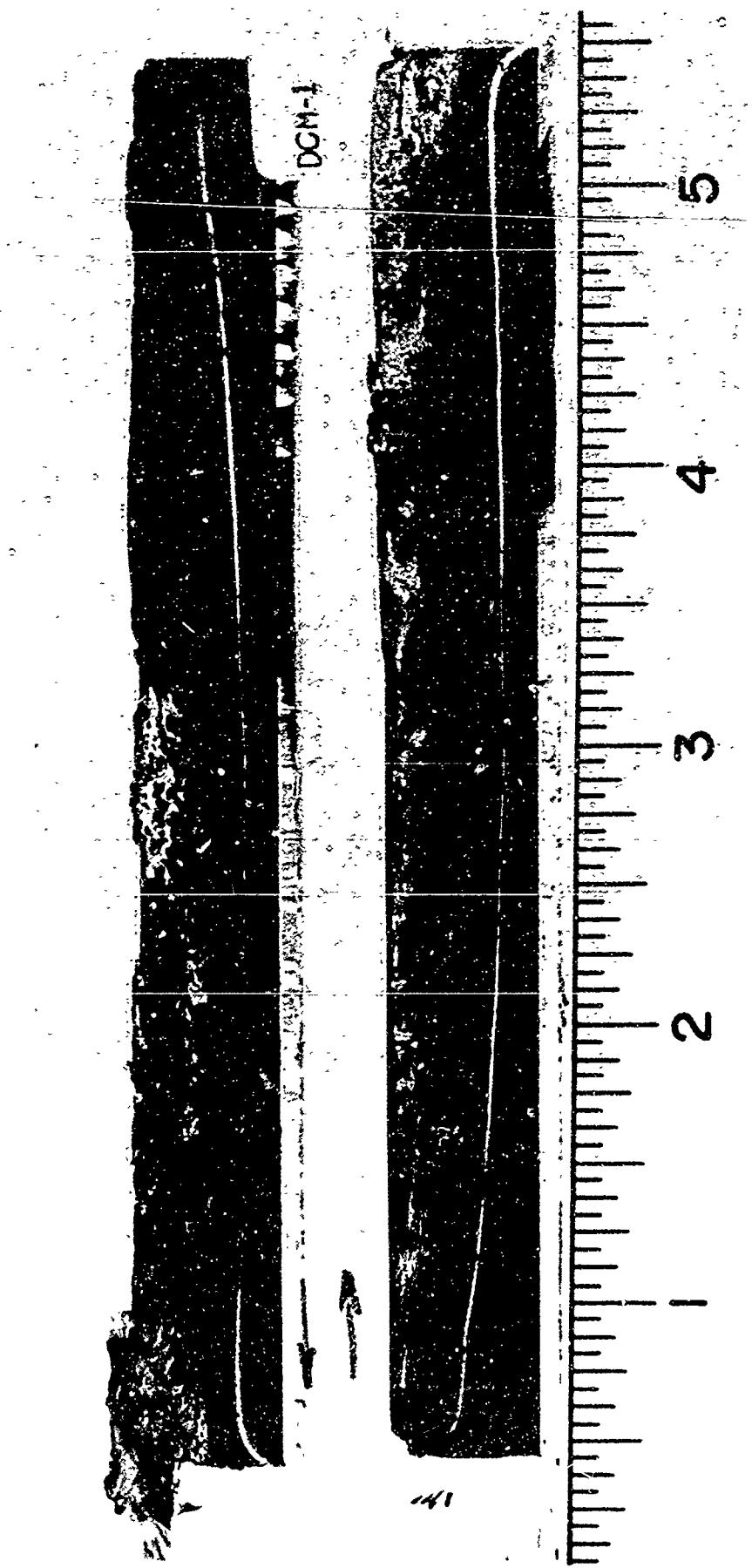
Figure 121. Ablated Specimen Cross Section DCM-1
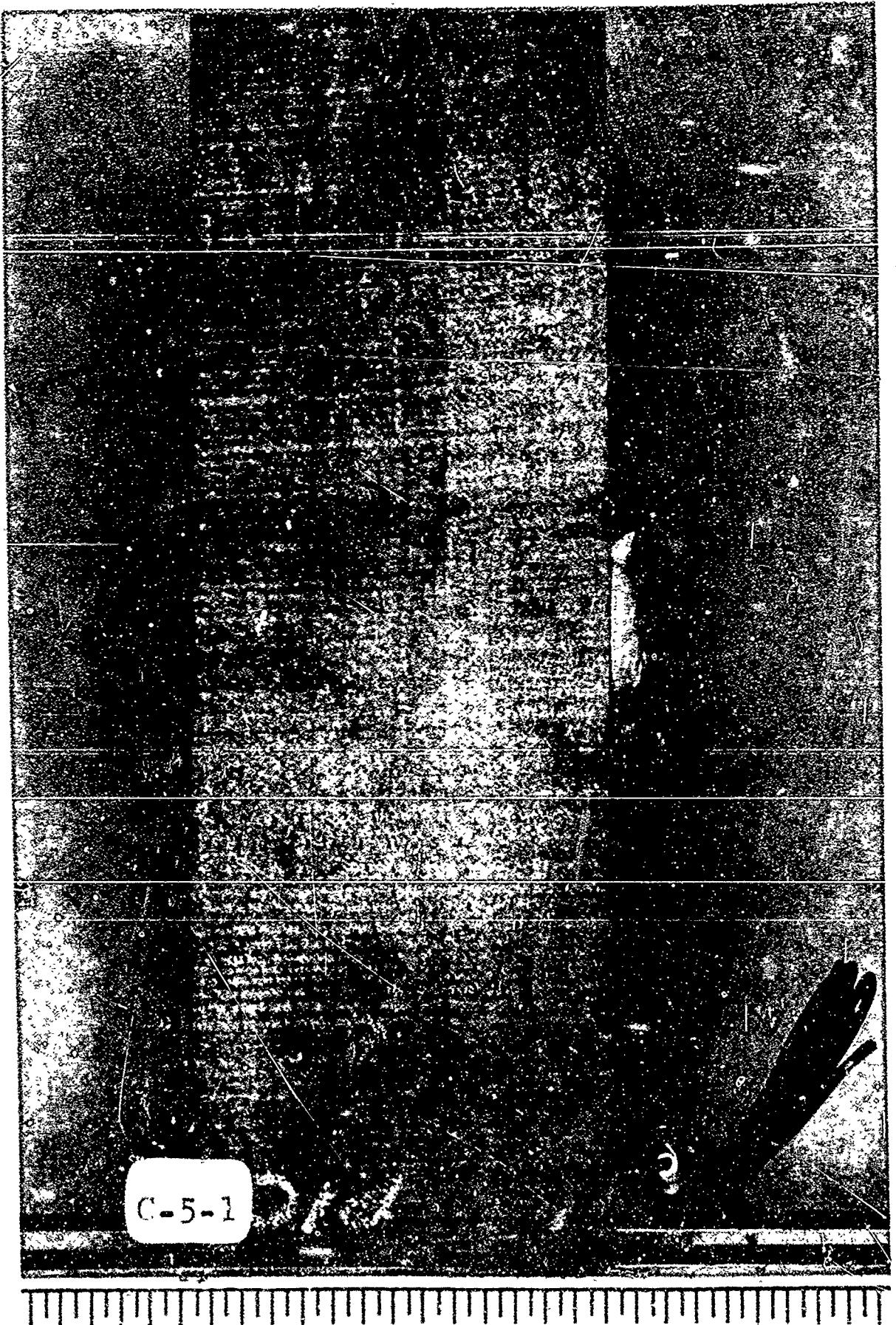
Figure 122.   Untested Specimen C5-1
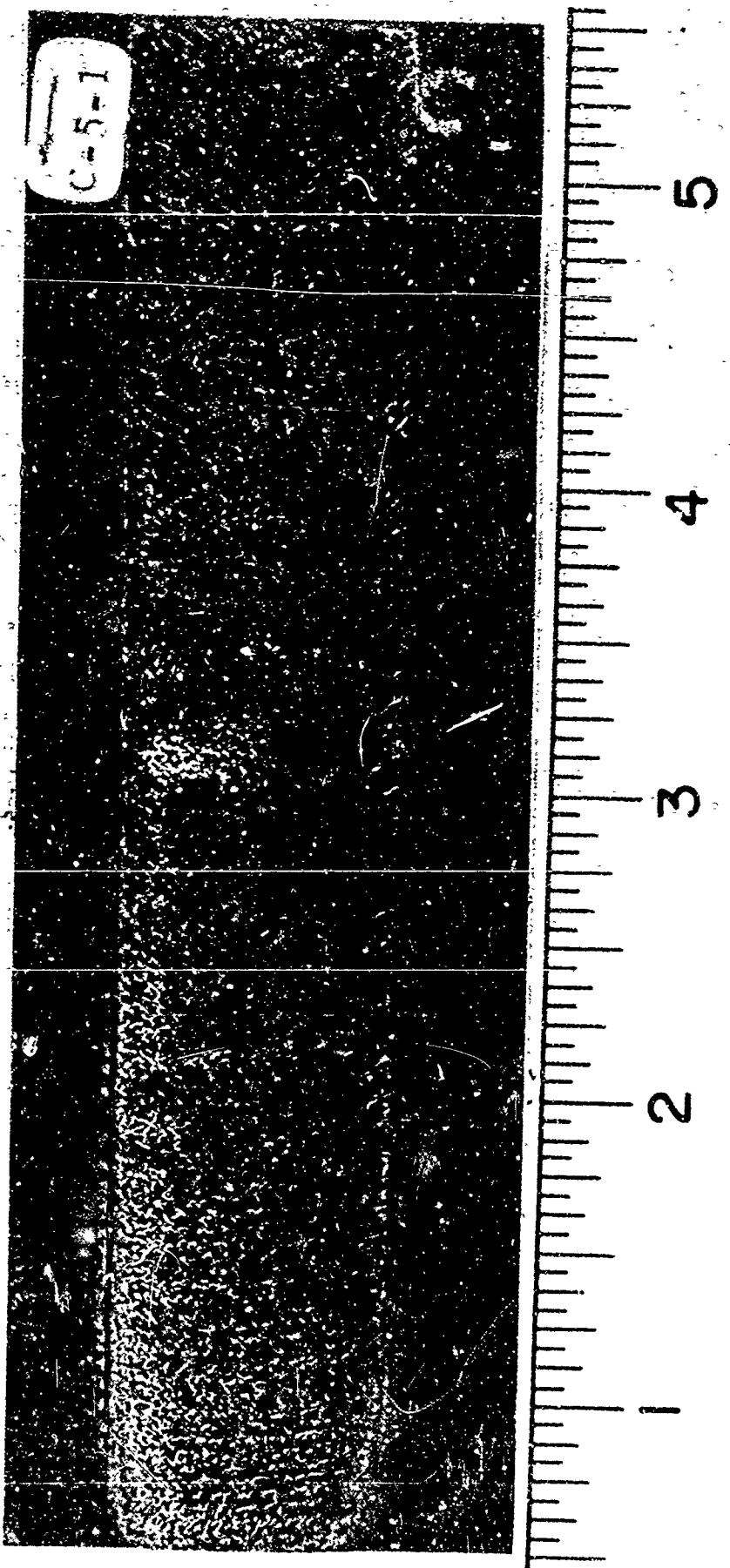
Figure 123. Ablated Specimen Top View C5-1

Figure 124. Ablated Specimen Three-Quarter View C5-1
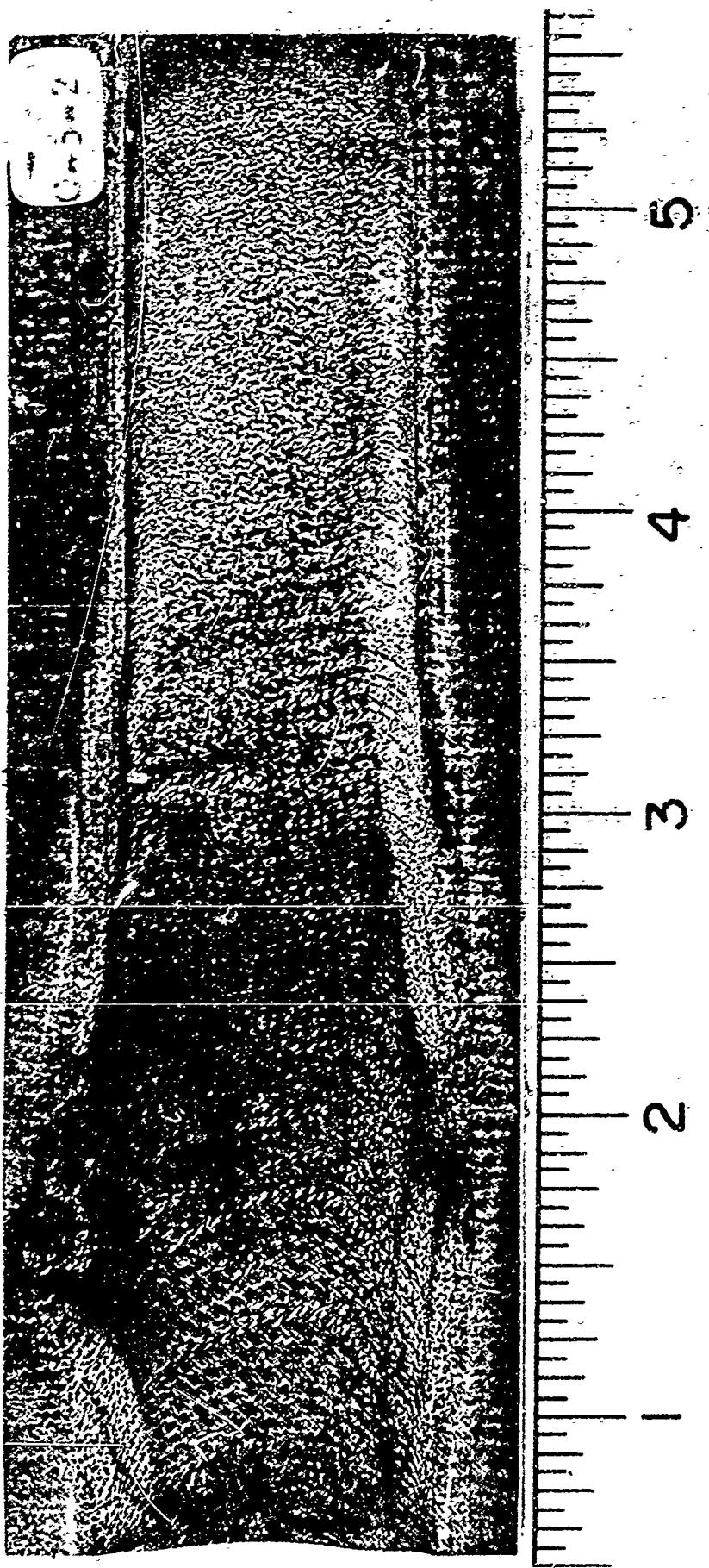
Figure 125. Ablated Specimen Top View C5-2.

115
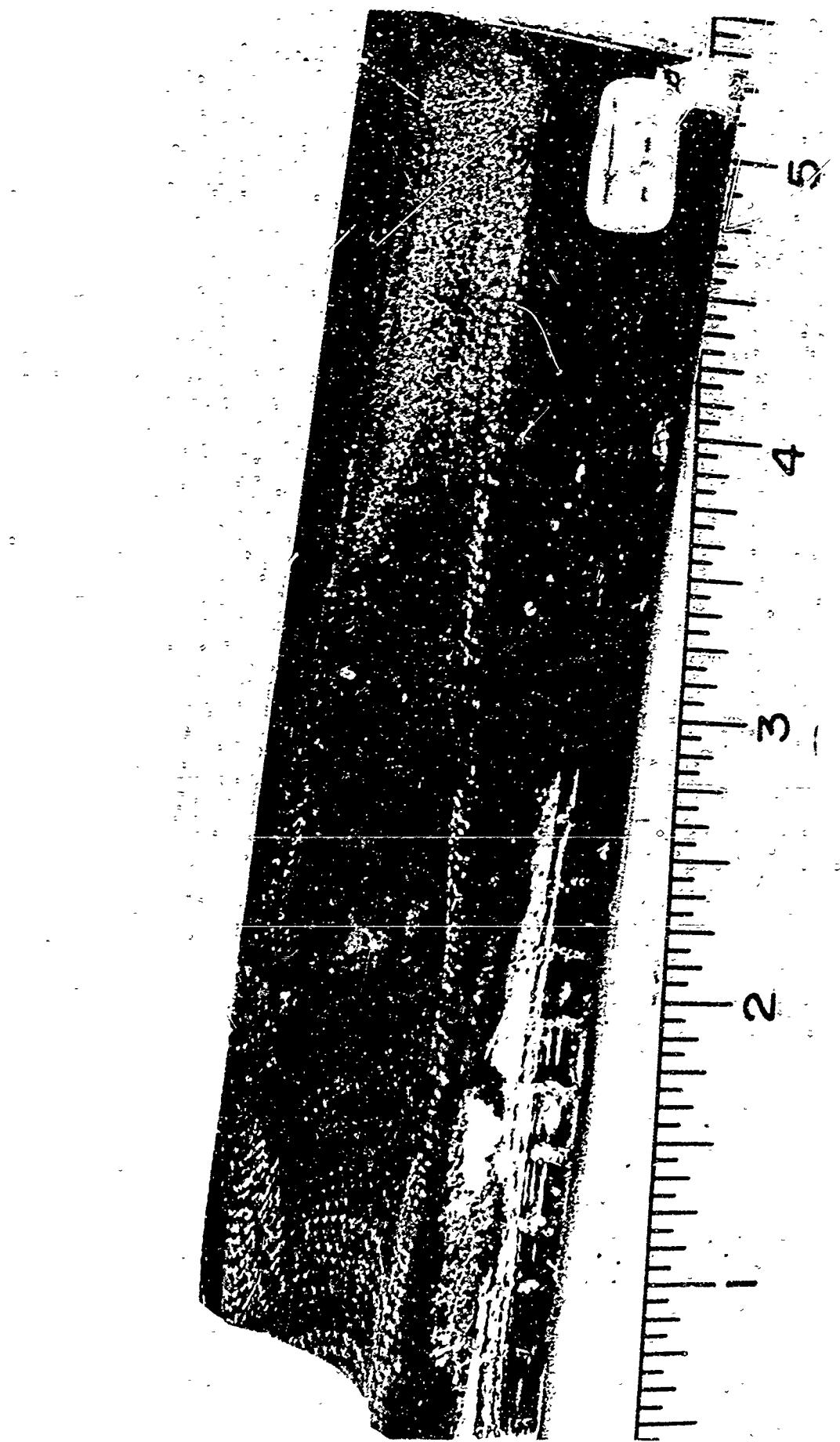
Figure 126. Ablated Specimen Three-Quarter View C5-2

116
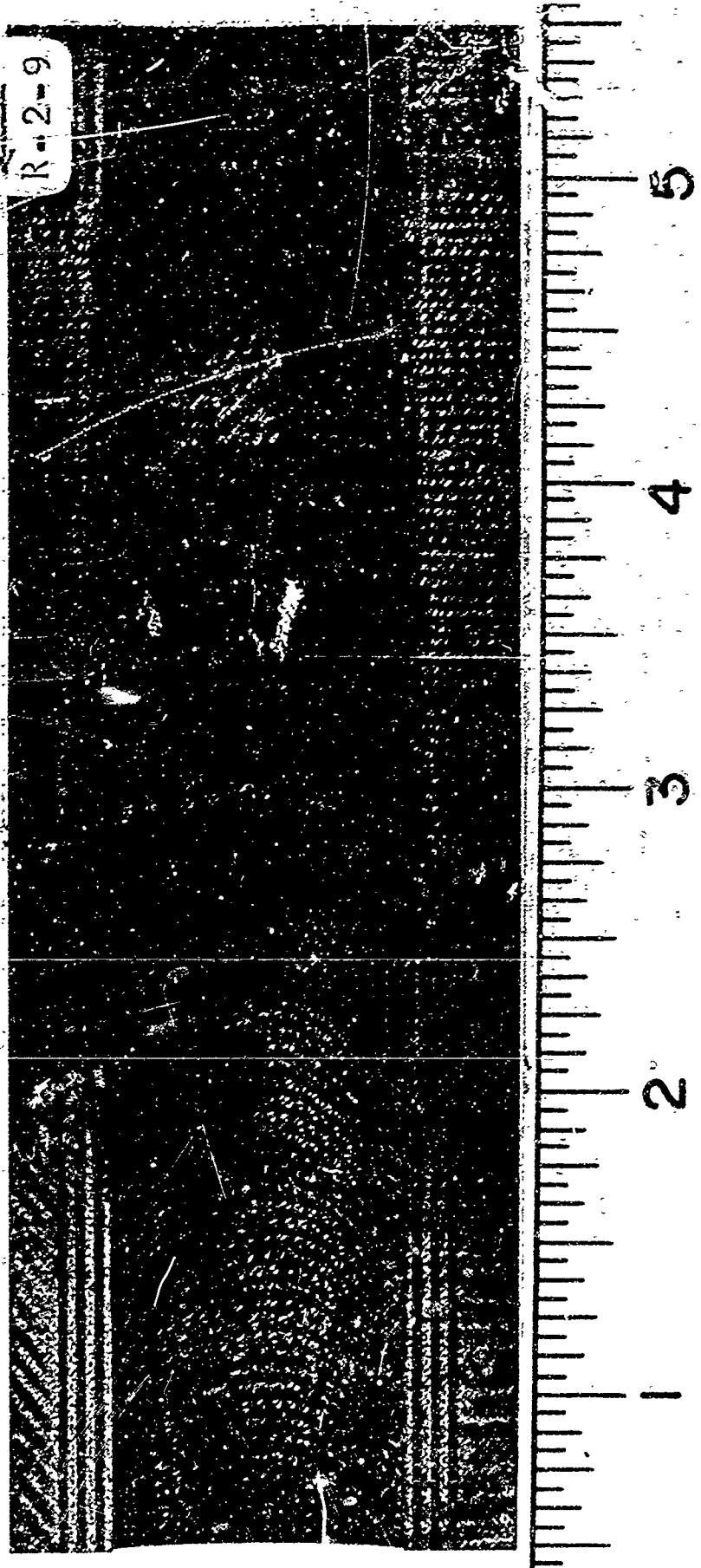
Figure 127. Ablated Specimen Top View R2-9

117

NOT REPRODUCIBLE
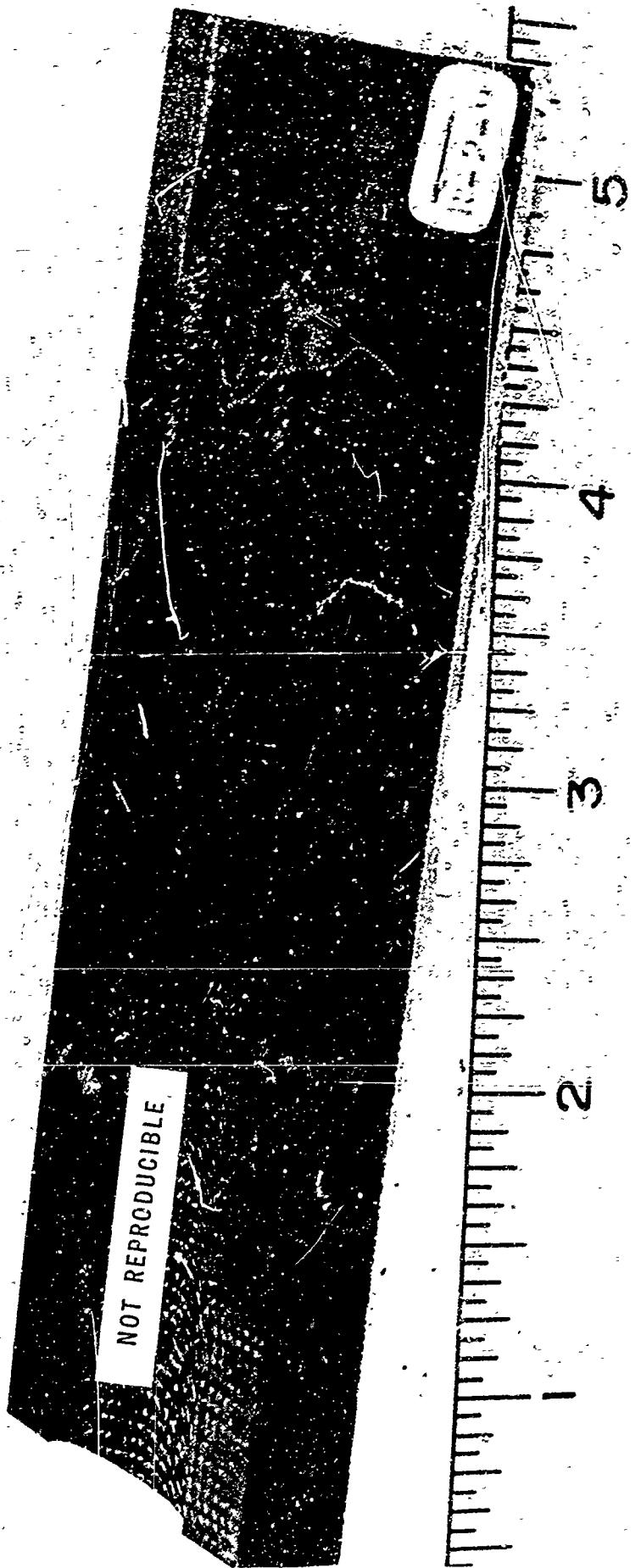
Figure 128. Ablated Specimen Three-Quarter View R2-9

118
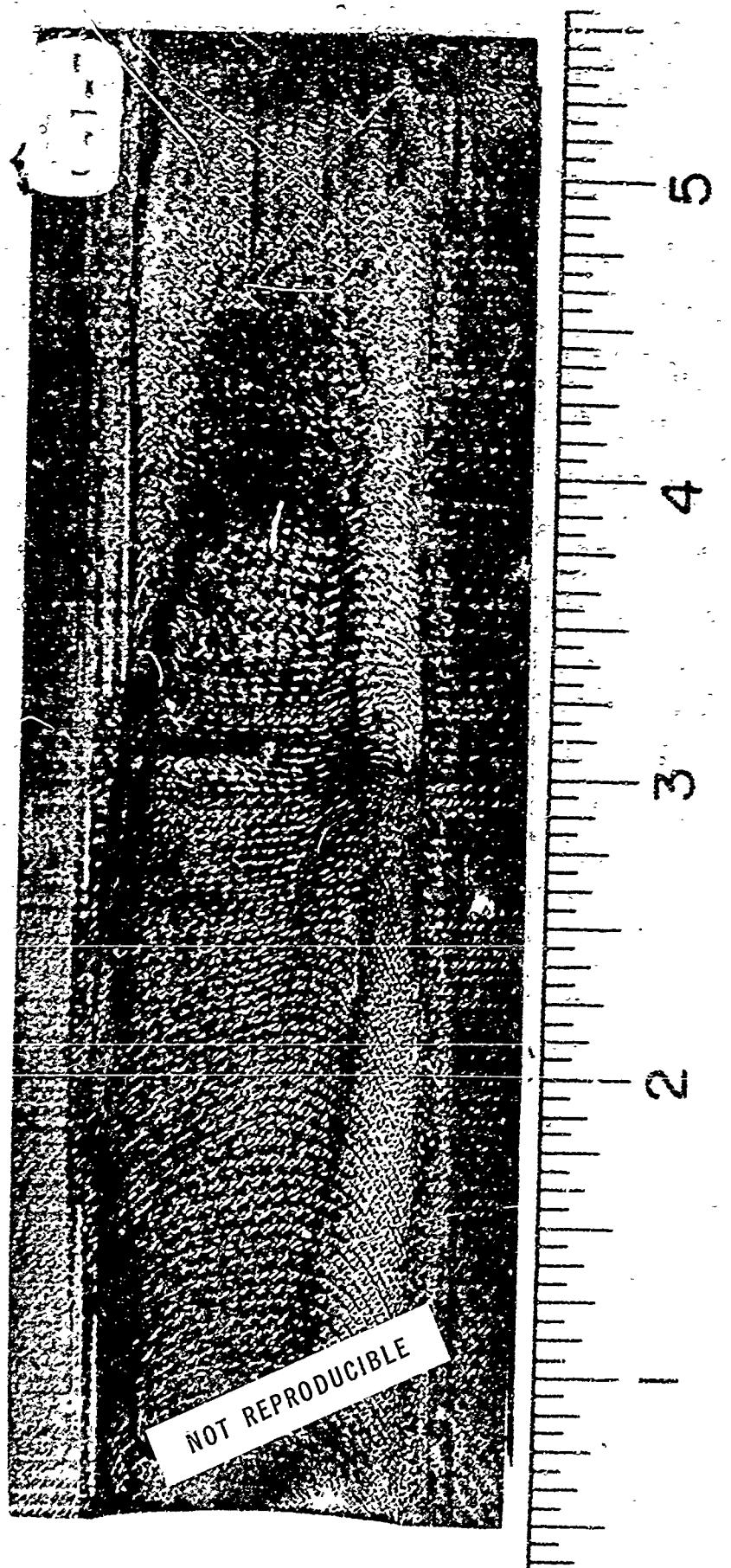
Figure 129. Ablated Specimen Top View C1-7

NOT REPRODUCIBLE

119
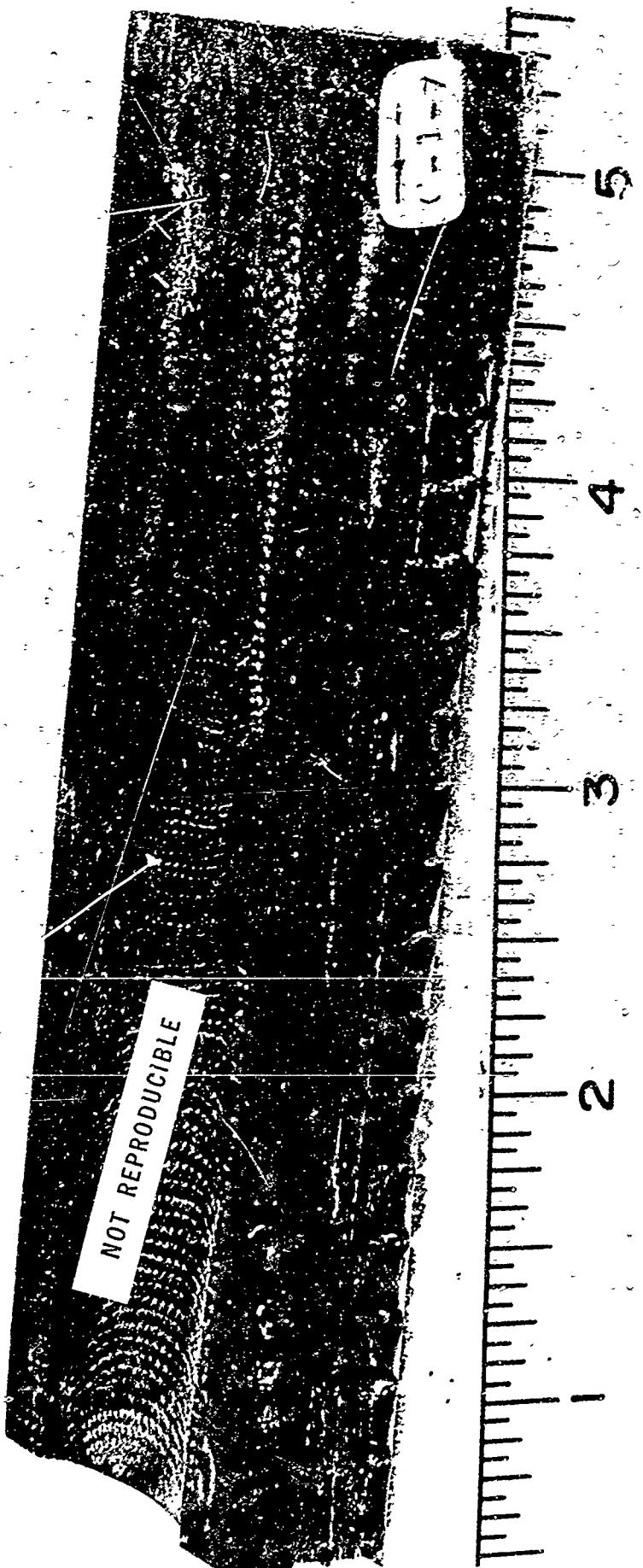
Figure 130. Ablated Specimen Three-Quarter View C1-7

NOT REPRODUCIBLE

120
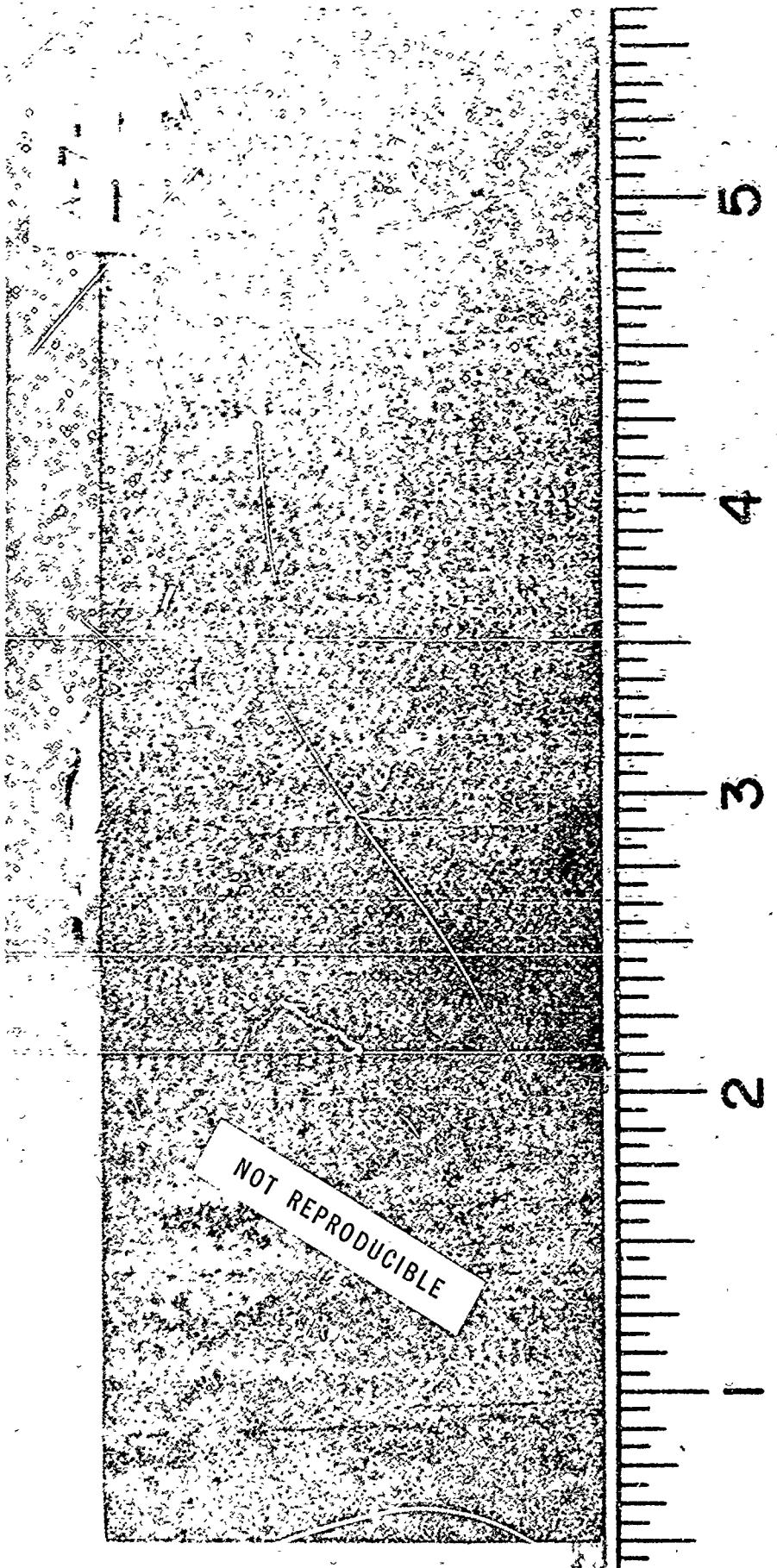
Figure 131. Untested Specimen Top View A7–1

NOT REPRODUCIBLE

NOT REPRODUCIBLE

GENERAL ⊕ ELECTRIC

Figure 132. Ablated Specimen Three-Quarter View A7-1

NOT REPRODUCIBLE
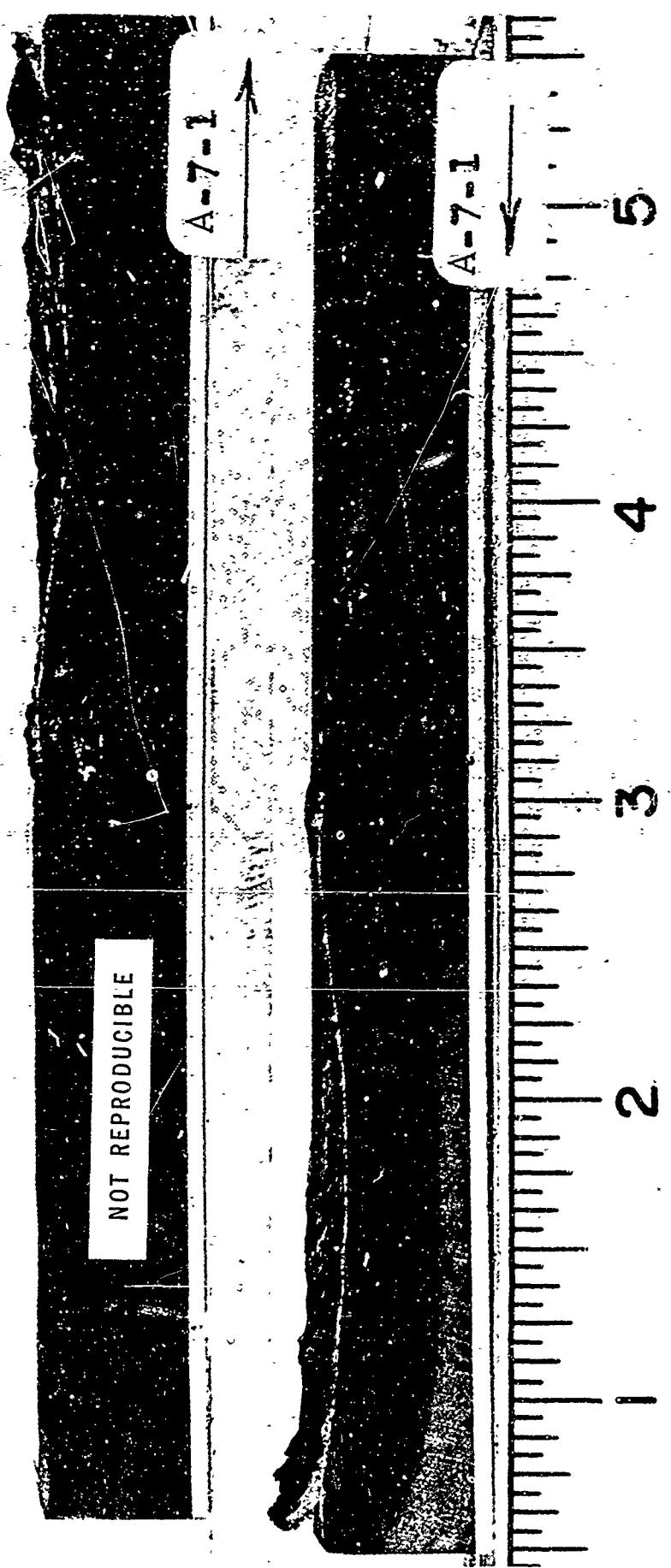
Figure 133. Ablated Specimen Cross Section A7-1

123
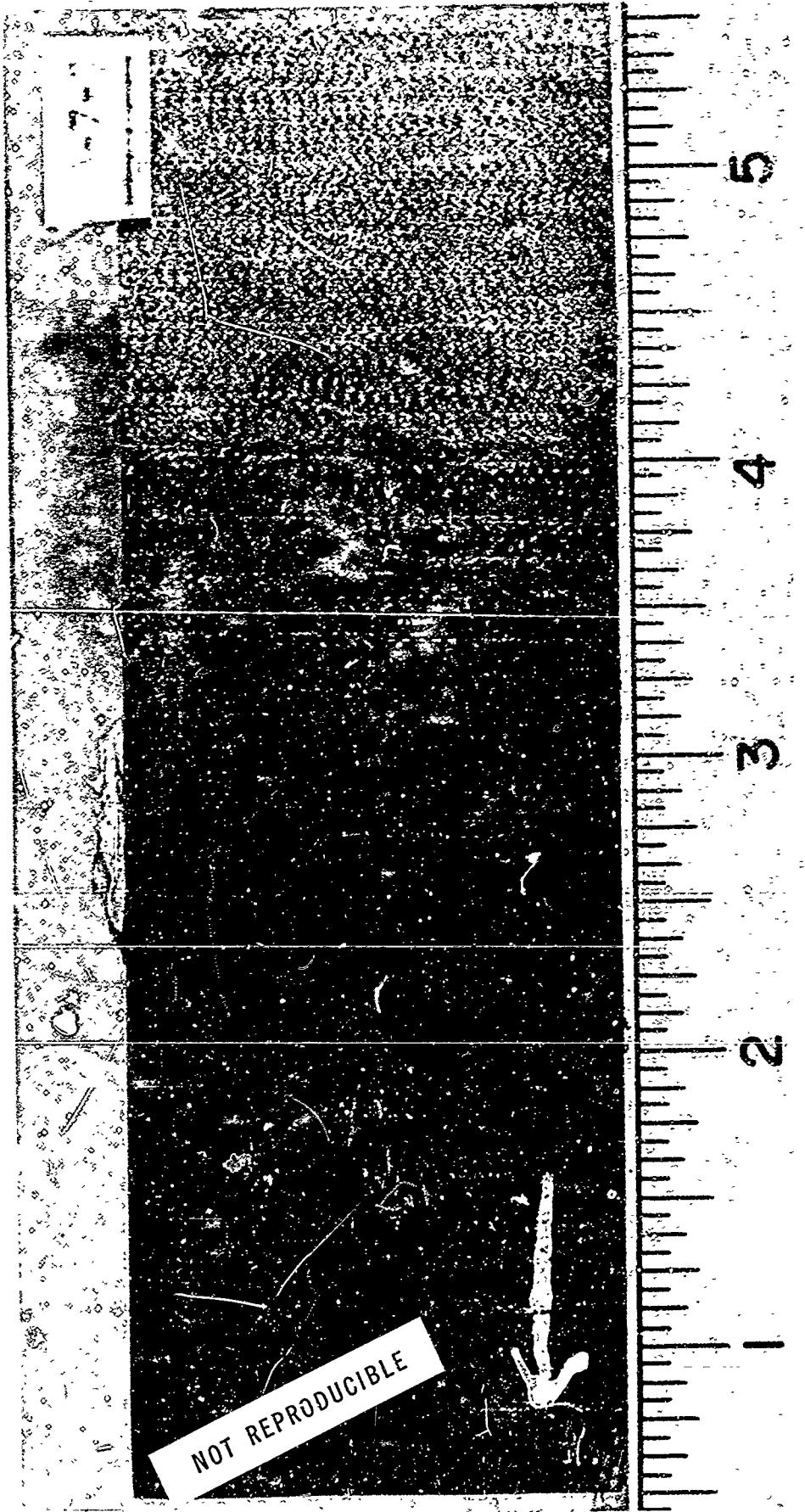
Figure 134. Untested Specimen Top View A7-3

NOT REPRODUCIBLE

124

A-7-3

NOT REPRODUCIBLE
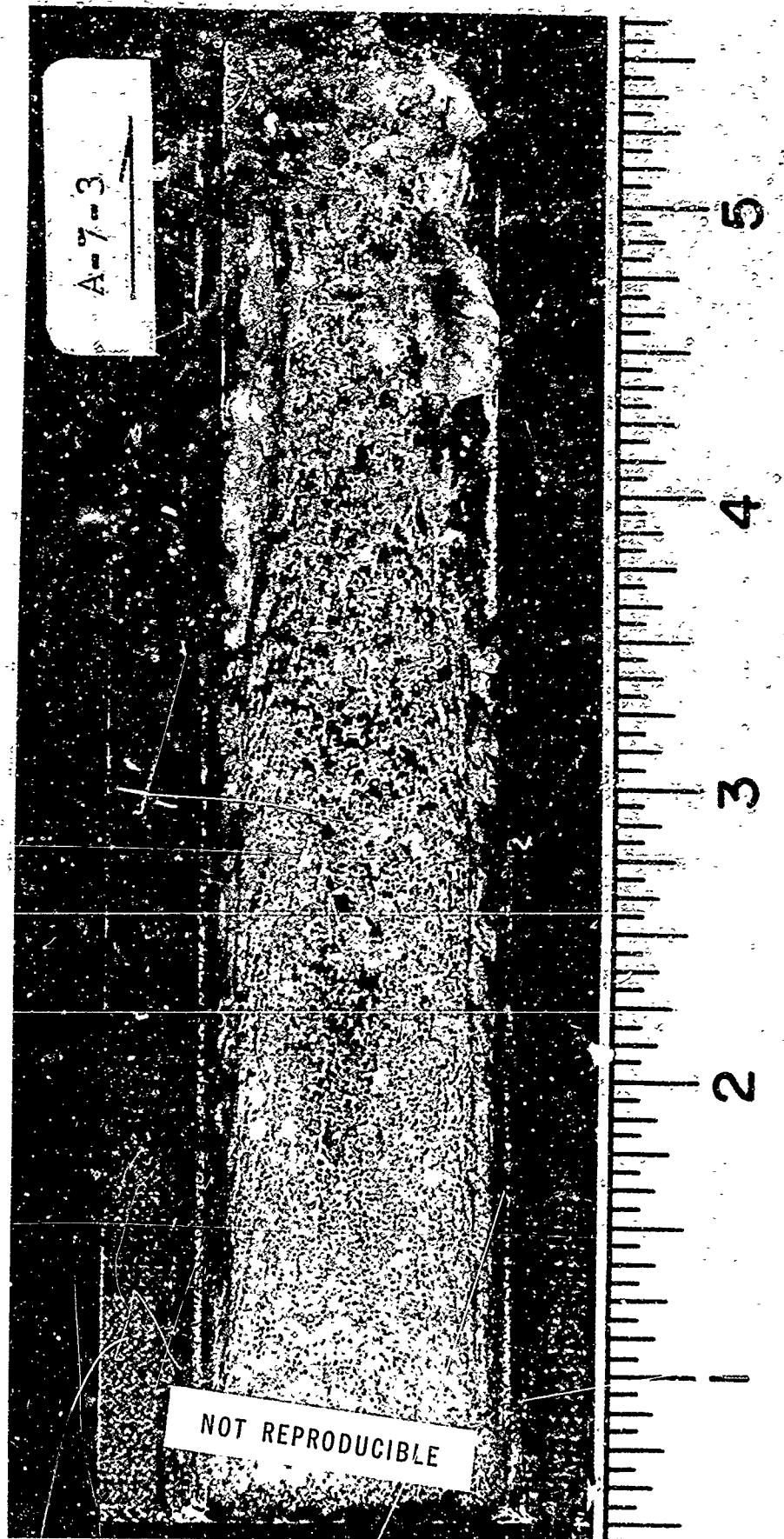
Figure 135. Ablated Specimen Top View A7-3

125

NOT REPRODUCIBLE

A-7-3

A-7-3

Figure 136. Ablated Specimen Sectioned A7-3

126

GE–M–2

NOT REPRODUCIBLE
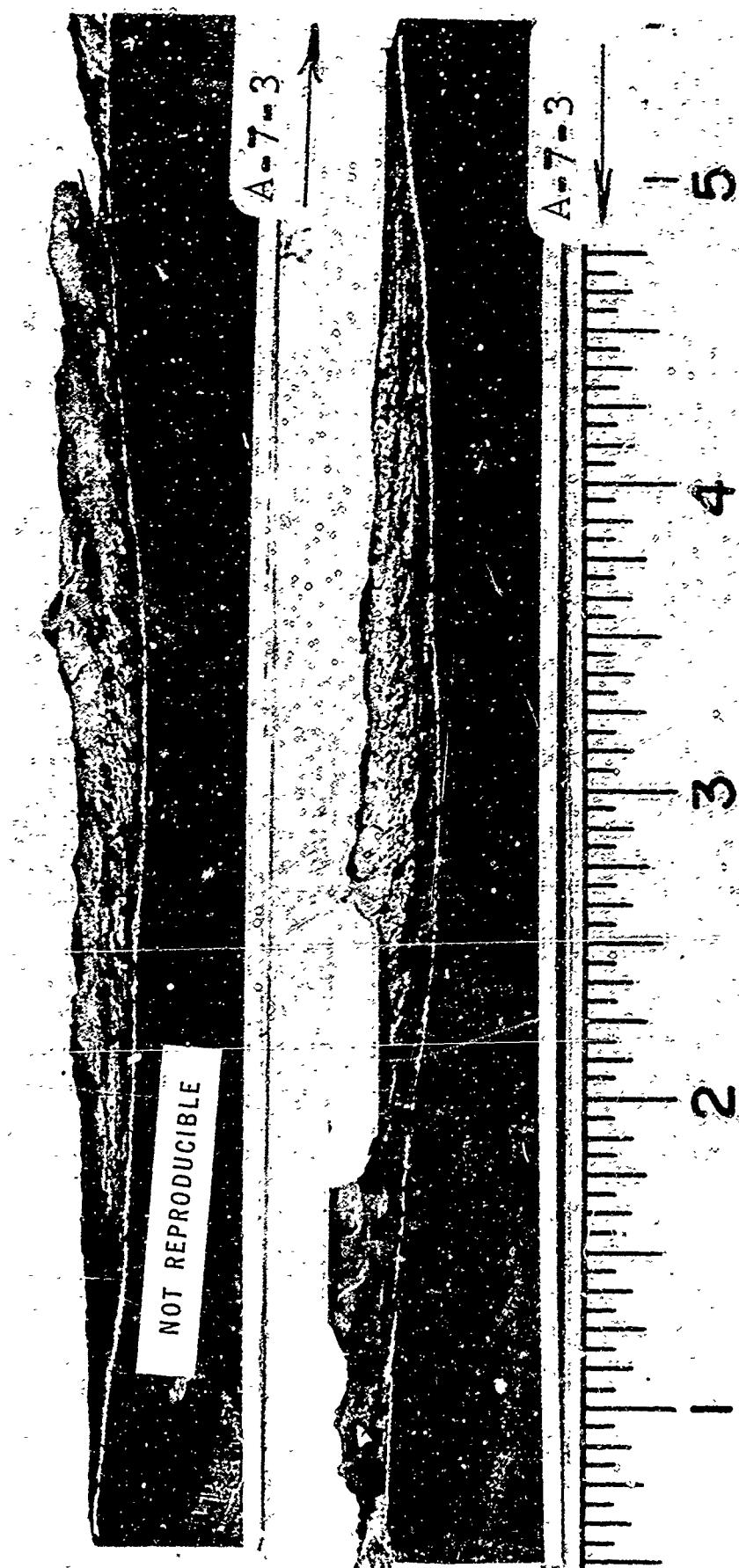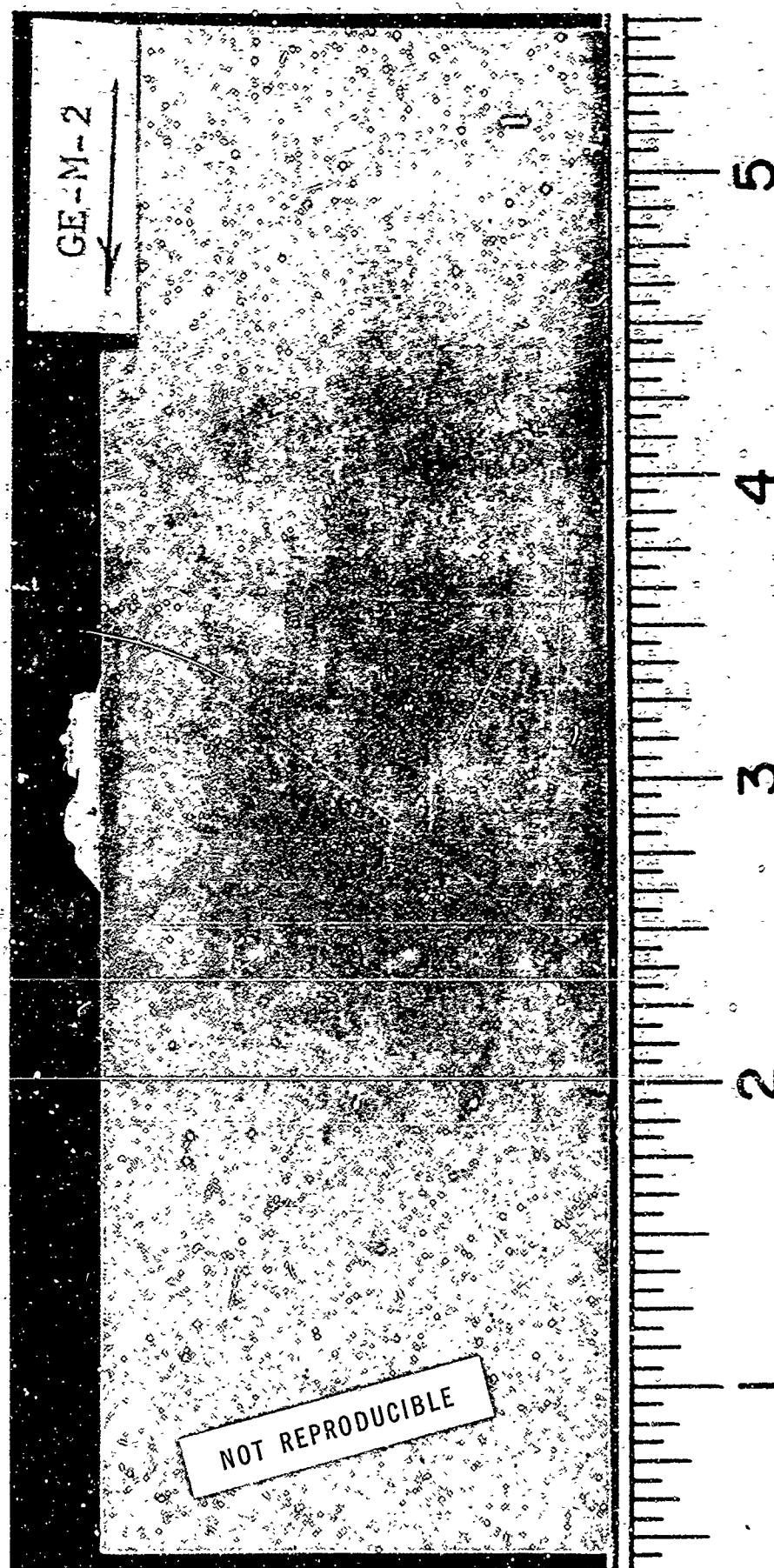
Figure 137. Untested Specimen Top View GEM–2

127

Figure 138. Ablated Specimen Three-Quarter View GEM-2

NOT REPRODUCIBLE

GE-M-2

GE-M-2

Figure 139. Ablated Specimen Sectioned GEM-2
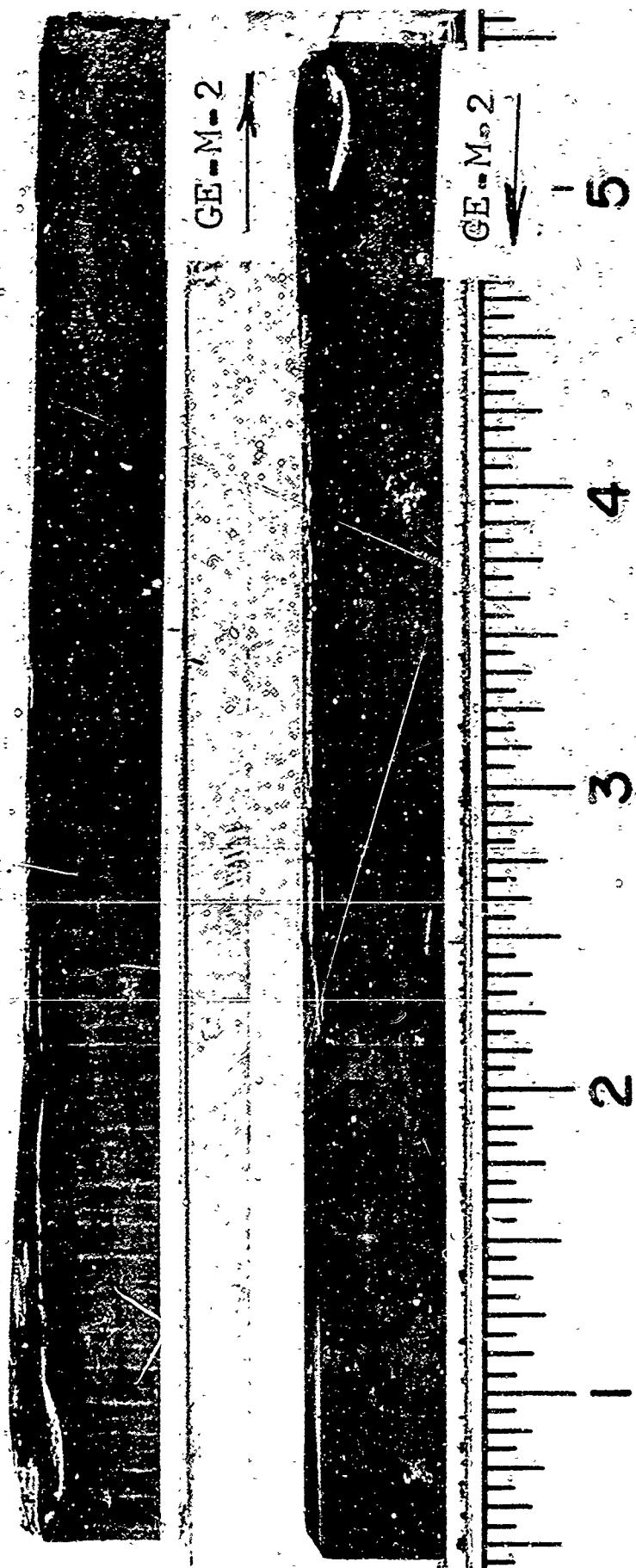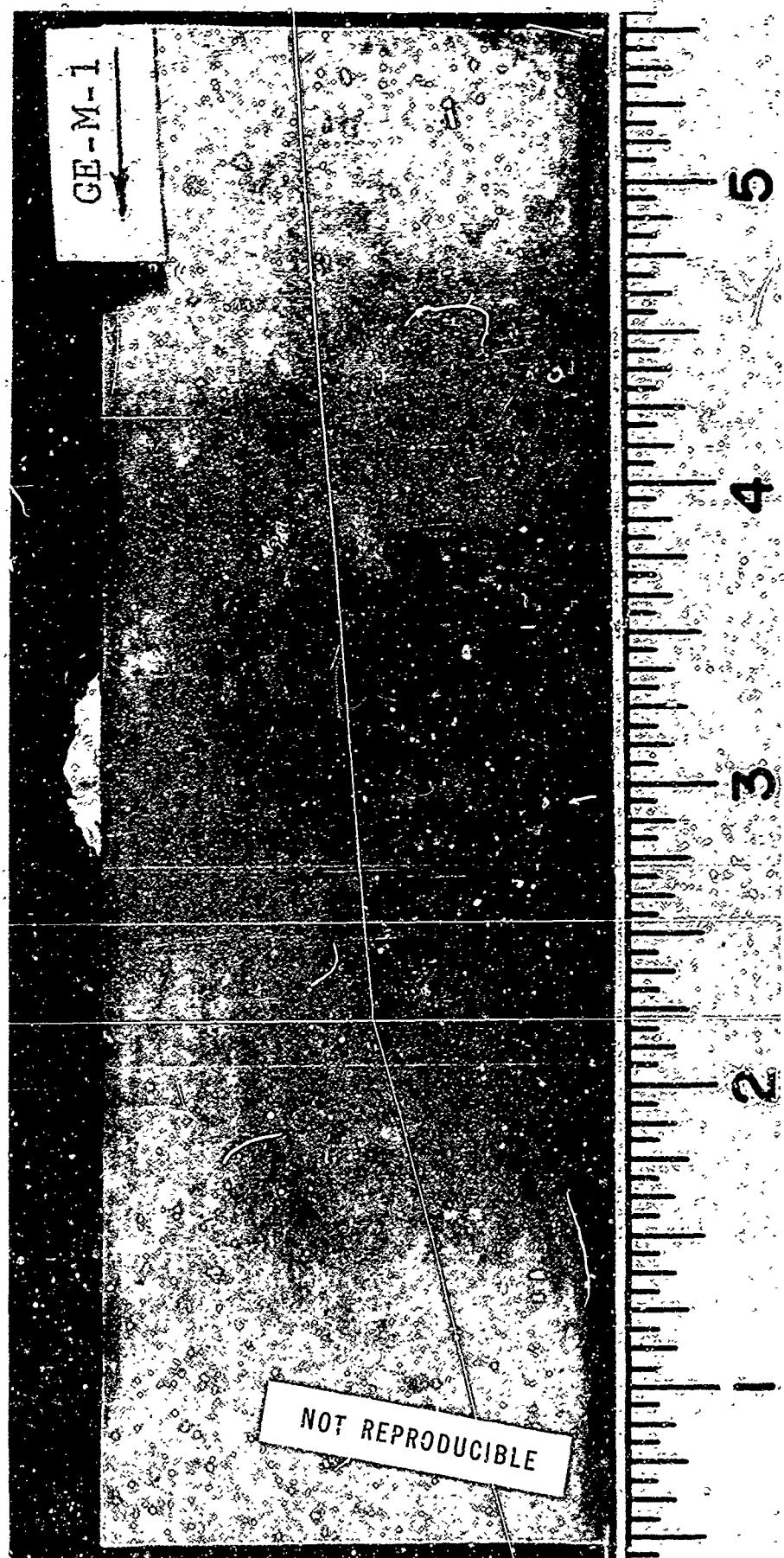
Figure 140. Untested Specimen Top View GEM-1
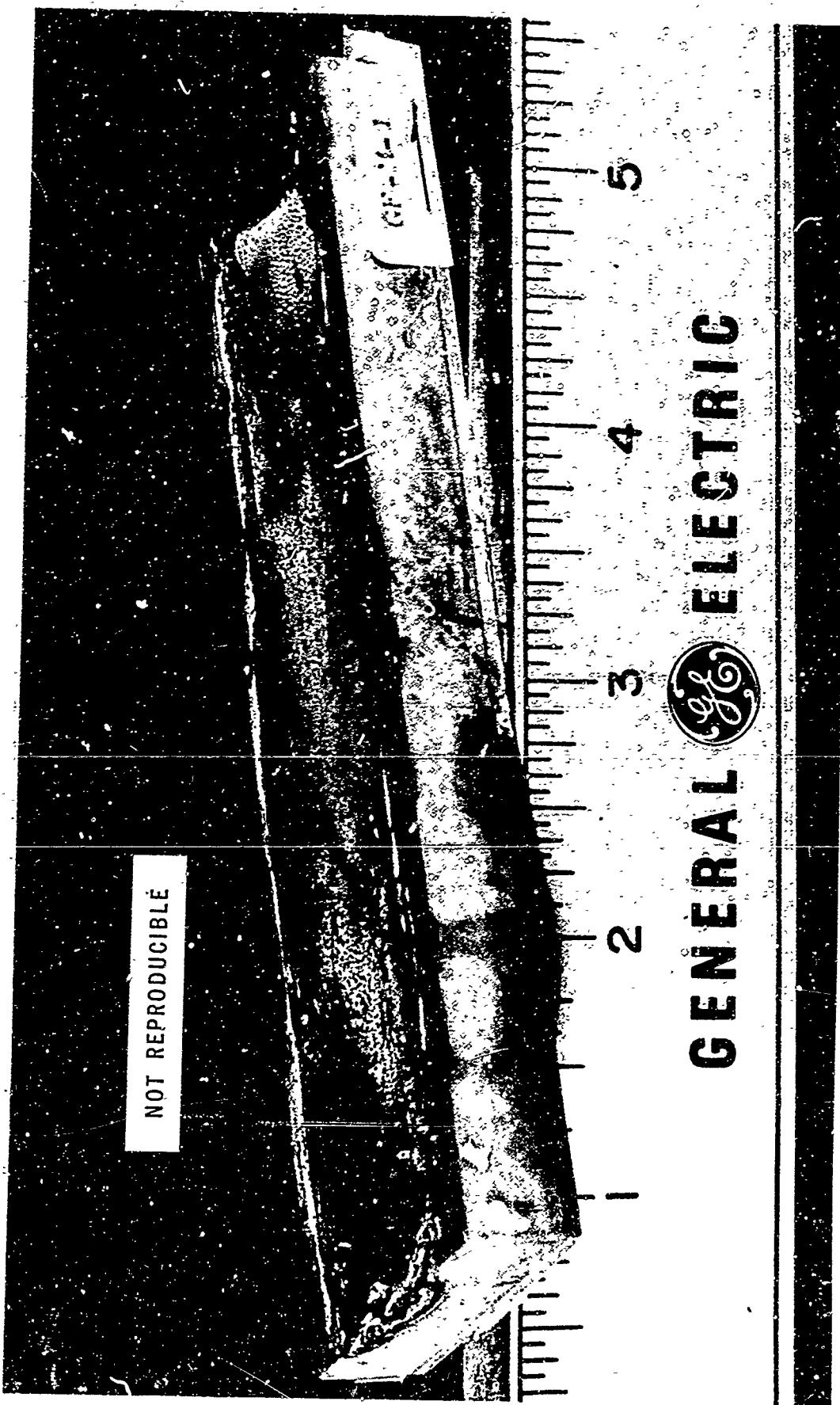
Figure 141. Ablated Specimen Three-Quarter View GEM-1

NOT REPRODUCIBLE

GENERAL ⊕ ELECTRIC

131
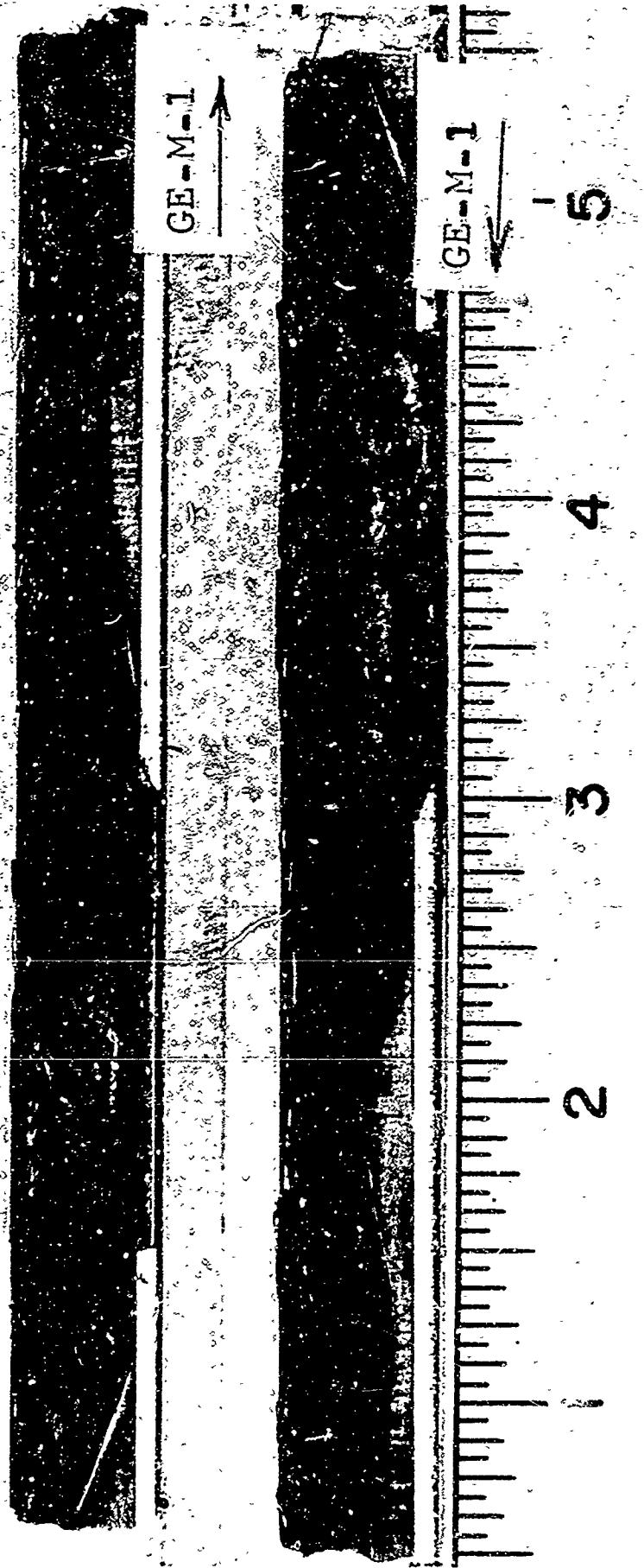
Figure 142. Ablated Specimen Sectioned GEM-1

NOT REPRODUCIBLE
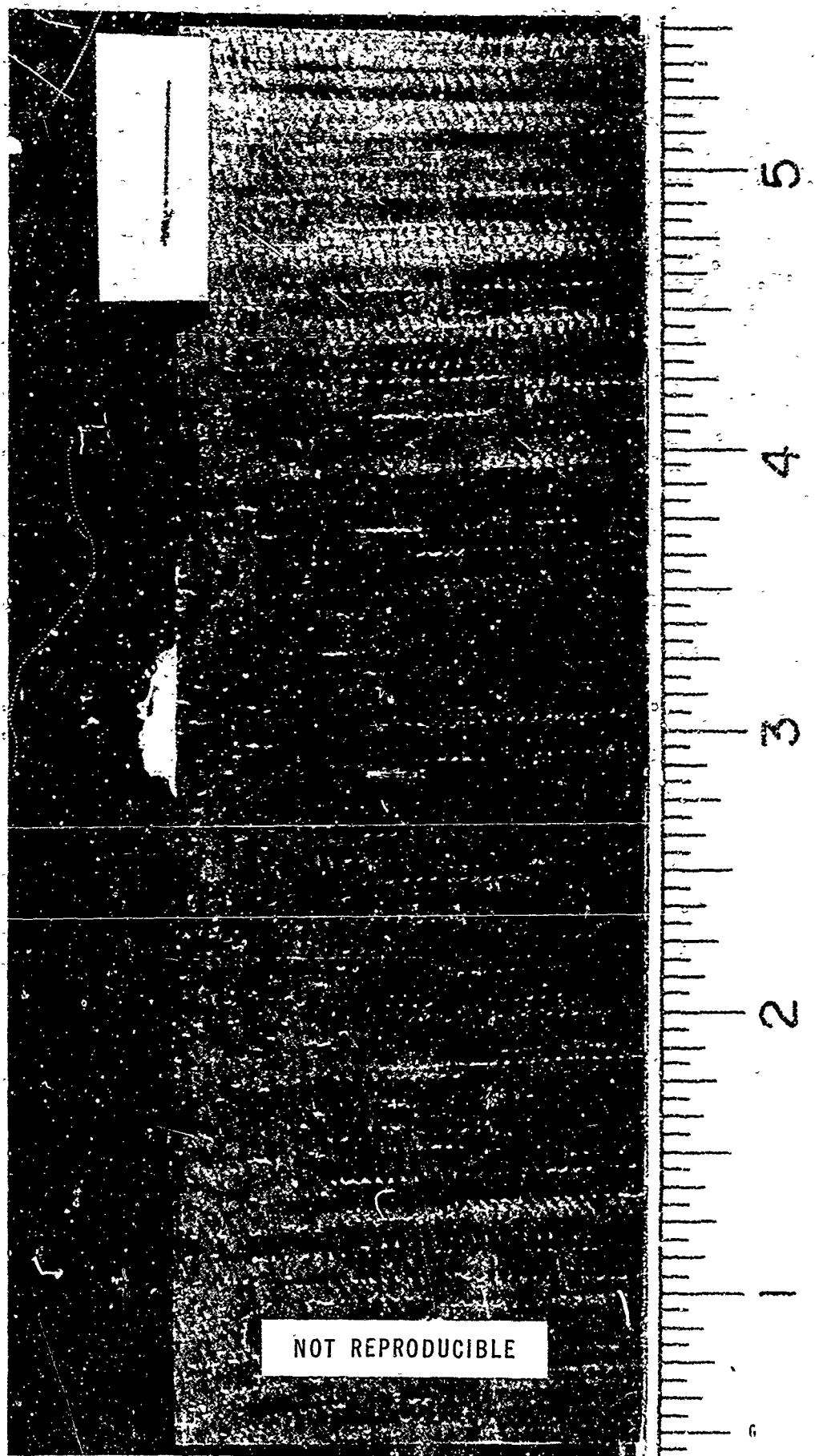
Figure 143. Untested Specimen Top View C4-1A
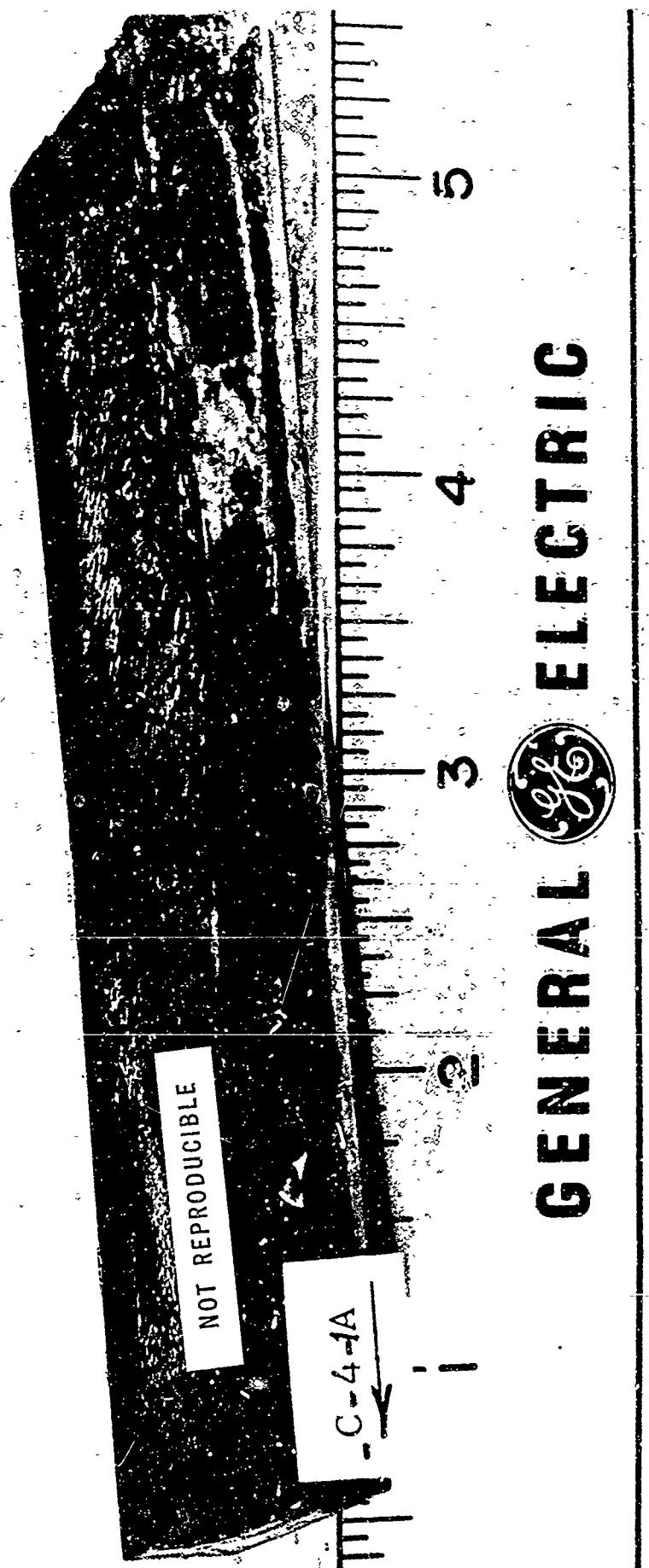
Figure 144. Ablated Specimen Three-Quarter View C4-1A

NOT REPRODUCIBLE

C-4-1A

GENERAL ⊕ ELECTRIC
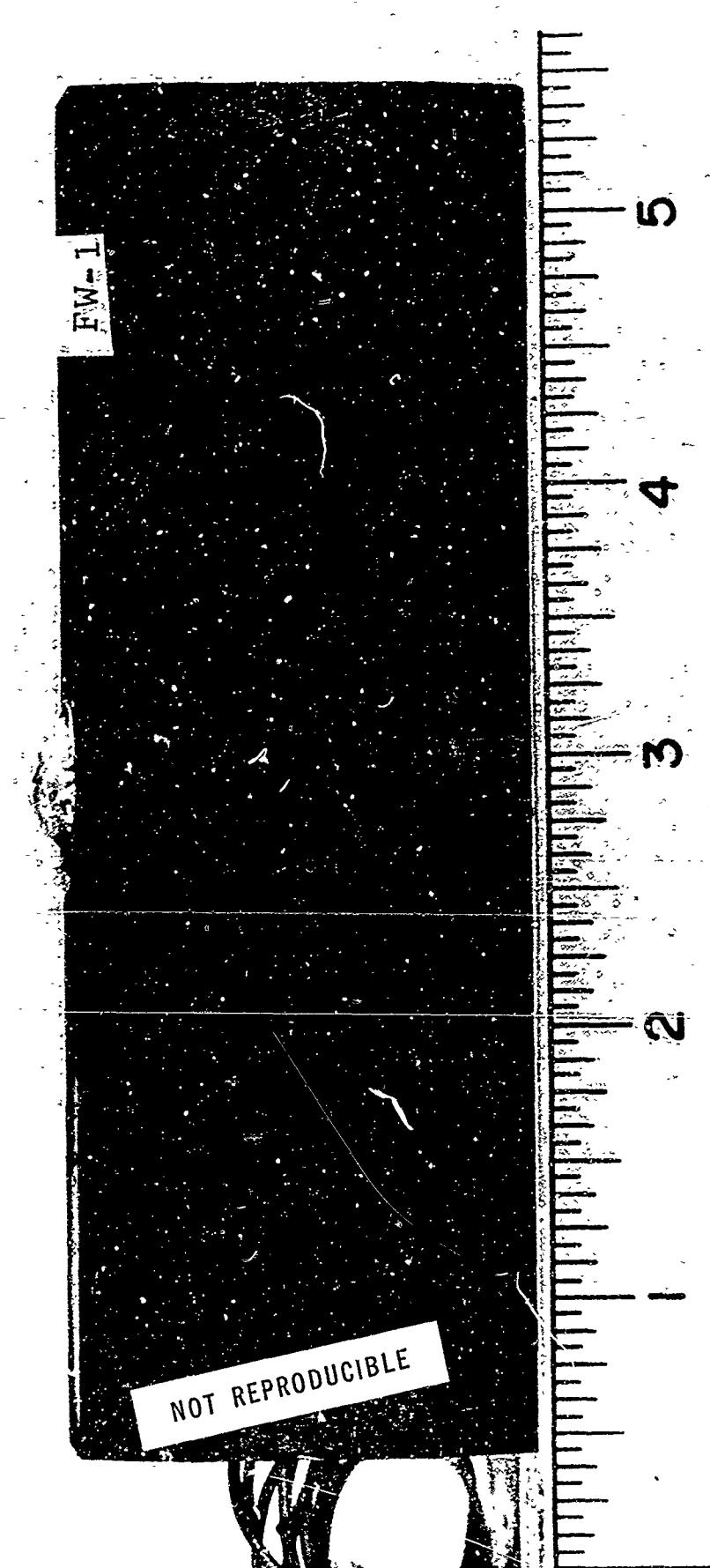
Figure 145. Untested Specimen FW-1

NOT REPRODUCIBLE

FW-1

135

NOT REPRODUCIBLE

GENERAL ⊛ ELECTRIC
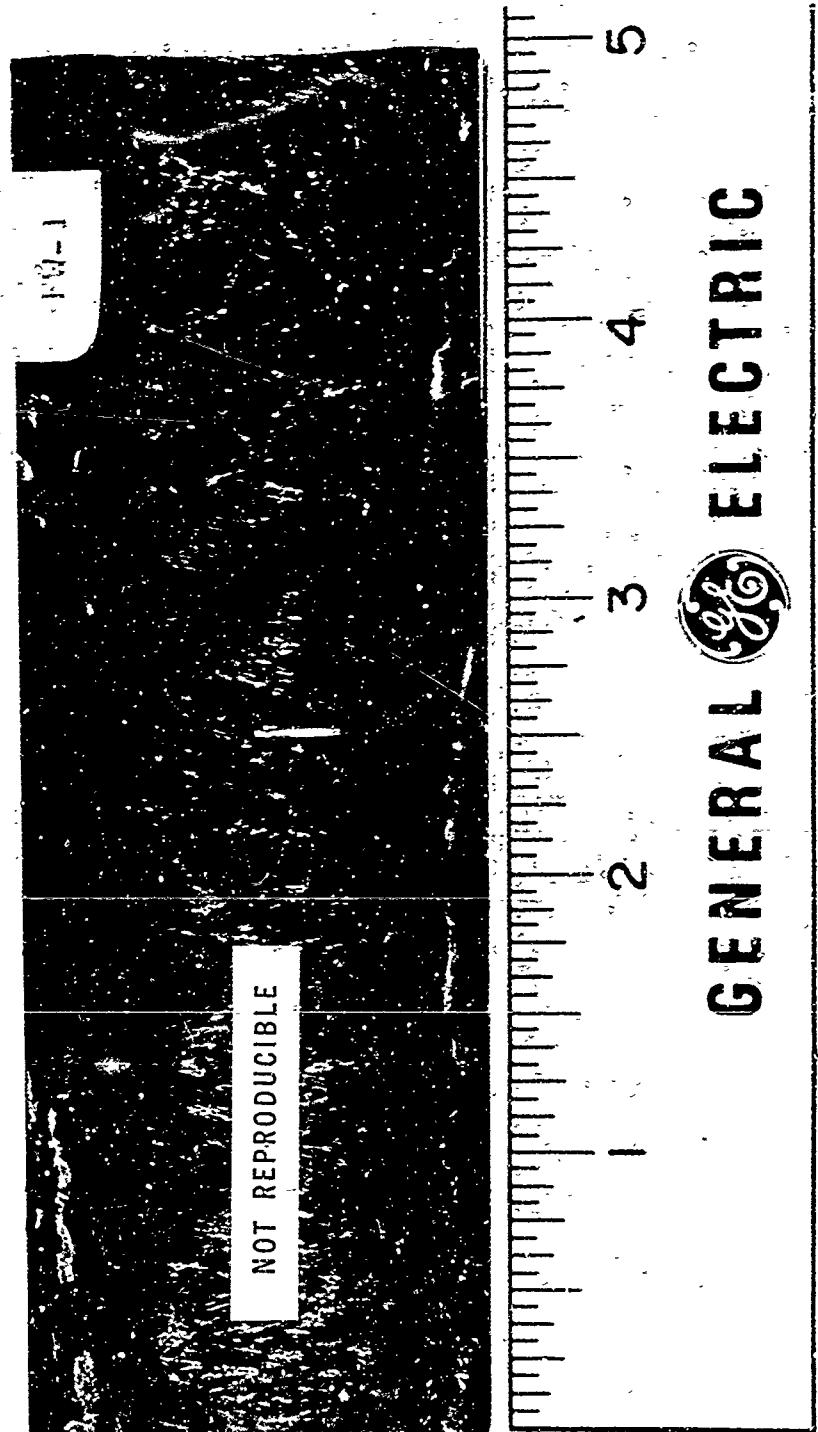
Figure 146. Ablated Specimen FW-1
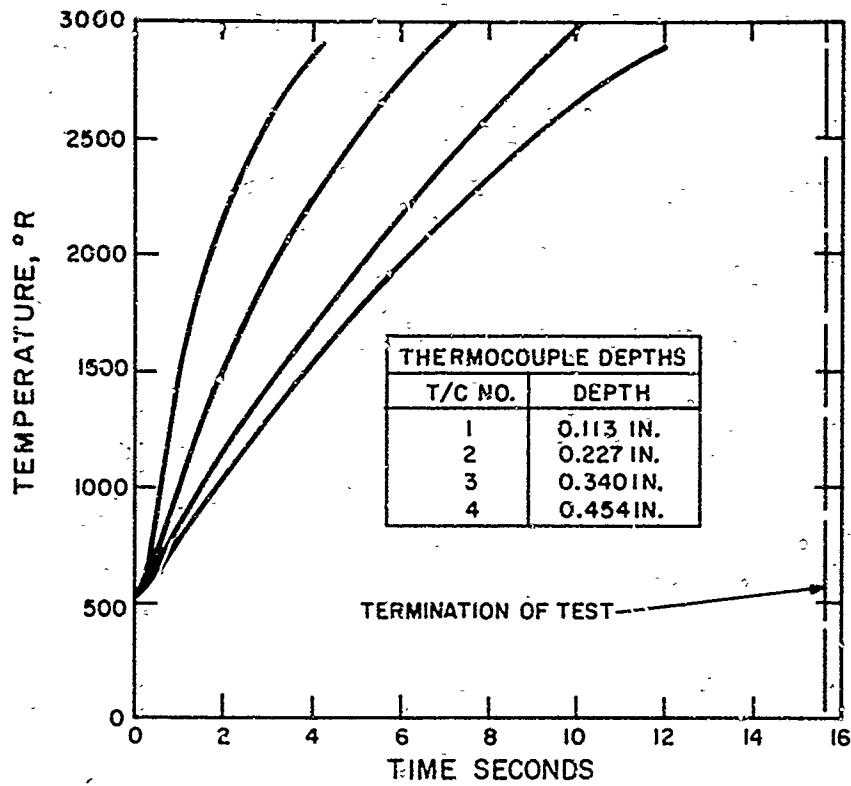
Figure 147. Thermocouple Response, ATJ Graphite
(Dual Channel Test)
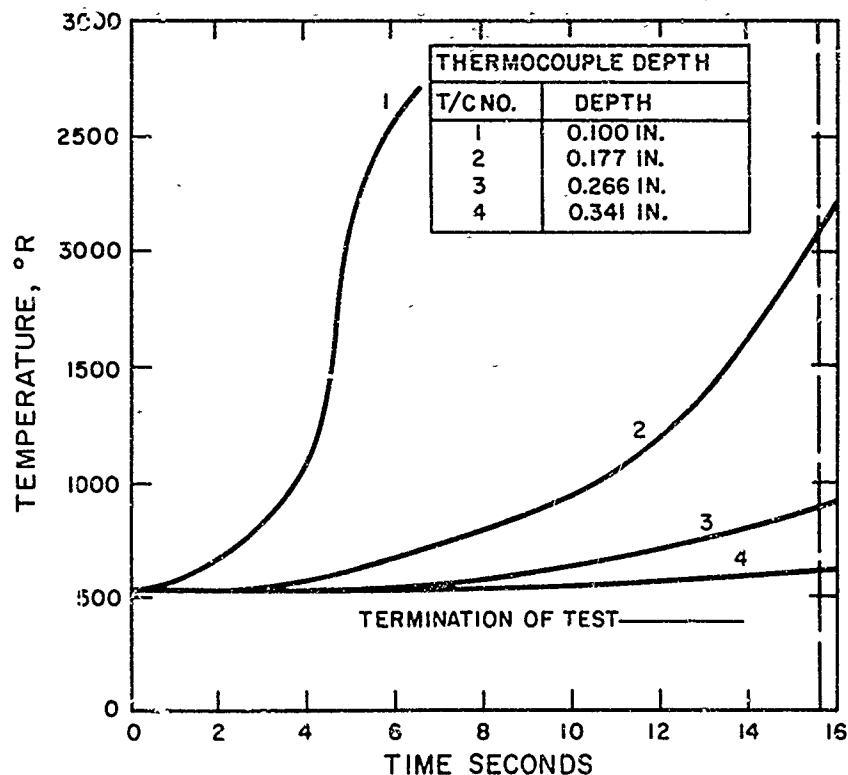
Figure 148. Thermocouple Response, CP109A (20° TW)
(Dual Channel Test)

137

THERMOCOUPLE DEPTHS

NO.1	0.100 IN.
NO.2	0.177 IN.
NO.3	0.266 IN.
NO.4	0.381 IN.
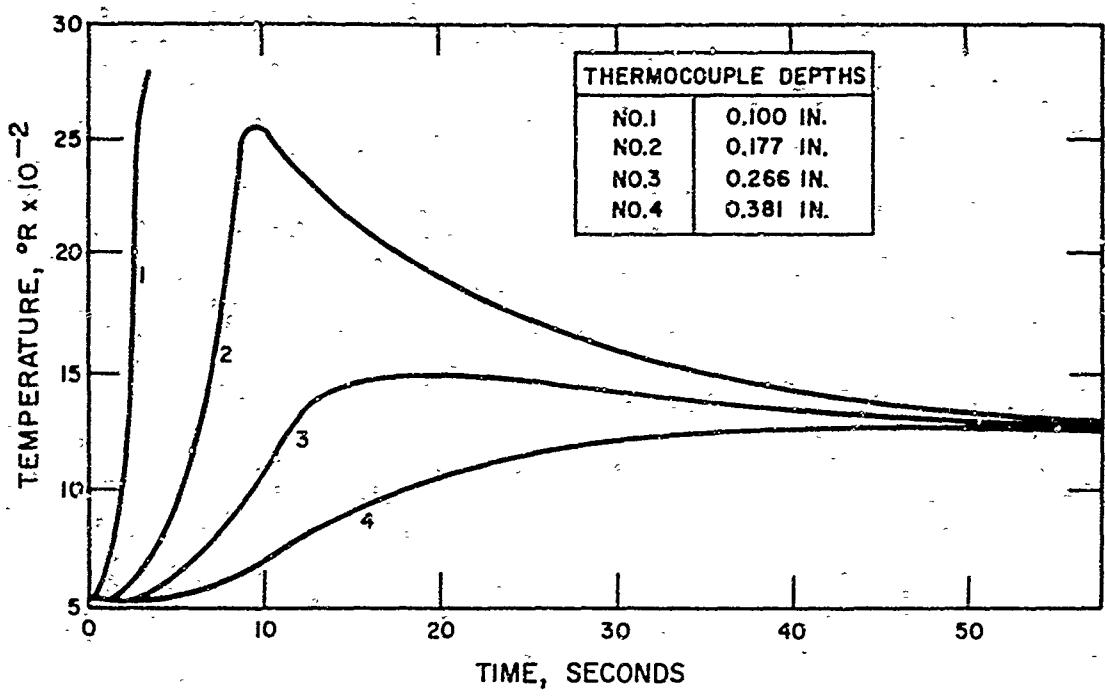
Figure 149. Thermocouple Response, CP 109A (20° TW)
(Dual Channel Test)
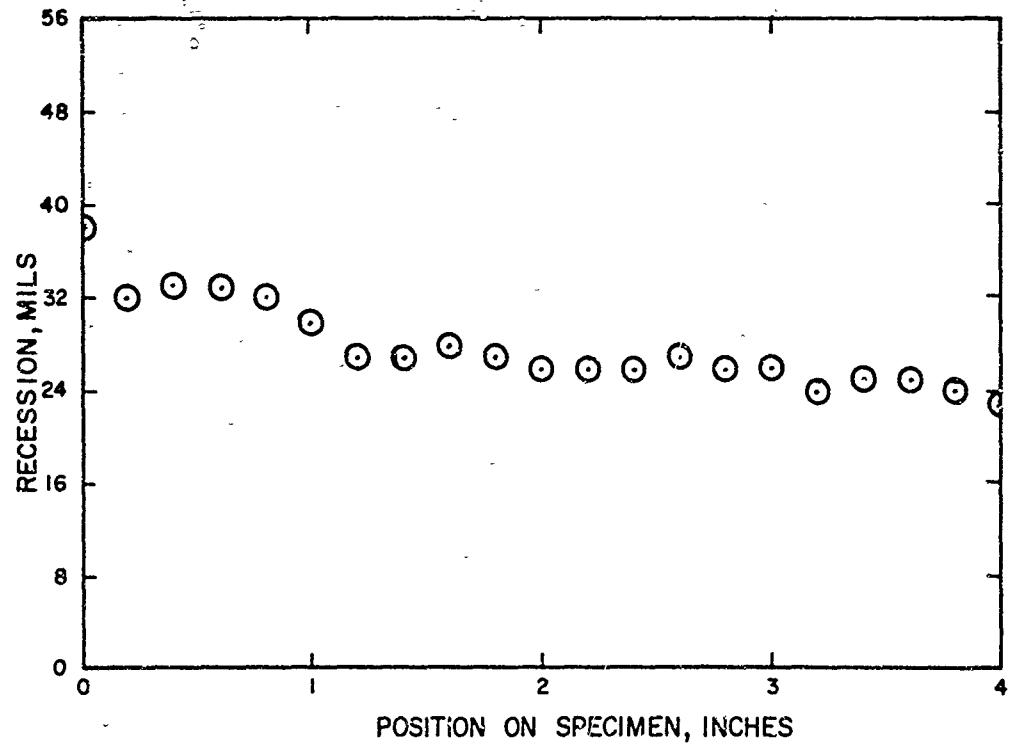
Figure 150. Recession Profile, ATJ Graphite
(Dual Channel Test)

138
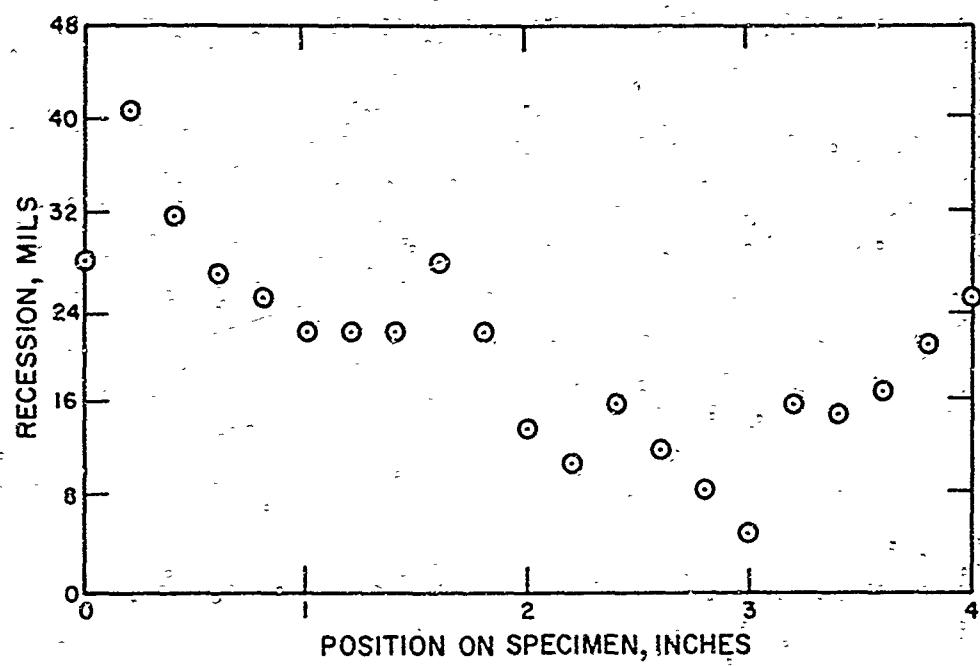
Figure 151. Recession Profile, Carbon Phenolic (20° TW)
(Dual Channel Test)

NOT REPRODUCIBLE
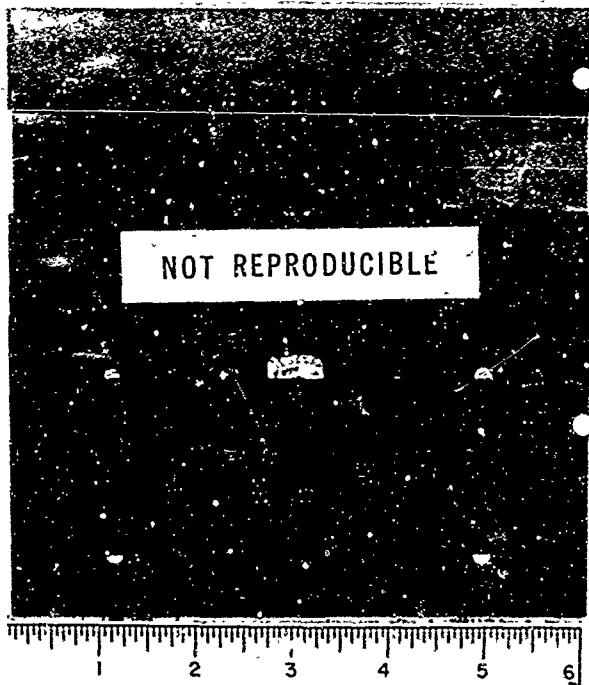
Figure 152. Dual Channel Plates Prior to Test (Upper – ATJ Graphite,
Lower – CP 109A 20° TW)
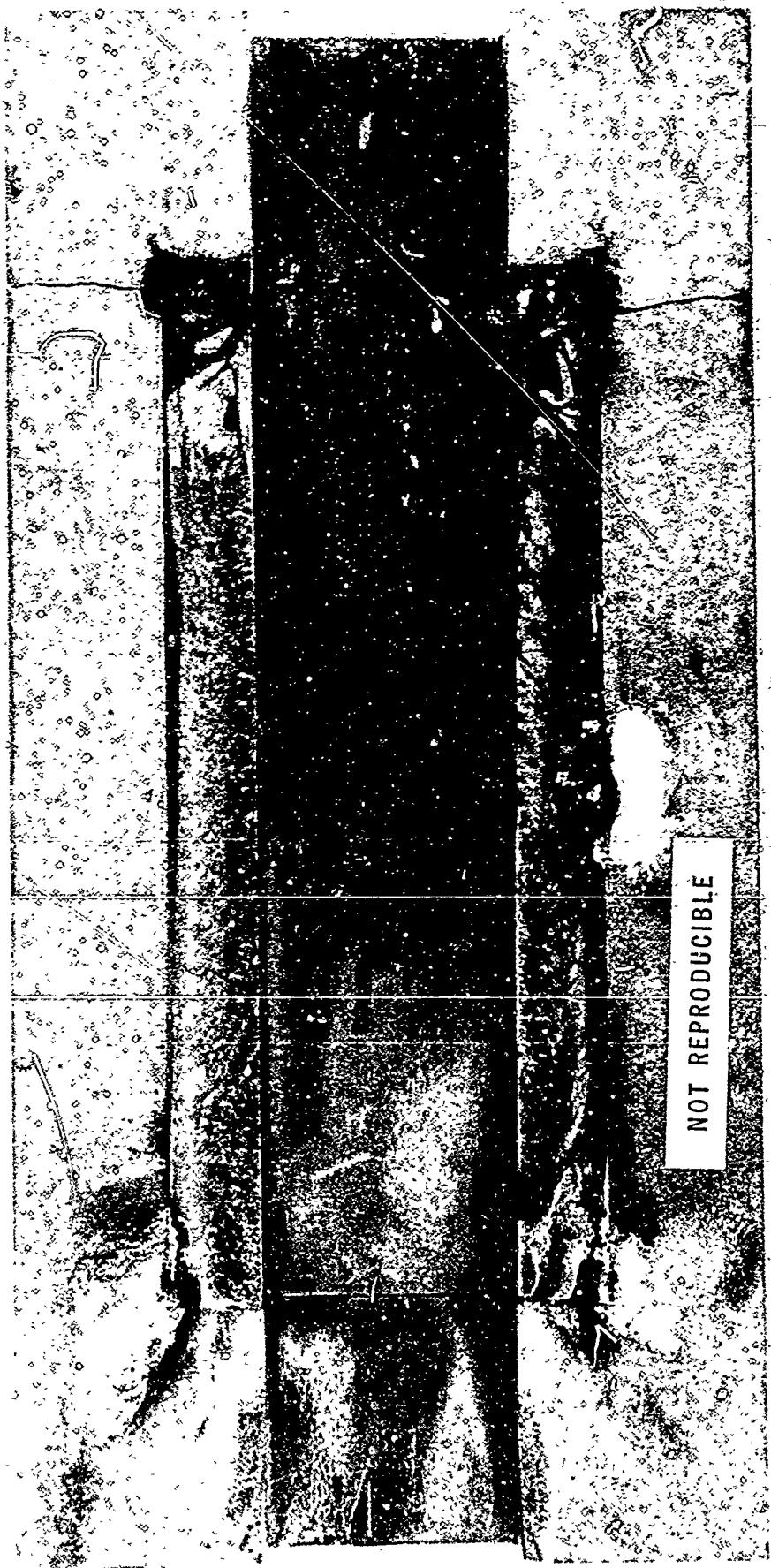
NOT REPRODUCIBLE

Figure 15c. ATJ Graphite after Test in Dual Channel Facility
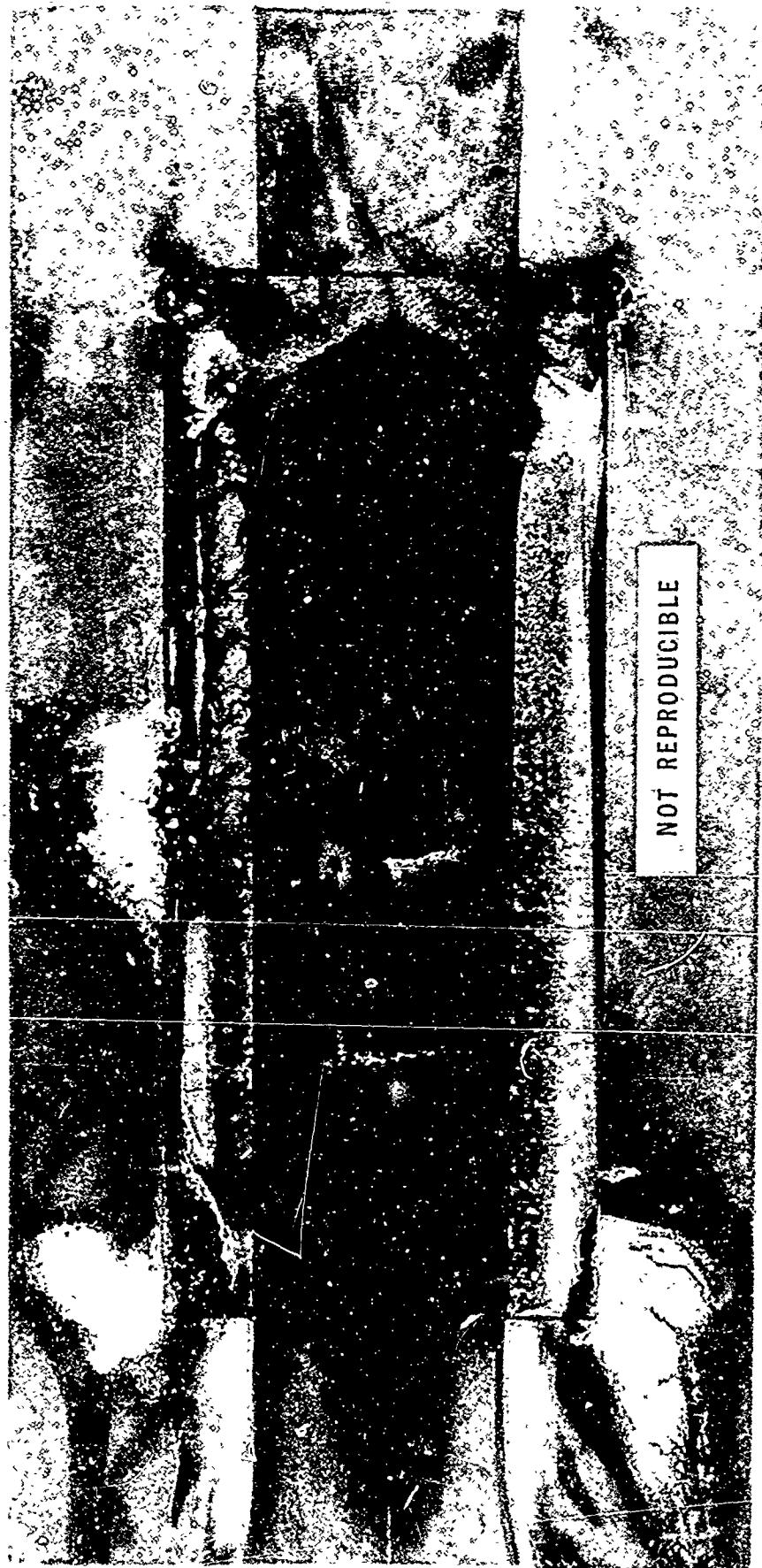
NOT REPRODUCIBLE

Figure 154. CP 109A (20° TW) after Test in Dual Channel Facility
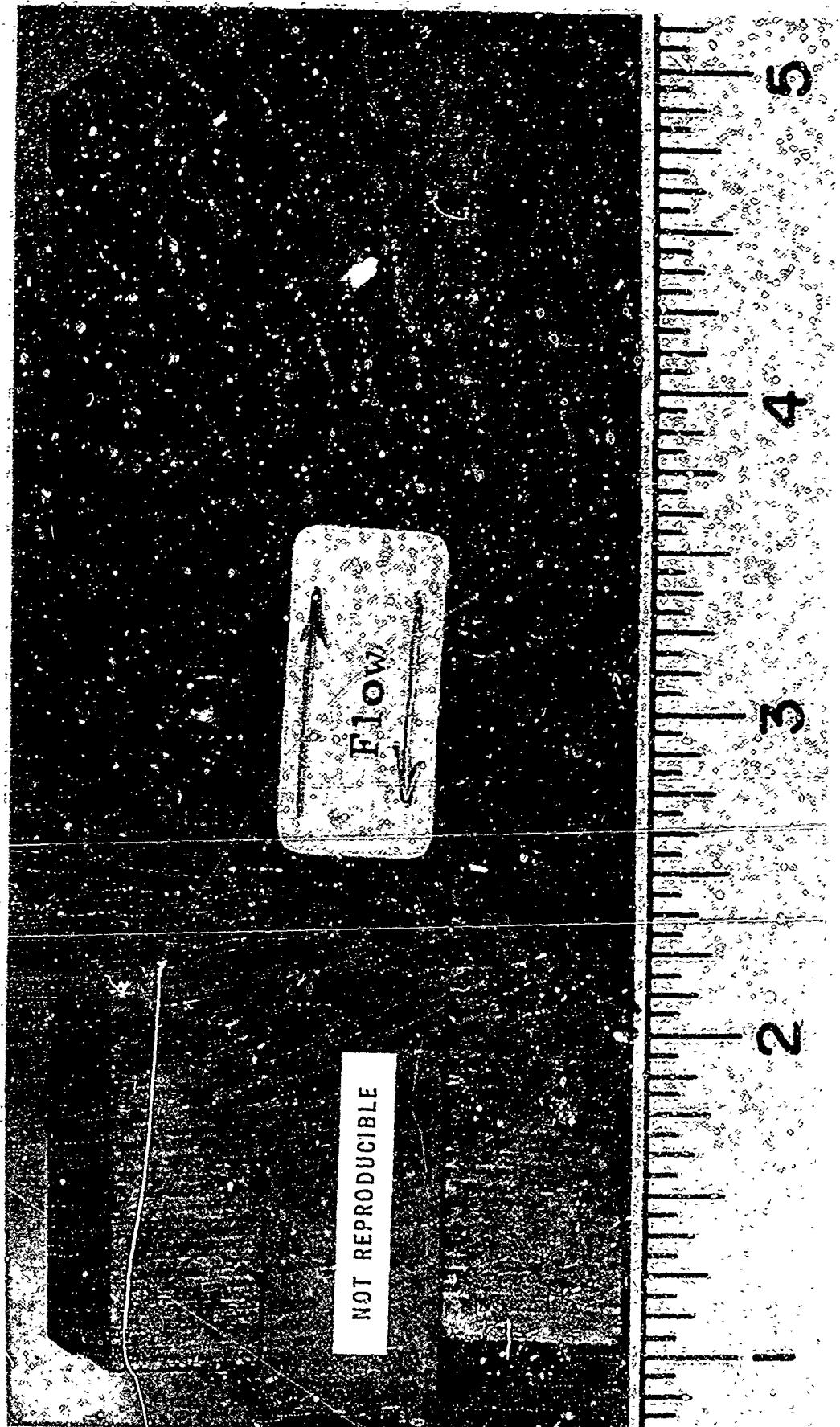
Figure 155. Sectional View of ATJ Graphite after Test

NOT REPRODUCIBLE

Flow
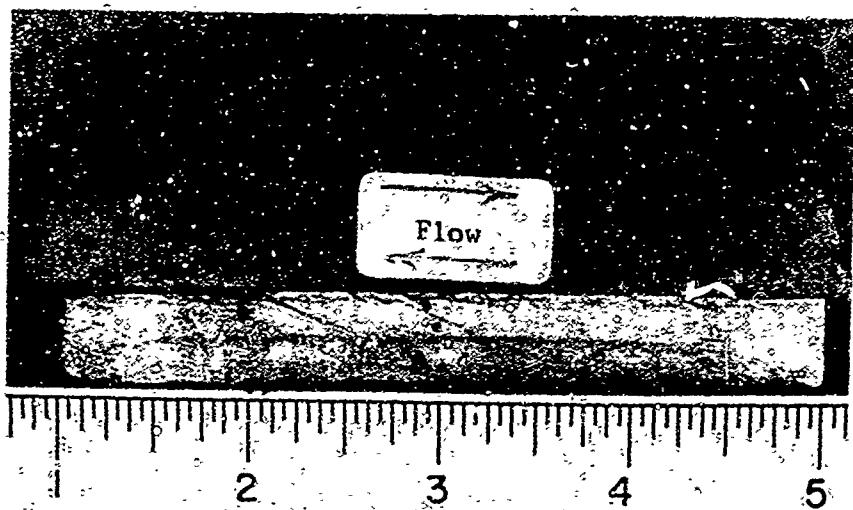
Figure 156. Sectional View of CP 109A (20° TW) after Test
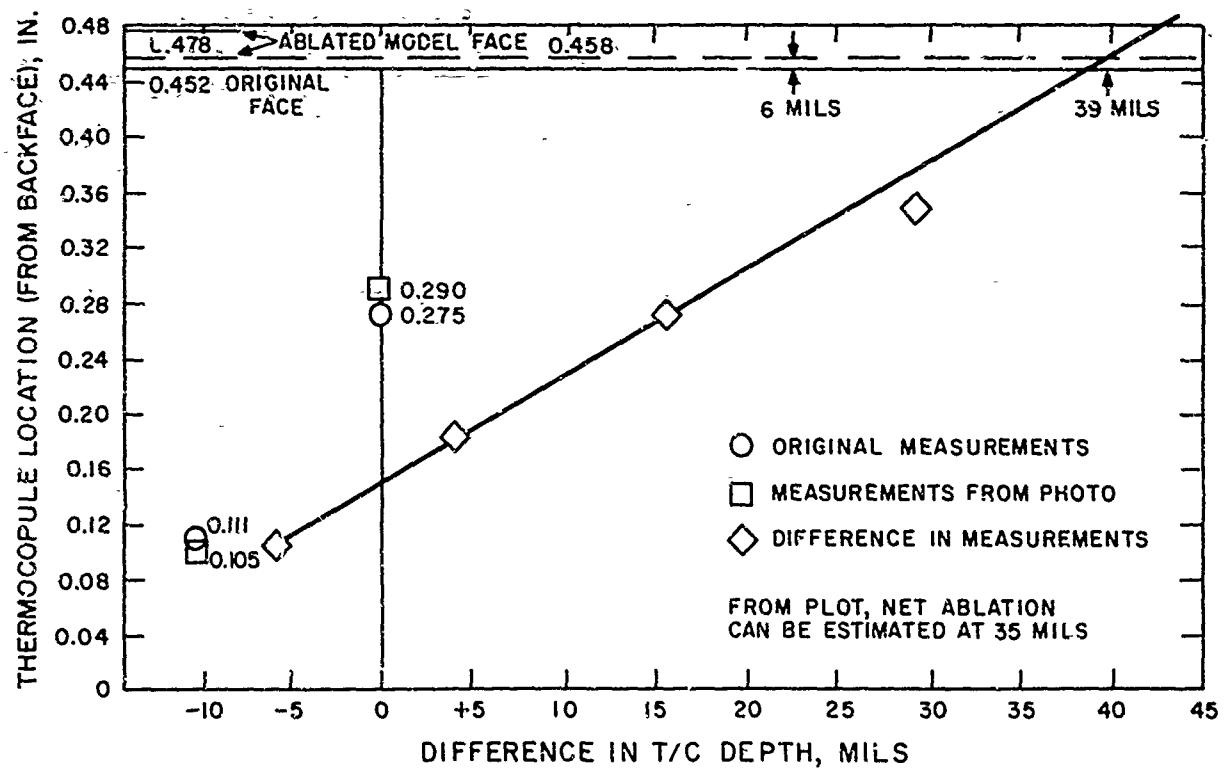
Figure 157. Analysis of Specimen Growth-CP 109A in Dual Channel Facility

143
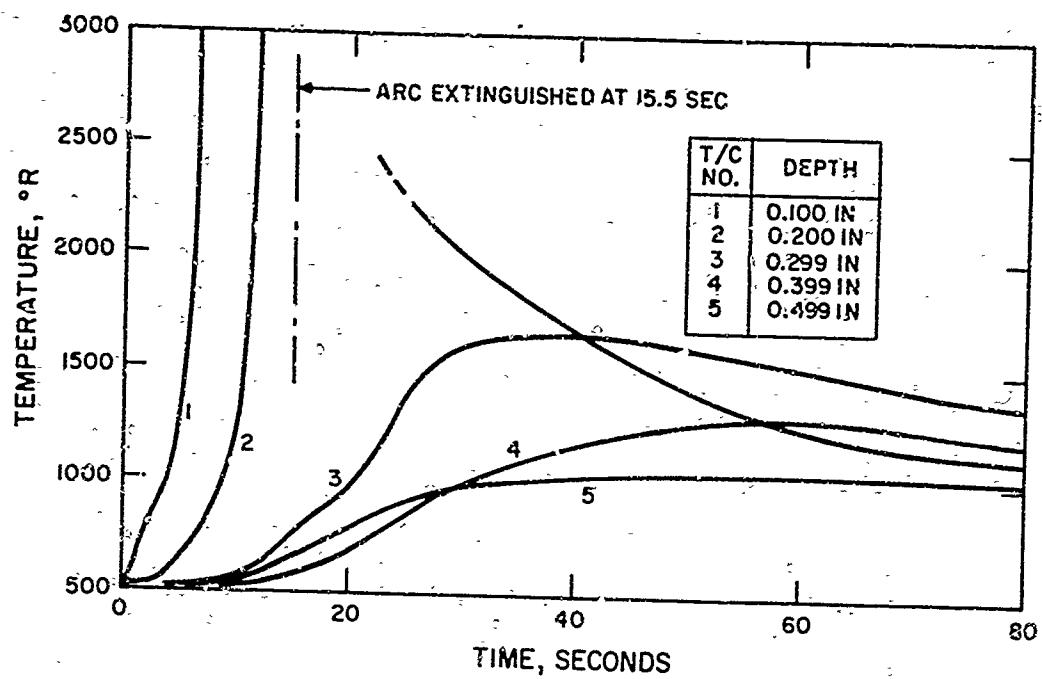
Figure 158. Thermocouple Response – Specimen A4-5
Run 22-71
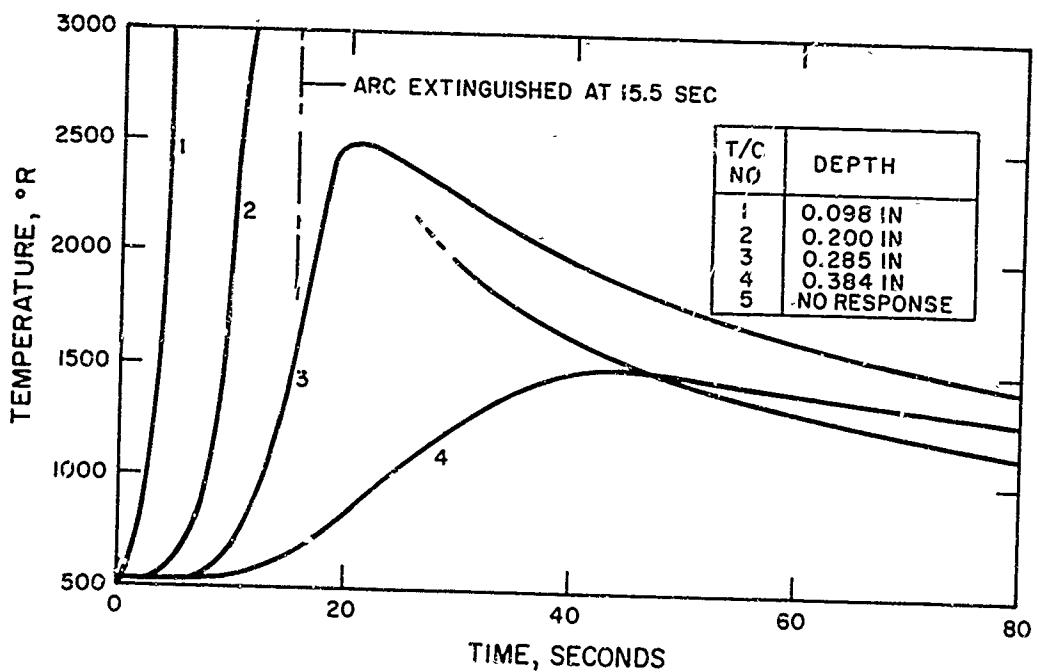
Figure 159. Thermocouple Response – Specimen A4-7
Run 22-71

144
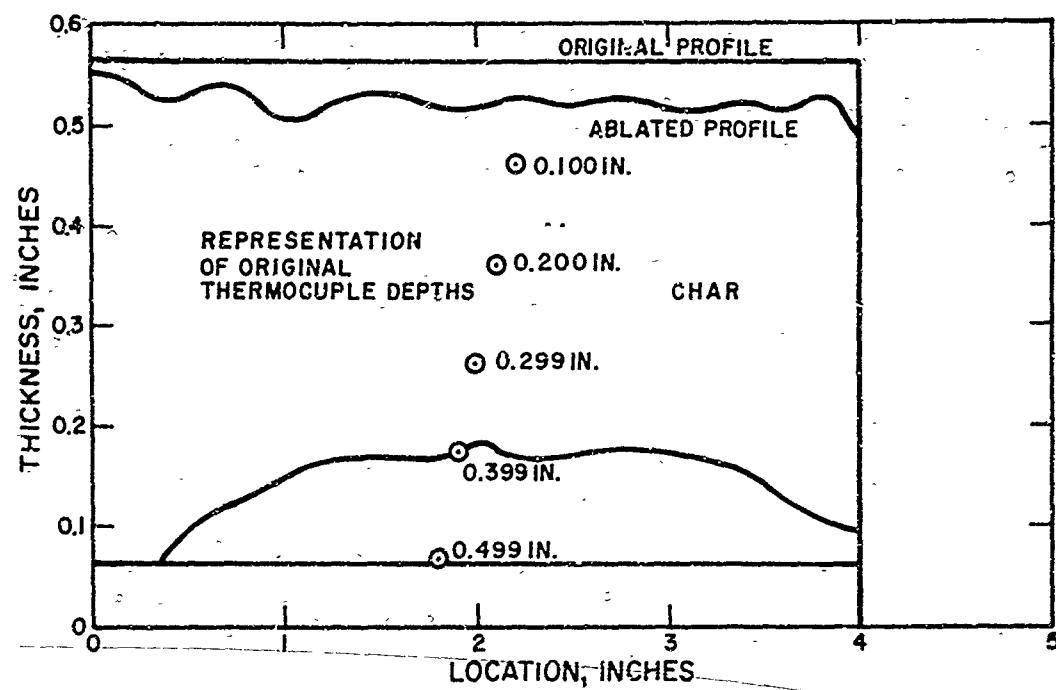
Figure 160. Recession Profile – Specimen A4-5 Run 22
(Dual Channel Test)
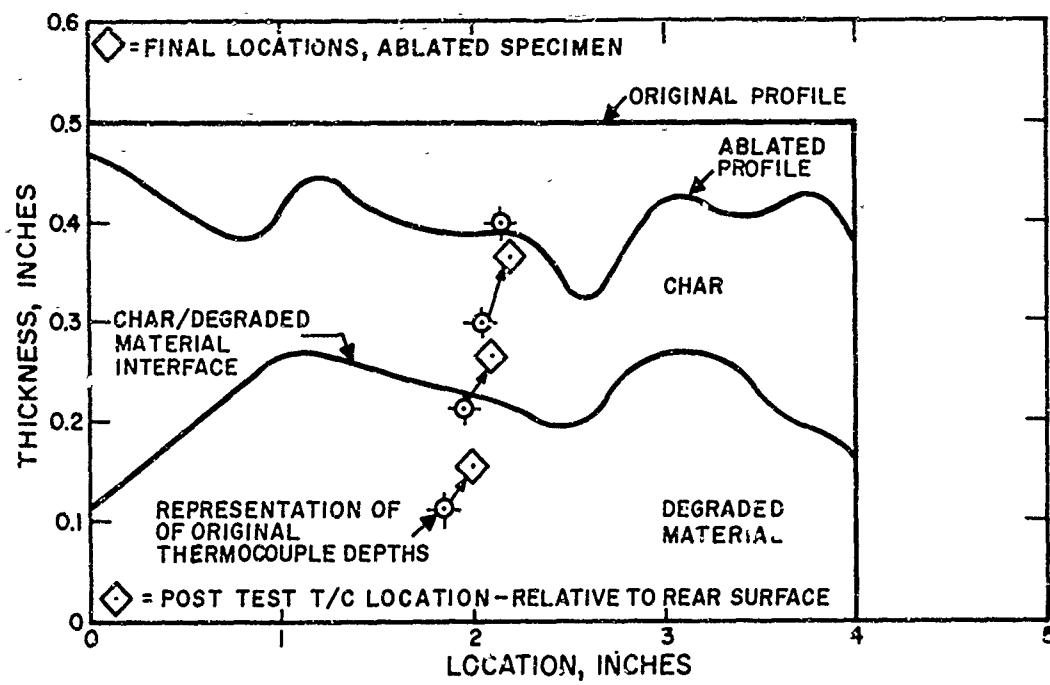
Figure 161. Recession Profile – Specimen A4-7 Run 22
(Dual Channel Test)

145
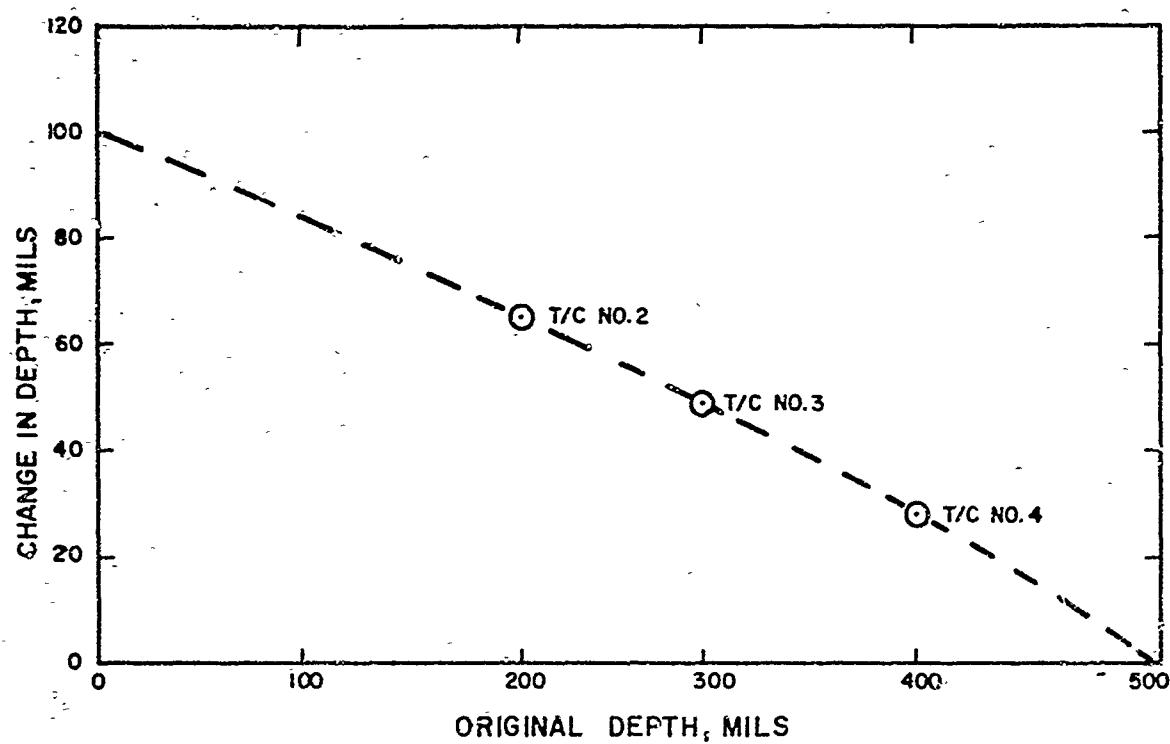
Figure 162. Depth Changes of Thermocouples (Projected Increase in Unablated Thickness) A4-7
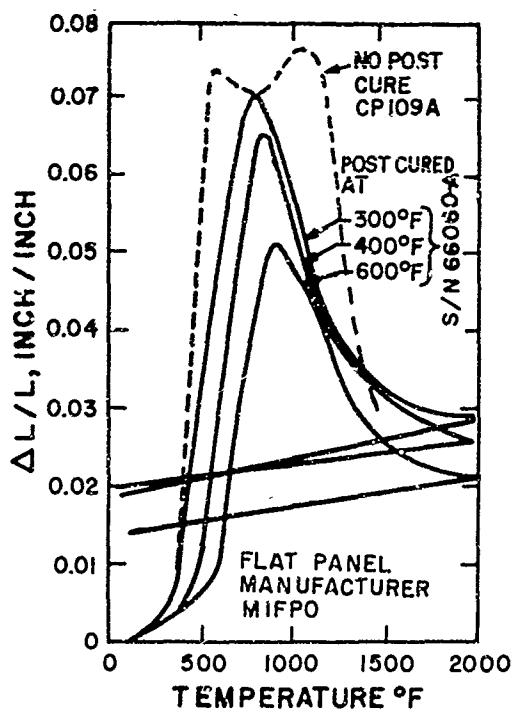
Figure 163. Thermal Expansion, Carbon Phenolic
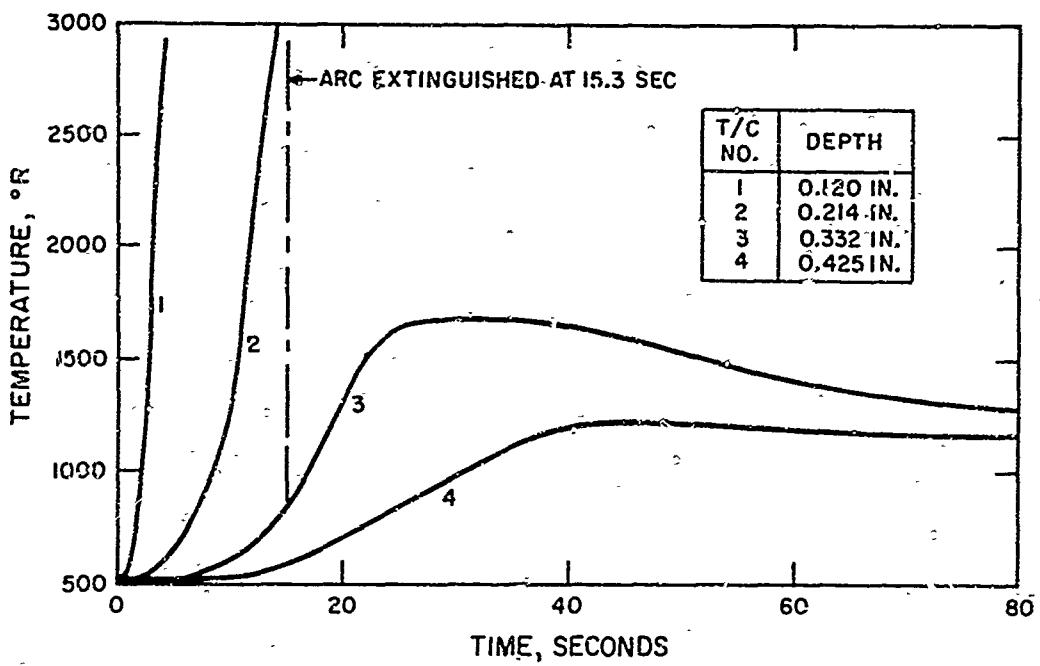
Figure 164. Thermocouple Response - Specimen A3-8 Run 23-71
(Dual Channel Test)
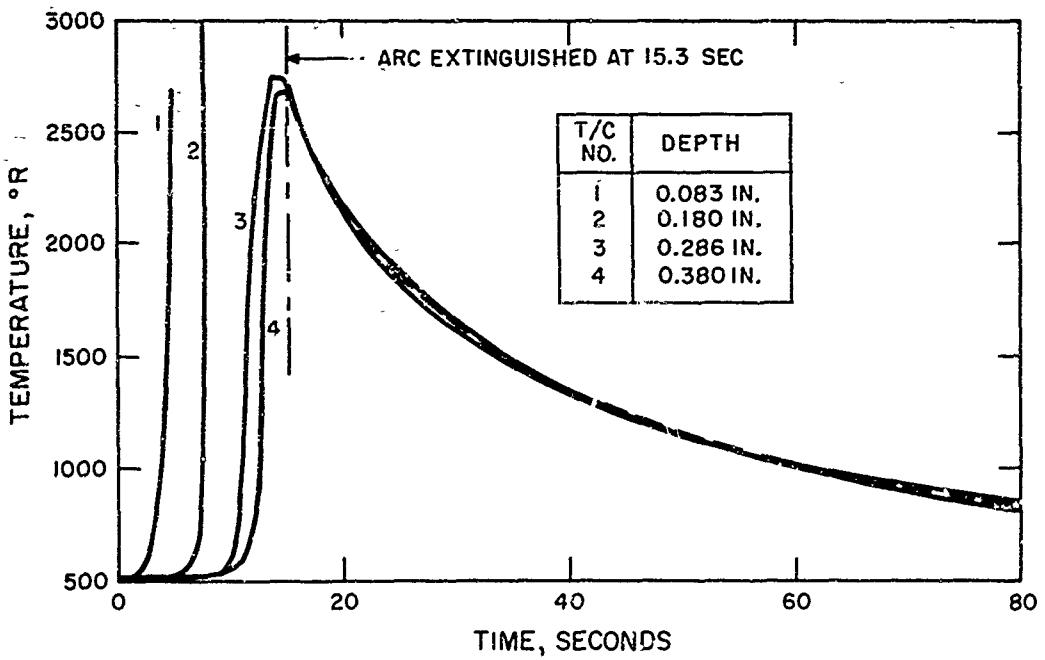
Figure 165. Thermocouple Response - Specimen A4-6 Run 23-71
(Dual Channel Test)

147
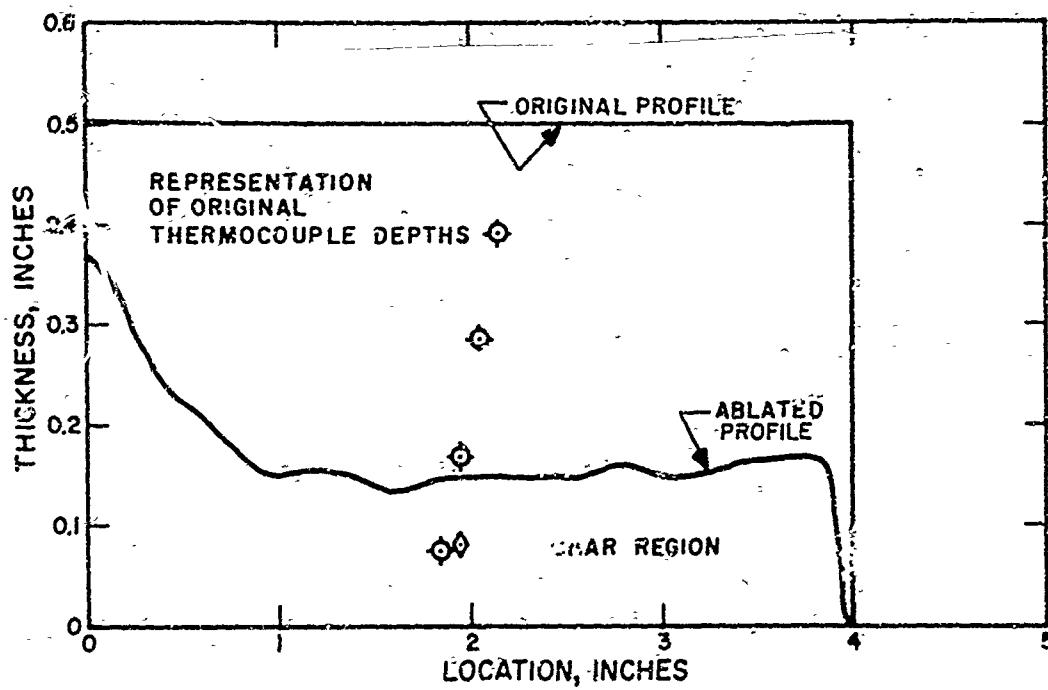
Figure 166. Recession Profile – Specimen A3-8 Run 23-71
(Dual Channel Test)
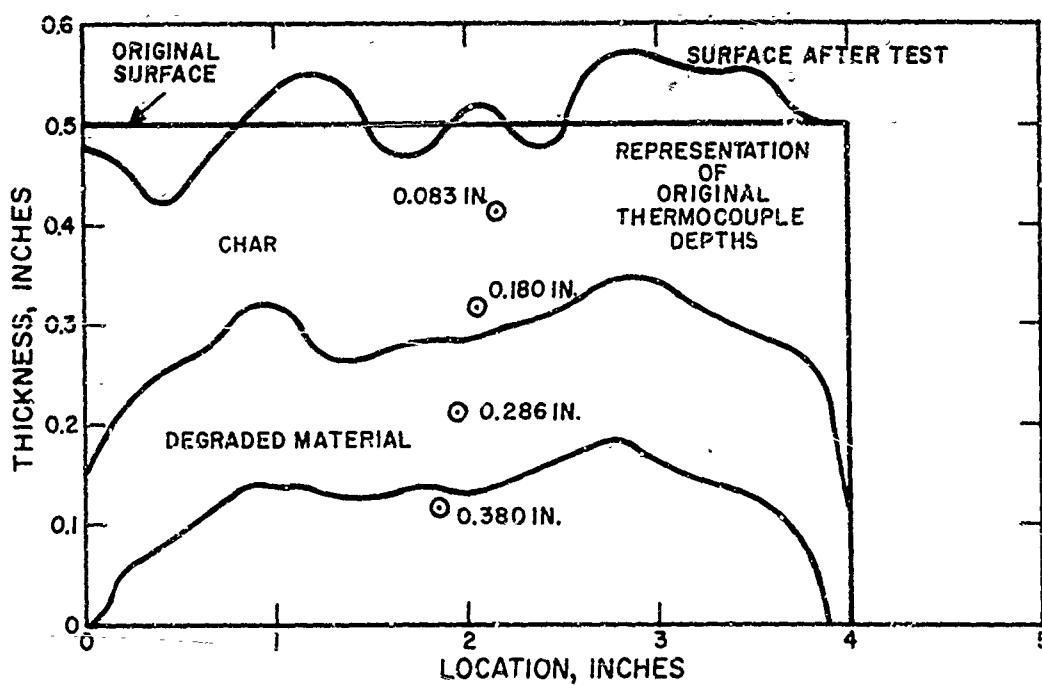
Figure 167. Recession Profile – Specimen A4-6 Run 23
(Dual Channel Test)
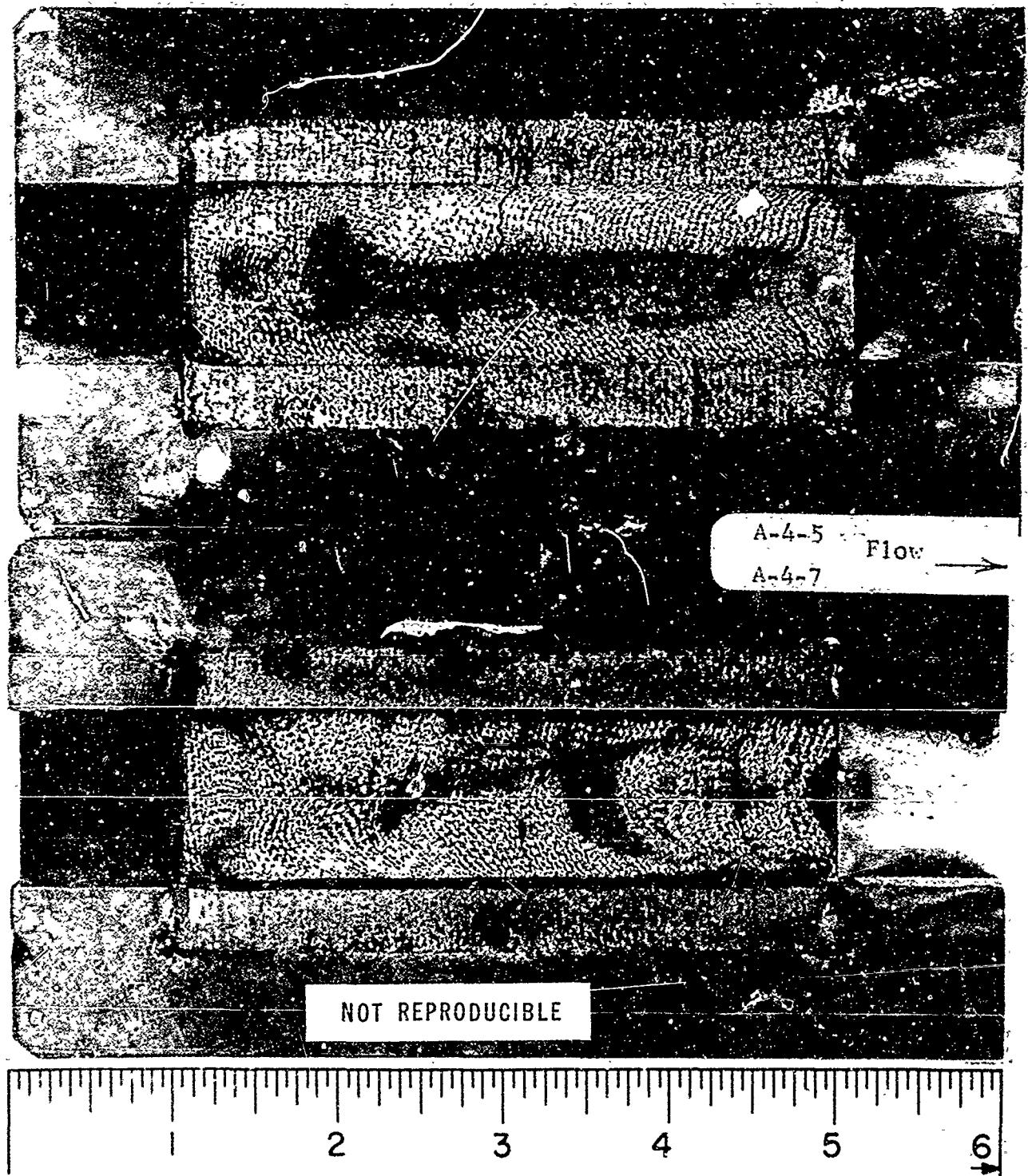
Figure 168. Ablated Specimens Top View A4-5 and A4-7

149
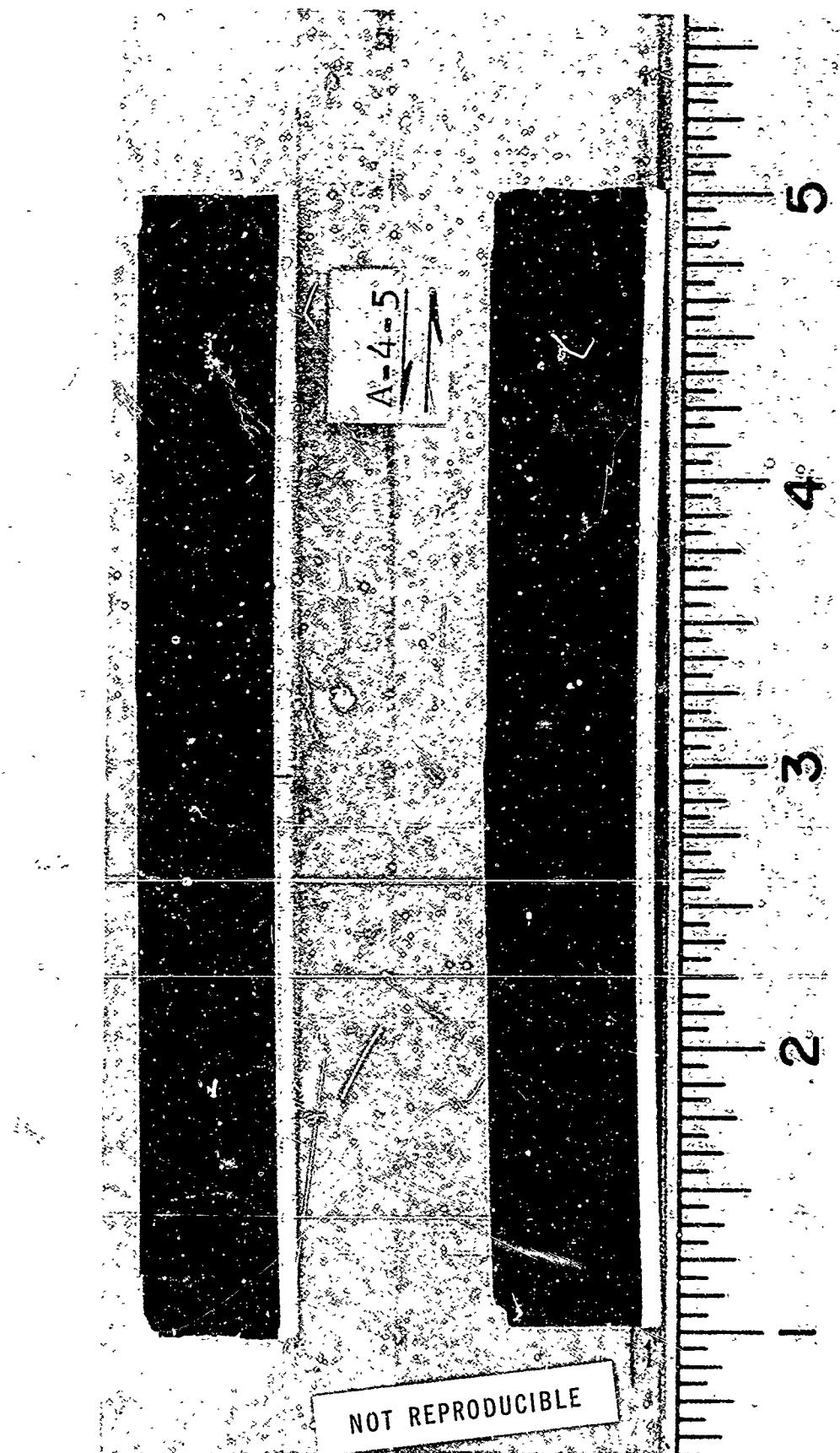
Figure 169. Ablated Specimens Sectioned A4-5

NOT REPRODUCIBLE

150

A4-7

NOT REPRODUCIBLE
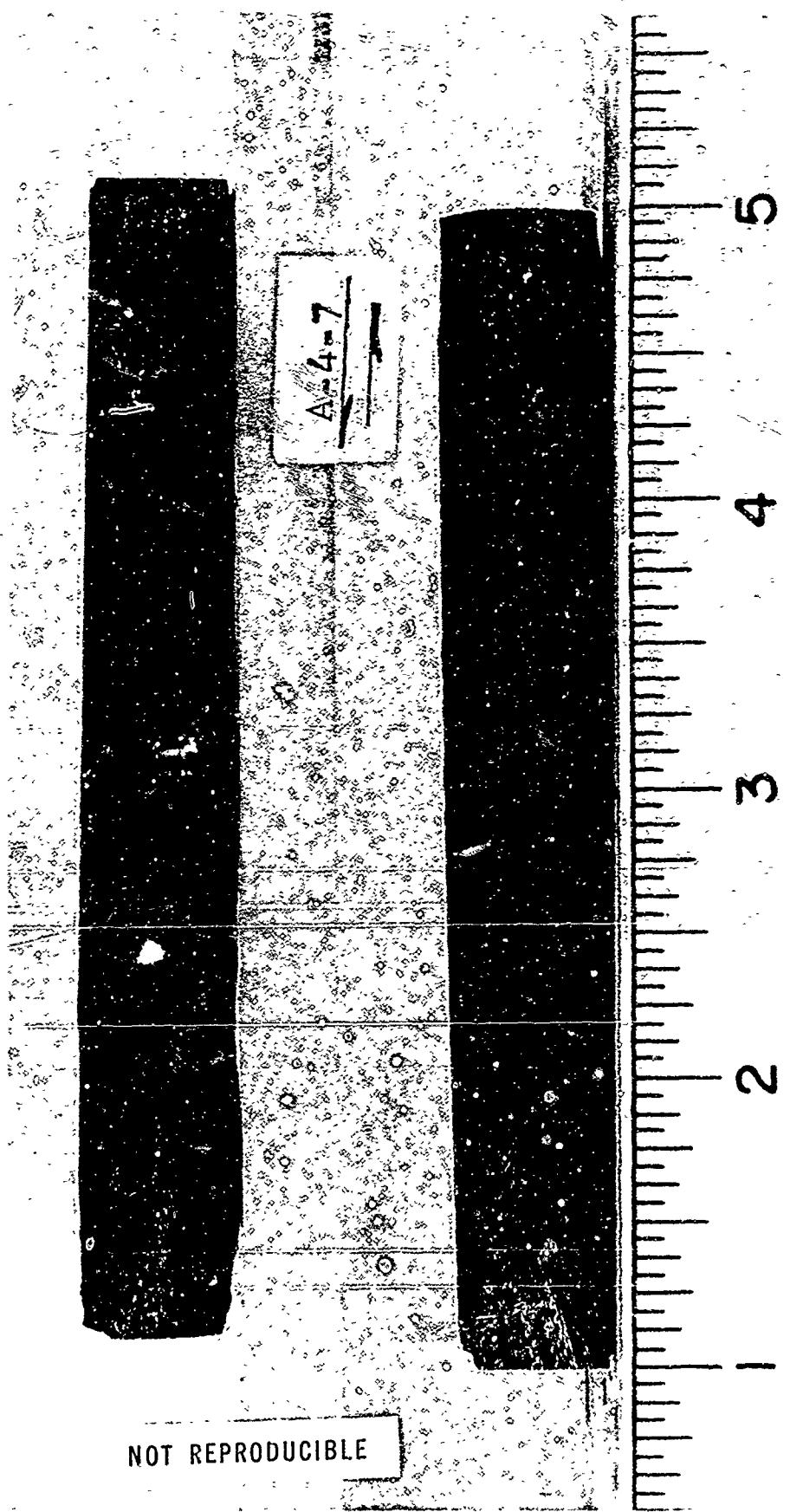
Figure 170. Ablated Specimens Sectioned A4-7

151
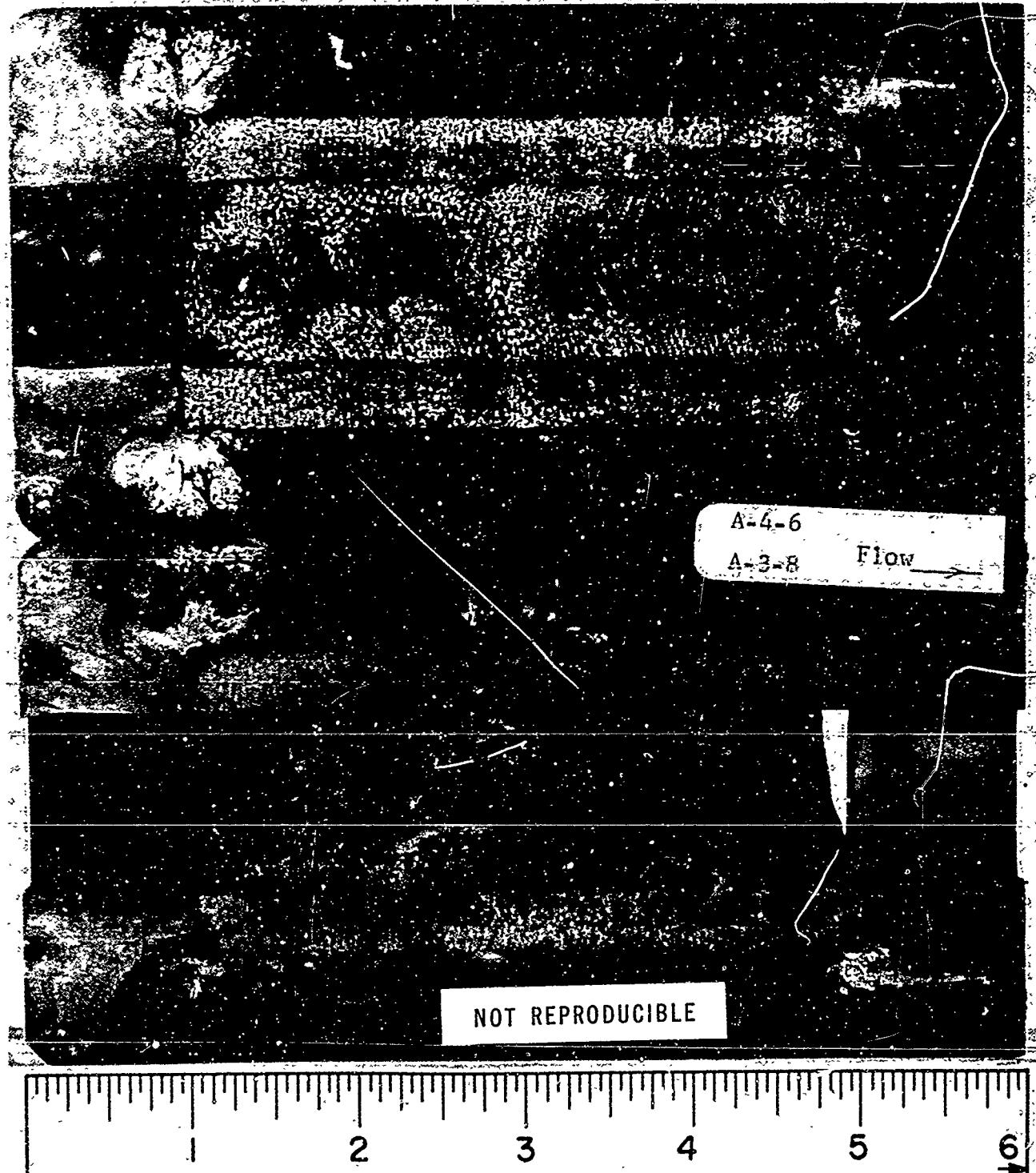
Figure 171. Ablated Specimens Top View A3-8 and A4-6

152
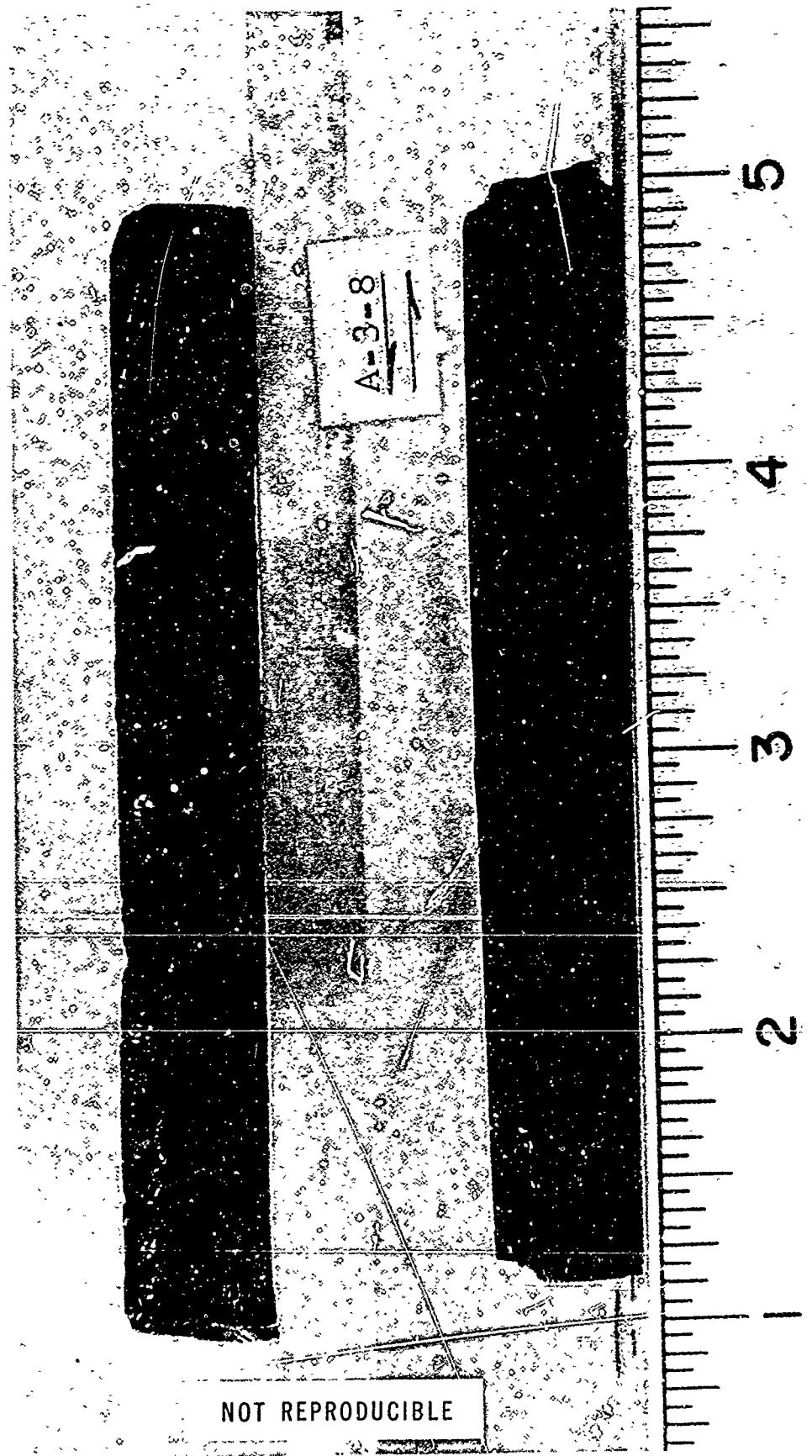
Figure 172. Ablated Specimens Sectioned A3-8

NOT REPRODUCIBLE

A-3-8
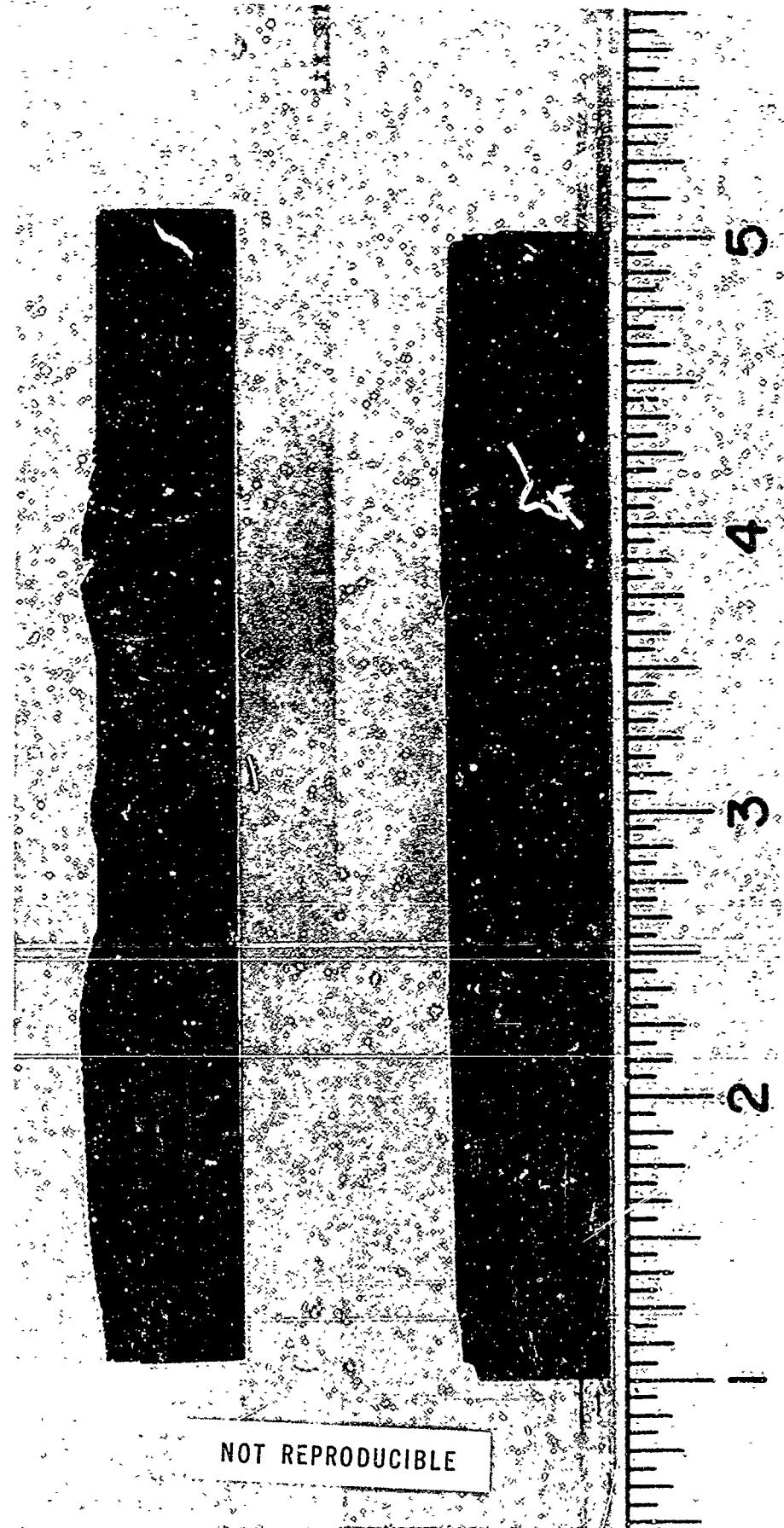
Figure 173. Ablated Specimens Sectioned A4-6

NOT REPRODUCIBLE

154
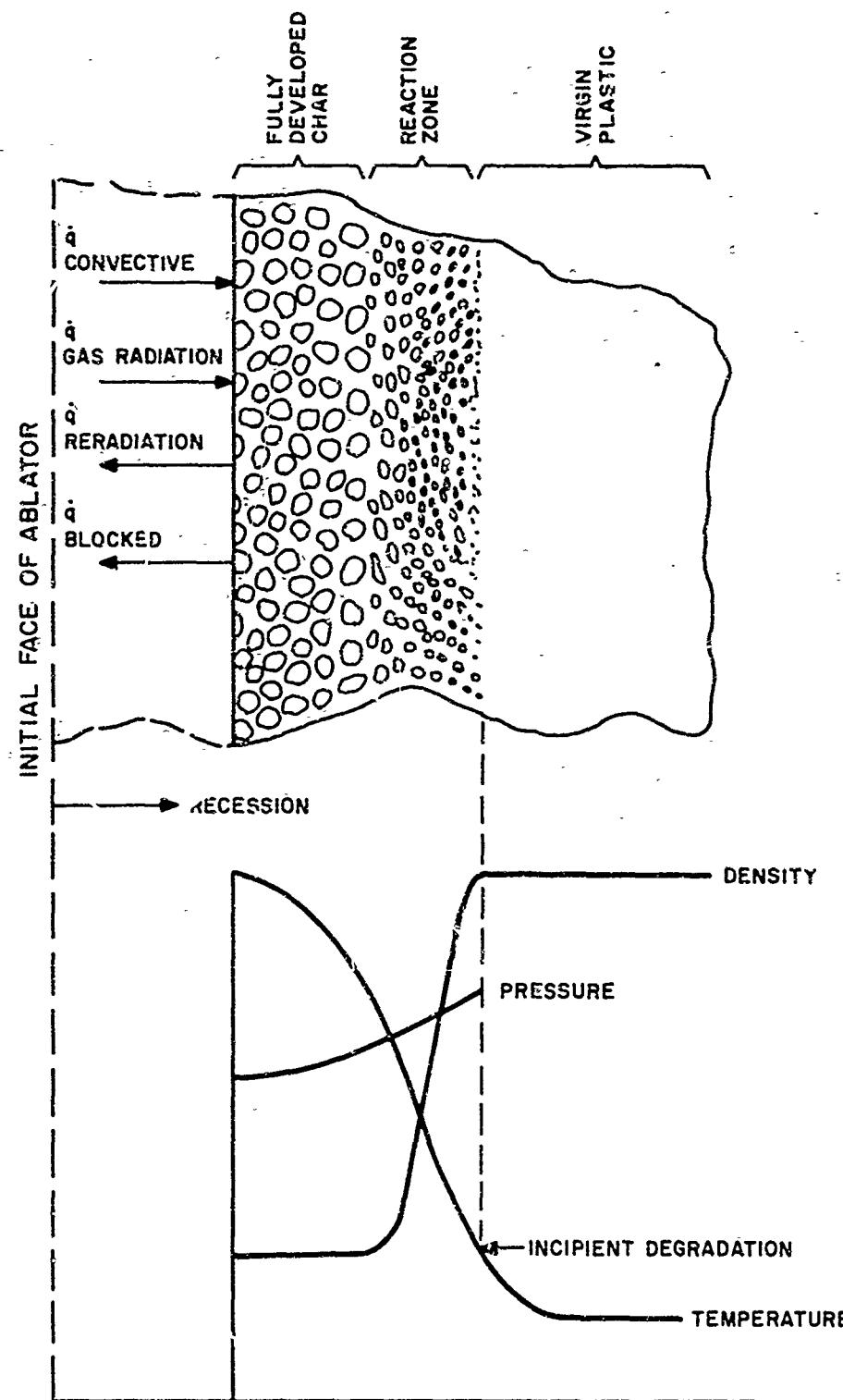
Figure 174. Representation of A Degrading Charring Plastic Ablator and
Corresponding Profiles

155
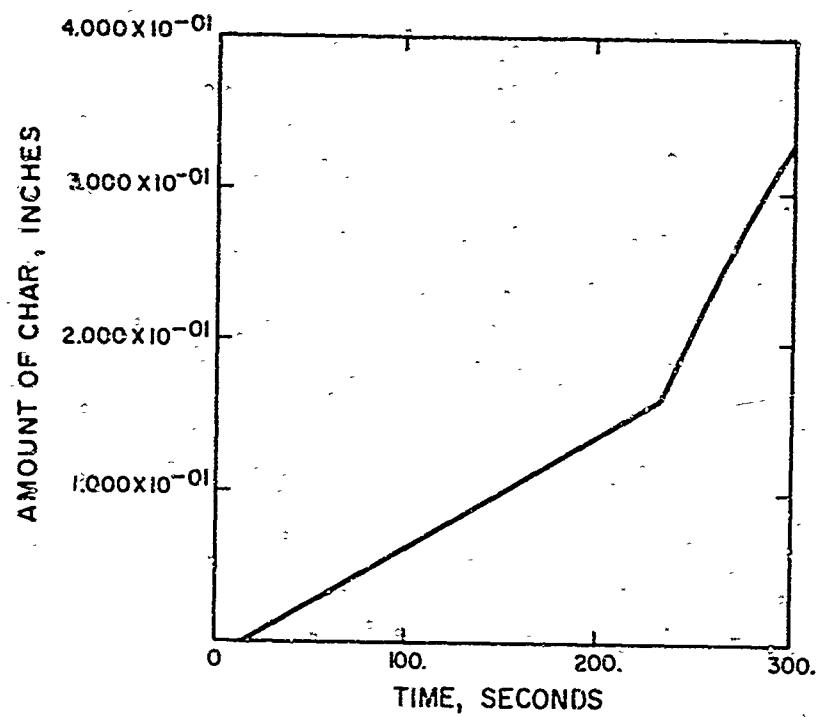
Figure 175. Composite C1 in Channel (T4M3) Char History
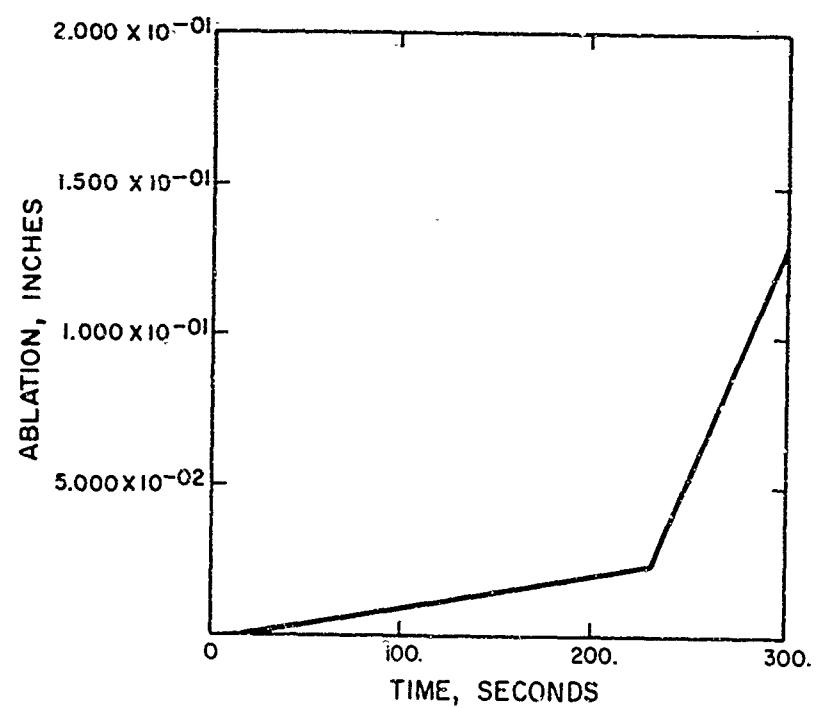
Figure 176. Composite C1 in Channel (T4M3) Ablation History

156
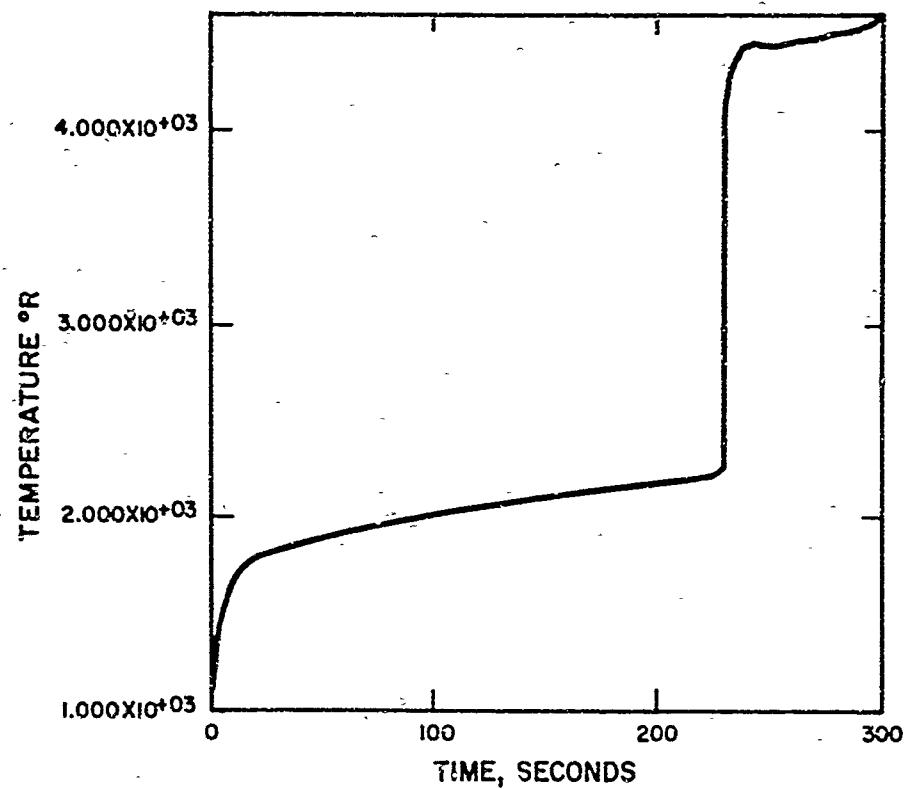
Figure 177. Composite C1 in Channel (T4M3) Surface
Temperature History
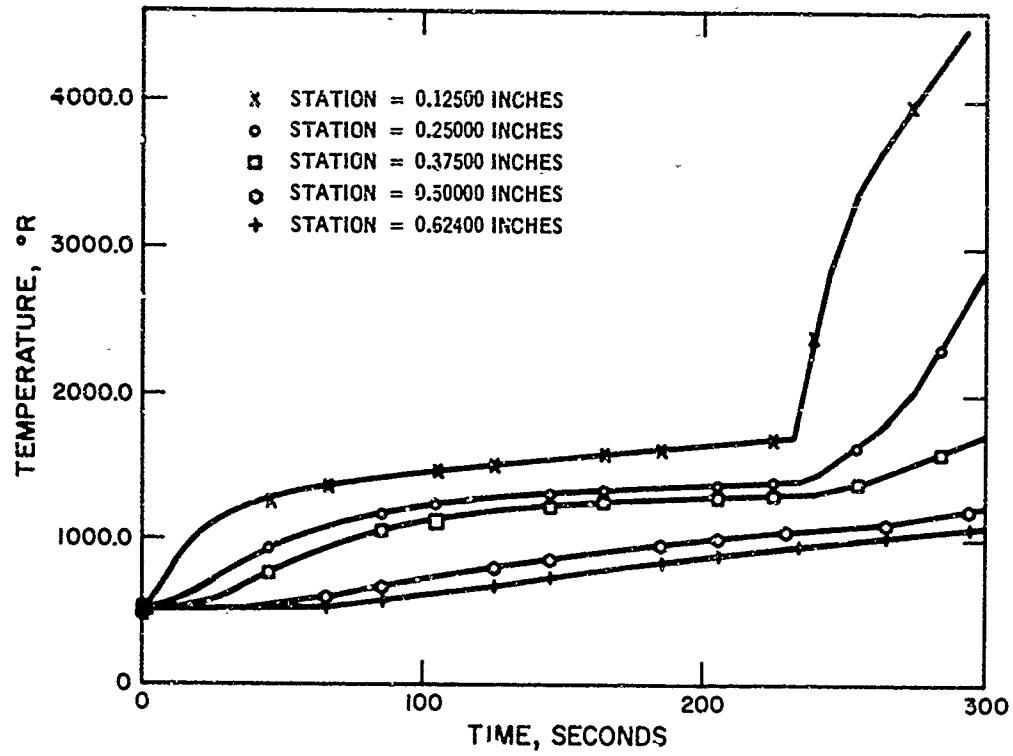
Figure 178. Composite C1 in Channel (T4M3) Temperature
History at Given Depths

157
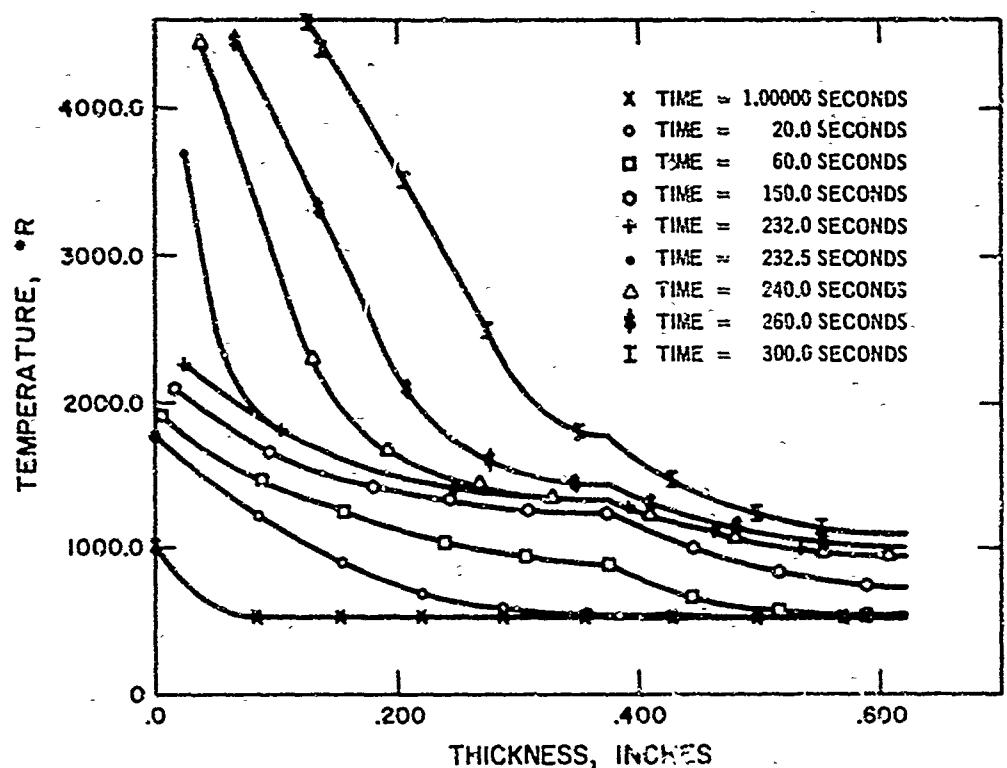
Figure 179. Composite C1 in Channel (T4M3) Temperature Profiles
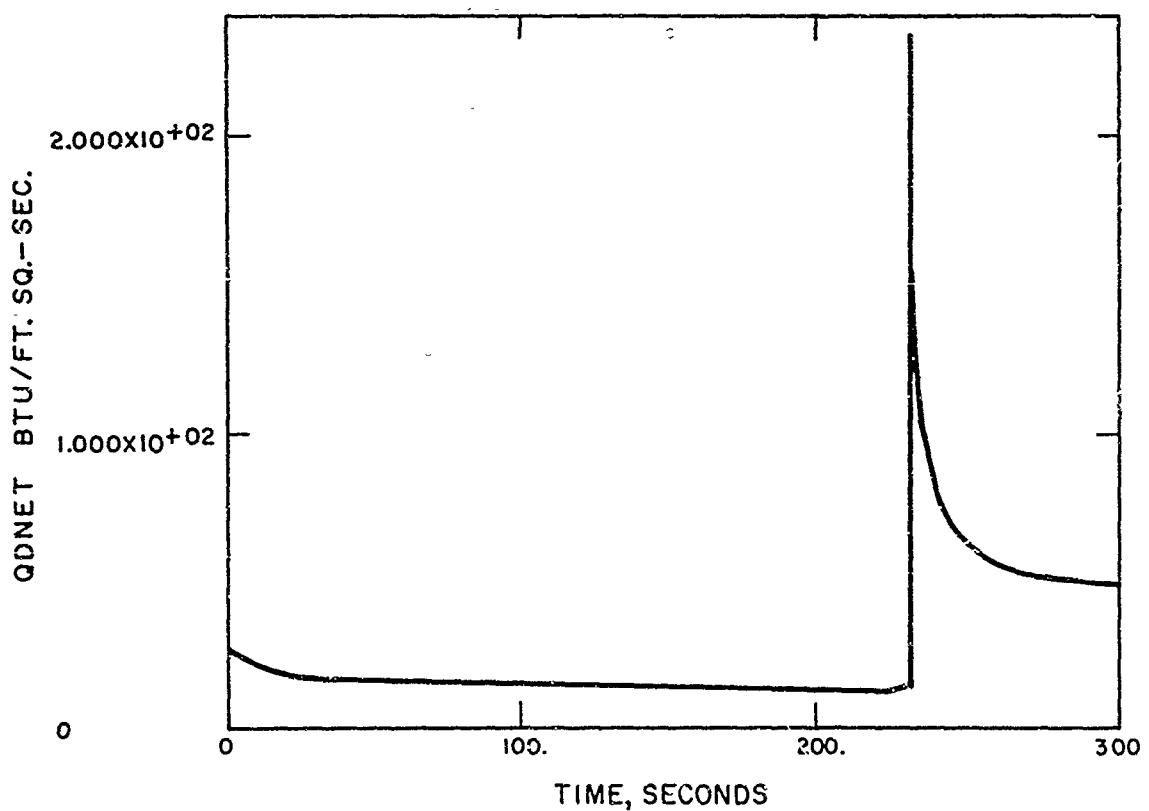
Figure 180. Composite C1 in Channel (T4M3) Heat Flux History

158
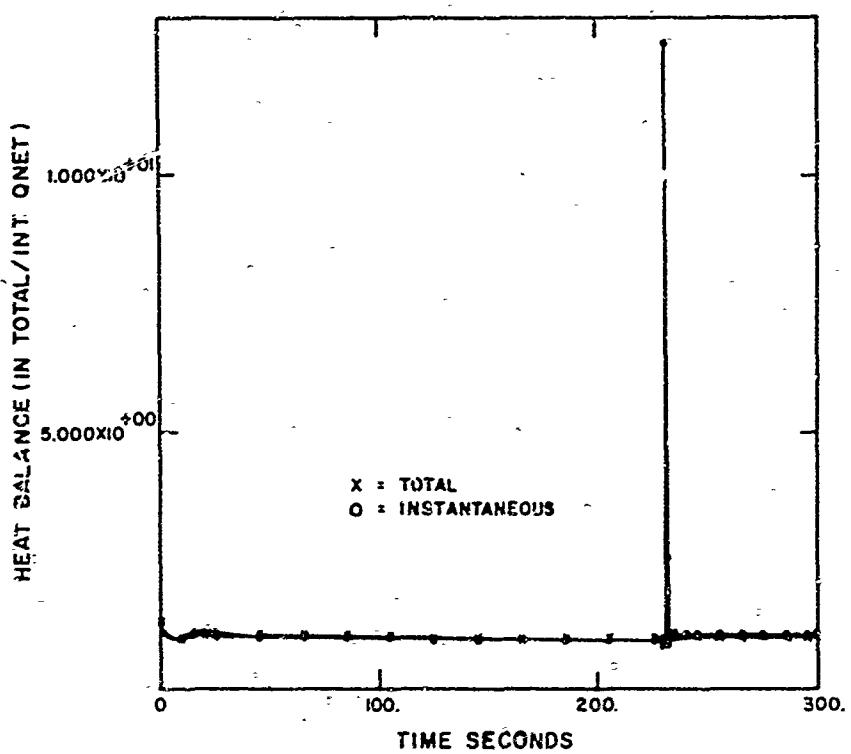
Figure 181. Composite C1 in Channel (T4M3) Heat Balance History
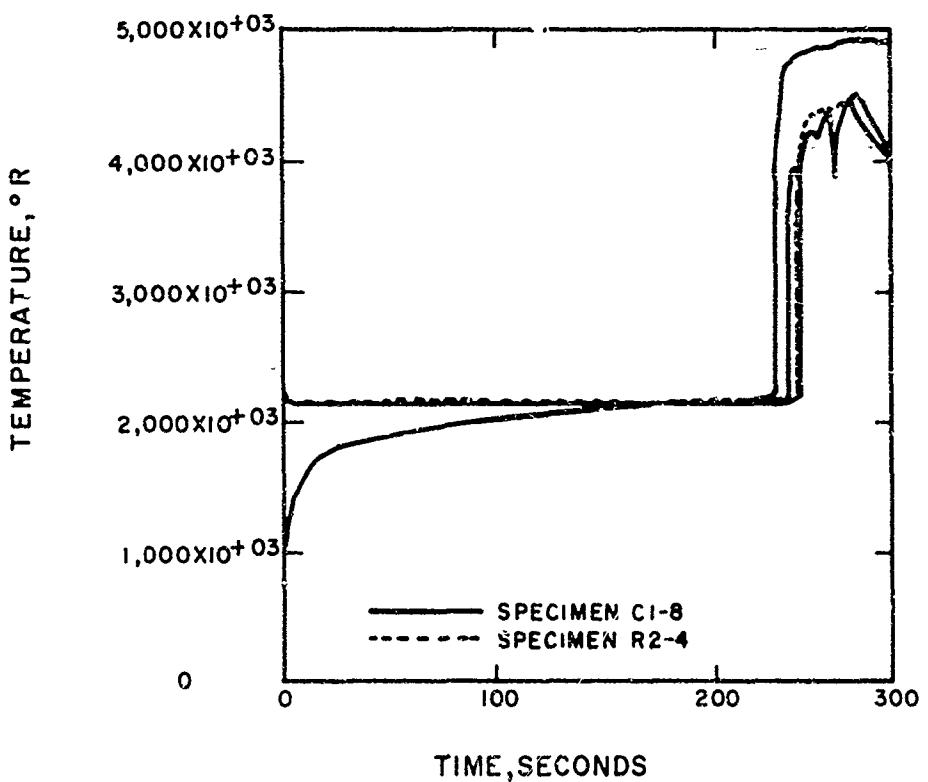
Figure 182. Carbon Phenolic, Channel Environment Surface Temperature History

159
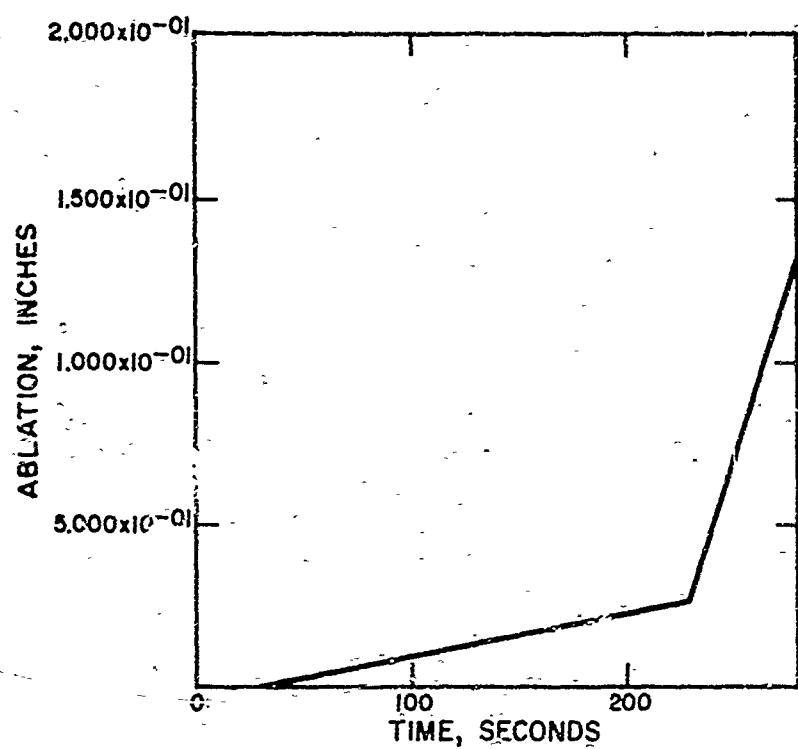
Figure 183. Carbon Phenolic, Channel Environment Ablation History
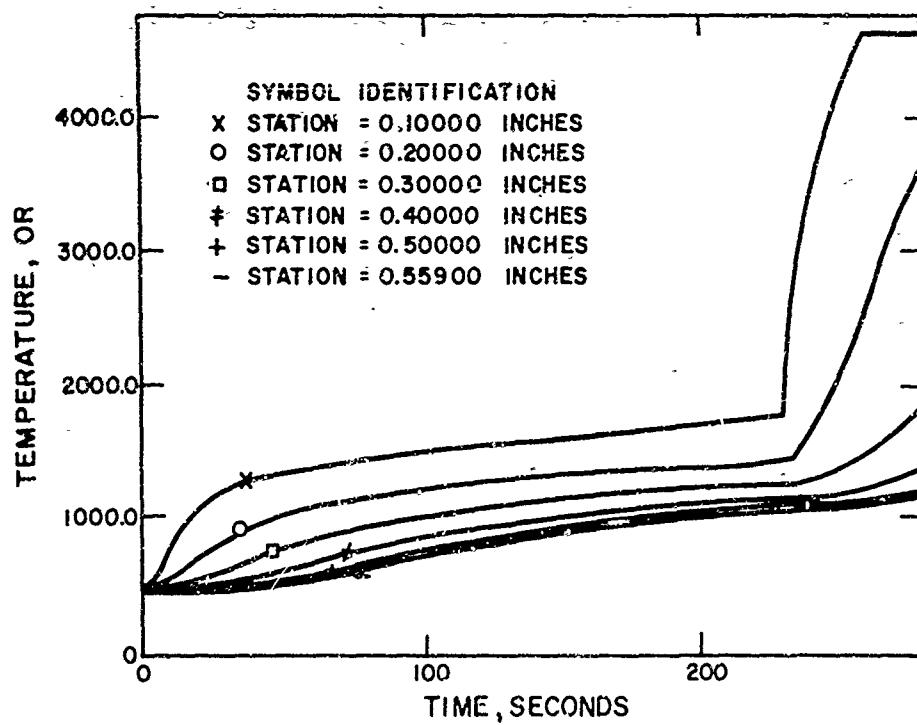
Figure 184. Carbon Phenolic, Channel Environment Temperature History
at Given Depths

160
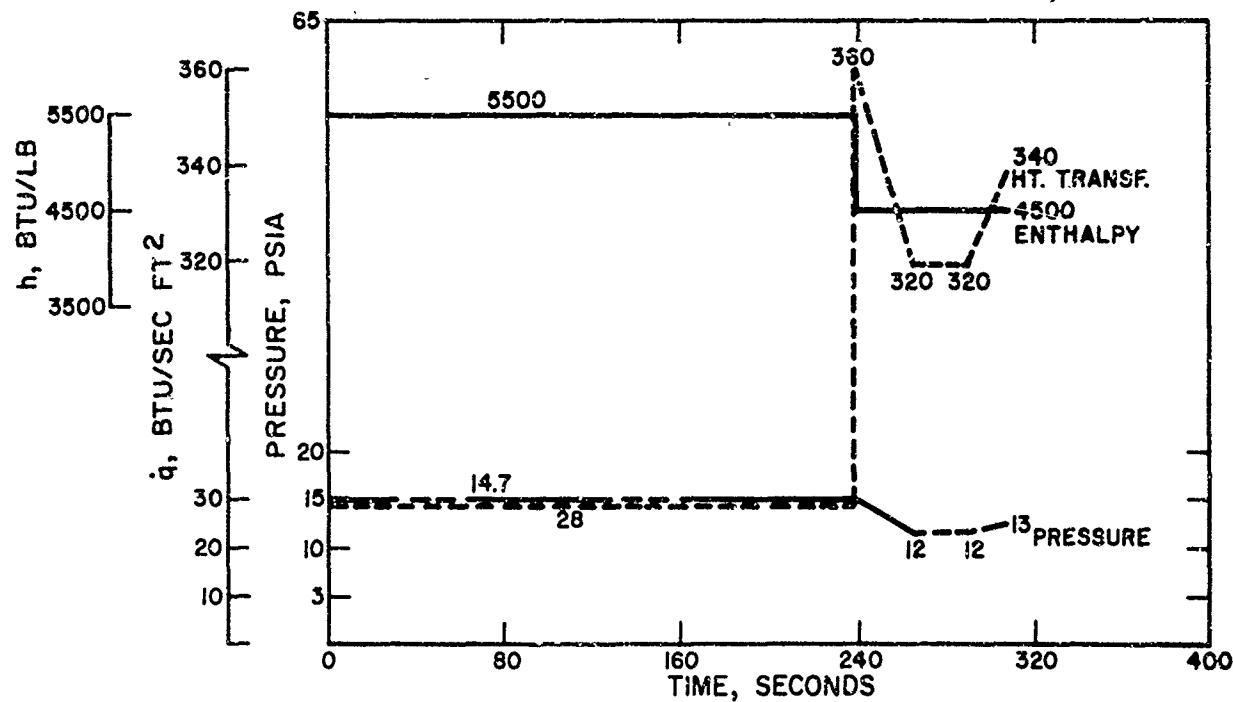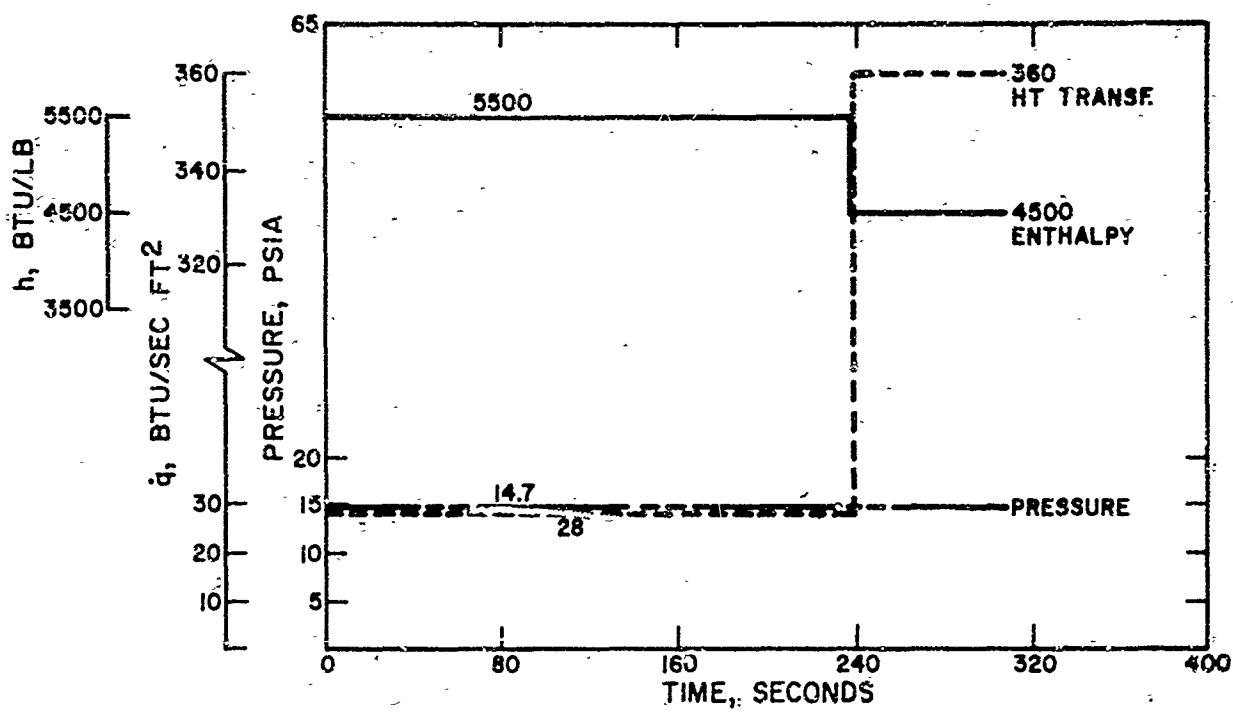
Figure 185. Inputs for Computer Models

161
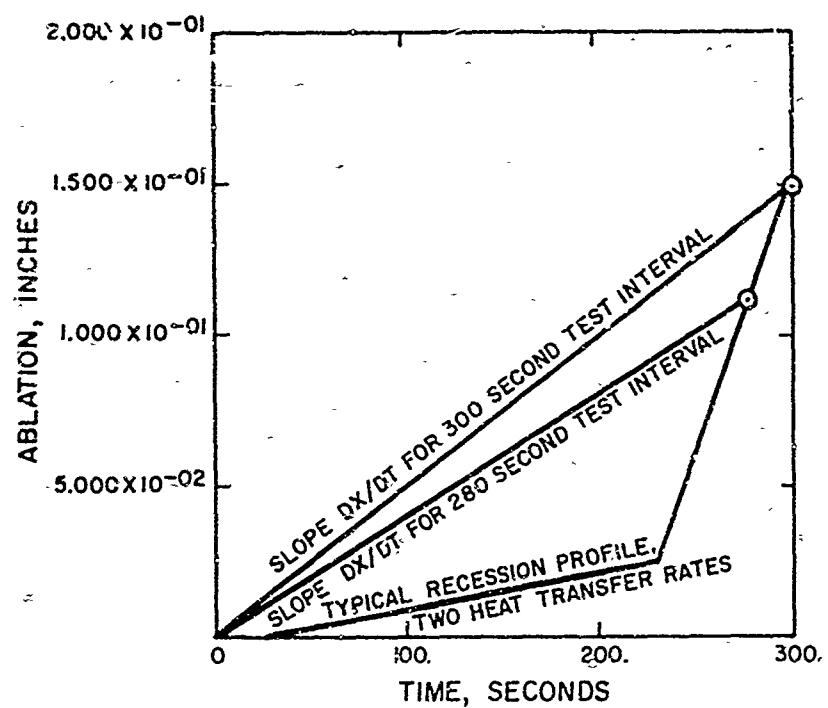
Figure 186. Carbon Phenolic – Channel Environment Ablation History
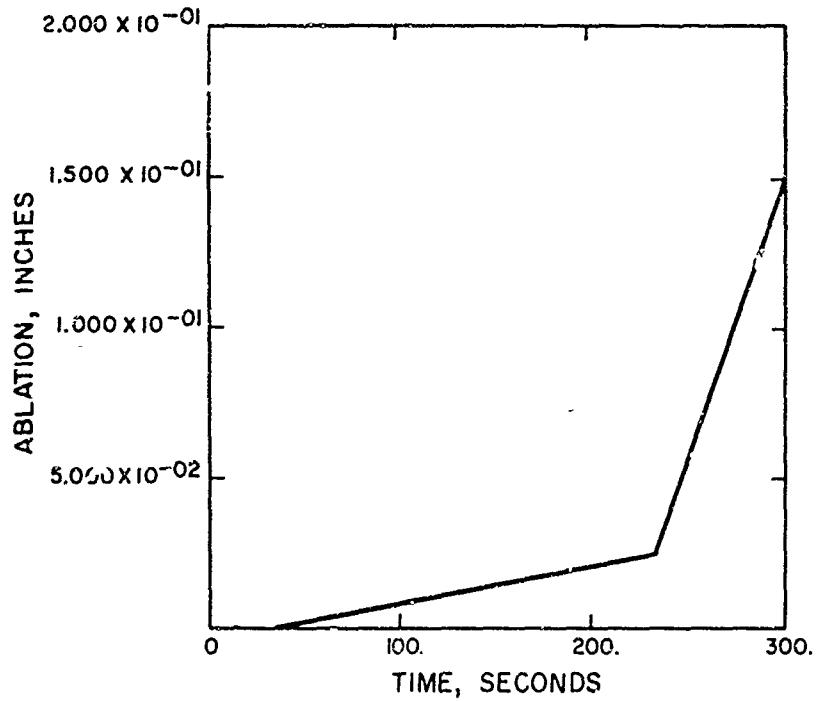
Figure 187. Carbon Phenolic, Channel Environment Ablation History (Model B)

162
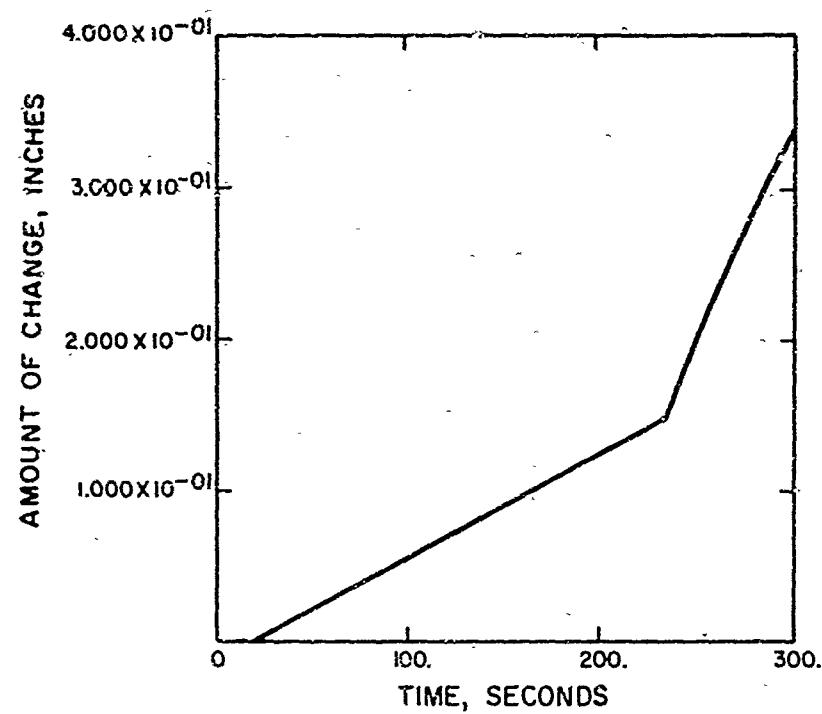
Figure 188. Carbon Phenolic, Channel Environment Char History
(Model "B")
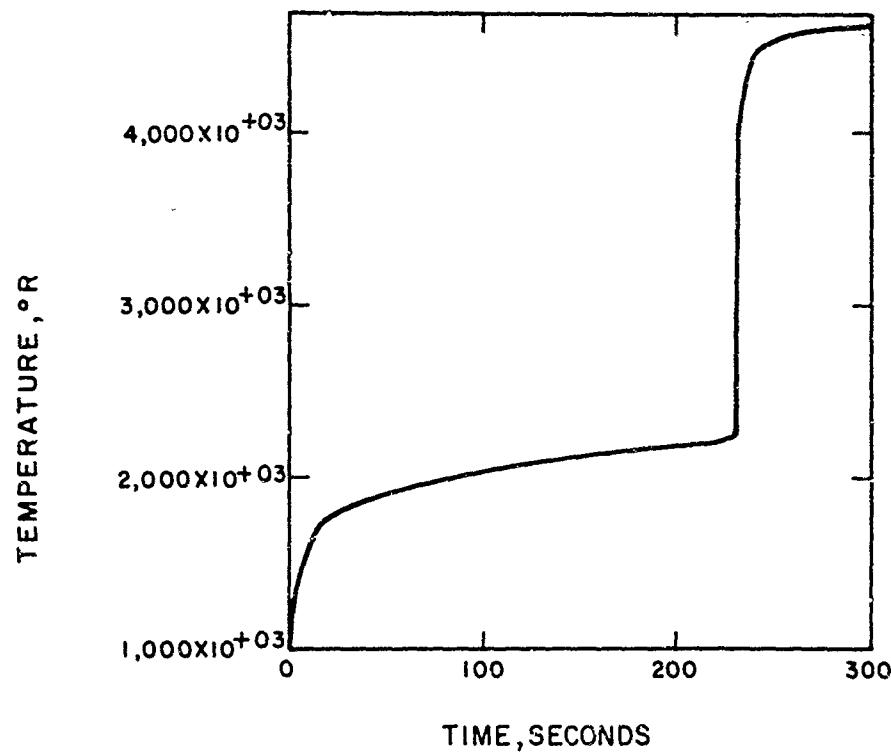
Figure 189. Carbon Phenolic, Channel Environment Surface Temperature History
(Model "B")

163
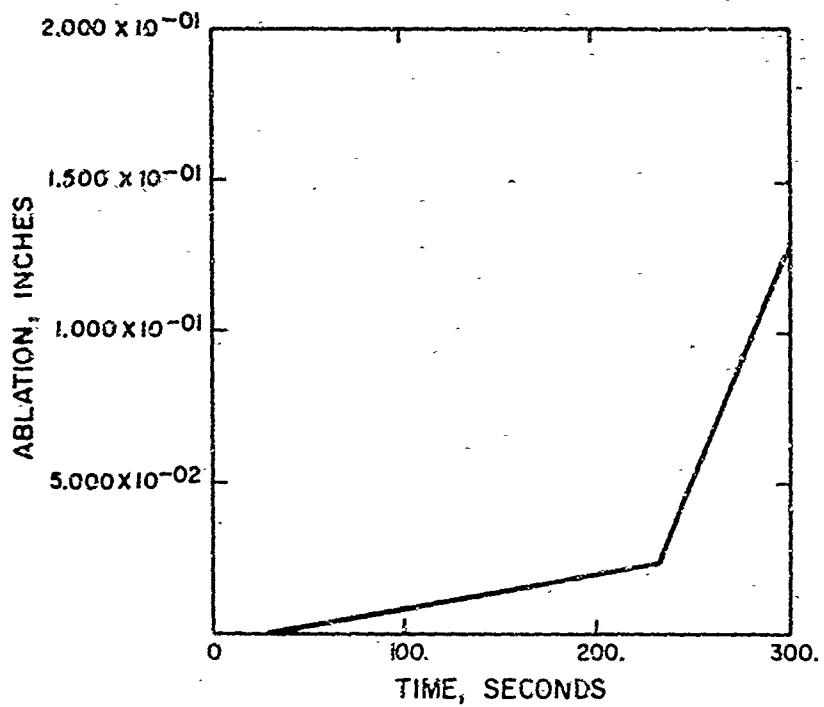
Figure 190. Carbon Phenolic, Channel Environment Ablation History
(Model "B")
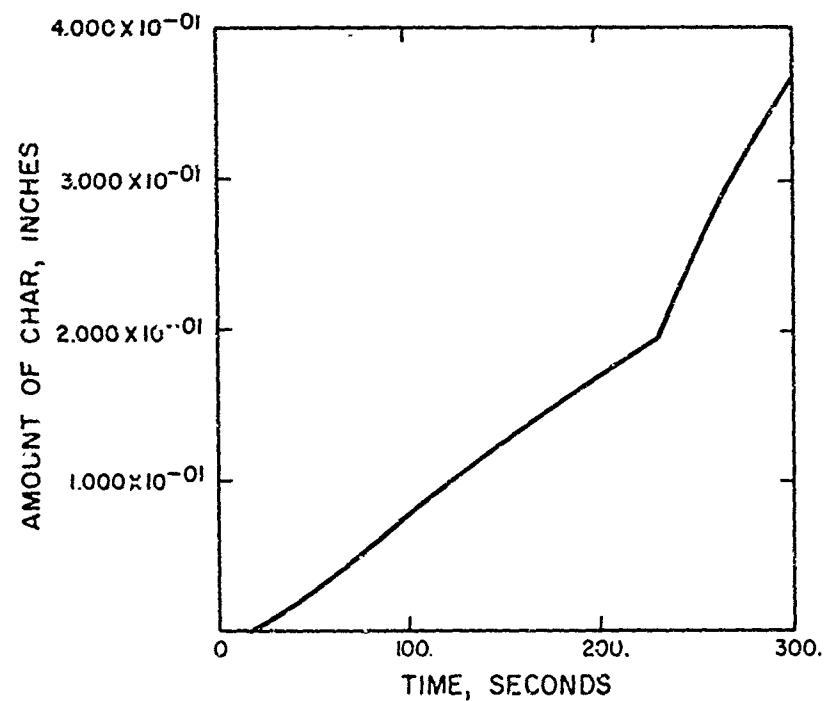
Figure 191. Carbon Phenolic, Channel Environment Char History
(Model "B")

164
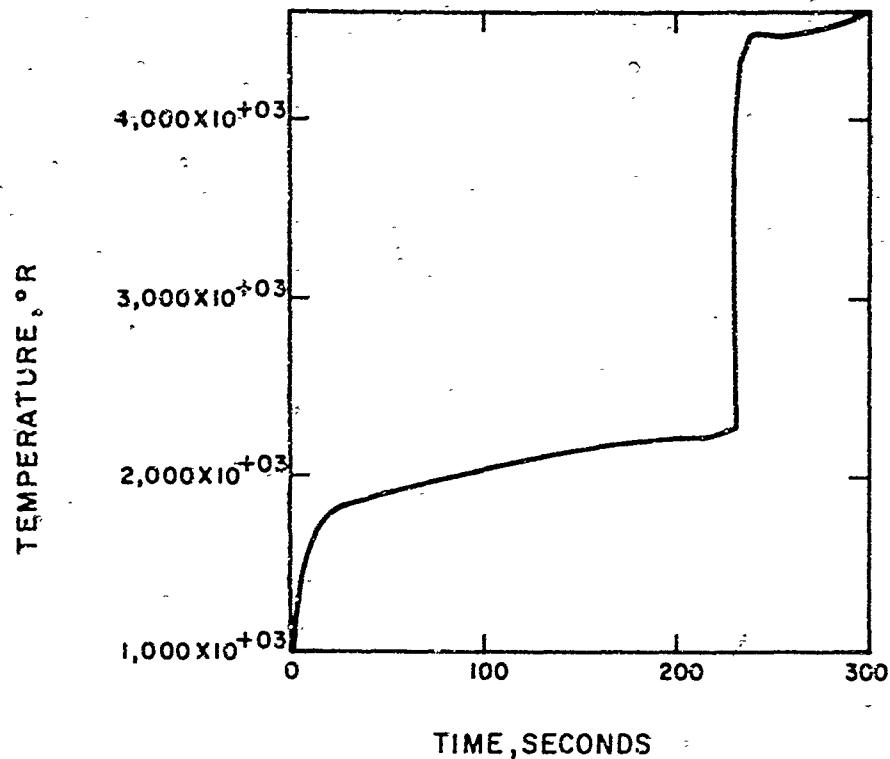
Figure 192. Carbon Phenolic, Channel Environment Surface Temperature History
(Model "C")
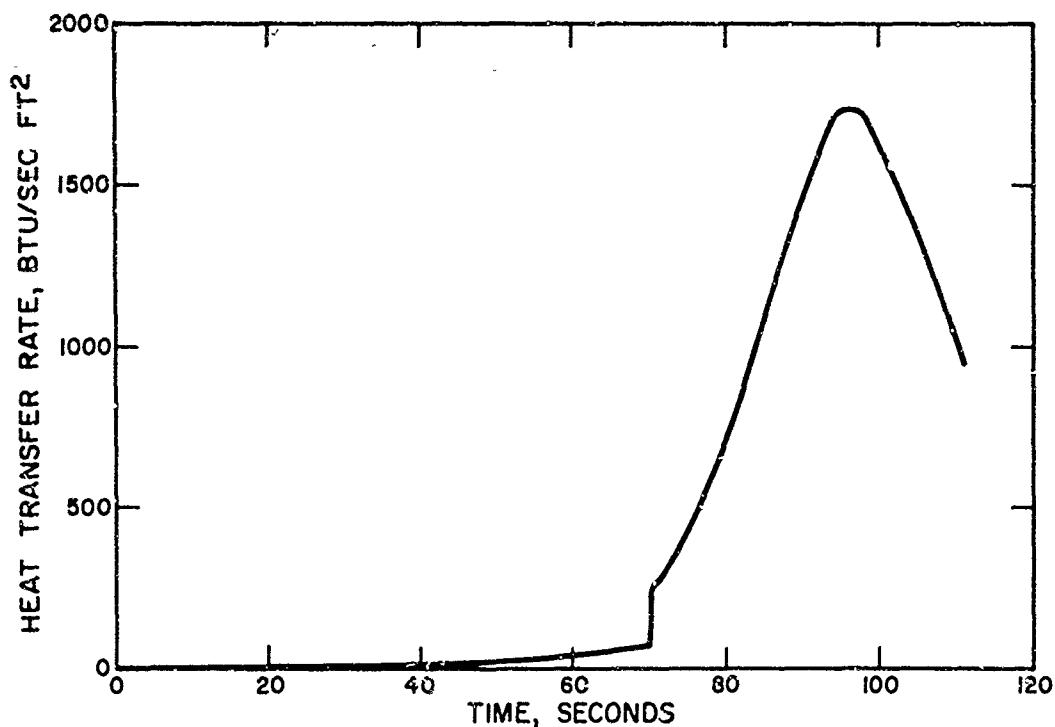
Figure 193. Typical High Integrated Heating Trajectory
(Frustum Station of Vehicle)
$\int \dot{q} dt = 46,500 \text{ Btu}/\text{Ft}^2$

165
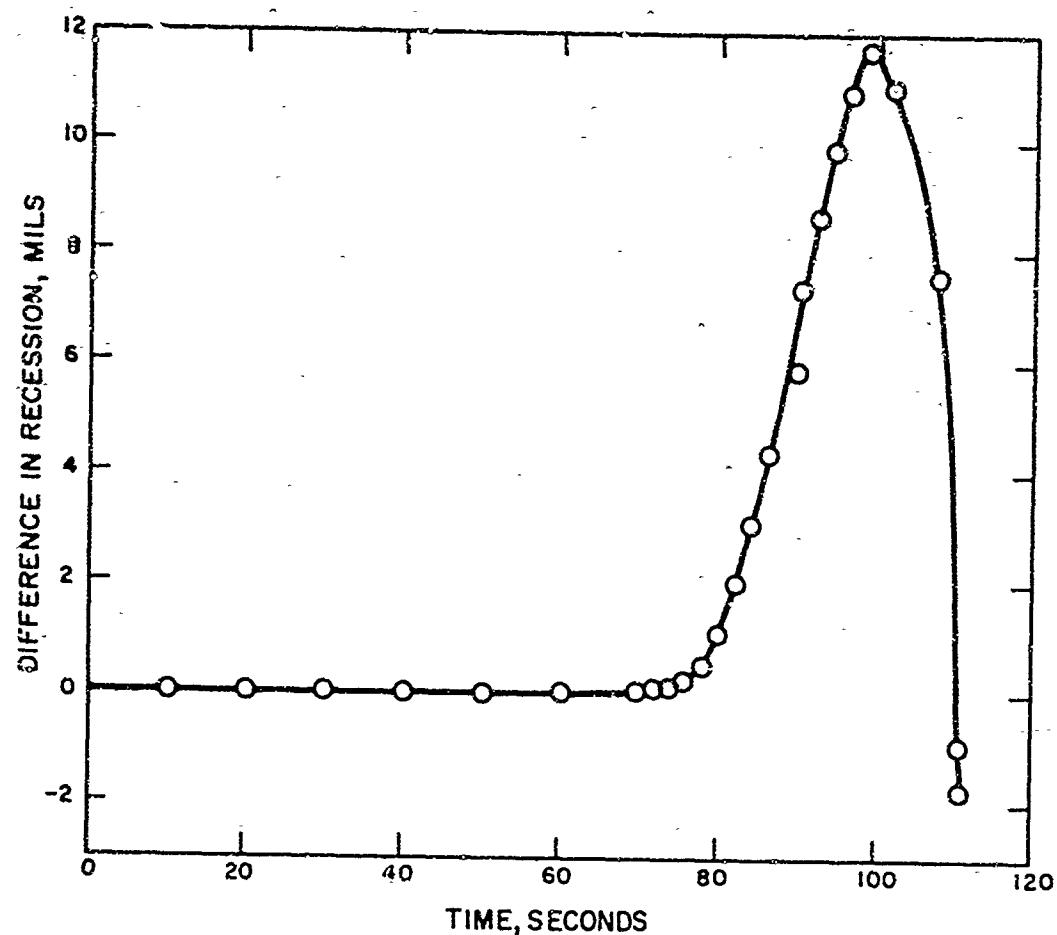
Figure 194. Recession Difference (Analytical Predictions)
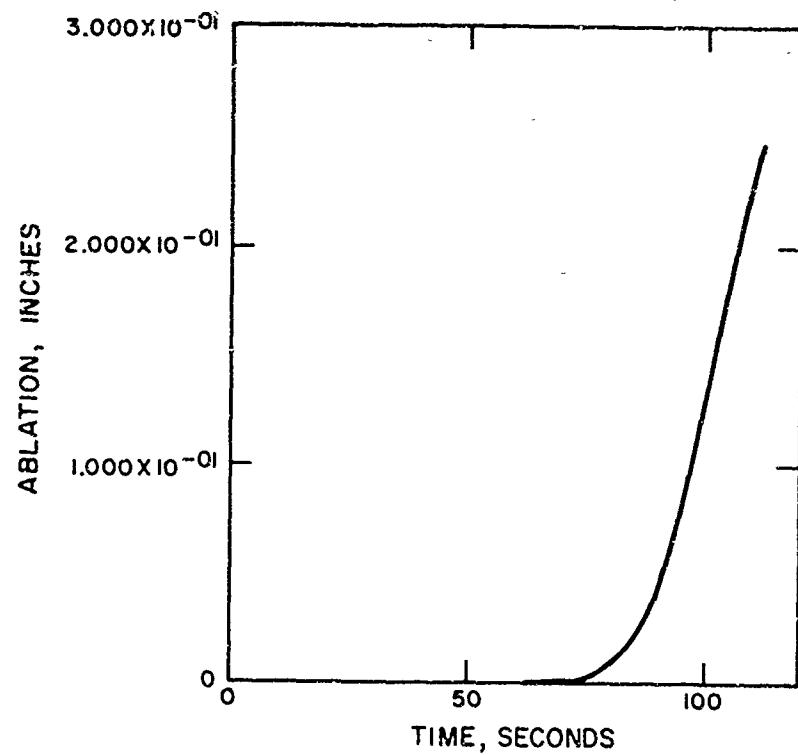
Figure 195. Station .75-CP/.04-EPON/.063-AL Ablation History
(Carbon Phenolic)

166
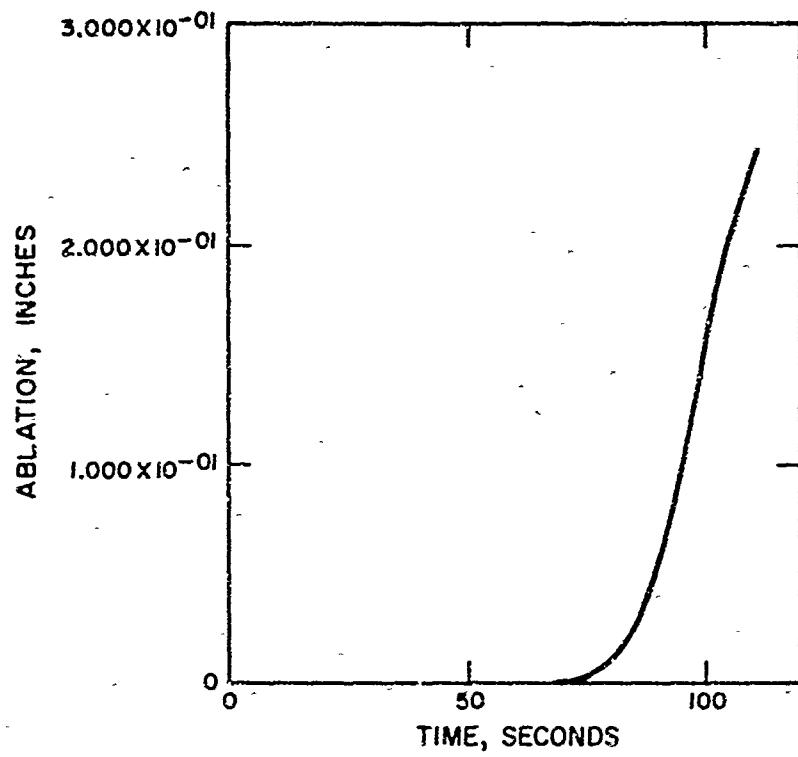
Figure 196. Station .75/CP/.04 EPON/.063-AL Ablation History
(Carbon Phenolic)

SYMBOL IDENTIFICATION

X TIME = 36.3 SECONDS
O TIME = 54.0 SECONDS
□ TIME = 71.2 SECONDS
‡ TIME = 80.0 SECONDS
+ TIME = 85.0 SECONDS
– TIME = 88.7 SECONDS
◻ TIME = 92.4 SECONDS
♣ TIME = 96.2 SECONDS
I TIME = 102.7 SECONDS
Q TIME = 111.0 SECONDS
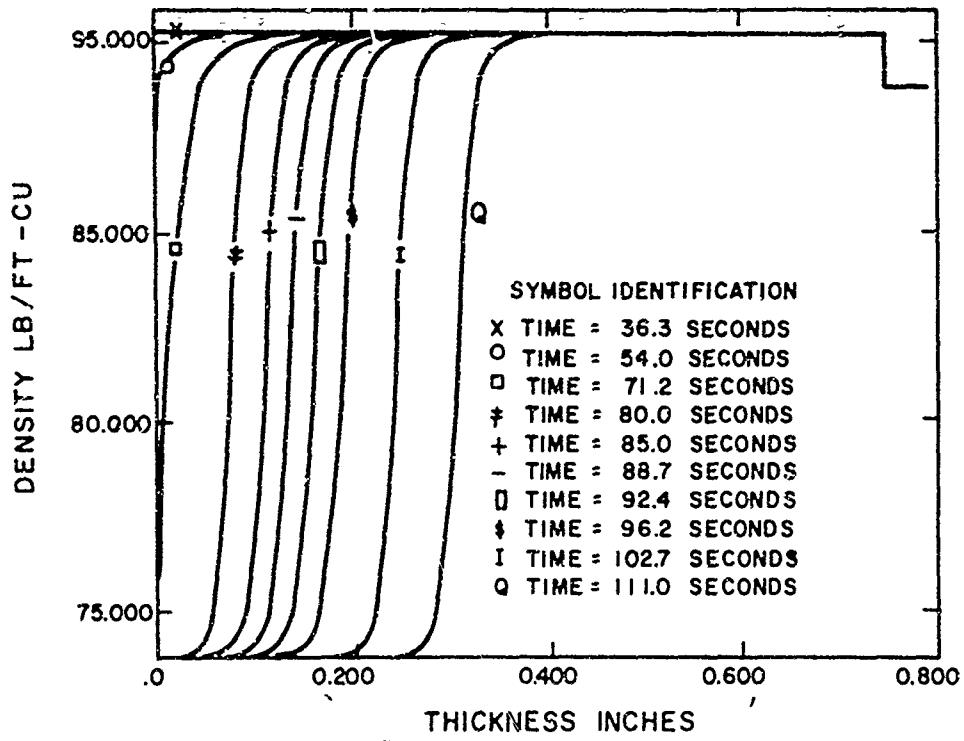
Figure 197. Station .75-CP/.04-EPON/.063-AL Density Profiles
(Carbon Phenolic)

167
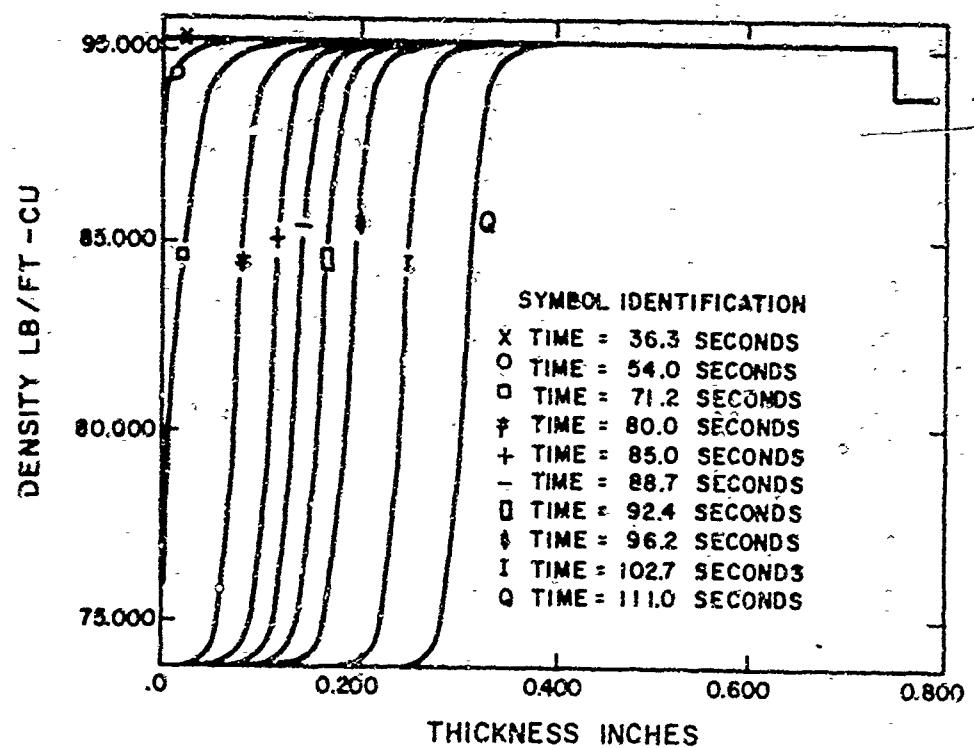
Figure 198. Station .75CP/.04EPON/.063-AL Density Profiles

DOCUMENT CONTROL DATA - R&D

(Security classification of title, body of abstract and indexing annotation must be entered when the overall report is classified)

1. ORIGINATING ACTIVITY (Corporate author)	2a. REPORT SECURITY CLASSIFICATION
General Electric Company Re-Entry and Environmental Systems Division Philadelphia, Pennsylvania 19101	UNCLASSIFIED
	2b. GROUP

3. REPORT TITLE

ABLATIVE MATERIALS FOR HIGH HEAT LOADS. PART II. HETEROCYCLIC RESINS, LAYERED COMPOSITES, ELASTOMERS, AND FILAMENT WOUND COMPOSITES

4. DESCRIPTIVE NOTES (Type of report and inclusive dates)

Interim Summary Report - March, 1970 to June, 1971

5. AUTHOR(S) (Last name, first name, initial)

P. W. Juneau, Jr.   R. M. Fenton
J. W. Metzger
F. F. Curtis

6. REPORT DATE	7a. TOTAL NO. OF PAGES	7b. NO. OF REFS
September, 1971	217	3

8a. CONTRACT OR GRANT NO. Contract No. F33615-69-C-1503	9a. ORIGINATOR'S REPORT NUMBER(S) AFML-TR-70-95, Part II
b. PROJECT NO. 7340	
c. Task No. 734001	9b. OTHER REPORT NO(S) (Any other numbers that may be assigned this report)
d.	

10. AVAILABILITY/LIMITATION NOTICES This document is subject to special export controls and each transmittal to foreign governments or foreign nationals may be made only with prior approval of the Plastics and Composites Branch, LNC, Nonmetallic Materials Laboratory, Wright-Patterson AFB, Ohio 45433.

| 11. SUPPLEMENTARY NOTES	12. SPONSORING MILITARY ACTIVITY Air Force Materials Laboratory (LNC) Air Force Systems Command Wright-Patterson Air Force Base, Ohio 45433

13. ABSTRACT

ABSTRACT

Ablative plastic composite materials were investigated and developed for long time heating environments. The desirable materials performance goals were low surface ablation, insulative ability, and low weight without asymmetrical ablation, char instability, spallation or other thermomechanical effects.

The candidate materials consisted of (a) carbon, quartz, and silica cloth reinforced polyimide resin, (b) loom woven, low density quartz (LDQ) insulative layers using polyimide resin, (c) carbon-quartz bifilament tape reinforced phenolic resin, (d) filled ablative silicone elastomers, and (e) a multiple interlock, filament wound (MIFW) carbon filament reinforced phenolic resin cylinder.

Candidate materials and reference carbon and silica cloth reinforced phenolic resinous composites were evaluated. Polyimide resin composites were generally comparable to the reference materials. LDQ proved an effective light weight insulator when used between a heat shield and aluminum structure. Outstanding carbon-quartz bifilament tape performance was obtained, but the results could not be adequately reproduced. There were no attractive performance features for the two remaining concepts.

The test environment was generated by a 5 megawatt air arc heater, which was operated stepwise over 300 seconds to give a 36,550 Btu/ft^2 heat load. Other nominal conditions over the 230- and 70-second heating intervals were 5000 and 5000 Btu/lb enthalpy; 25 and 440 Btu/ft^2-sec heat flux; 0.4 and 2.5 lb/ft^2 shear stress.

A high heat flux, dual channel characterization procedure was developed to investigate the ablative performance of materials under conditions more representative of advanced missile entry missions. Preliminary characterizations were conducted for selected reference and candidate composites.

An analytical study was made of materials response and to confirm experimental results. Good agreement was generally found between analytical and experimental results for carbon cloth reinforced phenolic resin and other composites.

DD ₁ FORM 1473
ᴶᴬᴺ ⁶⁴

14. KEY WORDS	LINK A		LINK B		LINK C	
	ROLE	WT	ROLE	WT	ROLE	WT
Ablation						
Ablative Materials						
Air Arc Heater Characterization						
Elastomers						
Filament Wound Composites						
Heterocyclic Resins						
Layered Composites						
Hyperthermal Environment						
Insulation						
Plastic Composites						
Reentry Environment						
Reinforced Plastics						

INSTRUCTIONS

1. ORIGINATING ACTIVITY: Enter the name and address of the contractor, subcontractor, grantee, Department of Defense activity or other organization (corporate author) issuing the report.

2a. REPORT SECURITY CLASSIFICATION: Enter the overall security classification of the report. Indicate whether "Restricted Data" is included. Marking is to be in accordance with appropriate security regulations.

2b. GROUP: Automatic downgrading is specified in DoD Directive 5200.10 and Armed Forces Industrial Manual. Enter the group number. Also, when applicable, show that optional markings have been used for Group 3 and Group 4 as authorized.

3. REPORT TITLE: Enter the complete report title in all capital letters. Titles in all cases should be unclassified. If a meaningful title cannot be selected without classification, show title classification in all capitals in parenthesis immediately following the title.

4. DESCRIPTIVE NOTES: If appropriate, enter the type of report, e.g., interim, progress, summary, annual, or final. Give the inclusive dates when a specific reporting period is covered.

5. AUTHOR(S): Enter the name(s) of author(s) as shown on or in the report. Enter last name, first name, middle initial. If military, show rank and branch of service. The name of the principal author is an absolute minimum requirement.

6. REPORT DATE: Enter the date of the report as day, month, year; or month, year. If more than one date appears on the report, use date of publication.

7a. TOTAL NUMBER OF PAGES: The total page count should follow normal pagination procedures, i.e., enter the number of pages containing information.

7b. NUMBER OF REFERENCES: Enter the total number of references cited in the report.

8a. CONTRACT OR GRANT NUMBER. If appropriate, enter the applicable number of the contract or grant under which the report was written.

8b, 8c, & 8d. PROJECT NUMBER. Enter the appropriate military department identification, such as project number, subproject number, system numbers, task number, etc.

9a. ORIGINATOR'S REPORT NUMBER(S) Enter the official report number by which the document will be identified and controlled by the originating activity. This number must be unique to this report.

9b. OTHER REPORT NUMBER(S): If the report has been assigned any other report numbers (either by the originator or by the sponsor), also enter this number(s).

10. AVAILABILITY/LIMITATION NOTICES: Enter any limitations on further dissemination of the report, other than those imposed by security classification, using standard statements such as:

(1) "Qualified requesters may obtain copies of this report from DDC."

(2) "Foreign announcement and dissemination of this report by DDC is not authorized."

(3) "U. S. Government agencies may obtain copies of this report directly from DDC. Other qualified DDC users shall request through
_____ ."

(4) "U. S. military agencies may obtain copies of this report directly from DDC. Other qualified users shall request through
_____ ."

(5) "All distribution of this report is controlled. Qualified DDC users shall request through
_____ ."

If the report has been furnished to the Office of Technical Services, Department of Commerce, for sale to the public, indicate this fact and enter the price, if known.

11. SUPPLEMENTARY NOTES: Use for additional explanatory notes.

12. SPONSORING MILITARY ACTIVITY. Enter the name of the departmental project office or laboratory sponsoring (paying for) the research and development. Include address.

13. ABSTRACT: Enter an abstract giving a brief and factual summary of the document indicative of the report, even though it may also appear elsewhere in the body of the technical report. If additional space is required, a continuation sheet shall be attached.

It is highly desirable that the abstract of classified reports be unclassified. Each paragraph of the abstract shall end with an indication of the military security classification of the information in the paragraph, represented as (TS), (S), (C), or (U).

There is no limitation on the length of the abstract. However, the suggested length is from 150 to 225 words.

14. KEY WORDS: Key words are technically meaningful terms or short phrases that characterize a report and may be used as index entries for cataloging the report. Key words must be selected so that no security classification is required. Identifiers, such as equipment model designation, trade name, military project code name, geographic location, may be used as key words but will be followed by an indication of technical context. The assignment of links, rules, and weights is optional.